Cycles biogéochimiques de la Mer Méditerranée : Processus et bilans

Fayçal Kessouri

Université de Toulouse

THÈSE

En vue de l'obtention du

DOCTORAT DE L'UNIVERSITÉ DE TOULOUSE

Délivré par :
Université Toulouse III Paul Sabatier (UT3 Paul Sabatier)

Discipline ou spécialité :

OCEANOGRAPHIE

Présentée et soutenue par :
M. Fayçal Kessouri

le : lundi 21 décembre 2015

Titre :

Cycles biogéochimiques de la mer Méditerranée: Processus et bilans

---

Ecole doctorale :
Sciences de l'Univers, de l'Environnement et de l'Espace (SDU2E)

Unité de recherche :
Laboratoire d'Aérologie UMR 5560

Directeur(s) de Thèse :
Me. Claude Estournel (LA - Univ. Toulouse)
Me. Caroline Ulses (LA - Univ. Toulouse)

Rapporteurs :

M. Maurizio Ribera d'Alcalà (Univ. Napoli)
Me. Marilaure Grégoire (Univ. Liège)

Membre(s) du jury :

Examinateurs:

Me. Isabelle Dadou (LEGOS - Univ. Toulouse)
M. Pascal Conan (LOMIC - Univ. Paris 6)
M. Xavier Durrieu de Madron (CEFREM - Univer. Perpignan)

Cycles biogéochimiques de la Mer Méditerranée :

Processus et bilans

« La Méditerranée, c'est mille choses à la fois. Non pas un paysage, mais d'innombrables paysages. Non pas une mer, mais une succession de mers. Non pas une civilisation, mais plusieurs civilisations superposées... La Méditerranée est un carrefour antique. Depuis des millénaires, tout conflue vers cette mer, bouleversant et enrichissant son histoire »

Fernand BRAUDEL, 1985

Fayçal Kessouri
Thèse de doctorat en océanographie
Laboratoire d'Aérologie – OMP, Université de Toulouse III Paul Sabatier

Résumé

La Méditerranée est caractérisée par une grande variété de régimes trophiques qui s'explique par les apports fluviaux, les ratios azote/phosphore particulièrement élevés dans le bassin oriental, et par les processus hydrodynamiques en particulier le mélange vertical dans les régions situées au nord. Cette thèse qui s'inscrit dans le cadre du projet MerMEX, composante du chantier MISTRALS, a pour objectif l'étude des cycles biogéochimiques en Méditerranée. Elle s'appuie en particulier sur les observations acquises dans le cadre du projet DeWEx et sur la modélisation couplée physique biogéochimie 3D. À l'échelle du bassin et à l'échelle régionale du sous-bassin occidental.

La première étude à l'échelle du bassin sur une période de 10 ans a permis d'effectuer une classification de régimes biogéochimiques, en fonction de leurs caractéristiques physiques et biogéochimiques. Les zones oligotrophes présentes au sud du bassin oriental et occidental sont caractérisées par une faible efflorescence et par de grandes profondeurs de nutriclines. Tandis qu'au nord du bassin, au large de Rhodes, en mer Adriatique et dans le bassin Liguro-provençal, le régime oligotrophe estival est suivi en hiver par une dynamique verticale intense, la convection profonde. Cette dernière est considérée comme le moteur de la circulation thermohaline. Elle entraine un enrichissement des eaux de surface en sels nutritifs qui permet une efflorescence rapide et intense au printemps. L'océan Atlantique représente une source de matière organique pour la Méditerranée. Cette mer représente en revanche une source de sels nutritifs pour l'Atlantique.

Ensuite, un modèle à très haute résolution a été imbriqué dans le modèle de bassin pour quantifier les processus physiques et biologiques qui déterminent la variabilité temporelle de la disponibilité et de la stœchiométrie des sels nutritifs en Méditerranée nord-occidentale. La convection profonde hivernale entraîne une homogénéisation des propriétés biogéochimiques sur la colonne d'eau, et une

stœchiométrie vers des valeurs estivales. Cette région bascule d'un régime d'eutrophie lors de la convection profonde vers un régime oligotrophe après le bloom de printemps. Lors du premier régime la production primaire est dominée par une production nouvelle en surface, alors que lors du deuxième régime la production phytoplanctonique de subsurface est essentiellement régénérée. Les masses d'eau adjacentes à la zone de convection et celles situées au sud sont caractérisées par une dominance de production régénérée toute l'année. Une partie de la matière organique particulaire est exportée en dessous de la couche épipélagique. Cet export de matière organique est variable et est fortement lié à la dynamique verticale des masses d'eau. **Mots clés :** Méditerranée, cycles saisonniers, cycles biogéochimiques, modélisation, régimes trophiques, stœchiométrie, bloom.

Abstract

The Mediterranean Sea is characterized by various trophic regimes due to river inputs, as well as heterogeneous nitrogen to phosphorus ratios and hydrodynamic processes, in particular vertical mixing. The objective of this thesis that was performed in the framework of the MISTRALS program is the study of the biogeochemical cycles of these various regimes that composed the Mediterranean. It is mainly based on the in situ observations collected during DeWEx project and on 3D physical/biogeochemical modeling at the scale of the entire basin and at the regional of the western sub-basin.

The first study is a ten-year basin scale study which allows an ecological classification, giving bioregions in function of their physical and biogeochemical properties. Southern oligotrophic areas in both eastern and western sub-basins are characterized by low efflorescence and deep nutriclines. While in the north, near Rhodes Island, in the southern Adriatic Sea and in the Liguro-Provencal sub-basin, the summer oligotrophic regime is altered annually by intense vertical dynamics, the deep convection. This process is considered as a driving force of the thermohaline circulation and entrains an enrichment of nutrients in surface layer which allows rapid and intense blooms in spring. The Mediterranean receives organic matter from the Atlantic Ocean, while, it is a source of inorganic matter for the Atlantic.

In a second part of this thesis, a high resolution model on the western sub-basin was embedded in the basin model to quantify the physical and biological processes that determine the temporal variability of the nutrient stocks and their stoichiometry. The north-western Mediterranean turns from an eutrophic regime during deep convection to an oligotrophic regime after the spring bloom. During the eutrophic regime new production dominates the primary production at the surface while during the

oligotrophic regime primary production is essentially associated to subsurface regenerated one. Adjacent water masses of the convection zone and west-southern regions are characterized by a dominance of regenerated production all over the year. **Key words:** Mediterranean Sea, seasonal cycles, biogeochemical cycles, modeling, trophic regimes, stoichiometry, bloom.

Table des matières

Table des matières 4
1 Introduction générale 8
1.1. La Méditerranée - Généralités 8
1.2. Objectifs de la thèse 10
1.3. Structure du manuscrit 12
2 CHAPITRE 1 : Description hydrodynamique 15
2.1. Description géographique des divers bassins 15
2.2. Structure verticale des masses d'eau 15
2.3. Circulation océanique en Méditerranée 16
2.4. La convection profonde 18
3 CHAPITRE 2 : Interaction entre dynamique et biogénèse 21
3.1. Les sels nutritifs 21
3.1.1 Les échanges des sels nutritifs 22
3.1.2 Impact du mélange sur les échanges verticaux de sels nutritifs 23
3.1.3 Enrichissement de surface par la convection profonde 24
3.2. La couche de mélange et le cycle de la chlorophylle 25
4 CHAPITRE 3 : Méthodologie 26
4.1. Etat de l'art sur la modélisation couplée physique biogéochimie en Mer Méditerranée 26
4.2. Les modèles couplés physique-biogéochimie 27
4.2.1 Les champs physiques 27
4.2.2 Le modèle biogéochimique (Eco3m-S) 28
4.2.3 Le couplage physique-biogéochimie 34
4.3. Les grilles de calcul 35
4.3.1 La grille à l'échelle du bassin méditerranéen 35

4.3.2 La grille du bassin occidental 35
1. Introduction 39
2. Methodology 40
2.1. The physical model 41
2.2. The biogeochemical model 41
2.3. Implementation on the Mediterranean basin 42
2.3.1. Biological boundary conditions 42
2.3.2. Initialization and spin up 43
3. Results and discussion 43
3.1. Evaluation of the model 44
3.1.1. Surface chlorophyll 44
3.1.2. Biogeochemical characteristics of water masses 47
3.2. Climatology 48
3.2.1 Mixed layer depth 48
3.2.2 Depth and magnitude of the Deep Chlorophyll Maximum (DCM) 50
3.2.3. Nutriclines 52
3.2.4. Net primary production (NPP) 54
3.2.5. Organic carbon export 56
3.3. Main pelagic ecological regimes of the Mediterranean Sea 58
3.3.1. Bloom like regime (group 1) 60
3.3.2. No-bloom regime of the western basin (group 3) 61
3.3.3. No-bloom regimes of the eastern basin (groups 4, 5, 6) 62
3.3.4. The Intermittent/Intermediate regime (group 2) 62
3.4. Nitrogen and phosphorus dynamics in the Mediterranean Sea 64
3.4.1. Biogeochemical processes 64
3.4.2. Fluxes at the straits 65
3.4.3. The global budget 65
4. Conclusion and perspectives 68
1. Introduction 75
2. Method 77
2.1. Observations 77
2.2. Modelling 78
2.2.1. Hydrodynamics 78
2.2.2. Biogeochemistry 79
2.2.3. Initial and boundary conditions 80
2.2.4. Derived variables 80

3. Results and discussion 80
3.1. Evaluation of the simulation 80
3.1.1. Surface chlorophyll 80
3.1.2. Horizontal and vertical biogeochemical patterns in winter and spring 81
3.1.3. Variability between April and September 2013 84
3.1.4. Annual cycle of the nutrients stocks 85
3.2. Atmospheric forcing and hydrology 86
3.3. Consequences of hydrological variability on biogeochemical processes and stoichiometry 87
3.3.1. Autumn 89
3.3.2. Winter 90
3.3.3. Spring 91
3.3.4. Summer 92
3.4. Budget of the nitrogen and phosphorus in the northwestern Mediterranean basin 93
4. Conclusion 95
Appendix – Model parameters 96
Table A.1: List of state variables 96
Appendix – State variables of the model 100
5. References 103
1. Introduction 110
2. Methods 112
2.1. The hydrodynamic model 112
2.2. The biogeochemical model 113
2.3. Areas of study 114
2.4. MODIS satellite dataset 114
2.5. Determination of the bloom onset 115
2.6. Calculation of the F-ratio 115
3. Model evaluation 115
4. Results and discussion 117
4.1. Atmospheric conditions 117
4.2. Vertical mixing and chlorophyll concentration 118
4.2.1. The Northern Gyre 118
4.2.2. The shallow convection area 120
4.2.3. The stratified region 120
4.3. Conditions at the onsets of the phytoplankton efflorescence 122
4.4. Primary production 124
4.5. Particulate organic carbon export 125

4.6 The trophic regimes 127
5. Conclusion 128
6. References 129
Bibliographie supplémentaire 134
5 Annexes 136
5.1 Annexe 1 : Déroulement de la thèse 136
5.2 Annexe 2 : Les bases de données et la calibration 139
2.1. Base de données Lavezza et al (2011) pour l'initialisation des sels nutritifs, et initialisation de l'oxygène 140
2.2. Le produit satellite MODIS 145
2.3. Les flotteurs BioArgo 149
2.4. Rappel de l'utilisation des bases de données pour la calibration et perfectionnement des modèles couplées 152
5.3 Annexes 3 : Les « groupes de travail (WP)» du chantier Méditerranéen MISTRALS et la modélisation 153
5.4 Annexes 4 : Paramètres du modèle biogéochimique 156

1 Introduction générale

1.1. La Méditerranée - Généralités

La Méditerranée s'est formée entre trois continents il y de cela 50 à 60 millions d'années entre le bloc africain et le bloc eurasien. La mer Méditerranée représente une des régions les plus riches au monde de par sa diversité naturelle et multiculturelle. La richesse de cette mer et de ses rivages est d'ordre géographique, historique, environnementale, géopolitique ou encore climatique. La société se pose désormais des questions pour se préparer aux changements menaçant l'équilibre de cette mer. Cela passe d'abord par savoir « comment fonctionne la Méditerranée ».

Dans ce registre très large, nous ne pouvons parler de la mer sans citer la terre, nous ne pouvons citer la terre sans parler du climat, nous ne pouvons parler du climat sans parler de notre civilisation qui est entièrement dépendante de la mer. On estime que l'Homme s'est installé sur les bords de la mer Méditerranée il y a de cela six à dix millénaires la mer Méditerranée était alors une barrière étendue jusqu'à l'horizon, une immensité énigmatique et obsédante. Aujourd'hui, elle est appréhendée comme une zone de profits, un parc marin et terrestre.

La Méditerranée est caractérisée par une forte insuffisance biologique. On parle de mer oligotrophe (Siokou-Frangou et al. 2010) Elle est quasiment dépourvue de plateaux continentaux essentiels à la prolifération d'espèces marines. Elle se serait vidée de ses ressources inorganiques trop exploitées, elle serait devenue très pauvre en plancton. Si la Méditerranée est pauvre en biomasse, sa biodiversité est finalement très importante.

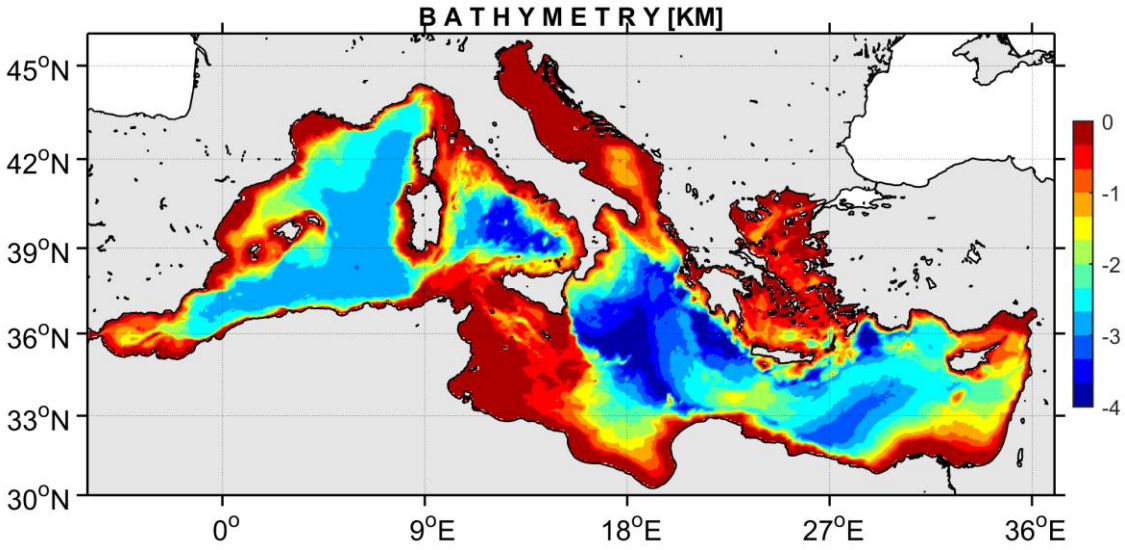

Figure 1.1: Bathymétrie en kilomètre de la Mer Méditerranée.

La Mer Méditerranée comporte des caractéristiques dynamiques et biologiques très variées que l'on retrouve dans le mécanisme global de l'océan mondial. Son étude permettrait donc la compréhension de phénomènes qui dépassent ses propres frontières.

Une question de saison

"Ce climat est unificateur des paysages et des genres de vie, construit par une double respiration, celle du Sahara au sud et celle de l'océan Atlantique à l'ouest" (F. Braudel, Le Méditerranée, « L'espace et l'histoire »)

Si je devais choisir un seul mot, pour sa signification scientifique (mais aussi philosophique et littéraire), qui qualifierait les rythmes de la physique, de la flore et de la faune méditerranéenne, ce serait "saisonnalité".

La Méditerranée oscille entre influence océanique et influence désertique qui s'imposent alternativement à un rythme saisonnier. « *Le désert s'efface quand intervient l'océan* », dès le mois d'octobre par son humidité liée à de grosses dépressions. Les vents les poussent vers l'orient jusqu'à changer la couleur de la surface de l'eau en bleu sombre ou en gris et recouvrir la mer d'écumes blanches. Pendant ces mois d'hiver les tempêtes sont impressionnantes, dévastatrices. Ces tempêtes permettent néanmoins d'enrichir les surfaces oligotrophes en matière nécessaire à la

prolifération des végétaux marins. Elles participent à l'équilibre thermique de la mer et sont aussi la source de phénomènes biologiques très importants : Les blooms phytoplanctoniques.

« *L'océan se retire quand souffle le désert* » à partir du mois de juin. L'air sec et brulant couvre l'étendue de la mer et en déborde largement ses limites vers le nord et l'ouest. Ce ciel d'été ne se voile que pour quelques jours lorsque soufflent des vents du sud chargés de sable qui ensemencent la surface d'un mélange de matière organique, inorganique et de métaux traces. Cette longue période est aussi appelée la saison oligotrophe car quasiment toute la surface de la mer est stable dynamiquement et dépourvue de sels nutritifs et de plancton végétal sur une large couche d'une centaine de mètres d'épaisseur.

Une forte sensibilité du et au climat

Cet équilibre saisonnier est en amont dépendant des variabilités climatiques. En effet, plusieurs études météorologiques ont montré que la Méditerranée est l'une des régions les plus sensibles aux variations climatiques (Giorgi et al. 2006 ; Somot et al. 2007 ; Herrmann et al. 2008). En 2007, Herrmann et al., grâce à la modélisation sur deux époques différentes, ont réalisé une première approche de l'étude du changement climatique sur les écosystèmes pélagiques. L'augmentation de la température de l'eau provoquerait une stratification plus forte et par conséquent une diminution de l'intensité des évènements de convection profonde, ce qui pourrait diminuer l'enrichissement des eaux de surface en sels nutritifs provoquant une diminution de l'efflorescence phytoplanctonique. Sachant que le phytoplancton est l'organisme à la base de la chaîne trophique, toute la chaîne serait donc face à d'importants bouleversements. Nous pouvons imaginer encore plus de modifications en prenant en compte également la diminution des débits des rivières et l'augmentation des effluents urbains qui toucheraient les écosystèmes par l'acidification de la mer.

1.2. Objectifs de la thèse

Les résultats scientifiques basés sur la modélisation régionale, obtenus dans les thèses de Marine Herrmann (2007) et Pierre-Amaël Auger (2011), ont mis l'accent sur la variabilité décennale et l'évolution à long terme de la biogéochimie des écosystèmes planctoniques du bassin nord occidental, en insistant sur l'impact des forçages atmosphériques et hydrologiques qui en découlent (Herrmann et al. 2008 ; 2009 ; 2013) et incluant des conséquences sur la biologie comme la répartition des groupes planctoniques et le découplage phytoplancton / zooplancton (Auger et al. 2011 ; 2014).

Mon travail de thèse s'inscrit dans la continuité de ces précédentes études. Il privilégie les échelles saisonnières, et se place également à plus large échelle spatiale considérant ainsi des régions au fonctionnement contrasté. Il est dédié à la compréhension du fonctionnement des premiers échelons trophiques en Méditerranée sous l'effet des forçages physiques. A l'échelle du bassin, la complexité vient du fait que le bassin est composé d'une mosaïque de régions aux fonctionnements contrastés (la prolifération des cellules végétales se répartit en fonction de l'éclairement solaire, de la disponibilité des éléments nutritifs et de la dynamique locale) mais qui peuvent interagir grâce au transit de la matière organique et inorganique. Une approche analytique est alors nécessaire pour comprendre comment la mosaïque est constituée, puis en analyser les principaux éléments à la lumière de ses relations avec ses voisins et de son hydrologie propre, puis de quantifier les différents processus physiques et biogéochimiques. Si de telles questions restent ouvertes, c'est en raison de la difficulté d'échantillonner des grandes zones à haute résolution spatiale et temporelle. La modélisation est donc un outil qui doit permettre de synthétiser les observations disponibles et d'aider à la quantification. C'est un des objectifs de cette thèse. Nous avons pour cela tenté de comprendre comment s'effectue l'enrichissement de la couche épipélagique, par quel mécanisme l'efflorescence gagne la couche superficielle, comment s'effectue la transition entre ces deux processus, tout ça dans différentes régions du bassin caractérisant les principaux régimes trophiques.

Dans un second temps, il apparaît que si cette démarche globale permet d'améliorer les connaissances sur le fonctionnement du bassin, ainsi que les modèles qui permettent de le représenter, de nombreuses zones d'ombre subsistent qui nécessitent d'aller plus en profondeur à l'intérieur des éléments de la mosaïque trophique. A ce titre, la communauté océanographique « biogéochimie » Méditerranéenne française regroupée dans le programme MerMeX (Marine ecosystem response in the Mediterranean Experiment) du méta programme MISTRALS consacré à l'étude pluridisciplinaire du bassin Méditerranéen a décidé de focaliser ses efforts sur une première zone qui joue un rôle majeur dans le bassin, la Méditerranée nord-occidentale. Cette zone est caractérisée par le processus physique de convection profonde qui impacte les écosystèmes marins par une remarquable efflorescence printanière. Un effort sans précédent dans la région a été entrepris pour échantillonner à la fois les paramètres physiques et biogéochimiques aux périodes clés de son cycle saisonnier. Les efforts de MerMex focalisés sur la biogéochimie et qui se sont traduits par la réalisation du projet DEWEX ont été complétés par un fort investissement du programme HyMeX (Hydrological Cycle in the Mediterranean Experiment) sur les processus physiques liés à la formation de l'eau dense. La modélisation est un volet majeur de cet effort, devant en assurer la synthèse en reconstruisant une vision spatio temporelle complète de l'hydrologie et de

la biogéochimie sur tout ce cycle saisonnier et en analysant les facteurs qui contrôlent le fonctionnement biogéochimique de la zone et finalement en dressant des bilans. L'équipe dans laquelle j'ai effectué ma thèse s'est fortement investie dans cette tâche et ma thèse en découle.

La première étape de cette modélisation a été tout d'abord de mettre au point une simulation aussi réaliste que possible de la physique et de la biogéochimie de la Méditerranée nord-occidentale pendant l'ensemble du cycle saisonnier échantillonné. La validation de la simulation à l'échelle saisonnière a donc pris une part importante en utilisant les observations qui étaient alors disponibles en particulier pendant les deux périodes clés que sont l'hiver avec la redistribution verticale des nutriments, et le printemps avec l'efflorescence. La simulation a ensuite été utilisée pour répondre à deux objectifs principaux. Le premier était de comprendre la dynamique des sels nutritifs dans la couche épipélagique. On a pour cela analysé comment les processus biologiques et physiques contrôlaient les stocks d'azote et de phosphore dans leur différentes formes et comment les rapports stœchiométriques étaient affectés. Un bilan de la couche épipélagique a ensuite été proposé. Le second objectif concernait la dynamique du phytoplancton. Nous avons tenté d'apporter des réponses aux questions qui concernent l'étendue de la zone enrichie en sels nutritifs et sa répercussion sur la distribution géographique de l'efflorescence printanière et étudié les conditions qui conduisent au déclenchement des blooms automnal et hivernal dans la zone convective. Nous avons ensuite comparé le fonctionnement de cette zone à celui de deux autres régions de Méditerranée occidentale caractérisées par un mélange hivernal plus faible. Le cycle saisonnier de la production primaire et de l'export de carbone organique particulaire a été également étudié dans ces différentes régions présentant des régimes trophiques différents.

1.3. Structure du manuscrit

Ce manuscrit de thèse est constitué comme suit :

Le chapitre 1 décrit la Méditerranée d'un point de vue hydrodynamique. On verra une description simplifiée des différentes masses d'eau que l'on trouve en Méditerranée et les circulations qui leur sont associées. Une courte description du processus de formation des eaux profondes, la convection, sera donnée.

Le chapitre 2 présente les relations entre les matériaux biogènes et la dynamique, en particulier les processus de mélange. Une approche des divers compartiments de la production primaire, des sels nutritifs à la chlorophylle sera discutée.

Au chapitre 3 la méthodologie utilisée dans ce travail sera développée. Cela couvre, d'une part, les aspects de la description des écosystèmes par biorégionalisation et d'autre part l'approche par la modélisation couplée hydrodynamique/biogéochimie.

Enfin les trois chapitres suivants sont constitués de projets d'articles.

1. **Le premier article** concerne la modélisation biogéochimique de l'ensemble du bassin méditerranéen, à l'aide du forçage physique NEMOMED12-Free (Hamon et al. In press) et du modèle biogéochimique Eco3m-S (Auger et al. 2014). Cette étude a bénéficié d'une collaboration entre les partenaires du projet SIMED impliqués sur la modélisation hydrodynamique du bassin (Mercator-Océan – CNRM) et le Laboratoire d'Aérologie. L'objet de cette publication est de constituer un groupement écologique des eaux pélagiques, en se basant sur une technique statistique utilisant les climatologies mensuelles des paramètres biologiques calculées à partir d'une simulation de 14 ans. Le but est d'expliquer les propriétés qui caractérisent les principaux groupes de biorégions du bassin dans un cadre de couplage dynamique, biogéochimique et biologique. Cet article a comme objectif final, l'exposition d'un bilan décennal du cycle de l'azote et du phosphore afin de mettre en évidence les flux des sels nutritifs et de la matière organique, la quantification des échanges avec l'océan Atlantique, ainsi que la quantification des processus biologiques qui interviennent dans la transformation de la matière biogène dans la couche supérieure et profonde des deux sous-bassins de la mer Méditerranée.

2. **Le deuxième article** fera partie du numéro spécial consacré à la formation de l'eau dense et à ses conséquences sur les cycles biogéochimiques. Il est consacré à l'étude de la modélisation du cycle saisonnier de l'azote et du phosphore dans le bassin occidental de la Méditerranée. La modélisation est réalisée à partir d'un couplage physique à l'aide du modèle SYMPHONIE (Estournel et al. 2005 ; Marsaleix et al. 2009 ; 2012) et biogéochimie avec le modèle Eco3m-S à très haute résolution (1 km). L'objectif est de reproduire le cycle des sels nutritifs pendant une année, entre l'automne 2012 et l'automne 2013. Les données issues des campagnes DeWEx 1 et 2 et MOOSE 2013 sont utilisées pour comparer et valider minutieusement le modèle en hiver, au printemps et en été 2013. Des diagnostiques sur le cycle saisonnier des processus biologiques, qui concernent le cycle de l'azote et du phosphore et sur la stœchiométrie, sont présentés dans la zone concernée par la convection profonde en Méditerranée nord-occidentale (Golfe du Lion). Cet article se termine par un bilan annuel des flux physiques et biogéochimiques d'azote et de phosphore dans la couche de surface.

3. **Le troisième article,** seconde contribution au volume spécial évoqué plus haut, a pour objectif la caractérisation spatio-temporelle du phytoplancton et l'étude du cycle saisonnier de la production primaire et l'export de carbone organique particulaire dans le bassin occidental méditerranéen. Il s'appuie sur la modélisation couplée physique-biogéochimie (SYMPHONIE-ECO3m-S) régionale validée dans le précédent article. Après une comparaison aux images couleur de l'eau MODIS, l'article se poursuit avec une analyse de la chlorophylle (i) dans la région de convection profonde, (ii) dans la région périphérique caractérisée par une convection peu profonde, et (iii) dans une région caractérisée par un faible mélange hivernal, composée en grande partie du bassin algérien. Une analyse des conditions atmosphériques à la surface de la mer, hydrodynamiques et biogéochimique lors du déclenchement des efflorescences phytoplanctoniques est ensuite proposée. Le cycle saisonnier de la production primaire et du flux du carbone organique particulaire influencé par la dynamique verticale d'une part et par les proliférations planctoniques d'une autre part est présenté dans les trois régions étudiées. Finalement, l'article propose une qualification des régimes trophiques régnant dans le bassin occidental.

Enfin, une conclusion à ce travail et des perspectives seront présentées à la fin du document.

La bibliographie des projets d'articles sera regroupée à la fin du document.

Nous proposons en annexes les détails des paramètres du modèle biogéochimique et une partie qui présentera l'historique de la modélisation en Méditerranée, suivie d'une description qui traitera alors de la calibration du système de modélisation mis en œuvre. Cette calibration sera présentée en parallèle des bases de données utilisées lors de cette étape primordiale dans mon travail de thèse.

2 CHAPITRE 1 : Description hydrodynamique

Avant de discuter dans la suite du manuscrit de la modélisation des systèmes de production biogéochimique présents en Méditerranée, il convient de faire une description des divers composants nécessaire à la compréhension des résultats que nous présenterons dans les articles en fin de ce document. Dans un premier temps on décrira les divers bassins qui constituent la Méditerranée. Ensuite, nous verrons une description de la structure verticale des masses d'eau ainsi que la circulation qui leur est associée. Enfin, nous présenterons un processus déterminant dans le maintien de la circulation générale de la Méditerranée : la convection profonde.

2.1. Description géographique des divers bassins

La mer Méditerranée se répartit en plusieurs sous bassins. Ce découpage naturel géographique a été géostratégique pour les anciens peuples. La répartition s'est organisée autour d'un grand nombre d'îles et de détroits. La figure 1.1 présente les différents bassins et détroits en Méditerranée. Les deux détroits les plus connus sont le détroit de Gibraltar qui représente la porte entre la Méditerranée et l'océan Atlantique, et le détroit de Sicile qui sépare les deux bassins occidental et oriental. Tout d'abord le bassin occidental est constitué, du bassin nord (comprenant la Ligurie (LIG), lles mer des Baléares, le bassin Provençal et le Golfe du Lion), au sud, le bassin Algérien et la mer d'Alboran et à l'est, la très accidentée mer Tyrrhénienne et le sous-bassin de Sicile. Dans le bassin oriental, on trouve la seconde partie du sous-bassin de Sicile ainsi que les deux grands bassins Ionien et Levantin. Au nord du bassin Levantin, l'arc égéen sépare le bassin Levantin de la mer Égée. Dans la mer Egée, le détroit des Dardanelles sépare la Méditerranée et la Mer Noire. A la limite entre le bassin nord Ionien et nord Levantin, on trouve la fosse la plus profonde de Méditerranée (4600 m de profondeur) au large du Cap Matapan. Enfin le détroit d'Otrante sépare le bassin Ionien de la mer Adriatique.

2.2. Structure verticale des masses d'eau

Le schéma (Fig. 2.1) montre la répartition des masses d'eaux principales qui composent la Méditerranée et leurs propriétés hydrologiques moyennes. Dans l'ensemble de sa partie pélagique, cette mer est constituée de trois couches distinctes. La couche supérieure est très sensible et constamment exposée aux forçages atmosphériques. Cette couche contient une sous-couche dans laquelle la densité est homogène, c'est la couche de mélange. En l'occurrence, nous considérons tout au long de ce manuscrit la couche de mélange comme la couche dans laquelle l'écart de la

masse volumique, à partir de 10 m de profondeur, est inférieur ou égale à 0.01 kg.m^{-3}. Au-dessus de cette couche on trouve la très fine couche de surface qui est très sensible en termes de réchauffement ou refroidissement temporaire. Au-dessous de la couche de mélange on trouve les pycnoclines saisonnière et principale. La pycnocline saisonnière est présente seulement durant la saison estivale. Elle disparaît sous l'action des forçages atmosphériques dans la période hivernale.

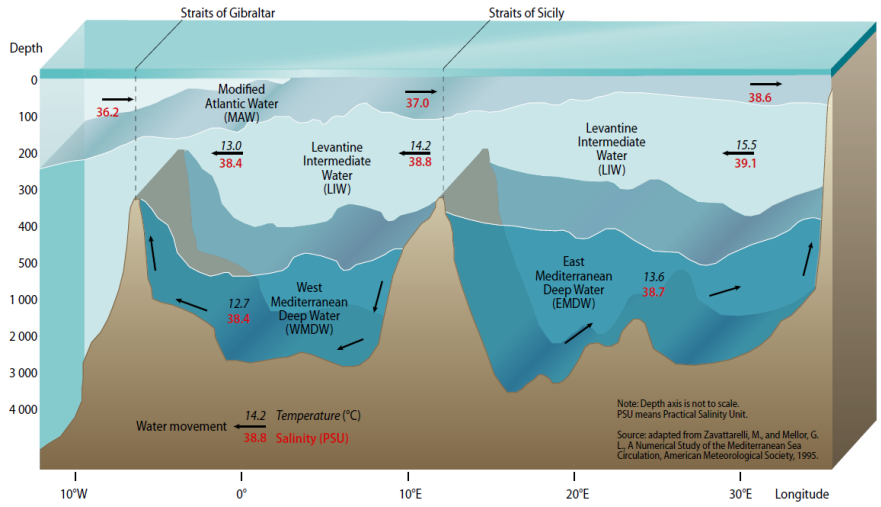

Figure 2.1: Schéma simplifié de la circulation en 3 couches de la Méditerranée, le long d'une radiale du détroit de Gibraltar, à la mer Levantine. Adapté de Zavattarelli et Mellor (1995).

Dans la couche supérieure circule l'eau d'origine Atlantique, nommée Modified Atlantic Water (MAW). La seconde couche correspond à la Levantine Intermediate Water (LIW), originaire de l'activité convective intermédiaire dans le bassin Levantin. Cette masse d'eau est salée et chaude. Le bassin Levantin subissant une forte évaporation est en effet caractérisé par la salinité la plus élevée de toute la Méditerranée. La couche intermédiaire du bassin occidental est constituée de toutes les eaux formées dans le bassin Levantin, Crétois et Egéen qui se mélangent au détroit de Sicile lors du passage vers le bassin occidental. Millot (2013) suggère d'appeler cette masse d'eau Eastern Intermediate Water (EIW). Enfin, on trouve une couche profonde plus dense (masse volumique > 1029 kg.m^{-3}), à l'est constituée suivant les périodes, d'eau formée dans l'Adriatique Sud ou de la Cretan Deep Water (CDW), originaire du bassin Crétois, et à l'ouest constituée de la Western Mediterranean Deep Water (WMDW) originaire du nord-ouest du bassin Provençal.

2.3. Circulation océanique en Méditerranée

De nombreux articles (en particulier ceux de Millot et al. 1997 ; Millot, 1999 ; 2005 ; 2013) décrivent la circulation générale en se basant sur la télédétection infrarouge et sur des mesures in situ en particulier à l'aide des CTD de différentes campagnes. Depuis une quinzaine d'années, les plateformes autonomes apportent des informations pertinentes quant à la dynamique à très fine échelle (Testor et al. 2006), notamment en ce qui concerne la structure des tourbillons méditerranéens. Leurs sources, leurs diamètres et leurs durées de vie sont variables et on pense

qu’ils constituent un vecteur de chaleur et de matière entre des zones mésotrophes et oligotrophes. D’autres auteurs se sont intéressés au transport des masses d’eau (Schroeder et al. 2010) après avoir sillonné la mer Méditerranée pour, par exemple, quantifier les flux aux principaux détroits.

Les principaux résultats de leurs travaux sont les suivants :

- La mer Méditerranée présente une évaporation importante qui excède l’eau apportée par la pluie et les apports de rivières. Elle présente donc un bilan évaporation/précipitation négatif de l’ordre de [0.5 – 1 m/an] (Ribera D’Alcalà et al. 2003). La perte d’eau est compensée par un apport de l’Océan Atlantique à travers le détroit de Gibraltar. Ce flux d’eau de surface entrant (AW pour Atlantic Water) est de l’ordre de [0.5 à 1 Sv, (1 Sv=1e6 m3/s)]. Cette eau est moins salée que l’eau de la Méditerranée. Elle est moins dense et circule par conséquent en surface, le long des côtes ou à l'aplomb des talus continentaux en circulation cyclonique (Figure 2.2a) dans les deux bassins (oriental et occidental).

- Pendant l’hiver, la Méditerranée connait des pertes de chaleurs intenses induites par les forts vents froids et secs venant du nord et causant la formation d’eau profonde et intermédiaire dans les deux bassins. En mer Levantine, la densification de l’eau de surface, provoque son approfondissement et création de l’eau intermédiaire levantine (LIW). Cette masse d'eau ainsi formée, circule dans le sens antihoraire (Figure 2.2b) à mi- profondeur longeant les côtes de la Grèce à l'Italie. Passé le détroit de Sicile, elle remonte alors vers le golfe de Gènes en se divisant de part et d'autre de la Sardaigne et la Corse. Elle poursuit sa course sous le courant Nord Méditerranéen pour finalement longer l'Espagne et sortir (en partie) de la Méditerranée via le détroit de Gibraltar. Une portion de cette eau recircule le long des côtes du Maghreb en direction du détroit de Sicile. Quand les flux air/mer sont très intenses, la densification de la AW est forte et provoque une formation d’eau profonde. Ce type de convection est observé en mer Egée, dans le Gyre de Rhodes, au sud de la mer Adriatique et dans le Golfe du Lion. Comme dans l'Océan global, cette formation d’eau profonde est le moteur essentiel de la circulation thermohaline. Ces eaux, les WMDW et EMDW (Fig. 2.2) circulent alors dans leur bassin respectif suivant à nouveau une circulation antihoraire (Fig 2.2c).

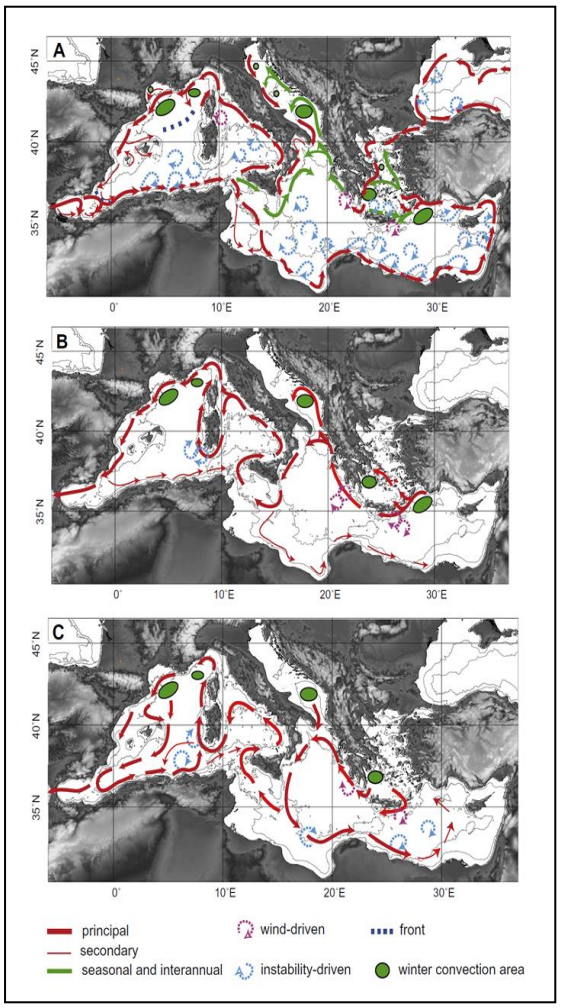

Figure 2.2: Schéma de la circulation sur trois couches (a- surface, b- intermédiaire, c-profonde). Tirée du (Durrieu de Madron et al., 2011).

- Le détroit de Sicile (400 m de profondeur seulement) se situant au centre du bassin, représente la porte d'échange entre les deux bassins oriental et occidental.

- La circulation thermohaline transporte les éléments biogéochimiques entre les sous-bassins méditerranéens. Cette circulation, associée aux transports verticaux qui l'alimentent, contrôle le développement du plancton qui donne une répartition spécifique des niveaux trophiques.

2.4. La convection profonde

L'équilibre qui régit la stratification de l'océan est détruit par les flux entre l'océan et l'atmosphère lors des évènements de convection profonde. Ces événements se produisent dans quelques régions particulières dans le monde. La mer Méditerranée connaît ce processus extrême quasiment chaque année dans quatre régions, trois situées à l'est et une située à l'ouest. Le processus le plus intense se situe dans le Golfe du Lion autour du point (42 °N; 5 °E), certaines années la convection peut s'étendre jusqu'au bassin Ligure (Damien, 2015).

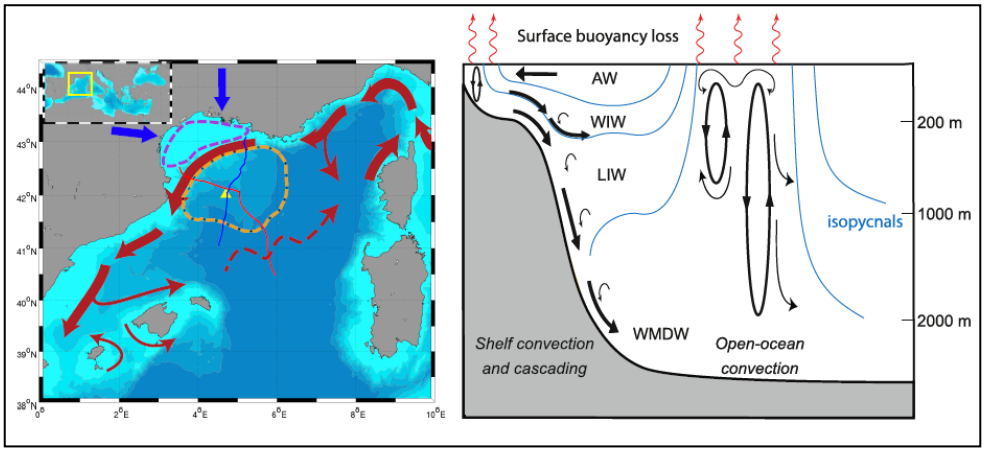

Figure 2.3: Schéma de la convection profonde en Méditerranée nord occidental.

Tiré de Durrieux et Madron et al. (2013) et de Puig et al. (2013).

La figure 2.3 (partie gauche), extraite de Puig et al. (2013a), schématise la circulation cyclonique dominante (flèches rouges) dans le sous-bassin nord occidental. La recirculation au sud du gyre représentée par des tirés rouges est très instable et limitée à la couche de surface. Elle est reliée à la position et à l'orientation du front des Baléares et sépare le gyre nord des eaux du sud (Millot, 1999 ; Testor et Gascard, 2006). La position géographique centrale de la convection profonde est montrée en traits orange. Le schéma de droite, résume le mouvement des masses d'eau liées à un événement de convection profonde.

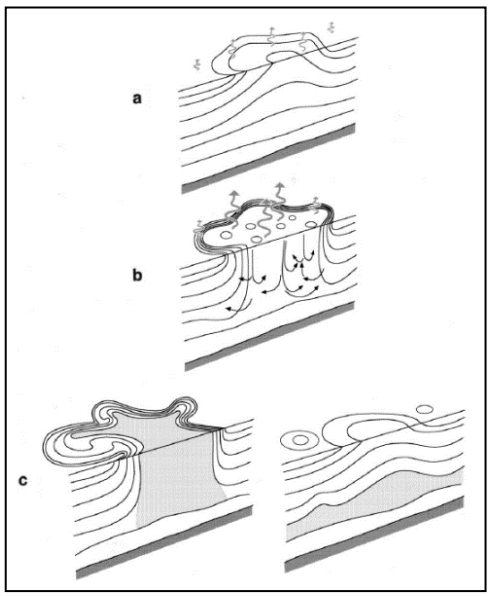

Figure 2.4: Mécanisme de la convection profonde suivant trois étapes : a. Préconditionnement. b. Mélange intense. c. Dispersion des eaux nouvellement formées. Tiré de Marshall et Schott (1999).

Le mécanisme de la convection profonde se fait en trois étapes. La première étape est le préconditionnement qui commence suite aux premiers coups de vent d'automne. Lié à la circulation cyclonique forcée par le vent, il se manifeste par un doming des isopycnes qui réduit l'épaisseur de la couche légère en surface favorisant la dé-stratification de la couche d'eau superficielle. Durant l'hiver, la perte de chaleur intense (causée principalement par la forte évaporation) suite à une série de coups de vents du nord) déclenche le mécanisme de convection profonde à l'intérieur du gyre cyclonique nord. Les mouvements convectifs se font dans de petites cellules appelées panache (ou plume) (Fig. 2.4b) (Voorgis et Webb, 1970 ; Schott et Leaman, 1991 ; Schott et al. 1996) dont la vitesse verticale descendante est de l'ordre de 10cm/s. La zone où se forment ces structures convectives s'étend éventuellement sur des dizaines de kilomètres. Les plumes convectives finissent par se rejoindre et créer un large patch d'eau dense. L'étendue de la zone de convection et son intensité en mélange dépendent des forçages atmosphériques (Herrmann et al., 2010). Lorsque le vent s'arrête, la dispersion des eaux denses et la stratification des eaux de surface commencent. En profondeur, l'eau nouvellement formée se disperse vers les zones adjacentes en partie par des tourbillons. Des instabilités naissent en périphérie du patch de convection. L'eau plus légère, transportée par des courants à moyenne échelle, vient recouvrir la zone mélangée.

L’impact de la convection profonde sur la distribution des éléments nutritifs et l’oxygène est difficilement observé et modélisé. Nous savons que la convection profonde joue un rôle dans la distribution de ces éléments. Étant donné que les concentrations des éléments biogènes ne sont pas uniformes sur la colonne d’eau, due à la présence d’un gradient fort en subsurface séparant les eaux enrichies des eaux appauvries, le mélange profond les rend accessibles pour la consommation en surface.

3 CHAPITRE 2 : Interaction entre dynamique et biogénèse

Dans un contexte pauvre en sels nutritifs, la biologie de la Méditerranée dépend des apports extérieurs et de la stimulation des processus liés à la formation et à la mise en mouvement des masses d'eaux de sub-surface (Yilmaz et Tugrul, 1998 ; Santinelli et al. 2012 ; Gacic et al. 2012 ; Estrada et al. 2014 ; Séverin et al. 2014 ; DeFommervault et al. 2015), favorisant un enrichissement planctonique en surface (Bethoux, 1989 ; Levy et al. 1999 ; Marty et Chiaverini, 2002 ; D'Ortenzio et Ribera d'Alcalà, 2009). Dans cette partie, nous caractériserons les sels nutritifs en Méditerranée ainsi que l'impact de la convection profonde sur leur répartition. Enfin, nous présenterons l'évolution de la chlorophylle dans la couche de subsurface, ce qui permettra d'identifier les conditions qui seront les plus favorables aux effllorescences lors des évènements que nous modéliserons.

3.1. Les sels nutritifs

Les sels nutritifs tels que le nitrate, le phosphate et le silicate sont distribués suivant un gradient vertical marqué, qui sépare les eaux de surface pauvres en nutriments des eaux de fond. L'ammonium, excrété par les hététrophes se trouve uniquement dans les eaux de surface. Cette distribution verticale des sels nutritifs majeurs s'explique en partie par les processus biogéochimiques. Les eaux de surface sont appauvries en sels nutritifs, consommés par le phytoplancton. Les eaux de fond, à l'inverse, sont riches en nutriments et les masses d'eau intermédiaires présentent souvent des valeurs de concentration en sels nutritifs légèrement plus fortes que les eaux de fond, du fait de la reminéralisation préférentielle de la matière organique par les bactéries dans cette couche.

Parallèlement au gradient vertical des concentrations en sels nutritifs, la mer Méditerranée présente des zones oligotrophes, c'est à dire pauvres en nutriments, avec un gradient marqué de l'ouest vers l'est. Les deux bassins occidental et oriental fonctionnent différemment : les concentrations en sels nutritifs dans les eaux intermédiaires et profondes du bassin occidental sont plus fortes que celles des eaux du bassin oriental. Le taux de production primaire, le positionnement vertical des processus biogéochimiques ainsi que leur intensité sont par conséquent différents.

L'étude de la stœchiométrie, en particulier l'étude du ratio stœchiométrique N/P (azote/phosphore) qui représente le rapport de la concentration en nitrate par la concentration en phosphate, est une discipline à part entière en Mer Méditerranée. La mer Méditerranée fonctionne différemment de l'océan global. Les rapports N/P dans les eaux profondes de l'Océan global sont de l'ordre 16:1

(rapport de Redfield). L'utilisation des sels nutritifs par les organismes marins est responsable de ce rapport (Copin-Montegut et Copin-Montegut, 1983). En mer Méditerranée, ce rapport n'est pas le même, il est beaucoup plus fort, estimé en moyenne à N/P = 24:1 (Béthoux et al. 2005). De plus, il présente un gradient horizontal marqué d'ouest en est. A l'ouest, la LIW et la WMDW présentent un rapport de 22:1 (Copin-Montegut, 1986) tandis qu'à l'est, le rapport atteint 27±3:1 en dessous de 200 m de profondeur dans le bassin Levantin et près de 30:1 en surface. Ce rapport est généralement plus élevé au-dessus de la nitracline. Ce fait s'explique par une préférence de consommation du phosphate par rapport au nitrate par les phytoplanctons (Raimbault et Coste, 1990). Ces ratios confirment que la Méditerranée est limitée en phosphate, en particulier dans le bassin est.

3.1.1 Les échanges des sels nutritifs

La variabilité spatiale et temporelle des sels nutritifs est par ailleurs liée aux différentes sources d'apport de sels nutritifs.

La mer Méditerranée représente une source nutritive pour l'Océan Atlantique (Ribera d'Alcalà et al. 2003). En effet, les eaux intermédiaires et une partie des eaux profondes de la mer Méditerranée, riches en sels nutritifs, sortent du bassin, grâce à la circulation thermohaline par le détroit de Gibraltar à hauteur de 1 ± 0.04 Sv. A l'inverse, la masse d'eau au-dessus de la thermocline est quasi-dépourvue de nutriments sur une très longue période de l'année (entre mars et décembre) sur l'ensemble de la mer Méditerranée pélagique. Au niveau du détroit de Gibraltar, ce sont les eaux de l'Océan Atlantique qui entrent en surface dans la Mer Méditerranée. Les sels nutritifs entrant ainsi par le détroit de Gibraltar sont rapidement consommés en mer d'Alboran et le long de la côte algérienne (Crise et al. 1999). L'eau de surface se disperse ensuite vers le nord et vers le bassin oriental très appauvri en nutriments.

Outre l'apport de nutriments en surface depuis le détroit de Gibraltar, d'autres sources potentielles de sels nutritifs ont été déterminées : les apports terrigènes par les fleuves et par les dépôts atmosphériques (Markaki et al. 2010 ; Coste et al. 1998). Les apports de nutriments des fleuves créent en général une forte productivité observée par images satellites par exemple à l'embouchure du Pô en Adriatique (Polimene et al., 2006). Les apports les plus importants sont fournis par le Rhône (débit moyen Qm= 1721 $m^3.s^{-1}$) dans le Golfe du Lion, l'Ebre (Qm= 416 $m^3.s^{-1}$) dans la mer des Baléares, l'Adige (Qm= 200 $m^3.s^{-1}$) et le Pô (Qm= 1569 $m^3.s^{-1}$) dans l'Adriatique, le Tevere (Qm= 216 $m^3.s^{-1}$) dans la mer Tyrrhénienne. Ludwig et al. (2010) montrent que la variabilité des débits des rivières est très forte, entraînant une variation importante des apports en sels nutritifs, en particulier

pour les apports en nitrate. Depuis les années 1980 et suite à la réduction imposée des phosphates dans les lessives sur la rive nord, les apports en phosphate à la mer par les fleuves ont beaucoup diminué conduisant probablement à un déséquilibre supplémentaire de la stœchiométrie du bassin.

Les apports atmosphériques pourraient également expliquer les rapports N:P élevés. D'après (Krom et al. 2004), les dépôts atmosphériques se composent de 60% d'azote et 30% de phosphore dans le bassin oriental Méditerranéen. D'un point de vue général, les apports atmosphériques jouent un rôle dans la fertilité des eaux de surface (Migon et al. 2002). Cet impact sur la fertilité est plus important en été pendant la période oligotrophe. Guerzoni et al (1999) montrent que l'impact des dépôts de la matière inorganique atmosphérique est plus important lorsqu'on s'éloigne des côtes vers le large, région moins variable et oligotrophe, loin des apports par les rivières et des zones dynamiquement actives par les processus d'upwelling et par la dynamique frontale.

3.1.2 Impact du mélange sur les échanges verticaux de sels nutritifs

Les périodes automnale et hivernale

La mer Méditerranée enregistre chaque année des évènements de vents impressionnants. Tout d'abord en automne, les premiers coups de vent ont une conséquence importante sur les écosystèmes planctoniques. Le vent mélange les eaux de subsurface. Les nutriments mis à disposition induisent des efflorescences automnales dans le bassin nord occidental et nord oriental. Le vent engendre un préconditionnement pour la convection profonde de la zone du Gyre Nord (GN) et celle du Gyre de Rhodes pour la convection profonde.

L'impact des forçages atmosphériques sur la mer est présenté sous forme de série temporelle du flux de l'énergie à l'interface air/mer (Fig. 2.1). Il s'agit du calcul du bilan radiatif. C'est l'énergie perdue par la mer (Qnet, $W.m^{-2}$) sous l'influence des masses d'air hivernales froides et sèches. Le bilan radiatif calculé est obtenu à partir des paramètres obtenus du La mer Méditerranée enregistre chaque année des événements de vents intenses. Tout d'abord en automne, les premiers coups de vent ont une conséquence importante sur les écosystèmes planctoniques. Le vent mélange les eaux de subsurface. Les nutriments mis à disposition induisent des efflorescences automnales dans tout le bassin.

La convection hivernale en Méditerranée nord occidentale représente la source la plus importante de sels nutritifs. Elle a été estimée pour l'hiver 2011 par Séverin et al (2014) à $1.3\ 10^{13}$ moles de NO_3+NO_2. L'enrichissement lors de la convection profonde a été mesuré à 8.9 µM de nitrate, de 0.4

µM de phosphate et de 7.7 µM de silicate en surface au centre du gyre nord en Méditerranée NW. Par ailleurs, Defommervault et al (2015) estiment que la concentration de surface résultant de la convection dépend de l'intensité de cette convection. Ils ont par conséquent estimé des valeurs de concentrations de nitrate et de phosphate en fonction de la MLD. Comme exemple, la concentration serait, pour respectivement le nitrate et le phosphate, de 6.93 et 0.28 µM pour une MLD de 110 m et de 7.78 et 0.37 µM à 1000 m dans le sous-bassin Ligure en Méditerranée nord-occidentale.

Dans les régions où la convection ne se produit pas, l'hiver voit principalement un épaississement de la couche de mélange qui en perçant les nutriclines se traduisent par des remontées de sels nutritifs limitées. Il semble cependant qu'au contraire des zones de convection où les sels nutritifs s'accumulent, ces nutriments soient rapidement consommés.

Les périodes printanière et estivale

La période de fin d'hiver début de printemps est une période clé pour la zone de convection de la Méditerranée nord-occidentale. C'est à ce moment-là que les sels nutritifs sont consommés. Les conditions de déclenchement du bloom sont encore controversées. Les images satellites ont montré que l'efflorescence phytoplanctonique en surface varie également d'une année à l'autre. Elle était par exemple intense en 2012 et en 2013, années de forte convection, et faible et courte en 2014, année caractérisée par un hiver chaud.

A partir du mois de mai, les flux de chaleur à la surface de la mer deviennent positifs. Cette dernière est réchauffée par la température de l'air. La température de surface passe de 13 °C à plus de 24 °C en été. Le mélange induit par le vent est réduit à de courtes périodes. En surface, les images des satellites ne détectent pas beaucoup d'activités mis à part aux embouchures de rivières. On observe une sorte « d'estivation » du plancton. C'est en subsurface que le maximum de chlorophylle (DCM) vient en fait se positionner. L'étude récentes de Lavigne et al (2015) ont bien résumé l'hétérogénéité de leur répartition géographique.

3.1.3 Enrichissement de surface par la convection profonde

La convection profonde en Méditerranée nord occidentale représente la source la plus importante en les nutritifs, estimé par Séverin et al (2014) à $1.3\ 10^{13}$ mole de NO_3+NO_2. L'enrichissement lors de la convection profonde a été mesuré à 8.9 µM de nitrate, de 0.4 µM de phosphate et de 7.7 µM de silicate en surface au centre du gyre nord en Méditerranée NW.

Defommervault et al (2015) estiment que la concentration de surface résultante de la convection

profonde dépend de l'intensité de la convection. Ils ont par conséquent estimé des valeurs de concentrations de nitrate et de phosphate en fonction de la MLD. Comme exemple, la concentration serait, pour respectivement le nitrate et le phosphate, de 6.93 et 0.28 µM pour une MLD de 110 m et de 7.78 et 0.37 µM à 1000m dans le sous-bassin ligure en Med NW.

3.2. La couche de mélange et le cycle de la chlorophylle

La chlorophylle en surface ou en subsurface est distribuée d'une manière hétérogène en mer Méditerranée. Cette distribution obéit à différents facteurs abiotiques (mélange vertical, lumière, température, disponibilité de nutriments…) et à des facteurs biotiques (prédation par le zooplancton, compétition interne et externe avec les bactéries). La variabilité de la couche de mélange, associée à l'exposition des cellules à la lumière et à l'enrichissement en sels nutritifs sont des paramètres clés pour les cycles des éléments nutritifs et la dynamique de la production planctonique. Ces paramètres sont donc également probablement les clés de la délimitation des biorégions en mer Méditerranée. C'est ce qu'a expliqué Lavigne (2014) dans son manuscrit de thèse après avoir repris une base de données historiques en se focalisant sur la biorégionalisation précédemment établie par D'Ortenzio et Ribera d'Alcalà (2009). Elle montre que le régime « no-bloom », est caractérisé par une efflorescence hivernale dès le mois de novembre, qui croît avec le mélange hivernal ; celui-ci enrichit la couche de surface en sels nutritifs et n'entraine pas de limitation par la lumière : c'est la théorie de "Entrainment Bloom" d'après Cullen et al. (2002). Au contraire, les régimes de bloom sont caractérisés par une décroissance phytoplanctonique pendant l'hiver ; dans ces régimes qui se situent dans les zones de convection, le mélange profond transporte les cellules végétales hors de la zone euphotique ce qui ralentit le processus de photosynthèse à cause de la limitation de la lumière : c'est la théorie "Detrainement Bloom" d'après Cullen et al (2002).

4 CHAPITRE 3 : Méthodologie

4.1. Etat de l'art sur la modélisation couplée physique biogéochimie en Mer Méditerranée

La variabilité spatiale et temporelle de la Méditerranée ainsi que la complexité des processus biologiques et des interactions entre la dynamique et la biogéochimie nécessitent le recours à la modélisation couplée dans un plan tridimensionnel afin de pouvoir en définir au mieux les contours et de mettre en évidence les subtilités de ce système du point de vue de la biogéochimie.

Les premiers modèles à avoir pris en compte ces aspects de couplage hydrodynamique-biogéochimie ont eu une approche unidimensionnelle représentant la dynamique d'une colonne d'eau, généralement représentative d'un sous-bassin. L'exemple le plus connu est celui de la station DYFAMED (43.5°N ; 7.25°E), au large de la côte niçoise. La présence d'une station de mesures hydrométéorologique donnant les propriétés dynamique et hydrologique, ainsi que d'une station de prélèvements biologiques et biogéochimiques, a abouti à une expertise sur les propriétés planctoniques de la colonne d'eau. Toutes ces observations ont permis la mise en place et la validation de modèles. L'application de modèle 1D sur cette station est aussi liée au fait que cette dernière se trouve dans un environnement dit « pélagique », faiblement influencée par le courant nord et suffisamment à l'intérieur du gyre nord pour que l'advection horizontale y soit considérée faible.

Les premiers modèles couplés 3D physique-biogéochimie pour le bassin méditerranéen ont été proposés par Crispi et al. (1998) et Crise et al. (1999). Ces derniers ont mis en évidence notamment la distribution hétérogène de la nitracline sur l'ensemble du bassin méditerranéen. Plus récemment Lazzari et al (2012) ont présenté une biorégionalisation du bassin en identifiant plusieurs régimes trophiques. Ils ont montré l'importance des processus physiques sur la dynamique phytoplanctonique dans les différentes biorégions. D'autre part, Macias et al. (2014) ont mis en lumière l'importance des processus biogéochimiques en subsurface, les structures de maximum de chlorophylle profond étant présent dans 73% des régions profondes du bassin. D'après ces auteurs, 62% de la production primaire annuelle aurait lieu dans ces structures.

D'autre part, plusieurs études (Tusseau et al. 1997 ; Lacroix and Nival, 1998 ; Lacroix and Grégoire, 2002) ont montré l'importance de la boucle microbienne pour une représentation correcte de la production primaire régénérée dont le rôle est prépondérant pendant la période stratifiée.

A l'échelle régionale, la modélisation tridimensionnelle centrée sur le Golfe du Lion a montré l'impact de la circulation induite par le vent, notamment des épisodes de convection sur la production primaire. Les travaux de Levy et al. (1998, 2000, 2001), ont relié la variabilité des caractéristiques biogéochimiques à la circulation océanique et aux variabilités spatiales de l'hydrodynamique à mésoéchelle. Herrmann et al (2013) et Auger et al (2014) ont étudié la variabilité interannuelle du développement des organismes planctoniques en réponse à celle des forçages atmosphériques et hydrodynamiques. Campbell et al (2013) ont montré l'impact d'un tourbillon dans le Golfe du Lion sur la production primaire en surface. Enfin, les travaux d'Auger et al (2011) et Fraysse et al (2013) ont montré que dans le Golfe du Lion, les eaux du Rhône jouent un rôle prépondérant dans la variabilité des écosystèmes.

4.2. Les modèles couplés physique-biogéochimie

Notre étude a reposé sur deux modèles couplés physique-biogéochimie régionaux : NEMO-Eco3m-S et SYMPHONIE-Eco3m-S. Les champs physiques puis le modèle biogéochimique sont présentés dans les deux sous chapitres suivants

4.2.1 Les champs physiques

Les champs physiques utilisés pour forcer en "mode offline" (soit la lecture en temps différé des champs physiques archivés dans des fichiers) la modélisation biogéochimique ont été calculés d'une part avec SYMPHONIE (modélisation à l'échelle du bassin occidental) et d'autre part avec NEMO (modélisation à l'échelle du bassin méditerranéen). Le modèle SYMPHONIE est développé par le laboratoire d'Aérologie et le modèle NEMO par le consortium européen du même nom (http://www.nemo-ocean.eu/). Ces deux modèles calculent les équations primitives pour la quantité de mouvement, les traceurs physiques, le niveau de la mer et les variables de la fermeture turbulente sur une grille Arakawa type C à l'aide de méthodes numériques aux différences/volumes finis conservant les principaux invariants linéaires (masse, quantité de mouvement, chaleur et sel) et non linéaires (énergie mécanique). Les deux modèles font l'hypothèse de Boussinesq et d'équilibre hydrostatique. Les différences notables se situent principalement au niveau des choix de la coordonnée verticale et de certaines paramétrisations (la turbulence notamment). Le modèle SYMPHONIE utilise un système de coordonnée sigma (surfaces de calcul déformables, tangentes aux surfaces limites de fond et de surface) et le modèle NEMO utilise une grille géopotentielle (surfaces de calcul normales à la gravitation terrestre). Le modèle SYMHONIE paramétrise les effets de la turbulence sous-maille avec soit le schéma de Gaspar (1990) (majoritairement utilisée dans

cette thèse) soit le schéma K-epsilon, alors que la version de NEMO mise en œuvre par MERCATOR sur la Méditerranée utilise le schéma de Blanke et Delecluse (1993). Le modèle SYMPHONIE est décrit en détail dans Marsaleix et al 2008, 2009, 2011, 2012 et le modèle NEMO dans Madec (2014).

4.2.2 Le modèle biogéochimique (Eco3m-S)

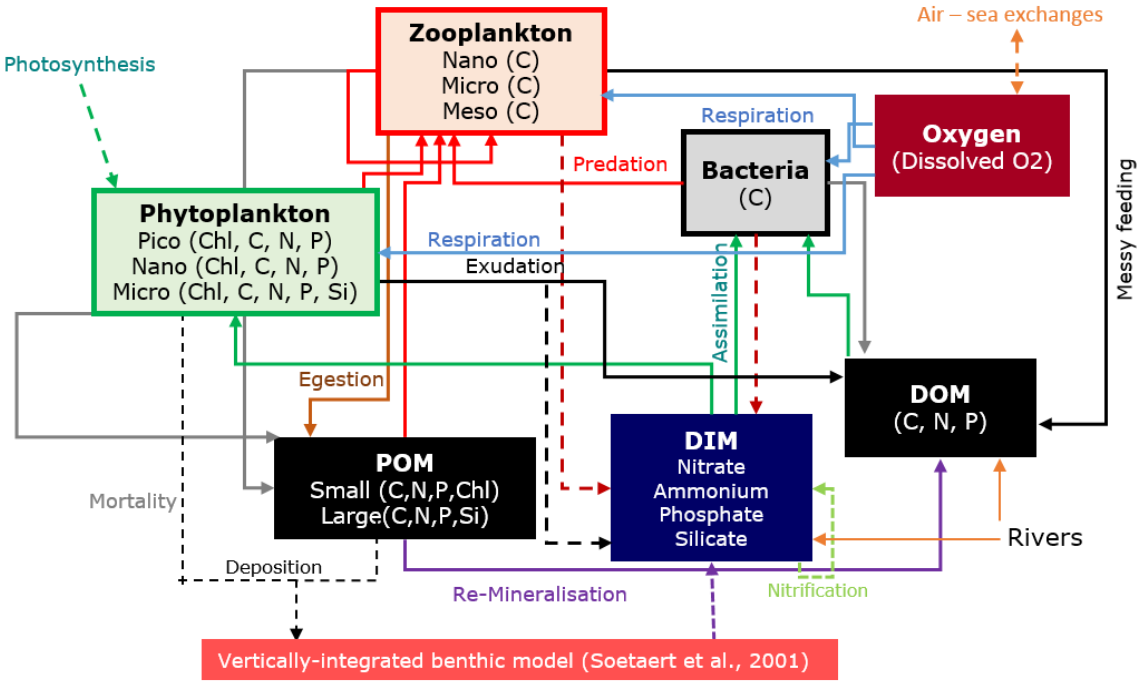

Figure 4.1: Représentation schématique du modèle Eco3m-S

Eco3m-S est un modèle biogéochimique multi-nutriment et multi-boites décrivant la dynamique du plancton pélagique. Le modèle décrit l'évolution temporelle de 33 variables d'état déjà présentes dans la version décrite par Herrmann (2007) et Auger (2011) ainsi que d'une variable représentant l'oxygène dissous que nous avons ajouté durant ma thèse. Le modèle représente les cycles des éléments suivants : l'azote (N), le phosphore (P), le silicium (Si), le carbone (C) et l'oxygène dissous (O_2d) et la chlorophylle (Chla). Le modèle est constitué des 8 compartiments suivants : la matière inorganique (ou sels nutritifs), le phytoplancton, le zooplancton, les bactéries, la matière organique dissoute, la matière organique particulaire et l'oxygène.

Ce modèle est une version nouvellement calibrée et complétée de la version du modèle présentée par (Hermann et al. 2013 ; Auger et al. 2014). Les équations d'état sont présentées dans les sections suivantes.

4.2.2.1 La matière inorganique dissoute

Ce compartiment est constitué du nitrate (NO_3), du phosphate (PO_4), du silicate ($Si(OH)_4$) et de l'ammonium (NH_4).

Le nitrate est consommé directement par les phytoplanctons, ce qui représente la production nouvelle. Il est produit par nitrification.

Taux de variation du nitrate=Nitrification-Absorption par le phytoplancton
$\frac{dNO_3}{dt} = Nitrif - \sum_{i=1}^{3} UptPhy_{i,NO_3}$

L'ammonium est produit par excrétion à partir des hétérotrophes (bactéries et zooplancton). Il est nitrifié, et consommé par les bactéries et le phytoplancton, la consommation par le phytoplancton correspondant à la production régénérée.

$\boldsymbol{Taux\ de\ variation\ de\ l'ammonuim = Excrétion\ par\ le\ zoo + Excrétion\ par\ les\ bactéries - Nitrification - Absorption\ par\ les\ phyto - Absorption\ par\ les\ bactéries}$
$\frac{dNH_4}{dt} = \sum_{i=1}^{3} ExcZoo_{i,NH_4} + ExcBac_{NH_4} - Nitrif - \sum_{i=1}^{3} UptPhy_{i,NH_4} - UptBac_{NH_4}$

Le phosphate est considéré comme l'élément le plus souvent limitant en mer Méditerranée (Thingstad et al., 2005). Il est excrété par les hétérotrophes (bactéries et zooplancton) et il est consommé par les bactéries et les phytoplanctons.

$\boldsymbol{Taux\ de\ variation\ du\ phosphate = Excrétion\ par\ le\ zoo + Excrétion\ par\ les\ bactéries - Absorption\ par\ les\ phyto - Absorption\ par\ les\ bactéries}$
$\frac{dPO_4}{dt} = \sum_{i=1}^{3} ExcZoo_{i,PO_4} + ExcBac_{PO_4} - \sum_{i=1}^{3} UptPhy_{i,PO_4} - UptBac_{PO_4}$

Le silicium est un élément limitant la croissance des diatomées (troisième classe de taille de phytoplancton dans le modèle). Le silicate est exsudé par le phytoplancton et produit par reminéralisation.

$\boldsymbol{Taux\ de\ variation\ du\ silicate = Exsdutation\ de\ la\ matière\ organique + Reminéralisation\ de\ la\ matière\ organique - Absorption\ par\ le\ phytoplancton}$

$$\frac{dSiO_4}{dt} = Exu_{3,Si} + Rem_{SiDet_S} + Rem_{SiDet_L} - UptPhy_{3,SiO_4}$$

4.2.2.2 Le phytoplancton

Le phytoplancton est représenté par trois groupes classés par taille (noté i=1(pico), 2(nano), 3(micro) dans les équations d'état et des processus) : le picophytoplancton (<2 microns), qu'on retrouve dans les milieux oligotrophes, le nanophytoplancton [2-20 microns], connu comme étant le plus abondant (Navarro et al., 2014) en Méditerranée et le microphytoplancton [>20 microns] constitué principalement par le groupe de diatomées. Le microphytoplancton a une vitesse de chute non nulle contrairement aux deux premières classes de phytoplancton. Le modèle de phytoplancton est dérivé du modèle Eco3M (Baklouti et al., 2006). Le fonctionnement du phytoplancton est régi par la production primaire, la synthèse de chlorophylle, la consommation de sels nutritifs, la respiration, l'exsudation, la mortalité et le broutage. Le phytoplancton possède des ratios internes variables. L'évolution temporelle des phytoplanctons est schématisée suivant les équations suivantes :

$$\textbf{Taux de variation du phytoplancton} = \textbf{Primary production} - \textbf{respiratioN} + \textbf{Absorption des sels nutritifs} - \textbf{exsudation} - \textbf{mortalité} - \textbf{broutage par le zooplancton}$$

$$\textbf{Taux de variation du phytoplancton} = \textbf{Primary production} - \textbf{respiratioN} + \textbf{Absorption des sels nutritifs} - \textbf{exsudation} - \textbf{mortalité} - \textbf{broutage par le zooplancton}$$

$$\frac{dCPhy_i}{dt} = GPP_i - RespPhy_i - Exu_{i,C} - MortPhy_{i,C} - \sum_{j=1}^{3} Graz_{j,CPhy_i}$$

$$\frac{dNPhy_i}{dt} = UptPhy_{i,NH_4} + UptPhy_{iNO_3} - Exu_{i,N} - MortPhy_{i,N} - \sum_{j=1}^{3} Graz_{j,NPhy_i}$$

$$\frac{dNPhy_i}{dt} = UptPhy_{i,NH_4} + UptPhy_{iNO_3} - Exu_{i,N} - MortPhy_{i,N} - \sum_{j=1}^{3} Graz_{j,NPhy_i}$$

$$\frac{dPPhy_i}{dt} = UptPhy_{i,PO_4} - Exu_{i,P} - MortPhy_{i,P} - \sum_{j=1}^{3} Graz_{j,PPhy_i}$$

$$\frac{dSiPhy_i}{dt} = UptPhy_{i,SiO_4} - Exu_{i,Si} - MortPhy_{i,Si} - \sum_{j=1}^{3} Graz_{j,SiPhy_i}$$

$$\frac{dChlPhy_i}{dt} = Synth_{i,Chl} - MortPhy_{i,Chl} - \sum_{j=1}^{3} Graz_{j,ChlPhy_i}$$

4.2.2.3 Le zooplancton

Le zooplancton est constitué de trois classes de taille (noté i=1(nano), 2(micro), 3(meso) dans les équations d'état et des processus) : le nano-zooplancton [diamètre < 20µm], le microzooplancton [20µm > diamètre > 200µm] et le mésozooplancton [diamètre> 200µm] qui se compose principalement de copépodes. Le modèle de zooplancton est basé sur le modèle développé par Anderson et Pondaven (2003) et adapté en mer Ligure par Raick et al. (2005). Le zooplancton possède des ratios internes constants. Le fonctionnement du zooplancton est régit par le broutage, la mortalité naturelle, la respiration basale, l'excrétion pour maintenir sa composition interne constante, l'égestion, le « Sloppy feeding » (nourriture broutée mais non assimilée), la prédation par les échelons trophiques supérieurs. L'évolution du zooplancton suit l'équation suivante :

$$\textbf{Taux de variation du zooplancton} = \textbf{broutage sur le phytoplancton} + \textbf{prédation du zooplancton carnivore} - \textbf{mortalité} - \textbf{respiration basale} - \textbf{egestion} - \textbf{excrétion de la matière organique dissoute} - \textbf{prédation par le zooplancton carnivore}$$

$$\textbf{Taux de variation du zooplancton} = \textbf{broutage sur le phytoplancton} + \textbf{prédation du zooplancton carnivore} - \textbf{mortalité} - \textbf{respiration basale} - \textbf{egestion} - \textbf{excrétion de la matière organique dissoute} - \textbf{prédation par le zooplancton carnivore}$$

$$\frac{dCZoo_i}{dt} = GrowthZoo_{i,C} - MortZoo_{i,C} - \sum_{j=1}^{3} Graz_{j,CZoo_i} - RespZoo_i^{add}$$

$$\frac{dCZoo_i}{dt} = GrowthZoo_{i,C} - MortZoo_{i,C} - \sum_{j=1}^{3} Graz_{j,CZoo_i} - RespZoo_i^{add}$$

4.2.2.4 Les bactéries

Le modèle de bactéries est également basé sur le modèle développé par Anderson et Pondaven (2003) et adapté en mer Ligure par Raick et al. (2005). Celles-ci possèdent également une composition interne constante. La consommation de matière organique dissoute et de nutriments, la respiration, l'excrétion, la mortalité naturelle et leur consommation par le nano-zooplancton sont les processus qui régissent leur fonctionnement. L'évolution des bactéries se fait dans le modèle d'après l'équation suivante :

$$\textbf{Taux de variation des bactéries} = \textbf{Absorption du carbone dissous et des sels nutritifs} - \textbf{respiration} - \textbf{mortalité} - \textbf{broutage par le zooplancton} - \textbf{excrétion de matière inorganique}$$

$$\frac{dCBac}{dt} = UptBac_{DOC} + UptBac_{x_iNut} - RespBac - MortBac_C - \sum_{j=1}^{3} Graz_{j,CBac} - ExcBac_{Nut}$$

x_i=phyto ; Nut= N, P

4.2.2.5 La matière organique particulaire

Ce compartiment contient des particules caractérisées par des petites vitesses de chute (0.7 m j^{-1}) et des particules avec de grandes vitesses de chute (90 m j^{-1}).

Les petits et grands détritus sont issus de la mortalité du phytoplancton et du zooplancton, de l'égestion du zooplancton. Ils sont consommés par le zooplancton et sont reminéralisés.

Taux de variation des petits détritus* = *mortalité du phytoplacton* + *mortalité du zooplancton* + *egestion du zooplancton* − *reminéralisation* − *broutage* − *prédation

Taux de variation des petits détritus* = *mortalité du phytoplacton* + *mortalité du zooplancton* + *egestion du zooplancton* − *reminéralisation* − *broutage* − *prédation

$$\frac{dCDet_S}{dt} = \sum_{i=1}^{3} MortPhy_{i,C} + \sum_{i=1}^{3} Eges_{i,C} + \sum_{i=1}^{2} fr_{Det_S}^{MortZoo_i} MortZoo_{i,C} + fr_{Det_S}^{MortZoo_3} PredZoo_{3,C} - Rem_{C,Det_S} - \sum_{i=1}^{3} Graz_{i,CDet_S}$$

$$\frac{dPDet_S}{dt} = \sum_{i=1}^{3} MortPhy_{i,P} + \sum_{i=1}^{3} Eges_{i,P} + \sum_{i=1}^{2} fr_{Det_S}^{MortZoo_i} MortZoo_{i,P} + fr_{Det_S}^{MortZoo_3} PredZoo_{3,P} - Rem_{P,Det_S} - \sum_{i=1}^{3} Graz_{i,PDet_S}$$

$$\frac{dNDet_S}{dt} = \sum_{i=1}^{3} MortPhy_{i,N} + \sum_{i=1}^{3} Eges_{i,N} + \sum_{i=1}^{2} fr_{Det_S}^{MortZoo_i} MortZoo_{i,N} + fr_{Det_S}^{MortZoo_3} PredZoo_{3,N} - Rem_{N,Det_S} - \sum_{i=1}^{3} Graz_{i,NDet_S}$$

$$\frac{dSiDet_S}{dt} = MortPhy_{3,Si} + fr_{Det_S}^{Eges_{Si}} . \sum_{i=2}^{3} Eges_{i,Si} - Rem_{Si,Det_S}$$

$$\frac{dChlDet_S}{dt} = \sum_{i=1}^{3} MortPhy_{i,Chl} + \sum_{i=2}^{3} Eges_{i,Chl} - Rem_{Chl,Det_S}$$

Taux de variation des grands détritus* = *mortalté du phytoplacton* + *mortalité du zooplancton* − *reminéralisation* − *broutage du zooplancton

$$\frac{dCDet_L}{dt} = \sum_{i=1}^{3} (1 - fr_{Det_S}^{MortZoo_i}) MortZoo_{i,C} + (1 - fr_{Det_S}^{MortZoo_3}) MortPhy_{i,C} - Rem_{C,Det_L} - \sum_{i=1}^{3} Graz_{i,CDet_L}$$

$$\frac{dPDet_L}{dt} = \sum_{i=1}^{3}(1 - fr_{Det_S}^{MortZoo_i})\, MortZoo_{i,P} + (1 - fr_{Det_S}^{MortZoo_3})\, MortPhy_{i,P} - Rem_{P,Det_L} - \sum_{i=1}^{3} Graz_{i,PDet_L}$$

$$\frac{dNDet_L}{dt} = \sum_{i=1}^{3}(1 - fr_{Det_S}^{MortZoo_i})\, MortZoo_{i,N} + (1 - fr_{Det_S}^{MortZoo_3})\, MortPhy_{i,N} - Rem_{N,Det_L} - \sum_{i=1}^{3} Graz_{i,NDet_L}$$

$$\frac{dSiDet_L}{dt} = (1 - fr_{Det_S}^{Eges_{Si}}).\sum_{i=2}^{3} Eges_{i,Si} - Rem_{Si,Det_L}$$

4.2.2.6 La matière organique dissoute

La matière organique dissoute est rejetée par exsudation par le phytoplancton et par « Sloppy feeding » par le zooplancton. Elle provient également de la reminéralisation de la matière organique particulaire et de la mortalité des bactéries. Elle est consommée par les bactéries :

$$\boldsymbol{Taux\ de\ variation\ du\ carbone\ organique\ dissous} = \boldsymbol{exsudation\ par\ le\ phytoplancton} + \boldsymbol{destructuration\ des\ proies\ avant\ leur\ consommation\ par\ le\ zooplancton} + \boldsymbol{mortalité\ des\ bactéries} + \boldsymbol{reminéralisation} - \boldsymbol{consommation\ par\ les\ bactéries}$$

$$\boldsymbol{Taux\ de\ variation\ du\ carbone\ organique\ dissous} = \boldsymbol{exsudation\ par\ le\ phytoplancton} + \boldsymbol{destructuration\ des\ proies\ avant\ leur\ consommation\ par\ le\ zooplancton} + \boldsymbol{mortalité\ des\ bactéries} + \boldsymbol{reminéralisation} - \boldsymbol{consommation\ par\ les\ bactéries}$$

$$\frac{dDOC}{dt} = \sum_{i=1}^{3} Exu_{i,C} + \sum_{i=1}^{3} SloppyFeed_{i,C} + MortBac_C + Rem_{CDet_S} + Rem_{CDet_L} - UptBac_{DOC}$$

$$\frac{dDOC}{dt} = \sum_{i=1}^{3} Exu_{i,C} + \sum_{i=1}^{3} SloppyFeed_{i,C} + MortBac_C + Rem_{CDet_S} + Rem_{CDet_L} - UptBac_{DOC}$$

4.2.2.7 L'oxygène dissous

$$\boldsymbol{Flux\ de\ l'oxygèneen\ surface} = Kw\ /\ 360\,000 * (oxygen_{sat} - oxygen)$$

$$Kw = (0.0283 * wind^3) * (Sc - 660)^{-0.5}$$

$$Sc = ox_A - (ox_B * T) + (ox_C * T^2) - (ox_D * T^3)$$

$$\boldsymbol{oxygen}\ \text{à}\ \boldsymbol{saturation} = (1000/22.3916) * \exp(x1)$$

Avec,

$$x1 = (ox_{A0} + ox_{A1} * T_s + ox_{A2} * T_s^2 + ox_{A3} * T_s^3 + ox_{A4} * T_s^4 + ox_{A5} * T_s^5) + (S * (ox_{B0} + ox_{B1} * T_s + ox_{B2} * T_s^2 + ox_{B3} * T_s^3) + ox_{C0} * S^2$$

Ainsi que,

$$Ts = \log(\,298.5 - T/273.15 + T)$$

Taux de variation de l'oxygen $= \boldsymbol{PPB} - \boldsymbol{Phytoplankton\ Respiration} - \boldsymbol{Zooplankton\ respiration} - \boldsymbol{bacteria\ respiration} + \boldsymbol{nitrification}$
$\frac{dO2}{dt} = (GPP_i \times C/O) - (RespPhy_i \times N/O) - (RespZoo_i^{add} \times N/O) - (RespBac \times N/O) - (Nitrif \times N/O)$

4.2.2.8 Le couplage benthique

Ce modèle est couplé avec une version simplifiée du méta-modèle benthique décrit par Soetaert et al. (2000). Les paramètres de ce dernier ont été fixés sur la base de l'étude de modélisation de Pastor et al., (2000) sur le plateau du Golfe du Lion.

4.2.3 Le couplage physique-biogéochimie

Nous venons de voir une description des modèles mis en œuvre au cours de mon travail de doctorat. Mais pour pouvoir réaliser une modélisation complète dynamique/biogéochimie, il s'agit maintenant de faire communiquer les différents compartiments de notre système. Cela se fait par le biais du couplage.

Après la phase d'initialisation des modèles physique et biogéochimique, le couplage se fait par les procédures suivantes :

- Calcul du taux de variation des variables biogéochimiques par Eco3m-S avec la prise en compte de l`effet de la pénétration de la lumière.
- Calcul du taux de variation total des variables biogéochimiques à l'aide d'une équation d'advection-diffusion par l'intermédiaire de la plateforme de couplage BLOOM (Biogeochemical & Lagrangian Offline Ocean Model, Marsaleix et al., 2014). Les champs physiques SYMPHONIE ou NEMO sont utilisés en offline pour le calcul du transport des variables biogéochimiques suivant l'équation suivante :

Le modèle physique a une échelle de temps beaucoup plus courte que celle du modèle biogéochimique. Par conséquent, les équations biogéochimiques sont résolues à une fréquence plus faible (~2h) que celle du transport eulérien par les champs physique (~15mn). Cette technique a été préalablement approuvée par Butenschon et al. (2012), c'est la technique du *Source Splitting*. En plus du gain de temps, les auteurs ont montré qu'elle diminuait les erreurs du calcul biologique.

Les conditions aux limites du système seront précisées pour les différentes études dans les chapitres dédiés.

4.3. Les grilles de calcul

4.3.1 La grille à l'échelle du bassin méditerranéen

A la différence de la modélisation physique du bassin occidental spécialement élaborée pendant la thèse pour répondre aux questionnements scientifiques soulevés par notre étude, la modélisation physique à l'échelle du bassin méditerranéen a été réalisée en dehors du Laboratoire d'Aérologie. Il s'agit concrètement des champs physiques calculés par une configuration régionale, MED12 (Lebeaupin Brossier et al., 2011, 2012 ; Beuvier et al., 2012) du modèle NEMO : Madec et l'équipe NEMO (2008), mise en place dans le cadre du programme SIMED par une équipe de MERCATOR-Océan, en collaboration avec le CNRM. Cette configuration, dont l'emprise spatiale est représentée sur la figure 4.2, couvre tout le bassin méditerranéen. La grille est caractérisée par une résolution horizontale de ~6 km (1/12°). Les niveaux verticaux sont au nombre de 75. La résolution verticale est de 1 m en surface et de plusieurs dizaines de mètres au fond.

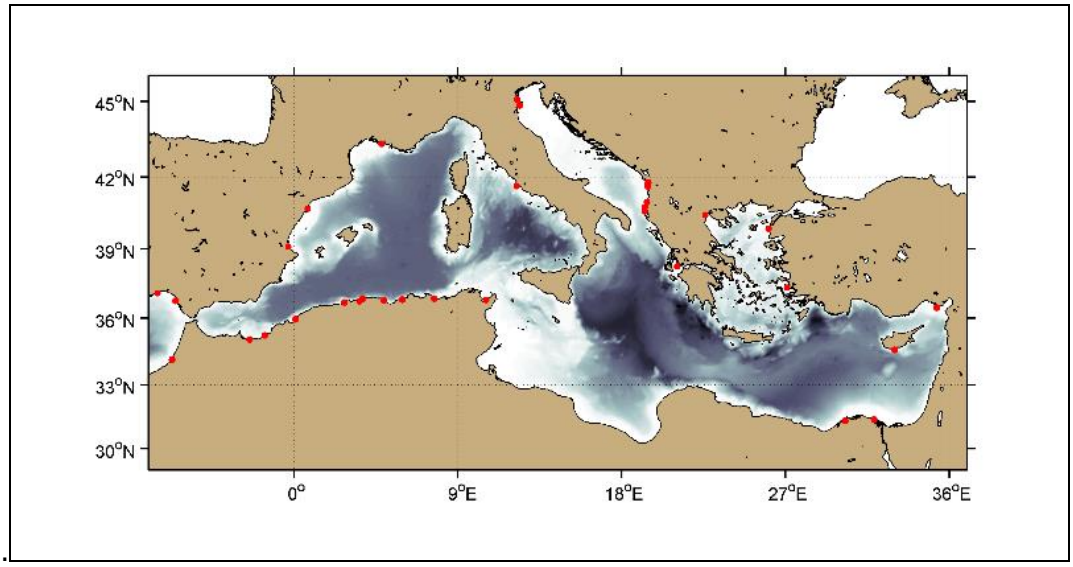

Figure 4.2: Extension et bathymétrie de la grille du modèle de forçage PSY2V2R4.

4.3.2 La grille du bassin occidental

Le modèle SYMPHONIE utilisé pour le bassin occidental a préalablement été utilisé en Méditerranée pour la simulation de la convection profonde au large du Golfe du Lion (Herrmann et al. 2009), ainsi que pour la formation d'eau dense côtière (Estournel et al. 2005 ; Ulses et al. 2008 ; Hermann et al.

2008 ; Ferré et al. 2008). Il a également été couplé au modèle Eco3m-S pour la modélisation de l'écosystème planctonique (Herrmann et al. 2013 ; 2014 ; Auger et al. 2011 ; 2014).

La grille spécialement élaborée pour les questions abordées pendant cette thèse recouvre une bonne partie du bassin occidental de la Mer Méditerranée (Fig. 4.2). Elle s'étend jusqu'à la limite entre le bassin algérien et la mer d'Alboran à l'Est, jusqu'au sous-bassin sicilien à l'Ouest et jusqu'à la côte africaine au Sud. Cette extension a été choisie afin (1) d'éloigner les frontières du modèle de la zone d'intérêt, la région nord-occidentale, pour éviter des perturbations dans cette zone liée aux conditions aux limites et (2) de la redistribution dans le bassin occidental qui est influencée par des structures tourbillonnaires à submésoéchelle (5-10 km) (Testor et Gascard, 2006). Pour une représentation correcte de ces structures qui jouent aussi un rôle important dans la formation d'eau dense (Herrmann et al., 2008) nous avons opté pour une résolution autour de 1 km. La grille, en sigma généralisée, est caractérisée par 40 niveaux verticaux, resserrés en surface dans les zones profondes.

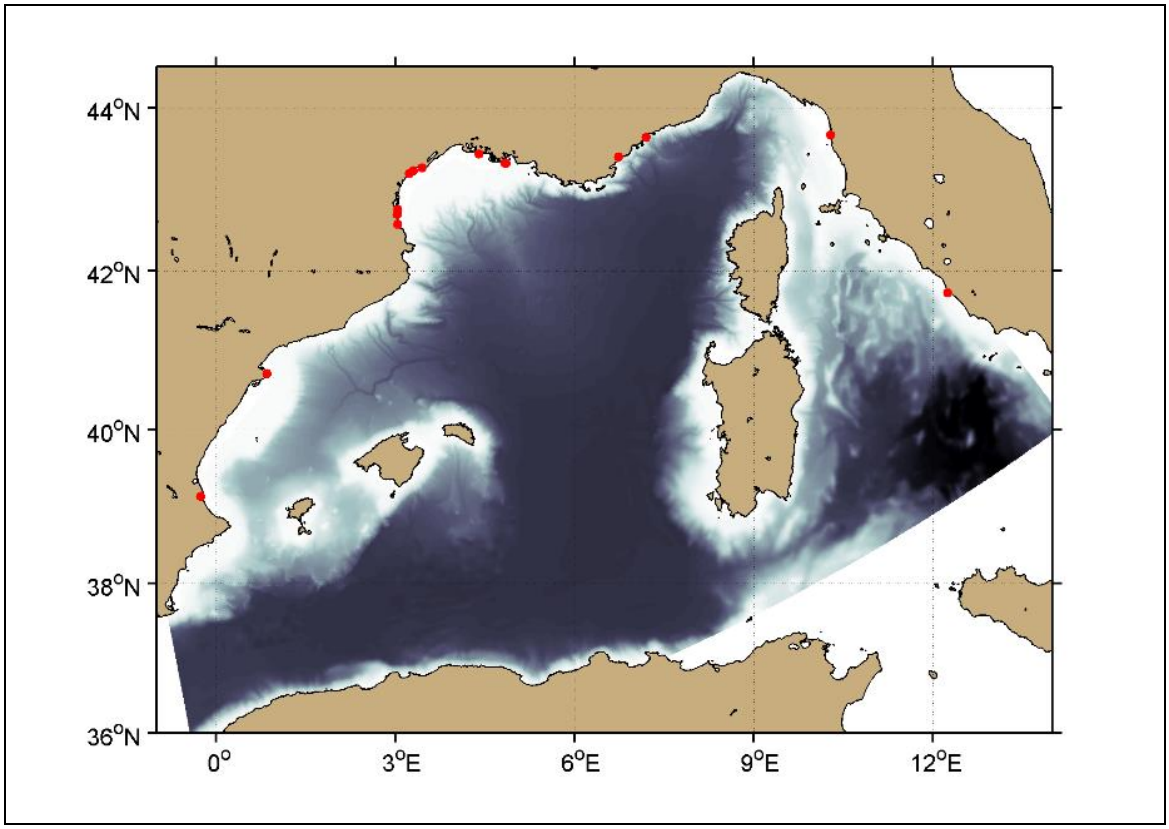

Figure 4.3: Extension et bathymétrie de la grille régionale du modèle SYMPHONIE

Title: Biogeochemical cycles of the Mediterranean Sea: climatologies and budget

Table des matières

1. Introduction 39
2. Methodology 40
   2.1. The physical model 41
   2.2. The biogeochemical model 41
   2.3. Implementation on the Mediterranean basin 42
      2.3.1. Biological boundary conditions 42
      2.3.2. Initialization and spin up 43
3. Results and discussion 43
   3.1. Evaluation of the model 44
      3.1.1. Surface chlorophyll 44
      3.1.2. Biogeochemical characteristics of water masses 47
   3.2. Climatology 48
      3.2.1 Mixed layer depth 48
      3.2.2 Depth and magnitude of the Deep Chlorophyll Maximum (DCM) 50
      3.2.3. Nutriclines 52
      3.2.4. Net primary production (NPP) 54
      3.2.5. Organic carbon export 56
   3.3. Main pelagic ecological regimes of the Mediterranean Sea 58
      3.3.1. Bloom like regime (group 1) 60
      3.3.2. No-bloom regime of the western basin (group 3) 61
      3.3.3. No-bloom regimes of the eastern basin (groups 4, 5, 6) 62
      3.3.4. The Intermittent/Intermediate regime (group 2) 62
   3.4. Nitrogen and phosphorus dynamics in the Mediterranean Sea 64
      3.4.1. Biogeochemical processes 64
      3.4.2. Fluxes at the straits 65
      3.4.3. The global budget 65
   4. Conclusion and perspectives 68

Authors

F. Kessouri[1], C. Ulses[1], P. Marsaleix[1], J. Beuvier[2,3], S. Somot[3], F. D'Ortenzio[4, 5], M. Pujo-Pay[6, 7], L. Prieur[5], C. Estournel[1]

[1] Laboratoire d'Aérologie, UMR 5560 CNRS, Université de Toulouse 3, 14 avenue Edouard Belin, 31400 Toulouse, France

[2] Mercator Océan, 10 rue Hermès, 31520 Ramonville-Saint-Agne, France

[3] Météo France, 42 av. Gaspard Coriolis, 31057 Toulouse CEDEX, France

[4] Sorbonne Universités, UPMC Univ Paris 06, UMR 7093, Laboratoire d'Océanographie de Villefranche, 06230 Villefranche-sur-Mer, France

[5] CNRS, UMR 7093, LOV, 06230 Villefranche-sur-Mer, France

[6] Sorbonne Universités, UPMC Univ Paris 06, UMR 7621, Laboratoire d'Océanographie Microbienne, Observatoire Océanologique, Avenue du Fontaulé, 66650 Banyuls/mer, France

[7] CNRS, UMR 7621, Laboratoire d'Océanographie Microbienne, Observatoire Océanologique, 66650 Banyuls/mer, France

Key points up to three (<100 characters)

- Decadal study using high resolution physical-biogeochemical model
- Biogeochemical climatologies based on modeling
- Ecological regionalization
- Mediterranean budgets of nitrogen and phosphorus

Abstract

The Mediterranean Sea is characterized by complex climatic characteristics, a well-developed thermohaline circulation at the scale of the western and eastern basins and energetic gyre and jet systems at sub-basin scale. These characteristics impact on the hydrological, biogeochemical and biological water mass properties. A ten years 1/12° offline simulation of the biogeochemical cycles of the Mediterranean Sea was performed using the ECO3M-S biogeochemical model and the daily averaged physical fields computed by the NEMO OGCM. The simulation is analyzed according to three thematic axes.

The first axis is a monthly climatology of mixed-layer depth and biogeochemical characteristics describing the seasonal cycles at sub-basins scale and the impact of key processes (such as deep-convection or seasonal stratification) on the nutriclines and DCM depth or biogenic inputs in the surface layer. The second axis is a regionalization based on physical and biogeochemical parameters leading to the identification of seven bioregions and four main trophic regimes, namely, the deep-convection regime (and ensuing phytoplankton blooms), the intermediate mixing regime, and the stratified regimes in the western and eastern basins. The third axis proposes a biogeochemical budget based on nitrogen and phosphorus fluxes through the straits and on transfers between organic and inorganic forms. At the Gibraltar strait, the inorganic nitrogen outflow is about 140 10^9 moles per year while the organic inflow is about 80 10^9 moles per year. The western basin is globally a source of organic matter, a substantial part of which is exported to the eastern basin. The eastern basin is a source of inorganic matter, a part of which is exported to the western basin by the circulation of the Levantine Intermediate Water.

The semi-enclosed Mediterranean Sea is driven by global dynamics forced by climate and thermohaline cyclonic circulation. Local regional dynamics impact on water masses properties and biological activity, as well as the amount of chemicals. An accurate budget of the Mediterranean needs accurate components of the water budget (inflows and outflows at the straits, runoff and precipitation) and an accurate determination of concentrations in these external inputs and in the different water masses. Budget of nutrients and processes analysis are the keys to understand biological ecosystem behavior. Front lines which meet these problematics were the work exposed in (Bethoux et al., 1988, Bethoux et al. 1990; Bethoux and Gentili, 1996; Bethoux, 1998).

Main biological processes were already well descripted in previous models. Lazzari et al., (2012), based on the "Longhurst biological classification" (Longhurst, 1995), qualified Mediterranean Sea as a "subtropical nutrient-limited winter spring production period bioregion" in adequacy with chlorophyll profiles exposed by (Lavigne et al., 2015; Mignot et al., 2014), where subsurface chlorophyll distribution in the Mediterranean Sea corresponds to some other subtropical regions. (Lazzari et al., 2012) have summarized the spatial gradient of net primary production (NPP) and its strong seasonal cycle over the basin. They demonstrated that this production depends on surface and integrated water properties. Crise et al., (1998) have mentioned west to east deepening of the nitracline, going from 50 m in Alboran Sea until 110m in Levantine Sea. Deep chlorophyll maximum (DCM) is globally superimposed on the nutriclines as studied by Macías et al., (2014). These authors have exposed that the DCM accounts for an important part of NPP and covers about 95% of the basin during the long oligotrophic period. Lavigne et al., (2015) thanks to a calibration of fluorescence derived chlorophyll of large historical datasets demonstrated that DCM should be estimated deeper than mentioned by Macías et al., (2014) and gave an estimation of a gradual deepening of DCM of 1.6m per longitudinal degree during stratified conditions.

Coupled physical/biogeochemical models meet limits because. Some limits are related to their physical component and associated atmospheric forcing. For example, a deeper MLD may cause an increased enrichment of surface waters. In contrary, weaker MLD than expected may cause a higher surface oligotrophy. Other problems may be linked to the calibration of biogeochemical model parameters which is difficult to obtain all over an area composed of regions with different biogeochemical functioning. The Mediterranean Sea is very heterogeneous and contains a large number of bioregions each one with its own biological functioning. Based on phytoplankton annual cycle, D'Ortenzio et al., (2009) classified the Mediterranean Sea into three groups: first, "Bloom-Like regime" characterized by quick and intense spring bloom. Then, "intermittent regime" characterized by long phytoplankton winter efflorescence and "NO-Bloom regime" present low chlorophyll concentration and their cycle seems like doming. To our knowledge, there are no coupled models able to represent these different trophic regimes.

Another important problem of modelling is related to the initialization and boundary forcing. Indeed, time of simulation is of

the order of the decade which is much lower than the residence time of water masses (Millot, 2005). Therefor specific initialization is required to attempt in short time the physical and the biogeochemical equilibrium states.

As mentioned by Macías et al., (2014), biological inputs from rivers, Atlantic and Black seas, and atmosphere suffer from large uncertainties. Important failures could be seen in shallow waters of western part of Alboran Sea, the Adriatic Sea and in the Gulf of Gabès.

Using modeling, this paper aims to describe the most important biogeochemical properties of the whole Mediterranean Sea, by identifying geographical distribution of each of them. An annual budget of biogenic matter circulating in the basin over the straits of Gibraltar and Sicily is also presented.

The paper is organized as follows: First the second section presents the modelling based methodology used in this study. Then results are presented in the third section, such as climatologies of the physical properties, together with climatologies of biogeochemical surface and water body properties, on the whole Mediterranean on a monthly climatological basis. Biogeochemical processes in four main regimes are quantified derived from a statistical clustering method, then discussed. A global nitrogen budget and nutrient fluxes at the Mediterranean straits are then presented to conclude the discussion. Conclusions and perspectives are given in the fourth section.

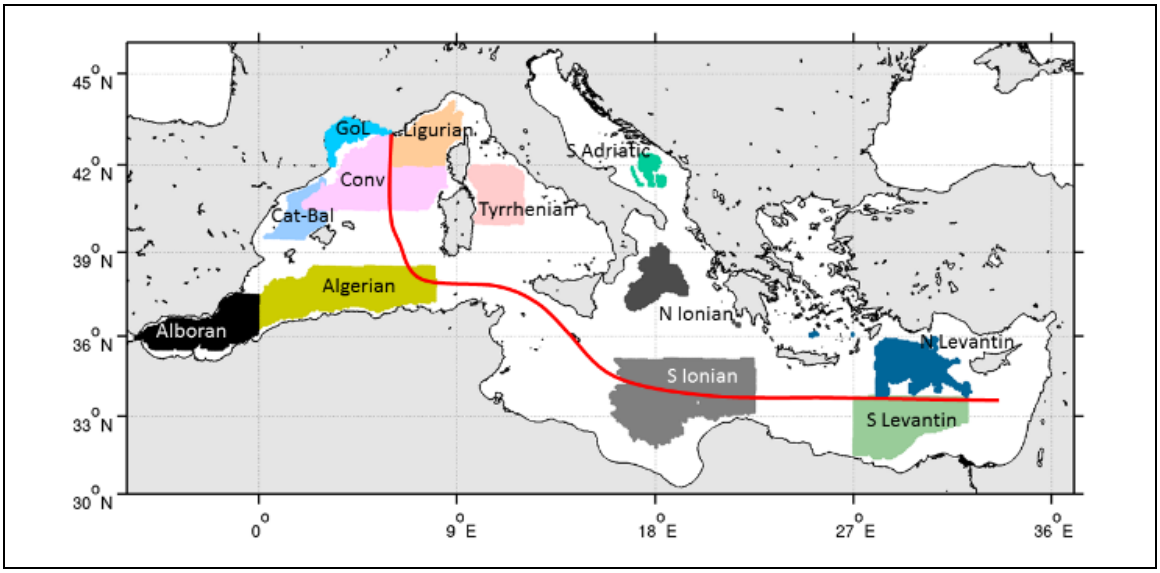

Figure 1: Position of the averaged regions in the chlorophyll validation section. Red line represents the transect performed by the oceanographic cruise BOUM in June and July 2008.

2. Methodology

In this study we have used a 3D coupled physical biogeochemical modeling. The biogeochemical multi-elements Eco3M-S

model (Auger et al., 2011, 2014), has been forced offline by the outputs of the hydrodynamic NEMO-MED12 model (Hamon et al., in revision) resolving mesoscale processes, via the BLOOM platform (pers. comm. P. Marsaleix).

2.1. The physical model

The configuration of the ocean general circulation NEMO model used was the regional configuration of the Mediterranean Sea, NEMO-MED12 (Hamon et al., in press), with a 1/12° (~ 7 km) horizontal resolution and 75 vertical z-levels with partial steps. The domain of modeling is indicated in Figure 1. It covers the whole Mediterranean Sea and a buffer zone west of the Strait of Gibraltar. The simulation, called NM12-FREE, described in (Hamon et al., in press) is a free run (i.e. without data assimilation) that starts in October 1979 and ends in June 2013. Initial conditions were provided by the monthly mean potential temperature and salinity 3-D fields from the state of the MEDATLAS-1979 climatology (Rixen et al., 2005) in the Mediterranean side and, in the Atlantic side, from the global ocean reanalysis ORAS4 (Balmaseda et al., 2013) at the same date. The exchanges with the Atlantic basin were performed through the buffer zone where 3-D temperature, salinity and sea level were relaxed toward ORAS4 monthly fields. River inputs were taken into account based on the climatological average of the dataset of Ludwig et al. (2009). For the 33 main rivers, the runoff values of the dataset were prescribed while for the other rivers, the value of runoff corresponded to an average in each subbasin. The Black Sea was not included in the model domain but represented a major source of freshwater. It was considered as a river for the Aegean Sea at the Dardanelles Strait. The model is forced by the 3-hourly atmospheric fluxes from an ALADIN-Climate simulation at 12 km of resolution (Herrmann et al., 2010), driven by the ERA-Interim atmospheric reanalysis, and called ALDERA (Hamon et al., in revision).

2.2. The biogeochemical model

The biogeochemical Eco3M-S model is a multi-nutrient and multi-plankton functional type model (Auger et al., 2011). It describes the cycles of C, N, P and Si. This model was previously used to study the multi-annual ecosystem variability in the NW Med (Auger et al. 2014; Herrmann et al. 2013) and the ecosystem functioning in the Gulf of Lions shelf influenced by the Rhone river inputs. We have re-calibrated the previous version described in Auger et al. (2014) in order to implement the model on the whole Mediterranean Sea. The different recalibrated parameters are described in (Kessouri et al., in prep-b). Eco3M-S consists of seven interconnected compartments (Fig. 2): (1) The inorganic compartment representing nitrate, ammonium, phosphate and silicate, (2) the dissolved organic matter compartment considered under the forms of carbon, nitrogen and phosphorus (3) particulate organic matter compartment (under the forms of C, N, P, Si and chlorophyll), divided in two weight classes, light and heavy, (4) the autotrophic compartment composed of three classes of phytoplankton classified by size: pico-phytoplankton (smaller than 2 microns, nano-phytoplankton (between 2 and 20 microns), and micro-phytoplankton (between 20 and 200 microns) that corresponds in the model to diatoms, (5) the zooplankton compartment composed of three size classes of zooplankton: nano-zooplankton [diameter < 20µm], micro-zooplankton [20µm > diameter

> 200µm] and meso-zooplankton [diameter> 200µm] and (6) the bacteria compartment. The relative internal composition, i.e. the stoichiometry, of each functional type is considered as variable for autotrophic organisms and constant for heterotrophic organisms. (7) Oxygen: Oxygen is consumed by plankton and bacteria; it is also produced inside the water mass through phytoplankton photosynthesis. Air-sea exchanges are performed throughout Wanninkhof and McGillis (1999) laws.

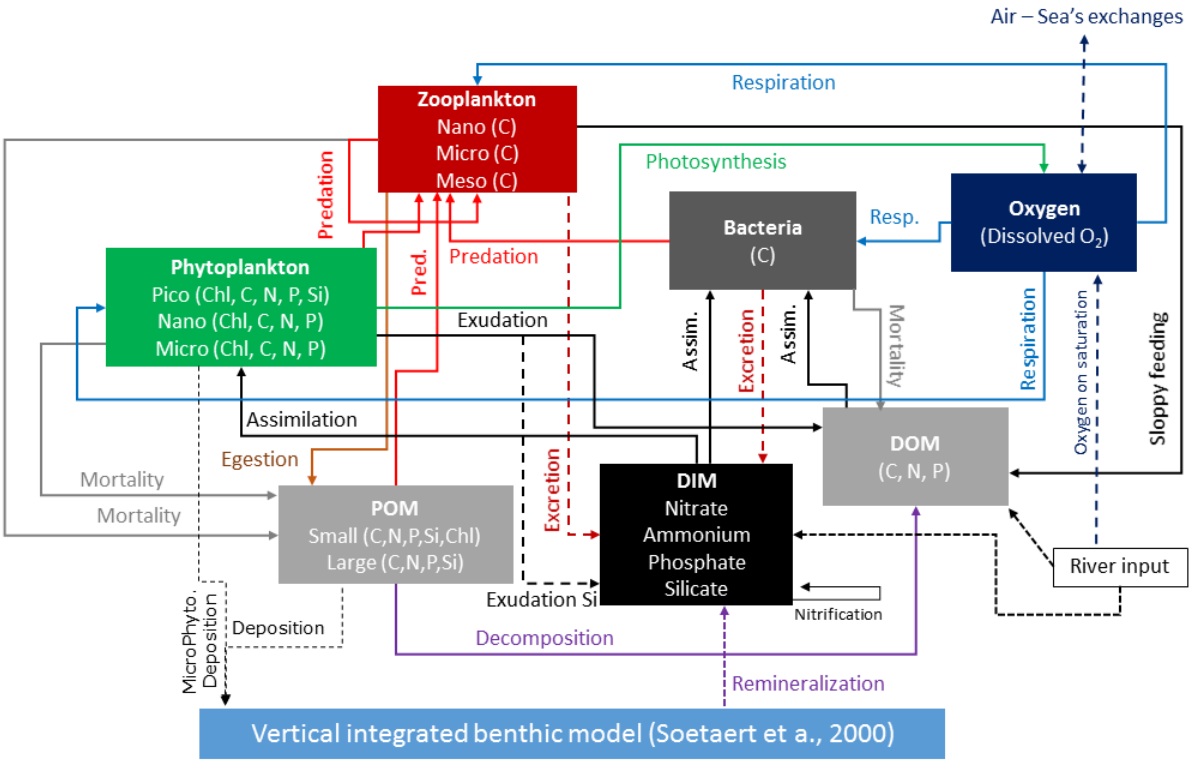

Figure 2: Scheme of the biogeochemical model Eco3m-S

2.3. Implementation on the Mediterranean basin

2.3.1. Biological boundary conditions

In the Atlantic Ocean, nutrients and oxygen have been prescribed using monthly profiles from "World Ocean Atlas 2009" climatology at 7.5° W. This boundary condition's limit has been chosen close to the Strait of Gibraltar to avoid spurious effects caused by relaxation on physical parameters in the buffer zone.

The Black Sea was not included in the model domain but it represents a major source of freshwater. It was considered in the NEMO-MED12 configuration as a river for the Aegean Sea at the Dardanelles Strait. At this strait, constant values for organic matter have been applied according to Copin Montegut (1993). Nutrient inputs have not been introduced at the Dardanelles Strait because of the null net flow (Tugrul et al., 2002).

At the runoff points, concentrations of nutrients have been imposed by region using dataset of Ludwig et al. (2010). As organic matter concentrations in the continental waters are most often unknown, constant values derived from the historical dataset of the Rhône River at Arles station (MOOSE program, pers. comm. Raimbault) have been imposed for these inputs.

At the sea surface, atmospheric deposition of inorganic matter has been prescribed as constant values for western (west to Sicily Strait) and eastern sub-basins based on "low" estimations reported by Ribera d'Alcalà et al. (2003). Deposition of organic matter has been deduced from relationships between inorganic and organic matter deduced from MOOSE network data collected south of France (pers. comm. Raimbault).

Nutrient fluxes at the water column/sediment interface have been obtained through a coupling of the biogeochemical model with a simplified version of the vertically-integrated benthic model described by Soetaert et al. (2000).

2.3.2. Initialization and spin up

In previous Mediterranean Sea modelling studies, initialization states were based either on climatology (Crise et al., 1998; Crispi et al., 2002) or, at sub-basin scale, on relationships between nutrients and physical properties of water masses (Prieur and Legendre, 1988; Auger et al., 2014). In this study, inorganic variables have been initialized using the historical database defined in 13 regions by Lavezza et al. (2011). Depending on the amount and spatial distribution of nutrients and hydrological salinity profiles in each bio-region, we have chosen one type of initialization mentioned above: we have used relations linking nutrients to salinity in the upper layer and intermediate waters, then a constant value in the deeper layer in the western basin where profiles are numerous and allow a seasonal description. In the eastern basin, because of the lack of the combined biological and physical datasets near coastal zones we have deduced nutrients' median profiles in each region defined by Lavezza et al. (2011).

The spin-up of a model is an important issue as its stability is required to calculate reliable budgets. Stable nutrient and organic matter stocks on the whole the basin have been obtained after four years of simulation (for instance, the total nitrate stock presents an annual variability around 0.05 %). Thus, the simulation has been started in 2000 using the final state of a first 2000-2004 simulation. It ends in 2013. In this paper we focus on the period 2003 – 2013.

3. Results and discussion

This section is divided in four parts:

First, we present an evaluation (1) of simulated surface chlorophyll patterns using daily 4km resolution outputs of MODIS Aqua satellite products and (2) of water mass properties, focusing on nutrient chlorophyll and DOC concentrations over the basin, based on the trans Mediterranean BOUM cruise dataset (Pujo-Pay et al., 2011; Moutin and Prieur, 2012) occurring in

summer 2008. To address the lack of temporal comparison, especially in winter, values were reported and compared to experiences mentioned in literature in the Gulf of Lions, in the Adriatic Sea and in the Rhodes Gyre.

In the second part, the monthly climatologies of hydrological and biogeochemical parameters calculated over the [2003 – 2013] decade from model outputs are presented and discussed.

In the third part, the functioning of four kinds of regimes is described throughout clustering analysis using models output using selected parameters. Finally, matter exchanges and flux at the straits of the Mediterranean Sea and biological fluxes in the eastern and the western basins are highlighted.

3.1. Evaluation of the model

3.1.1. Surface chlorophyll

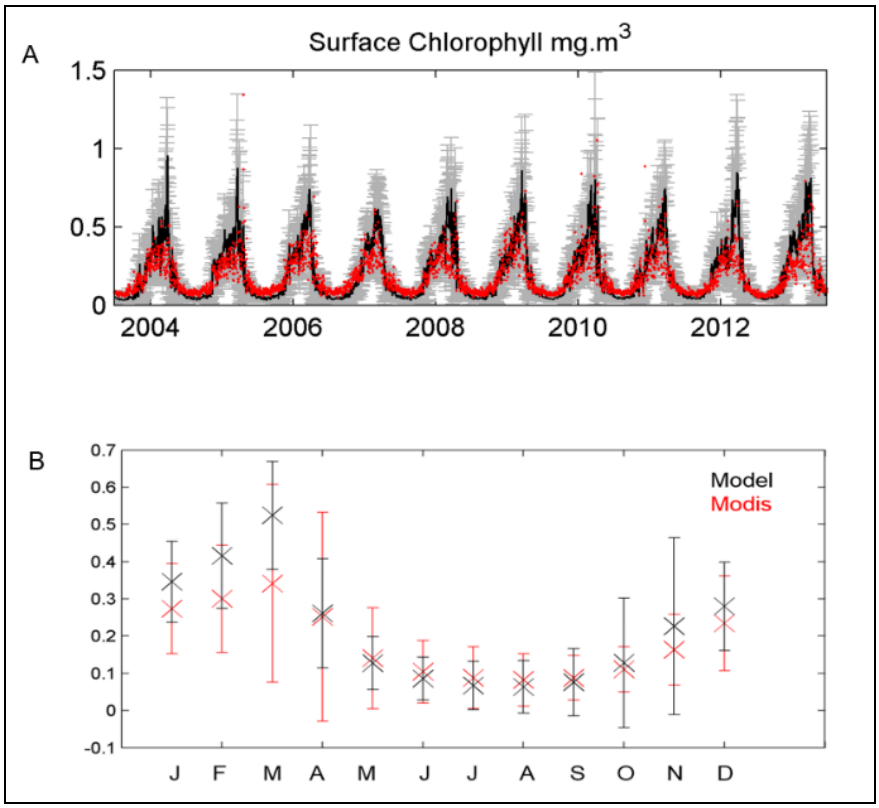

Figure 3: A. Observed (MODIS at 4 km resolution, in black) and modeled (red) surface chlorophyll concentration (mg m^{-3}) averaged over the whole Mediterranean basin Grey points represent standard deviation in model outputs. B. Modeled (black) and observed (red) monthly average and standard deviation of surface chlorophyll concentration.

Figure 3-A presents a comparison between simulated (without considering penetration depth) and observed surface

chlorophyll concentrations averaged over pelagic areas (bathymetry > 500m) of the whole basin from summer 2003 to summer 2013. Model results show a good agreement in the temporal evolution with the observations. The Spearman correlation coefficient between data and model outputs is equal to 0.93 ($p<0.01$). The difference between model outputs and observations is maximum in winter (January, February and March) when the mean concentration is strong (Fig. 3-B). Its annual mean value is equal to 0.02 $mg.m^{-3}$. The timing of the maximum is also generally well represented except in some cases where it is anticipated by about 5 to 7 days as in 2005. Statistics (mean, RMSD, standard deviation) concerning each subbasin (Fig. 1) are presented in Tab. 1. The mean concentration for each subbasin is very close between observations and model outputs. However, the standard deviation in model outputs are higher than in observations and RMSD (Friedrichs et al., 2009) higher than the mean values in eastern regions.

Regions	Alboran	Algerian	Conv.	Ligurian	Cat-Bal	Adriatic	N Ionian	S Ionian	N Levantin	S Levantin
STD obs	0.35	0.18	0.36	0.34	0.19	0.10	0.07	0.05	0.06	0.04
STD mod	0.31	0.23	0.37	0.36	0.32	0.23	0.19	0.12	0.18	0.12
MEAN obs	0.43	0.24	0.33	0.32	0.26	0.18	0.13	0.09	0.10	0.07
MEAN mod	0.38	0.26	0.33	0.32	0.30	0.14	0.13	0.10	0.13	0.08
RMSD obs vs mod	0.34	0.13	0.31	0.31	0.23	0.20	0.15	0.08	0.14	0.09

Table 1: Statistics of surface chlorophyll from the model and from Modis by region showed in Fig. 1.

Figure 4 displays a comparison between observed and simulated monthly surface chlorophyll concentration 2D fields. The model reproduces correctly the East-West and South-North concentration gradients. Seasonal variability in each region is well reproduced. Chlorophyll concentration is generally maximal during winter (in the whole basin except in the north-western subbasin) or spring (in the north-western subbasin), and low during the long oligotrophic period, from May until October. The model reproduces correctly the autumn (November – December) efflorescence observed by satellite particularly in the western basin. Nevertheless, an overestimation of 0.4 $mg.m^{-3}$ is noteworthy in the south Adriatic, northern Ionian and northern Levantine subbasins in February and March. This difference could be caused by an overestimation of the deepening of the mixed layer as it will be seen in section 3.2.1. In contrary, the Alboran Sea is less productive in the model than in the observations. This default could be due to the fact that we didn't take into account tides that could favor nutrients upwelling through increased vertical diffusivities (Sanchez-Vidal et al., 2008; Renault et al., 2012). An underestimation of chlorophyll in the model is also visible along the African coast in the thin Algerian current, which is weaker in the model than in the estimations performed by Millot (1999) based on MEDIPROC data set.

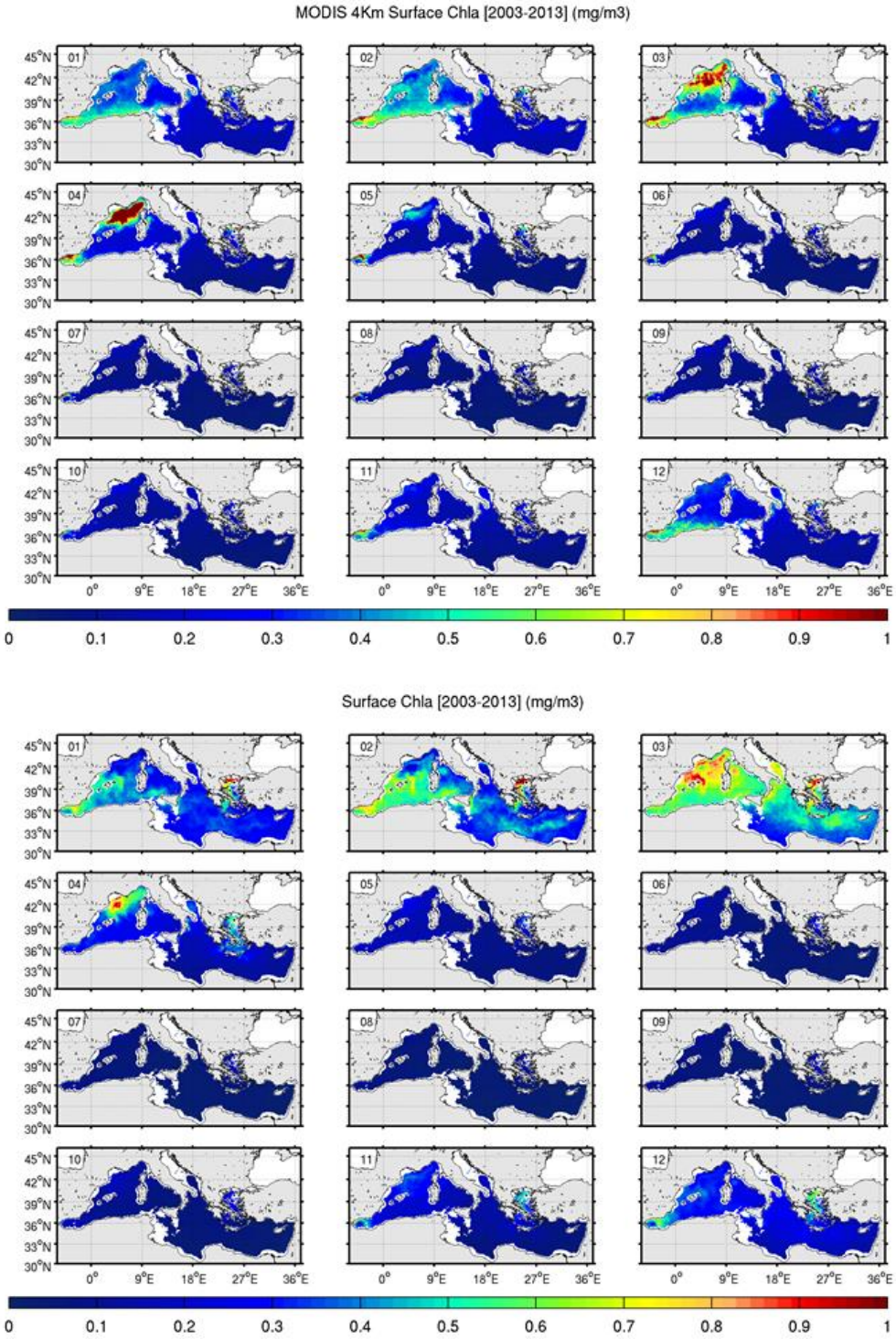

Figure 4: 10-year (2003-2013) average of observed (top) and modeled (down) monthly surface chlorophyll concentrations

3.1.2. Biogeochemical characteristics of water masses

The ability of the model to represent the biogeochemical characteristics of the different water masses has been evaluated trough a confrontation of model results against the observations of the BOUM cruise (Moutin & Prieur, 2012) along transects from North to South in the western basin and from West to East in the eastern basin (indicated on Figure 1). The cruise lasted for one month and a half between June and July 2008. We have averaged the model outputs during the period of the cruise (July to August 2008).

Over the entire transect, observed and simulated nutrients (nitrate and phosphate) show extremely low concentrations in the surface layer (Fig. 5). Nitracline has been defined here as the depth where nitrate is equal to 1 mmol.m^{-3}, and for the phosphacline the threshold concentration has been chosen equal to 0.05 mmol.m^{-3} (Lazzari et al., 2012). As in the observations, nitracline is localized at 60 m depth in the western basin and gradually deepens to attain 120 m in the eastern Levantine basin. Phosphacline is close to the nitracline in the western basin but a gradual decoupling between both nutriclines is then observed to the east. The difference between both depths could reach 40 m in some locations in the eastern part of the Levantine Sea.

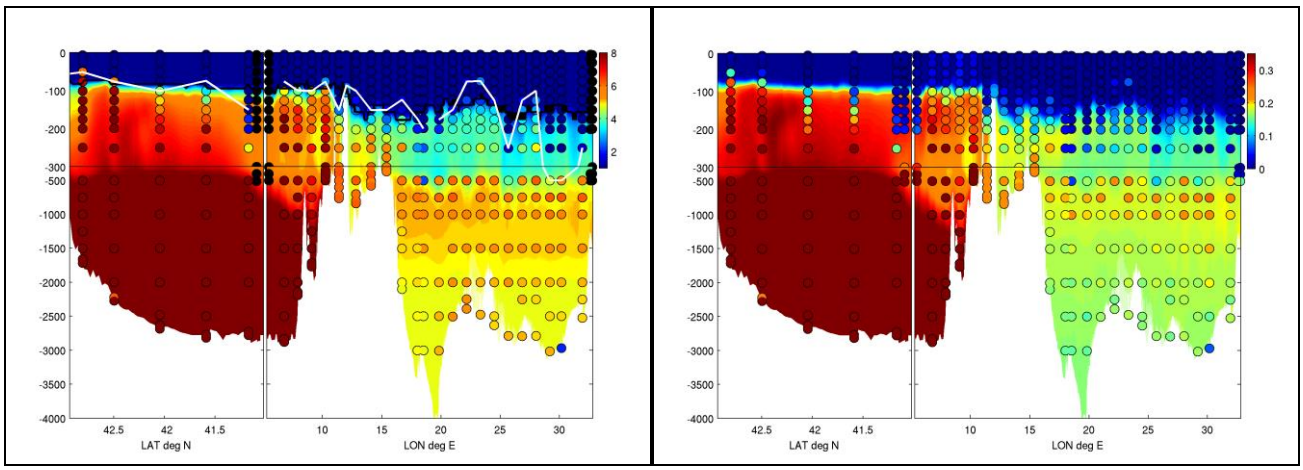

Figure 5: Left panel Nitrate concentration [mmol.m^{-3}] comparison, between model's outputs (background) and BOUM transect observations (dots). Same for phosphate in the right panel. Black dots are missed data in the left panel.

In the eastern sub-basin, local deepening of the nutriclines are observed at some stations, due to the presence of anticyclonic eddies (Moutin and Prieur, 2012). This pattern is represented in model outputs but it is not clearly visible in the modeled averaged outputs presented in Figure 5. The model reproduces maximum concentrations of nitrate (~5.5 mmol.m^{-3}) and phosphate (~0.25 mMol.m^{-3}) observed in the intermediate waters (250 - 500m) in the eastern basin. Nevertheless, these maxima are slightly underestimated (by 0.5 mmol.m^{-3} for nitrate, and 0.05 mmol.m^{-3} for phosphate). In the western basin below the nutriclines, concentrations increase from 1 to 7 mmol.m^{-3} for nitrate, and from 0.05 to 0.3 mmol.m^{-3} for

phosphate in less than 100 m. However, intermediate waters seem to be less concentrated in the model by a gap of about ~0.5 mmol.m^{-3} for nitrate and ~0.025 mmol.m^{-3} for phosphate in some western zones. For instance, the deepening of the nitracline is more important at the latitude 41 which is not represented in the model. Like observations, modeled deep water masses are characterized by values higher than 8 mmol.m^{-3} for nitrate, and higher than 0.4 mmol.m^{-3} for phosphate as also observed by (Béthoux et al., 1998; Pujo-Pay et al., 2011; Severin et al., 2014).

Simulated deep chlorophyll maximum (DCM, showed in figure 6) deepens from West to East as the nutriclines. The depth of the DCM is around 55 m in the north-west region and gradually attains 110 m near the eastern boundary of the transect in the central Levantine sub-basin. Observation and modeled data have the same patterns.

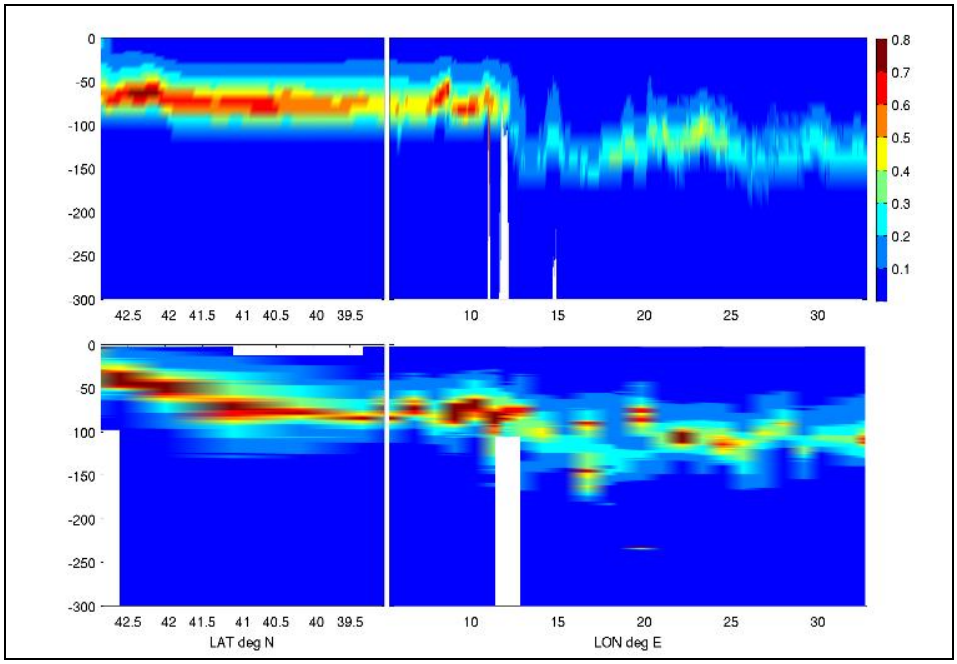

Figure 6: Chlorophyll [mgChl/m^{-3}] (zoom 0-300m depth) comparison between model (upper) and BOUM in situ data (lower).

3.2. Climatology

First, climatologies of the mixed layer depth (MLD) are presented. Then we present a climatology for biogeochemical properties (DCM, nutriclines, amount of nitrate in the top 150m layer and surface oxygen concentration) and biological fluxes (net primary production or organic carbon export).

3.2.1 Mixed layer depth

The MLD has been defined here as the depth where the potential density increases by 0.01 kg.m^{-3} relatively to the 10 m depth. The climatology of the MLD (Fig. 7) shows two key periods. The first period is a vertical mixing season between

October and April and the second one is a stratified period between May and September. During winter, only coastal regions (not shown) under the influence of freshwater discharges as well as the North Aegean influenced by the inflow of the Black Sea present a thin MLD.

The thickest MLD are found in February. The patterns of thick MLD (> 100 m) are generally close to those presented by Houpert et al. (2015) in its climatology based on *in situ* observations. They are located in the Gulf of Lions and the Tyrrhenian Sea for the western basin, the south Adriatic and North Ionian Sea for the central basin and the Levantine Sea for the Eastern basin. Among these regions of important winter vertical mixing, some of them correspond to well-known convection zones (Gulf of Lions, south Adriatic, north Ionian Sea and Rhodes Gyre). Nevertheless, climatology doesn't represent the extreme values observed in these areas. This is partly due to the spatial and mainly temporal variabilities in the intensity of the convection episodes. For example, convection in the Gulf of Lions reaches certain years its maximum depth in January and other years in February or even in March. Moreover, the decadal variability is believed to be important as a response to the variability of heat losses (Grignon et al., 2010) which would make it difficult to compare our climatology based on a 10–year period to the climatology performed by Houpert et al. (2015) based on a 40-year period. The convection events occurring in the eastern basin present, in the model results, much less interannual variability than in the Gulf of Lions. In the north Ionian and Levantine subbasins, it results in an overestimation of mixing compared to observations presented by Houpert et al. (2015). Not shown time-series in the model presents some high values over 300 m depth in some regions of the eastern basin.

The Algerian basin presents a weak MLD that does not deepen at more than 60 m in winter. In this basin vertical mixing starts in early December and stops in February. A return to stratified conditions is observed in early March. Local spatial variability is observed, which is related to the mesoscale activity. This concerns for example the anticyclonic eddies evolving near the coast.

In the climatology of Houpert et al. (2015), the Alboran Sea is in winter the most stratified region of the Mediterranean. More into details, the Alboran Sea presents a strong mesoscale activity impacting on vertical motion through the northern front near the Spanish coast and the southern anticyclonic West Alboran Gyre (WAG). Our MLD climatology shows an important difference between these two parts of the Alboran Sea. The northern front has a MLD lower than 40 m, all the year while in the anticyclonic WAG the MLD fluctuates between 70 and 90 m depth from December to April.

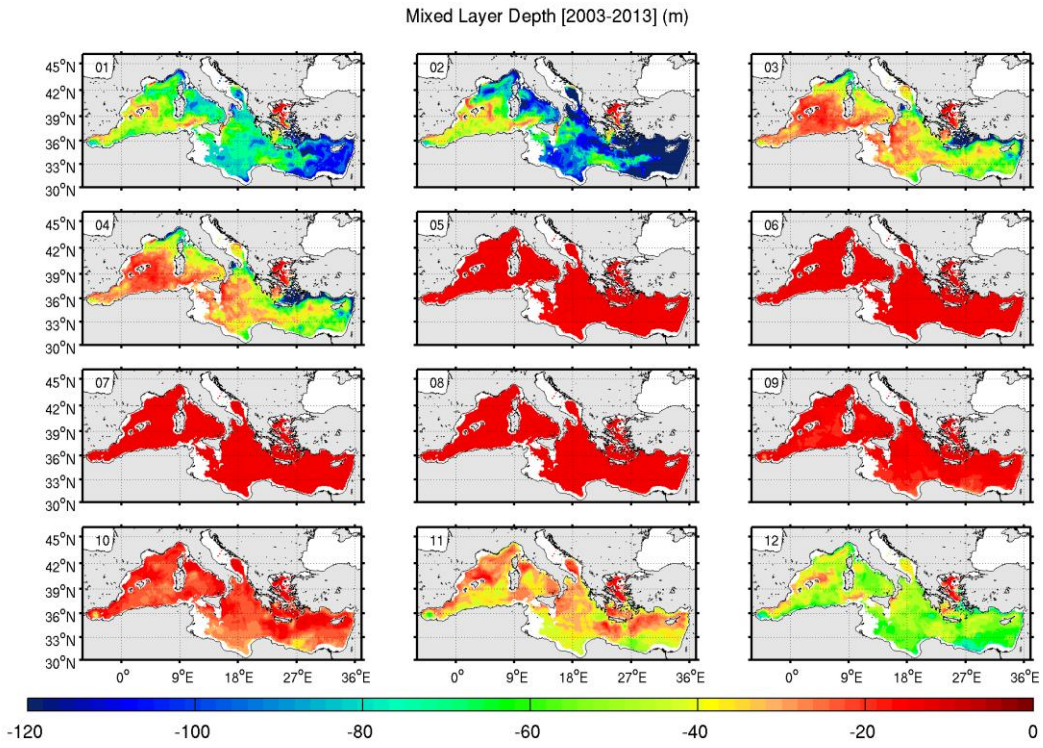

Figure 7: Modeled MLD climatology

3.2.2 Depth and magnitude of the Deep Chlorophyll Maximum (DCM)

Figure 8 presents the monthly climatology of the depth and magnitude of the model-computed DCM. The chlorophyll maximum is located at the surface in January and February over the entire basin. From March to July, the DCM progressively deepens. This deepening presents a general West-East gradient, characterized by a value of 1.66 $m.l^{-1}$ longitudinal. This estimation is close to the result of Crispi (1999) based on 3D modelling approach and of Lavigne et al. (2015) based on *in situ* observations. Maximal values of DCM depth are reached in July and August, when it attains 60 m in the western and north-eastern subbasins, 90 m in the central eastern basins and 120 m near the south-eastern coast. In autumn, the DCM becomes shallower. In November, the chlorophyll concentration is maximum at the surface in the Alboran Sea, in the north-western region and in the Aegean Sea. Finally in December, the chlorophyll maximum is again located at the surface in the whole basin except in some areas, which are: Tyrrhenian, Ionian and Levantine subbasins. The DCM is therefore present over a wide part of the year, in particular in south-eastern regions. This seasonal cycle of the depth of the DCM is in consistency with the modelling study of Macias et al. (2014).

The DCM presents relatively low concentrations, from October to January. At this period, it is of the order of 0.1-0.2 mg m^{-3} in the south-eastern regions, and of 0.5 mg m^{-3} in the rest of the basin. In spring and summer, maxima (higher than 0.7 mg m^{-3}) are visible in the Alboran Sea, north-western region, Adriatic, north-Ionian, and Aegean Seas.

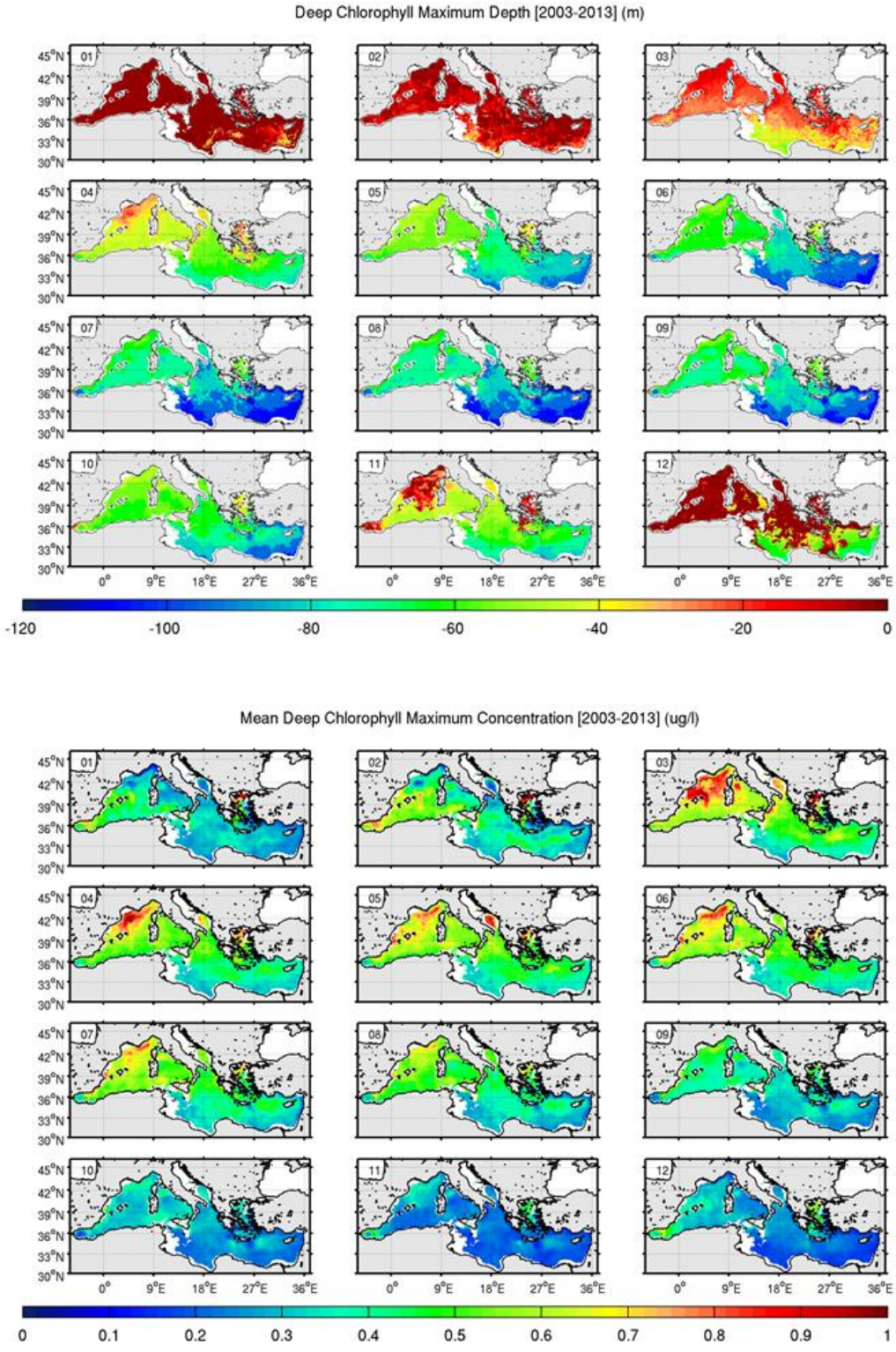

Figure 8: Modeled DCM depth (upper) and chlorophyll maximum concentration (lower) climatologies

3.2.3. Nutriclines

Climatologies of modeled nitracline and phosphacline depths are presented in Fig. 9. West to East and North to South deepening of nutriclines over the basin are globally obtained. Both nutriclines follow the same seasonal evolution. The depths of the top of nutriclines are maximum in August and September. During winter, the nutriclines disappear in the northern parts of the basin, while their depths are minimum in the rest of the basin.

A West-East progressive deepening of phosphacline related to nitracline is also noticeable. The difference of nutriclines depths is maximum in winter in both subbasins. From May to December, this difference is around 8 m in the Levantine subbasin and close to zero in the Algerian subbasin. In February, it is around 50 m in the Levantine subbasin and 10 m in the Algerian subbasin.

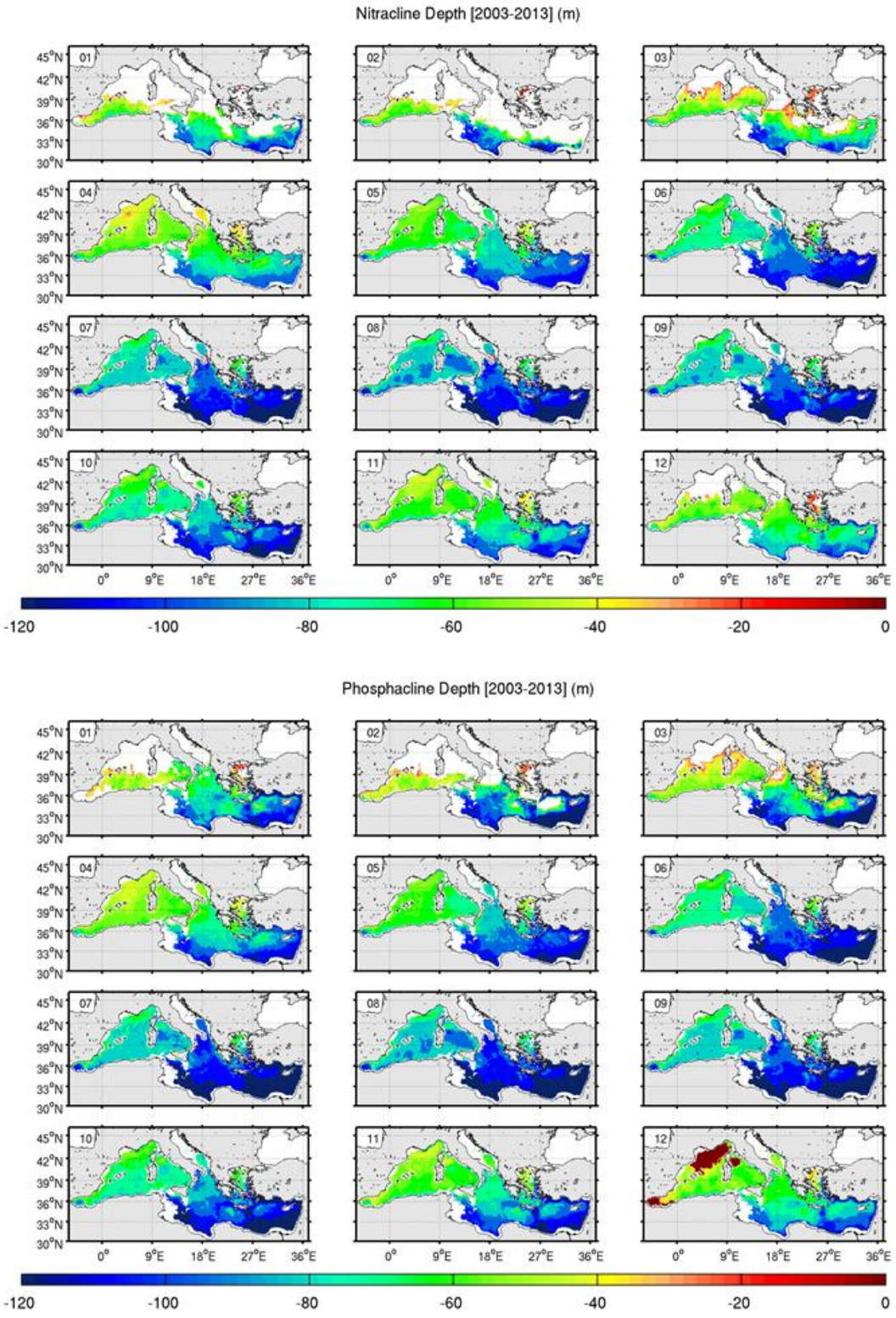

Figure 9: Modeled nitracline (upper) and phosphacline (lower) climatologies

3.2.4. Net primary production (NPP)

The NPP is heterogeneous over the Mediterranean Sea (Fig. 10). Highest values are estimated in the Alboran Sea, where PPN never decreases under 0.5 $gC.m^{-2}.d^{-1}$ and attains locally 1 $gC.m^{-2}.d^{-1}$ in winter and in spring. At the same time, the WAG contains very lower production which is caused by its anticyclonic circulation. This anticyclone is surrounded by the most productive dynamics of the Mediterranean Sea in a frontal zone. Minima are estimated in the extreme eastern Levantine basin by 0.1 $gC.m^{-2}.d^{-1}$ in autumn and 0.4 $gC.m^{-2}.d^{-1}$ in winter. The NPP is particularly heterogeneous in the NW, where northern gyre (NG) and the surrounding area show antagonist patterns in winter and spring. In winter, low PPN is simulated in the NG while high values are visible in peripheral zones, and inversely in spring. When the high production triggers, the surrounded waters become less productive. The NPP reaches inside the NG 0.2 $gC.m^{-2}.d^{-1}$ in winter and 0.9 $gC.m^{-2}.d^{-1}$ in spring. These values are close to estimates from observations described by Uitz et al. (2012).

NPP seasonal evolution is different from the one of the surface chlorophyll concentrations: high production is simulated at the end of spring and beginning of summer (Fig. 10) when the lowest values are simulated and observed for surface chlorophyll (Fig. 4). In the Algerian basin, there is accumulated nutrients in the euphotic layer. During this period, chlorophyll profiles get globally a homogeneous form but some local features such as eddies favor “high surface chlorophyll” (HSC) profiles shape described by (Lavigne et al., 2015) when nutriclines become shallow (not shown).

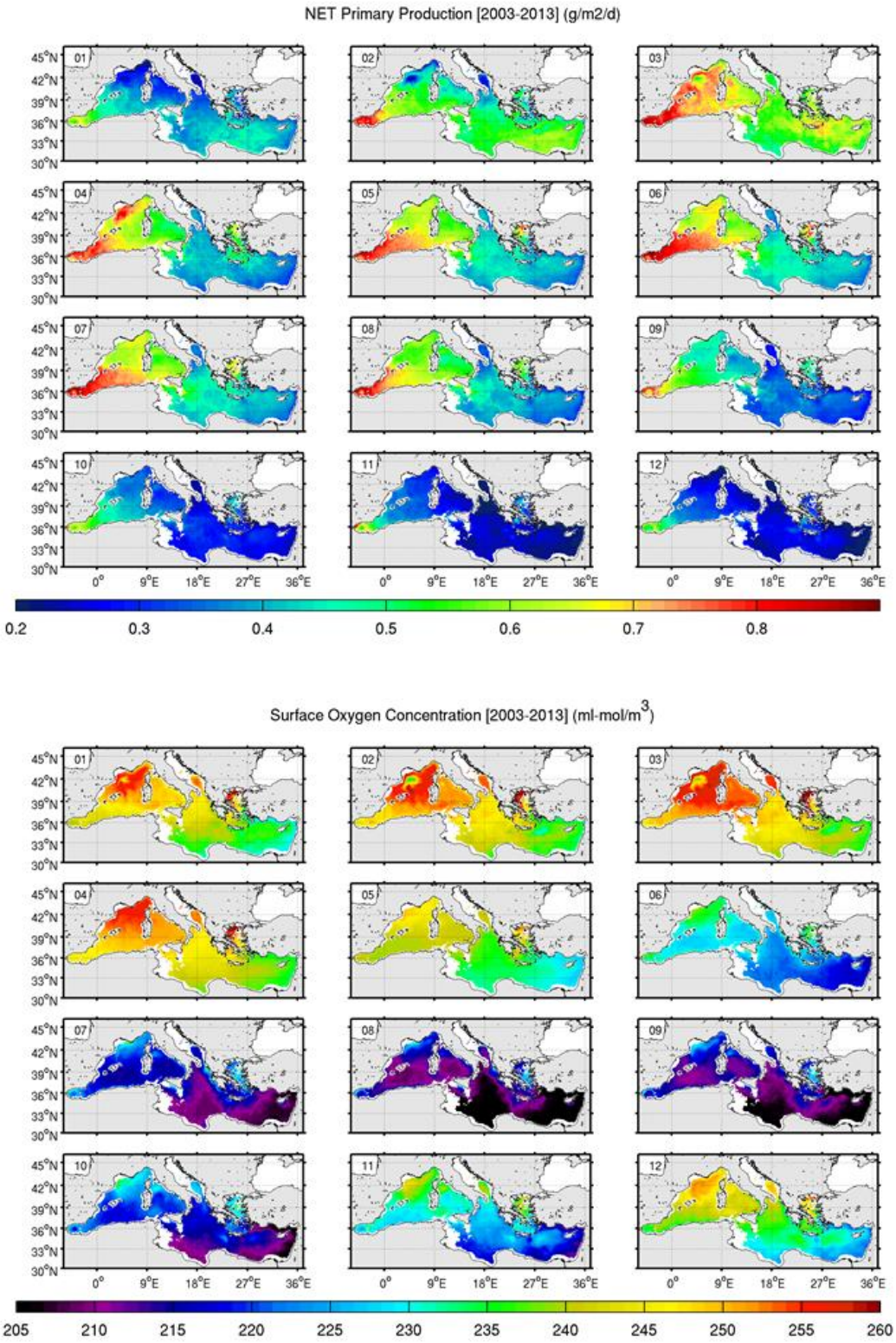

Figure 10: Modeled NPP (upper) and Surface oxygen concentration (lower) climatologies

3.2.5. Organic carbon export

We have computed the export at 200 m depth because production processes take place above this threshold in the entire basin.

The DOC export (Fig. 11) presents high values [>20 $mgC.m^{-2}.d^{-1}$] in winter in the northwestern region, north Ionian and the Levantine Seas. The rest of the year it is relatively weak. Some mesoscale features provoking import and export of DOC can be distinguished over the entire basin.

The export of POC (Fig. 11) is high during winter in the whole basin except in the south Ionian and south Levantine subbasins. It ranges between 15 and 25 $mgC.m^{-2}.d^{-1}$ from winter to spring in the NW and Northern Ionian Sea. Maximum export in the NG reaches 100 $mgC.m^{-2}.d^{-1}$ in February and March in the NW. Between May and September, the POC export is about 10 $mgC.m^{-2}.d^{-1}$ in the most productive areas of the NE or NW basins. Meanwhile, SW and SE basins do not show important values in summer and autumn.

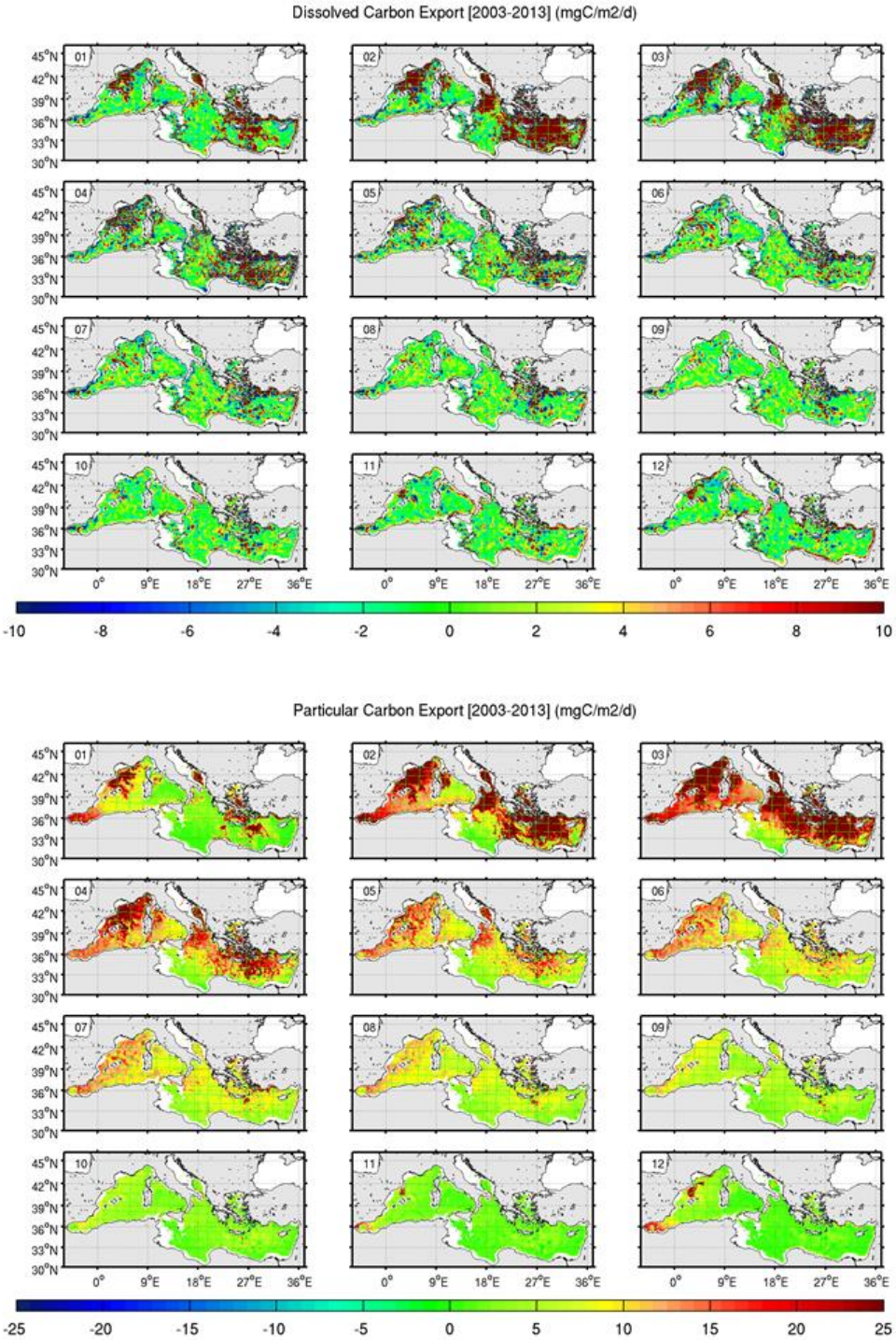

Figure 11: DOC export (upper) and POC export (lower) climatologies

3.3. Main pelagic ecological regimes of the Mediterranean Sea

In the previous section, climatologies of hydrodynamic and biogeochemical variables have been presented in order to gain in understanding of the functioning of the pelagic ecosystem of the Mediterranean Sea. Large spatial heterogeneities have been noticed in both north-south and west-east directions. Here we propose to use a statistical method of clustering to simplify this complex picture and to identify bio-regions characterized by similar seasonal cycles. This objective identification of bioregions is a step forward compared to a fixed division of regions based on geography. Such a regionalization has been proposed for the Mediterranean by D'Ortenzio and Ribera D'Alcalà (2009) from a detailed analysis of the surface chlorophyll seasonal cycle. The different seasonal cycles found with this classification identified different "trophic regimes" present in the classification of Longhurst (1998). They also showed that the structure of the seasonal cycle is tightly coupled with the dynamic range of biomass characterizing the productivity of the region. The idea of repeating this exercise with a model is to have benefit of the large volume of information given by a coupled model not only at the surface but also in the sub-surface as the values of the surface chlorophyll are negligible during a large part of the year although primary production is still active in the DCM.

For clustering, we classified each pixels on the basis of the climatological values of the surface and depth-integrated chlorophyll, the primary production, the nitrate uptake, the amount of nitrate in the upper layer [0-150m], nitrate concentration in the intermediate layer (500 m), the mixed layer depth and the stratification index. Then, for each bioregions we calculated the mean time series. The first three parameters inform about the biological surface and subsurface properties, the nitrate uptake about the ability of phytoplankton to consume nutrients, the amount of nitrate represents the balance between the nutrients imports by vertical dynamics and their consumption and the last parameter characterize the global patterns of the hydrology.

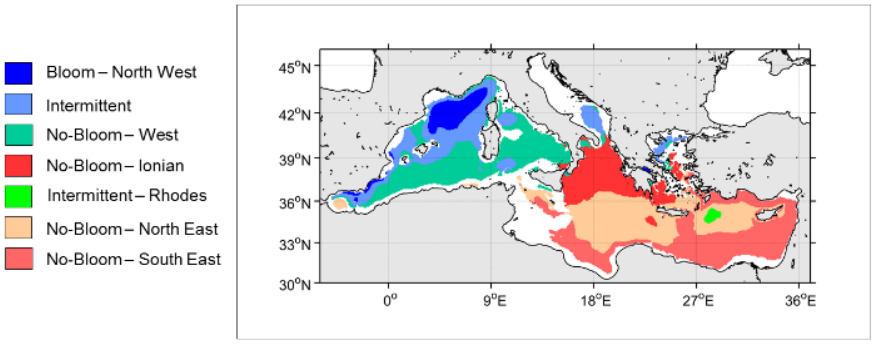

Figure 12: Spatial distribution of bioregions extracted by k-means clustering from physical and biogeochemical datasets derived from the model's outputs.

The k-means clustering using Euclidian distance has been chosen despite the difficulty in the choice of the number of groups. Several tests with different numbers have been performed. The western basin is few sensitive to this number with a final robust repartition in three groups. It is

not the case in the eastern basin where the number of groups is sensitive. The choice has been made on a configuration with four specific groups in this basin.

The repartition of these different groups is shown on Fig. 12. The western basin consists of group 1 in the deep northwest basin where dense water formation occurs, group 2 mainly encircling group 1, group 3 in the Algerian and the south Tyrrhenian basins. The eastern basin consists of one group to the north similar to group 2, and 3 groups more or less organized as west east bands. Group 4 is mainly present in the Ionian and Aegean seas, group 5 in the mid Levantine and mid Ionian and group 6 following the southern and eastern coasts of the subbasin. Finally, a small region (group 7) corresponds to the region of the Rhodes gyre. Note also that the anticyclonic West Alboran gyre belongs to group 5. The seasonal cycle of the surface and depth-integrated chlorophyll is given for the different groups in Figure 13.

A comparison with the classification of D'Ortenzio and Ribera d'Alcalà (2009) (DR09) shows some similarities and differences. First, the "Bloom" bioregion of DR09 is very similar to group 1 for the geographical region as well as the surface signature. In the same way, the "Intermittently" bioregion of DR09 has strong similarities with group 2, at the whole periphery of group 1, in the northern Tyrrhenian gyre, in the south Adriatic and along the northern coast of the Alboran Sea. As in DR09, the surface maximum is earlier than in group 1 but it looks more pronounced in the model. The "No Bloom 3" cluster of DR09 could correspond to group 3 although in DR09, it does not extend in the southern Tyrrhenian. The surface chlorophyll cycle presents differences with DR09: a small peak is present in March and starting from this peak, the simulated concentration decreases too quickly. The eastern basin is dominated in DR09 by two "No bloom clusters". Our eastern clusters have the same drawbacks than the group 3 cluster of the western basin. In the following, we keep the denomination of DR09 for our clusters even if the No-Bloom denomination could look a little abusive if the small increase of surface chlorophyll in March is considered.

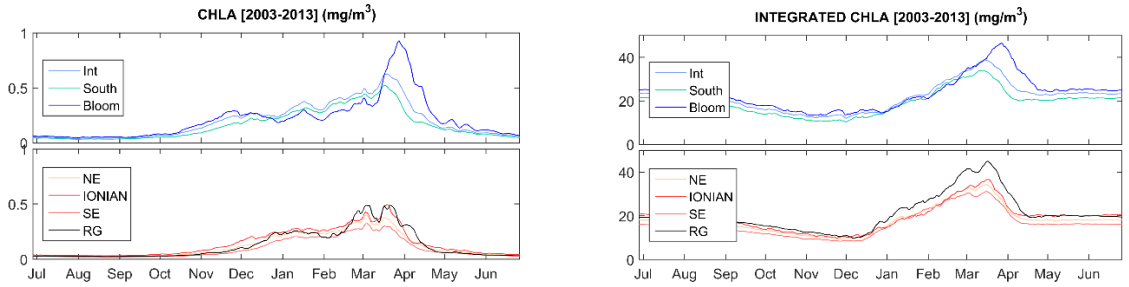

Figure 13: Time-series of surface and integrated chlorophyll climatologies by bioregion (colours mentioned in the maps Fig. 12).

3.3.1. Bloom like regime (group 1)

The first regime corresponds to the “Bloom Like” regime mostly localized in the Northern Gyre (northwestern sub-basin). It is characterized by a strong nutrient enrichment in the surface layer in winter, a temporary accumulation of nutrients in this layer and a huge spring bloom (Fig. 13). In this regime, the DCM disappears progressively starting from December during mixing events and appears again permanently in May (Fig. 14). During winters characterized by deep mixing, surface nutrient concentrations can reach the bottom values. In these cases, the efflorescence is delayed in March-April. The delay of the bloom is caused by winter phytoplankton growth inhibition at the surface caused itself by light limitation when vegetal cells are exported out of the photic layer. Fig.15 indicate that in the NW Bloom box the MLD is much deeper than the nutriclines both positioned at the same depth.

In this region, deep mixing exposes plankton cells and detritus to dilution and favors POC export in January and February. The carbon is also exported under dissolved form as explained by (Santinelli et al., 2010). .Winter particulate export is estimated around 25 $mgC.m^{-2}.d^{-1}$ on average with much higher values, in mesoscale structures. These values have the magnitude as the sediment traps measurements reported by (Martin et al., 2010). The weak plankton development in winter could appear in contradiction with the strong export of organic matter. First, a part of the winter export is due to the organic matter produced in the subsurface during autumn. Second, even if the surface biomass concentrations are weak, the depth-integrated biomasses are not negligible (Kessouri et al., in prep-c). Finally vertical mixing and large vertical velocities affecting the whole water column and associated to submesoscale processes in convective regimes favor the export.

In early spring, by the end of the deep mixing period, phytoplankton forms an intense bloom (Fig. 13). In some locations and for some years, chlorophyll concentrations reach more than 2 $mg.m^{-3}$ (not shown) and primary production exceeds 0.9 $gC.m^{-2}.d^{-1}$. We expect that the carbon export recorded in spring is associated to the sedimentation of the bloom of large cells. At the end of the bloom, nutriclines (N, P) deepen progressively, but remain vulnerable to occasional gales which characterize this transition period (Bernardello et al., 2012). These gales produce local nutrient enrichment (not shown). Globally, phytoplankton gradually consumes nutrients in the surface layer during one month approximately until depletion. The f-ratio represents the ratio of the new production on total production. The model indicates that the f-ratio in the NW region is in February and March the highest of the basin (after the Adriatic) which is consistent with the strong vertical inputs of nutrients.

Starting in May with the depletion of the surface layer, the DCM progressively deepens to reach its maximum depth in August at 60 m depth. Summer is the period where the f-ratio is minimum indicating the importance of the regenerated production to sustain the production in the DCM. Globally, the net primary production in the northwestern subbasin is not so negligible. The POC export is progressively declining but remains then not negligible. In autumn the DCM starts to rise progressively with the isopycnals between August and the end of November due to wind intensification episodes inducing

preconditioning of the northern gyre. The first wind storms inject nutrients in the MLD which progressively thickens. As a consequence the f-ratio increases. This period corresponds to the autumnal bloom.

3.3.2. No-bloom regime of the western basin (group 3)

The No-bloom regime of the western basin concerns the Algerian and Tyrrhenian subbasins. This region, with more than 200-250 $gC.m^{-2}.y^{-1}$, represents in our model the second most productive region of the Mediterranean Sea after the Alboran Sea. The group 3 regime is characterized by regular supplies of nutrient in the surface layer especially between December and February as indicated by the values of the f-ratio, without intense accumulation of nutrients in this layer coupled with a continuous consumption. However, as already discussed, our model does not reproduce correctly this feature as the surface chlorophyll maximum is found in March while the satellite climatology shows the maximum rather at the end of January, beginning of February (DR09). One explanation could be that the vertical injection of nutrients lasts too long (see intermediate values of the f-ratio in March).

This regime presents the less variable MLD and nutriclines evolutions in the whole Mediterranean (Fig. 14). Two periods emerge from the seasonal cycle:

The first period is the mixing season, from November to March. In both subbasins, the mixing starts during the first autumnal heat losses, from which the DCM begins to shallow. The DCM undergoes a fairly rapid surfacing and disappears in January during the efflorescence.

This regime presents properties close to the Atlantic subtropical gyre where the mixing is rapidly followed by a phytoplankton development. As the model shows, the MLD does not clearly exceed the epipelagic layer. On the other hand, the MLD is close to the nutriclines all along the winter. These characteristics are at the origin of the regular increase of the phytoplankton biomass synchronized with the nutrients inputs. However, it should be noted that the Algerian sub-basin is characterized in winter by the minimum f-ratio of the basin. The vertical input of nutrients seems therefore too low or too irregular to ensure the winter production which could then combine alternations of new and regenerated productions.

The simulation indicates that due to the duration of the efflorescence, the time-integrated productivity is high. A POC export maximum from February to April is associated to this production.

The second period corresponds to the stratified period between April and October. From April, the DCM starts deepening all over the sub-basins to reach in average 55 m depth in summer (Fig. 14). In the center of some local anticyclonic features of the Algerian basin where it could be deeper. Then the DCM remains stable until September. Subsurface water masses contain important phytoplankton concentrations (0.5 – 0.7 mg m^{-3}) forming a particularly thick DCM (not shown), as mentioned by Lavigne et al., (2015). The Algerian subbasin remains then productive in summer and autumn at subsurface

depths. The production is significant in this DCM as the simulated net primary production is 0.7 $gC.m^{-2}.d^{-1}$ (between 0.25 – 0.75 with different satellite based algorithms of primary production of Uitz et al., 2012). The f-ratio is at the minimum value of the basin, 0.18, meaning that 82% of the production is regenerated.

3.3.3. No-bloom regimes of the eastern basin (groups 4, 5, 6)

The eastern basin includes the No-bloom northeastern, southeastern and Ionian bioregions (Fig. 12). It is characterized by deep DCM in summer and weak nitrate supply to the surface. Deep nutrient concentrations are 40% less important than in the western basin.

Two main periods are distinguishable (winter and summer).

In winter, phytoplankton blooming depends on phosphacline depth pierced during mixing events as mentioned by (Lazzari et al., 2012). As shown in Fig. 14, MLD exceeds the phosphacline depths over short periods in February and March for groups 4 and 5. In the no-bloom southeastern regime (group 6), the averaged MLD is never located under the top of the phosphacline. These regimes display low primary production at the beginning of winter. The model overestimates it with values generally in the range 0.45 – 0.55 $gC.m^{-2}.d^{-1}$ between January and March while (Uitz et al., 2012) gave estimates between 0.15 and 0.45. Like in the western no-bloom regime, vertical mixing allows a weak enrichment by nutrients to maintain subsurface phytoplankton production. The new production represents 40 to 50 % of the total production at this period.

During the stratified period, in summer, the DCM reaches its maximum depth. The DCM depth is increasing from west to east. Maximum depth (120 m) is found in the Levantine Sea in August and September (Figs. 8 & 14). Chlorophyll concentration in the DCM is low and decreases from spring to summer from 0.4 to 0.25 mg m^{-3} (Fig. 8). The regenerated production represents about 80% of the total production.

In the no-bloom regimes of the Eastern basin, phosphacline gradually deepens related to the nitracline towards the east. The maximum difference between the phosphacline and nitracline can reach 48 m in the Levantine Sea in February and March. This sub-basin presents the poorest surface and subsurface waters of the Mediterranean in terms of nutrients concentrations and biological activity.

3.3.4. The Intermittent/Intermediate regime (group 2)

This regime characterizes waters surrounding the deep convection area of the northwest Mediterranean as well as regions with moderate to strong mixing (Bonifacio gyre, Adriatic) and stratified regions of the Alboran Sea. The first category is characterized by permanent currents associated to density fronts, as the Northern Current, the North Balearic front where winter mixing can reach 200 m. In the north Alboran Sea, the MLD is shallow all over the year but the vertical dynamics

promoting nutrient enrichment is strong at the periphery of the permanent mesoscale features. Such a variety of regions in this cluster has been also highlighted by DR09.

The common point to these regions is probably an enrichment which is intermediate between the bloom and the no-bloom regimes. This is clear on Fig. 14 where the MLD is significantly deeper than the nutriclines during winter while, first, in the no-bloom regions these interfaces are closer from each other, and, second, in the bloom region, the difference is much larger. Another consequence is that the MLD is generally not deep enough to inhibit production (the southern Adriatic should be an exception). Whatever the injection of nutrients is done by convection (Adriatic) or by frontal dynamics (NW and north frontal zone of the Alboran Sea) with immediate consumption. In the first case, the MLD is significantly deeper than in the second one, and in the second case, the frontal dynamics allows to inject nutrients directly in the MLD.

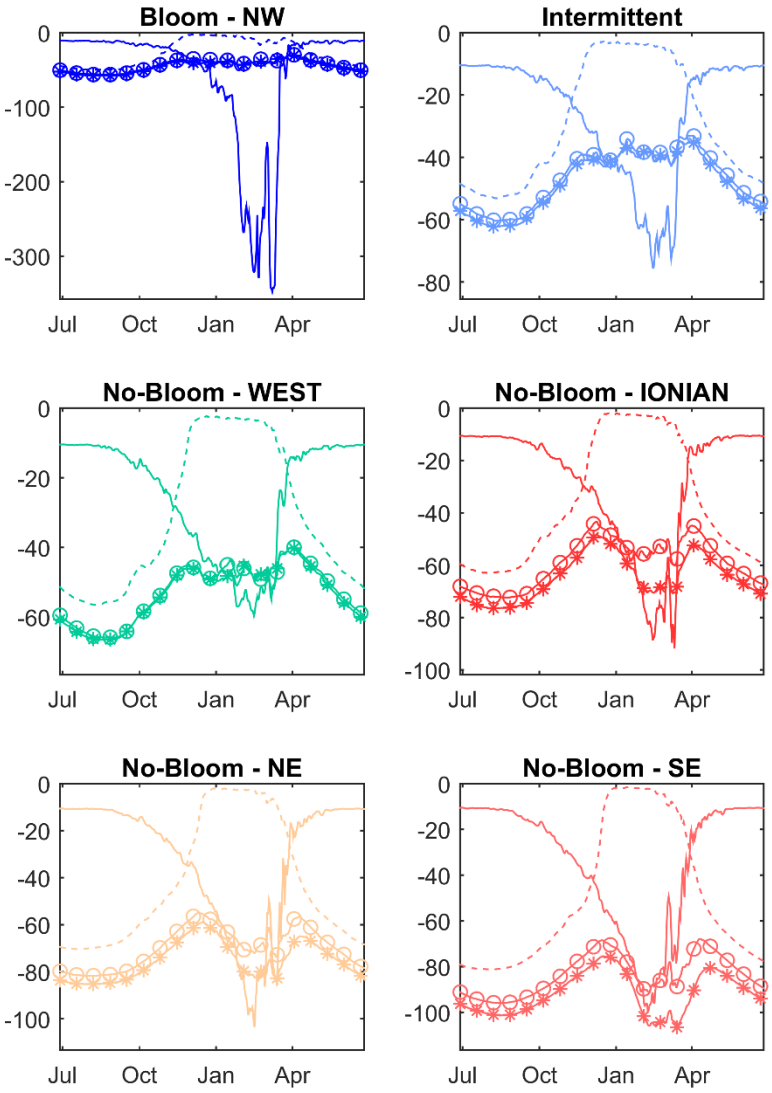

Figure 14: Climatological time-series of MLD (solid line), DCM (dashed line), nitracline (circles) and phosphacline (stars) by region. Colors are mentioned in Figure 13.

However, it can be noted an important difference between the two types of regions forming this group. In the “mixing” regions like the Adriatic, the primary production is apparently lower than in the frontal regions (see Alboran) but a larger part of this production is attributed to new production (maximum f-ratio of 0.66 in February in the Adriatic and only 0.39 in January in Alboran).

The Alboran Sea is very particular. It is the most productive region of the Mediterranean Sea with over 400 $gC.m^{-2}.y^{-1}$. Some regions of this basin are the most productive area of the Mediterranean Sea (Fig. 10), because a high vertical dynamics exist and thus very high NPP is

registered every winter in the frontal zone, which is a fine area close to the Spanish coast. According to the classification of (D'Ortenzio and Ribera d'Alcalà, 2009) a northern part of this area could be considered as a "Bloom-like" regime. If we take a comparison to the south, inside the western anticyclonic gyre (WAG), this part is slightly less productive and following our classification, it is considered bio-geochemically too close to the eastern regimes with low production and deep nutriclines (Fig. 12). These remarks are consistent with the time series of (Uitz et al., 2012). All over the year, frontal area in the north is demarcated from the southern part in terms of PPN. POC export is maintained at high values around 15 $mgC.m^{-2}.d^{-1}$ all over the year inside the frontal zone with some pics in winter as higher as those of the NWMed.

The Alboran Sea frontal zone DCM cycle presents two periods. First, between May and October, where the new production inside the DCM is constantly fed by nutrients upwelling. This dynamic is comparable to upwelling zones of Atlantic Subtropical Ocean (Eppley et al., 1981) characterized by winter unimodal chlorophyll profiles (Herbland 1983) or HSC (Lavigne et al 2015) representing maximum chlorophyll at the surface, surrounded by less productive water categorized by "Karabashev" (Herbland, 1983) or "Complex" (Lavigne et al., 2015) chlorophyll profile shape with highly significant values (> 0.4 mg/m3) by 40-50 meters. At the same time, constant presence of 500 to 650 $mMolN.m^{-2}$ inside the epipelagic layer. During the second part of the year, between November and April, nitrate amount inside the epipelagic layer stays maintained at higher values.

3.4. Nitrogen and phosphorus dynamics in the Mediterranean Sea

3.4.1. Biogeochemical processes

The processes involved in the nitrogen and phosphorus cycles are highlighted within the passage from organic to inorganic forms and vice versa through excretion of inorganic matter and uptake of inorganic matter. In the model, the excretion of inorganic matter is done by heterotrophs (zooplankton and bacteria) and the absorption of inorganic matter is done by autotrophs and bacteria.

We have divided the western and eastern sub-basins in two layers, surface [0-200m] and deep layer [200m-bottom] and thereby averaging the biogeochemical flux on the ten years of simulation [2003 - 2013].

The result shows that in the western surface layer, organic matter is produced by uptake of nutrients in amounts of 4.1772 10^{12} $molN.y^{-1}$ and 1.7382 10^{11} $molP.y^{-1}$ while nutrients excretion is weaker with 4.0961 10^{12} $molN.y^{-1}$ and 1.698_10^{11} $molP.y^{-1}$. The budget of these two processes is about 2% of the value of the individual processes. In the deep layer, the nutrients uptake are considerably lower (5.8122 10^{8} $molN.y^{-1}$ and 4.6760 10^{7} $molP.y^{-1}$) while the nutrients excretion is two orders of magnitude lower than in the surface layer (5.9487 10^{10} $molN.y^{-1}$ and 4.1017 10^{9} $molP.y^{-1}$).

Organic matter production is then larger than nutrients excretion in the western basin by +23 10^9 molN.y^{-1} and 2.7 10^7 molP.y^{-1}.

In the eastern basin, the uptake of nutrients is 7.4625 10^{12} molN.y^{-1} and 1.8091 10^{11} molP.y^{-1} in the surface layer while the nutrients excretion is 7.3395 10^{12} molN.y^{-1} and 1.7349 10^{11} molP.y^{-1}. In the deep layer, the uptake is 4.9147 10^9 molN.y^{-1} and 3.6898 10^8 molP.y^{-1} while deep nutrients excretion is 1.7299 10^{11} molN.y^{-1} and 1.1241 10^{10} molP.y^{-1}. The functioning of the eastern basin is opposite to the one of the western basin. Nutrients excretion is larger than organic matter production. This can be explained by a stronger export of organic matter under 200 m (196 10^9 molN.y^{-1} in the eastern sub-basin vs 70 molN.y^{-1} in the western sub-basin), and a lower import of inorganic matter in the surface layer related to organic matter export (50 % in the eastern vs 87 % in the western). An excess of inorganic matter is then produced and a part is exported to the western basin. Figures 16 and 17 present the net budget of nitrogen and phosphorus for each basin.

3.4.2. Fluxes at the straits

Horizontal organic and inorganic fluxes across Gibraltar Strait (GS) and Sicilian Strait (SS) have been extracted daily from the model, then averaged between June 2003 and June 2013. At the GS, the model shows a deep outflow of 0.735 Sv and a surface inflow of 0.782 Sv. Net inorganic matter outflow to the Atlantic is equal to 142 10^9 molN.y^{-1} and 6.6 10^9 molP.y^{-1}. This estimation is very close to the one of Huertas et al. (2012) based on observations with 139 10^9 molN.y^{-1} and 4.8 10^9 molP.y^{-1}. This budget consists of a deep outflow of inorganic matter of 174 10^9 molN.y^{-1} and 6.6 10^9 molP.y^{-1} and a surface inflow of 34 10^9 molN.y^{-1} and 1.53 10^9 molP.y^{-1}. The surface inflow is nevertheless questionable, as nutrients have been forced at 7°W (125 km from GS) using WOA09 monthly climatologies. The nutrients at the surface coming from the Atlantic support the productivity of the Alboran Sea. Nitrate represents 95% of the total inorganic nitrogen flux while ammonium represents 5%. Concerning the organic form, the net inflow at Gibraltar is estimated to 73 10^9 molN.y^{-1} and 6.3 10^9 molP.y^{-1}.

Because of the contrasted biogeochemical functioning of the two basins, important exchanges of inorganic and organic matter take place at the SS between the eastern and western basins (see chlorophyll at longitude~11°E in Fig. 7). A deep flow directed from the east to the west of 1.0055 Sv is the main vector of a net nutrient flux of 86 10^9 molN.y^{-1} and 3.88 10^9 molP.y^{-1}, close to the estimations of Huertas et al. (2012) of 92 10^9 molN.y^{-1} and 4.1 10^9 molP.y^{-1}. The surface eastward flow of 0.9508 Sv is enriched in organic matter and is the main vector of the net eastward flux of 78 10^9 molN.y^{-1} and 4 10^9 molP.y^{-1}.

3.4.3. The global budget

Before discussing the budget, the evolution of the nutrients stocks is important to judge of the model stability. Compared to the state of 2003, the inorganic nitrogen in 2013 presents a mean deficit of 36 10^9 molN.y^{-1} in the western basin and a gain of 38 10^9 molN.y^{-1} in the eastern basin, while the total stock is equal to about 1.1043 10^{13} molN in the western basin and

1.1268 10^{13} molN in the eastern basin. This annual variation represents 0.3% of the stock of each sub-basin and is very low for the entire basin. The accumulation of nutrients in the eastern basin and the deficit in the western basin may have different combined causes. A too high export of organic matter from the western basin to the eastern basin due to an incorrect positioning of the depths of remineralization of organic matter, itself a compromise between the sedimentation velocity of organic matter and its decomposition rate could be a good candidate. This is compatible with the loss of nutrients in the western basin which affects the [300 - 1200 m] layer (not shown) while the accumulation in the eastern basin affects the [130 - 400 m] layer. On the other hand, biases in the general circulation including the exchanges at the straits and convection intensity could also participate to this imbalance. We can finally note that the subsurface accumulation of nutrients to the east could be responsible of the too high production suggested by the comparison of chlorophyll with satellite (Fig. 4).

Despite these imbalances, some conclusions can be drawn from this budget.

The western basin is more productive than the eastern one as long as the uptake and the excretion rate by surface unit are compared. The simulated uptake is 5.22 and 4.66 molN.m^{-2}.y^{-1} for the western and eastern basins respectively while the excretion is 5.1 and 4.59 molN.m^{-2}.y^{-1}.

The western basin seems to be responsible of a large transfer of organic matter to the eastern basin (even if it could be overestimated as discussed above). A large flux of organic matter entering into the western basin has been found throughout the Gibraltar Strait representing half the outflow of inorganic nitrogen and the total outflow of inorganic phosphorus. This imbalance of these two elements reflects the increase of the N:P ratio along the path of the water in the Mediterranean basin. Besides, the inorganic matter flux from the eastern basin to the western basin has been found equal to 60% of the outflow to the Atlantic meaning that the western basin contributes by 40% to the outflow at Gibraltar.

In our simulation, the amount of nutrients coming from the rivers (Ludwig et al., 2010) and Black Sea (Tugrul et al., 2002) is estimated equal to 47 % (23 %) of the inorganic nitrogen (resp. phosphorus) exported throughout Gibraltar, which gives to the river inputs an important role in the global budget of the Mediterranean Sea. Finally, atmospheric inputs are not negligible in the global budget of the Mediterranean.

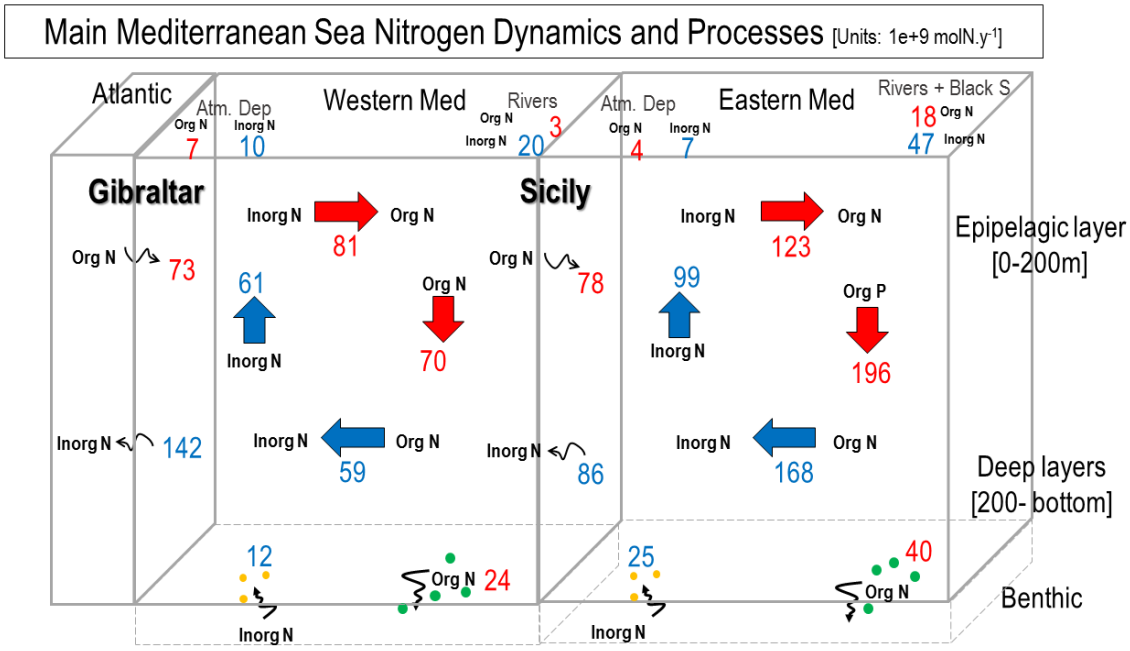

Figure 16: Mediterranean nitrogen cycle. **Org** represents the organic matter and **Inorg** represents the inorganic matter amount. Only the net biogeochemical flux is given. Unit: 10^9 molN.y^{-1}.

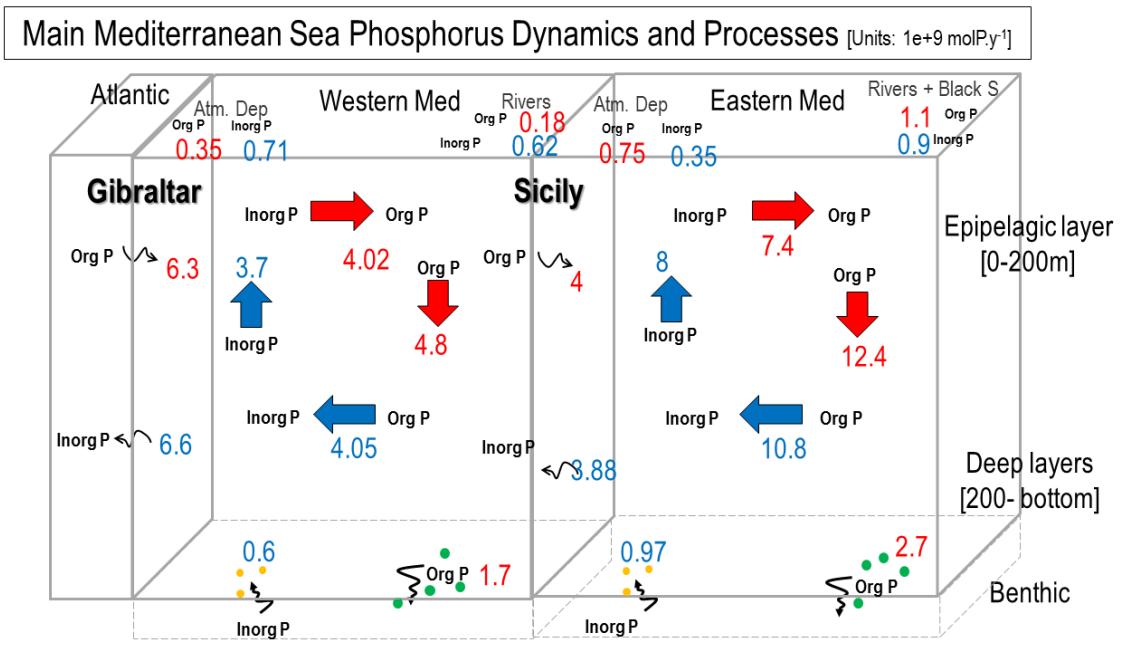

Figure 16: Mediterranean phosphorus cycle. **Org** represents the organic matter and **Inorg** represents the inorganic matter amount. Unit: 10^9 molP.y^{-1}.

Uncertainties should therefore be reduced regarding rivers inputs and atmospheric deposition. Indeed, atmospheric deposition used in the model comes from the lowest average basin scale and yearly estimations of (Ribera d'Alcalà, 2003). Improvement should be applied for future applications not only for the total deposition but also concerning the spatial

heterogeneity of the deposits and their timing as these inputs are highly intermittent. In the same way, the discharge and the nutrients concentration in a large number of rivers of the Mediterranean are poorly known.

Nutrients deposition play an important role on the surface concerning the new primary production by direct uptake (Loye-Pilot et al, 1993; Kouvarakis et al, 2001; Herut et al, 2002; Kocak et al, 2015). Add to that, in situ experiments (Guieu et al., 2014a) showed another way of nutrient utilization, which consists on a temporal fortification of the bacterial activity at the surface water.

4. Conclusion and perspectives

A 3D physical/biogeochemical modeling have been carried out over a 13-year period to study the impact of hydrodynamic processes on the plankton ecosystem dynamics in the Mediterranean basin. The biogeochemical model previously used to study the planktonic functioning in the north-western region has been re-calibrated to represent the different regimes present in the whole basin. The model results have been confronted to various datasets (MODIS satellite images, BOUM cruise in situ observations). The comparisons of model results with observations shows the ability of the model to correctly represent (1) the spatial variation of nutrient profiles across the basin in summer, (2) the general temporal evolution of surface chlorophyll in the different open sea regions of the basin, despite an overestimation of the efflorescence in March in oligotrophic eastern regions, and (3) the spatial variations of magnitude and depth of DCM across the basin in summer.

Climatologies of MLD and biogeochemical variables and fluxes have been presented and helps to confirm results of previous modeling experiments (Lazzari et al., 2012, Macias et al., 2014):

- The southwestern subbasin is annually the most productive area of the open sea region of the basin. However, during spring season, the northwestern subbasin appears the most productive region. This production is based on new production due to vertical import of a huge amount of nutrients into the surface layer during deep convection.

- The development of a DCM in summer.

- Summer is more appropriate for microbial cycle which represents the other role in productivity by remineralization of the organic matter at the DCM depths.

- The Mediterranean is heterogeneous in terms of trophic regime: the Eastern basin appears oligotrophic, and a large part of the western basin is mesotrophic.

In this study a new cluster of Mediterranean Sea regions has been proposed based on surface and vertical biogeochemical properties in order to complete the previous clusters and descriptions of the biogeochemical functioning of the bio-regions constituting the Mediterranean Sea (Longhurst, 1995, D'Ortenzio et al., 2009 and Lazzari et al., 2014).

We have described four different regimes. DCM, nutriclines, their intensity and decoupling, primary production and associated carbon export evolution are specific for each regime.

Finally, a budget of nutrients (N and P) has been performed on the whole basin. It show that

- Cycling and transformation are the main driven processes for the nutrients cycles (Huertas et al., 2012), quantification have been extracted from our model during the last decade.

- The rivers discharge controls the productivity (Macias et al., 2014) with other external inputs such as atmospheric deposition which have local roles (Guieu et al., 2014), allow also the annual stability of the model. Indeed, their cumulative annual amount represents 50% of the exported flux of nutrients into the Atlantic across Gibraltar Straits.

Although the model represents reasonably well the global functioning of the Mediterranean Sea regions, the present results suffer from certain deficiencies.

Microbial loops are a lack for most biogeochemical models from the moment they did not separate different type of bacteria over the water column. Add to that, the good representation of the LIW which represents the water mass concerned by the remineralization, its formation in the eastern subbasins needs to be well modeled. An implementation of nested very high resolution models to represent well the high dynamics which characterize the deep and intermediate convection.

The nitrogen balance shows the important role of the benthic coupling in terms of global budget. Remineralization process is very intense mainly in coastal environment and impact on the nutrient supply in the deep water masses. The balance of the model depends on the contributions of rivers outputs and atmospheric deposits of biogenic matter.

The sensitivity of the response of the ecosystem is very vulnerable for phytoplankton dynamics in the subsurface depths, where the biological activity and mesoscale dynamics are intensified. It is true mainly in oligotrophic region. For this, circulation model and parameterization of the vertical speed could be improved in our coupling in order to work on understanding the dome shape we saw in the chlorophyll time series in the south-eastern basin particularly. Understanding the eastern basin variability is a complicated challenge and may need specific submesoscale modelling.

References:

- Auger, P. a., Diaz, F., Ulses, C., Estournel, C., Neveux, J., Joux, F., Pujo-Pay, M. and Naudin, J. J.: Functioning of the planktonic ecosystem on the Gulf of Lions shelf (NW Mediterranean) during spring and its impact on the carbon deposition: A field data and 3-D modelling combined approach, Biogeosciences, 8(11), 3231–3261, doi:10.5194/bg-8-3231-2011, 2011.

- Auger, P. a., Ulses, C., Estournel, C., Stemmann, L., Somot, S. and Diaz, F.: Interannual control of plankton communities by deep winter mixing and prey/predator interactions in the NW Mediterranean: Results from a 30-year 3D modeling study, Prog. Oceanogr., 124, 12–27, doi:10.1016/j.pocean.2014.04.004, 2014.
- Béthoux, J. P.: Oxygen consumption, new production, vertical advection and environmental evolution in the Mediterranean Sea, Deep Sea Res. Part A. Oceanogr. Res. Pap., 36(5), 769–781, doi:10.1016/0198-0149(89)90150-7, 1989.
- Béthoux JP and Copin-Montégut G. Biological fixation of atmospheric nitrogen in the Mediterranean Sea. Limnol. Oceanogr. ;(United States), 31(6), 1986.
- Béthoux, J. P., Gentili, B. et Tailliez, D.: Warming and freshwater budget change in the Mediterranean since the 1940s, their possible relation to the greenhouse effect. Geophys. Res. Lett., 25(7), 1023-1026, 1998.
- Copin-Montégut, G. et Avril, B.: Vertical distribution and temporal variation of dissolved organic carbon in the north-western Mediterranean Sea, Deep-Sea Res. PT 1, 40(10), 1963-1972, 1993.
- Crise, a., Crispi, G. and Mauri, E.: A seasonal three-dimensional study of the nitrogen cycle in the Mediterranean Sea Part I. Model implementation and numerical results, J. Mar. Syst., 18(1-3), 287–312, doi:10.1016/S0924-7963(98)00016-5, 1998.
- Crispi, G., Crise, a. and Mauri, E.: A seasonal three-dimensional study of the nitrogen cycle in the Mediterranean Sea: Part II. Verification of the energy constrained trophic model, J. Mar. Syst., 20(1-4), 357–379, doi:10.1016/S0924-7963(98)00085-2, 1999.
- D'Ortenzio, F., S. Le Reste, H. Lavigne, F. Besson, H. Claustre, L. Coppola, A. Dufour, V. 1050 Dutreuil, A. Laes, and E. Leymarie (2012), Autonomously profiling the nitrate concentrations 1051 in the ocean: the Pronuts project, Mercator Ocean–CORIOLIS Quarterly Newsletter(45), 8-11.
- D'Ortenzio, F. and Ribera d'Alcalà, M.: On the trophic regimes of the Mediterranean Sea: a satellite analysis, Biogeosciences Discuss., 5(4), 2959–2983, doi:10.5194/bgd-5-2959-2008, 2009.
- Friedrichs et al., Assessing the uncertainties of model estimates of primary productivity in the tropical Pacific Ocean. Journal of Marine Systems 76 (2009) 113–133. doi:10.1016/j.jmarsys.2008.05.010.
- Grignon, L., Smeed, D.A., Bryden, H.L., Schroeder, K., 2010. Importance of the variability of hydrographic preconditioning for deep convection in the Gulf of Lion, NW Mediterranean. Ocean Science 6, 573–586.
- Guieu, C., Ridame, C., Pulido-Villena, E., Bressac, M., Desboeufs, and Dulac,. Dust deposition in an oligotrophic marine environment: impact on the carbon budget. Biogeosciences Discussions, 11(1) : 1707–1738, 2014. doi : 10.5194/bgd-11-1707-2014. URL http://www.biogeosciences-discuss.net/11/1707/2014/.
- Hamon. M, Beuvier. J, Somot. S, M. Lellouche .J.M. , Greiner. E, Jordà. G , Bouin. M.N , Arsouze. T, Béranger. K, Sevault. F, Dubois. C, Drevillon. M, and Drillet. Y. Design and validation of MEDRYS, a Mediterranean Sea reanalysis over 1992–2013. Sci. In revision.

- Herbland, .A., Le Borgne. R., Le Bouteiller, A., Voituriez, B. (1983). Structure hydrologique et production primaire dans l'Atlantique tropical oriental Oceanogr Trop. 17: 15-25
- Herrmann, M., Sevault, F., Beuvier, J. and Somot, S.: What induced the exceptional 2005 convection event in the northwestern Mediterranean basin? Answers from a modeling study, J. Geophys. Res. Ocean., 115(12), 1–19, doi:10.1029/2010JC006162, 2010.
- Herrmann, M., Diaz, F., Estournel, C., Marsaleix, P., Ulses, C. Impact of atmospheric and oceanic interannual variability on the Northwestern Mediterranean Sea pelagic planktonic ecosystem and associated carbon cycle. Journal of Geophysical Research – Oceans 118, 5792–5813. 2013
- Herut, B., Collier, R., Krom, M. D., 2002 : The role of dust in supplying nitrogen and phosphorus to the Southeast Mediterranean. Limnology and Oceanorgraphy, 47, 870-878.
- Houpert, L., Testor, P., Madron, X. D. De, Somot, S. and Ortenzio, F. D.: Seasonal cycle of the mixed layer depth , of the seasonal thermocline and of the upper-ocean heat rate in the Mediterranean Sea : an observational approach, Geophys. Res. Abstr., 16, 15100, doi:10.1016/j.pocean.2014.11.004, 2014.
- Huertas, I. E., Ríos, a. F., García-Lafuente, J., Navarro, G., Makaoui, a., Sánchez-Román, a., Rodriguez-Galvez, S., Orbi, a., Ruíz, J. and Pérez, F. F.: Atlantic forcing of the Mediterranean oligotrophy, Global Biogeochem. Cycles, 26(2), n/a–n/a, doi:10.1029/2011GB004167, 2012.
- Lavezza, R., Dubroca, L., Conversano, F., Iudicone, D., Kress, N. and Herut, B.: MED – Nut , a new Quality Controlled nutrient data base for the Mediterranean Sea, , (November), 1–42, doi:10.1594/PANGAEA.771907.1, 2011.
- Lavigne, H., D'Ortenzio, F., Ribera D'Alcalà, M., Claustre, H., Sauzède, R. and Gacic, M.: On the vertical distribution of the chlorophyll a concentration in the Mediterranean Sea: a basin scale and seasonal approach, Biogeosciences Discuss., 12(5), 4139–4181, doi:10.5194/bgd-12-4139-2015, 2015.
- Lavigne, H., F. D'Ortenzio, C. Migon, H. Claustre, P. Testor, M. R. d'Alcalà, R. Lavezza, L. 1156 Houpert, and L. Prieur (2013), Enhancing the comprehension of mixed layer depth control on 1157 the Mediterranean phytoplankton phenology, Journal of Geophysical Research: Oceans, 1158 118(7), 3416-3430, doi:10.1002/jgrc.20251.
- Kessouri et al., Phytoplankton dynamics and biogeochemical fluxes in the western Mediterranean Sea using a 3D physical/biogeochemical coupled model (In prep-c).
- Koçak M.,: Solubility of Atmospheric Nutrients over the Eastern Mediterranean: Comparison between Pure-Water and Sea-Water, Implications Regarding Marine Production, Turk. J. Fish. Aquat., Sci. 15: 59-71. 2015.
- Kouvarakis, G., Mihalopoulos, N., Tselepides, A.,Stavrakaki, S., 2001 : On the importance of atmospheric inputs of inorganic nitrogen species on the productivity of the eastern Mediterranean Sea. Global Biogeochemical Cycles, 15.
- Lazzari, P., Solidoro, C., Ibello, V., Salon, S., Teruzzi, a., Béranger, K., Colella, S. and Crise, a.: Seasonal and inter-annual variability of plankton chlorophyll and primary production in the Mediterranean Sea: A modelling approach, Biogeosciences, 9(1), 217–233, doi:10.5194/bg-9-217-2012, 2012.

- Longhurst, a.: Seasonal cycles of pelagic production and consumption, Prog. Oceanogr., 36(2), 77–167, doi:10.1016/0079-6611(95)00015-1, 1995.
- Loye-Pilot, M.D., Klein, C. and Martin, J.M., 1993 : Major inorganic elements in north western Mediterranean aerosols: Concentrations and sources, Estimation of dry deposition of soluble inorganic nitrogen, in Water Pollution Reports, edited by J.M. Martin and H. Barth, Rep. 20, pp. 271-277, Eur. Union, Brussels
- Ludwig, W., Bouwman, a. F., Dumont, E. and Lespinas, F.: Water and nutrient fluxes from major Mediterranean and Black Sea rivers: Past and future trends and their implications for the basin-scale budgets, Global Biogeochem. Cycles, 24(4), 1–14, doi:10.1029/2009GB003594, 2010.
- Macías, D., Stips, A. and Garcia-Gorriz, E.: The relevance of deep chlorophyll maximum in the open Mediterranean Sea evaluated through 3D hydrodynamic-biogeochemical coupled simulations, Ecol. Modell., 281, 26–37, doi:10.1016/j.ecolmodel.2014.03.002, 2014.
- Martin J., Miquel J.C., Khripounoff. A. Impact of open sea deep convection on sediment remobilization in the western Mediterranean. Geophy. Res. Lett. doi:10.1029/2010GL043704, 2010.
- Mignot, A., Claustre, H., Uitz, J., Poteau, A., D'Ortenzio, F., and Xing, X.: Understanding the seasonal dynamics of phytoplankton biomass and the deep chlorophyll maximum in oligotrophic environments: a Bio-Argo float investigation, Global Biogeochem. Cy., 28, 856–876, 2014.
- Millot, C.: Circulation in the Western Mediterranean Sea, J. Mar. Syst., 20(1-4), 423–442 [online] Available from: http://linkinghub.elsevier.com/retrieve/pii/S0924796398000785, 1999.
- Millot, C.: Circulation in the Mediterranean Sea: evidences, debates and unanswered questions, Sci. Mar., 69(June), 5–21, doi:10.3989/scimar.2005.69s15, 2005.
- Moutin, T. and Prieur, L.: Influence of anticyclonic eddies on the Biogeochemistry from the Oligotrophic to the Ultraoligotrophic Mediterranean(BOUM cruise), Biogeosciences [online] Available from: http://biogeosciences.net/9/3827/2012/bg-9-3827-2012.pdf (Accessed 3 April 2013), 2012.
- Pujo-Pay, M., Conan, P., Oriol, L., Cornet-Barthaux, V., Falco, C., Ghiglione, J. F., Goyet, C., Moutin, T. and Prieur, L.: Integrated survey of elemental stoichiometry (C, N, P) from the western to eastern Mediterranean Sea, Biogeosciences, 8(4), 883–899, doi:10.5194/bg-8-883-2011, 2011.
- Renault, L., Oguz, T., Pascual, a., Vizoso, G. and Tintore, J.: Surface circulation in the Alborn Sea (western Mediterranean) inferred from remotely sensed data, J. Geophys. Res. Ocean., 117(8), 1–11, doi:10.1029/2011JC007659, 2012.
- Ribera d'Alcalà, M.: Nutrient ratios and fluxes hint at overlooked processes in the Mediterranean Sea, J. Geophys. Res., 108(C9), doi:10.1029/2002JC001650, 2003.
- Rixen, M., Beckers, J. M., Levitus, S., Antonov, J., Boyer, T., Maillard, C., Fichaut, M., Balopoulos, E., Iona, S., Dooley, H., Garcia, M. J., Manca, B., Giorgetti, a., Manzella, G., Mikhailov, N., Pinardi, N. and Zavatarelli, M.: The Western

Mediterranean Deep Water: A proxy for climate change, Geophys. Res. Lett., 32(12), 1–4, doi:10.1029/2005GL022702, 2005.

- Sanchez-Vidal, A., Pasqual, C., Kerhervé, P., Calafat, a., Heussner, S., Palanques, a., Durrieu de Madron, X., Canals, M. and Puig, P.: Impact of dense shelf water cascading on the transfer of organic matter to the deep western Mediterranean basin, Geophys. Res. Lett., 35(5), 1–5, doi:10.1029/2007GL032825, 2008.
- Santinelli, C., Nannicini, L. and Seritti, A.: DOC dynamics in the meso and bathypelagic layers of the Mediterranean Sea, Deep. Res. Part II Top. Stud. Oceanogr., 57(16), 1446–1459, doi:10.1016/j.dsr2.2010.02.014, 2010.
- Severin, T., Conan, P., Durrieu De Madron, X., Houpert, L., Oliver, M. J., Oriol, L., Caparros, J. and Pujo-Pay, M.: Impact of open-ocean convection on nutrient, phytoplankton biomass and activity, Deep Sea Res. Part I Oceanogr. Res. Pap., Submitted, 62–71, doi:10.1016/j.dsr.2014.07.015, 2014.
- Soetaert, K., Herman, P. M. J., Middelburg, J. J., Heip, C., Smith, C. L., Tett, P. and Wild-Allen, K.: Numerical modelling of the shelf break ecosystem: Reproducing benthic and pelagic measurements, Deep. Res. Part II Top. Stud. Oceanogr., 48(14-15), 3141–3177, doi:10.1016/S0967-0645(01)00035-2, 2001.
- Tuğrul, S., Beşiktepe, Ş. T. and Salihoğlu, I.: Nutrient exchange fluxes between the Aegean and Black Seas through the marmara sea, Mediterr. Mar. Sci., 3(1), 33–42, doi:10.12681/mms.256, 2002.
- Uitz, J., Claustre, H., Morel, A., Hooker, S.B., 2006. Vertical distribution of phytoplankton communities in open ocean: An assessment based on surface chlorophyll. J. Geophys. Res. 111. doi:10.1029/2005JC003207.
- Wanninkhof, R. and McGillis, W. R.: A cubic relationship between air-sea CO2 exchange and wind speed, Geophys. Res. Lett., 26(13), 1889–1892, doi:10.1029/1999GL900363, 1999.

Title: Nitrogen and phosphorus cycles in the western Mediterranean Sea using high resolution modeling: Processes and budget

Table des matières

1. Introduction 75
2. Method 77
2.1. Observations 77
2.2. Modelling 78
2.2.1. Hydrodynamics 78
2.2.2. Biogeochemistry 79
2.2.3. Initial and boundary conditions 80
2.2.4. Derived variables 80
3. Results and discussion 80
3.1. Evaluation of the simulation 80
3.1.1. Surface chlorophyll 80
3.1.2. Horizontal and vertical biogeochemical patterns in winter and spring 81
3.1.3. Variability between April and September 2013 84
3.1.4. Annual cycle of the nutrients stocks 85
3.2. Atmospheric forcing and hydrology 86
3.3. Consequences of hydrological variability on biogeochemical processes and stoichiometry 87
3.3.1. Autumn 89
3.3.2. Winter 90
3.3.3. Spring 91
3.3.4. Summer 92
3.4. Budget of the nitrogen and phosphorus in the northwestern Mediterranean basin 93
4. Conclusion 95
5. References 103

Authors:

F. Kessouri[1], C. Estournel[1], C. Ulses[1], P. Marsaleix[1], and DeWEx Groups

[1] Laboratoire d'Aérologie, UMR 5560 CNRS, Université de Toulouse 3, 14 avenue Edouard Belin, 31400 Toulouse, France

Key points up to three (<100 characters)

- Seasonality of nutrients (nitrate, phosphate) concentrations

- Deep convection
- Phytoplankton bloom
- New and regenerated production
- Budget and nutrient vertical and horizontal fluxes
- Stoichiometry

Abstract

The aim of the DeWEX project is to understand the biogeochemical functioning of the North-Western Mediterranean Sea, the only region in the whole Mediterranean Sea with a marked "spring bloom" behavior related to the winter dense water formation characterizing this area. The data set collected by several cruises spread over one year (summer 2012 to summer 2013) was used to calibrate and validate a multi-element biogeochemical model forced by a 1 km resolution hydrodynamical model of the western Mediterranean Sea. As a first step, the simulation was validated using satellite derived chlorophyll and in situ nutrients observations. The nitrogen and phosphorus seasonal cycles are analyzed following two complementary directions. The first direction is the temporal variability of the stoichiometry in the dense water formation area. Biogeochemical and physical processes impacting the distribution of inorganic nitrogen and phosphorus were quantified. The different processes responsible for the stoichiometric variability at the seasonal scale were then disentangled. Autumnal and spring blooms tend to counter mixing and convection effects. Indeed, while the convective deepening of the mixed layer reduces the N:P ratio of surface waters (N:P ratio = 22:1), strong consumption by phytoplankton increases the ratio up to 30:1. The second direction is the quantification of nitrogen and phosphorus budgets within the surface layer of the deep convection area. At the annual scale, the exchanges of nitrate and phosphate with the peripheric regions are nil. More generally, the horizontal export of nitrogen (ammonium export higher than organic matter import) balances vertical inflow coming from deeper layers (nitrate import higher than organic matter export). As far as phosphorus is concerned, vertical import of phosphate is quasi balanced by organic matter export. Last, the nitrate based new production, as an annual average, is responsible for 22 to 47% of the total production.

1. Introduction : **Nitrogen and phosphorus cycles in the western Mediterranean Sea using high resolution modeling: Processes and budget**

The winter climate of the North-western Mediterranean Sea (NW Med) is characterized by cold and dry local winds blowing from the north and inducing high evaporation and cooling of the sea surface layer, at the origin of open sea convection process. This process induces the formation of intermediate and deep water masses in the north-western basin (Medoc Group, 1970), the south Adriatic (Pollak et al, 1951), the Aegean (Nittis et al., 2003) and the Rhodes Gyre (Ovchinnikov et al, 1984). In the NW Med, the cold Mistral and Tramontane winds are at the origin of oceanic heat losses which promote convection with strong

interannual variability (Mertens and Schott, 1998). When reaching the seafloor, the NW Med Open Ocean Deep Convection is responsible for the formation of the deep water of the western basin.

Medoc Group (1970) gave the first description of the three phases of the deep water formation in the NM Med: (i) preconditioning, characterized by the northern gyre cyclonic circulation which creates an isopycnal dome; (ii) formation of convective plumes which mix the water column over the preconditioned site; and (iii) sinking and spreading of the newly formed waters. Since early 90's, Tchernia and Gamberoni (1985) then Bethoux et al., (1990) have mentioned that climate change impacts deep water masses characteristics. These long-term changes are superimposed to larger variations occurring at interannual and decadal scales (Schroeder et al., 2013). For example, the Western Mediterranean Transient, an abrupt increase of the heat and salt content in the deep waters of the western basin, had been related to the combination of the severe winter 2005 and a salt and heat accumulation in the intermediate levels, due to the arrival of the Eastern Mediterranean Transient in the Ligurian basin in 2004.

NW Med convection produces a large footprint on the regional biogeochemistry cycles and marine ecosystems, mostly through the import of deep waters enriched in nutrients to the surface (Severin et al., 2014). This enrichment changes the biogeochemical characteristics of the surface layers (Durrieu de Madron et al., 2011; Herrmann et al., 2013, Auger et al., 2014), promoting a large phytoplankton bloom (D'Ortenzio et al., 2009; Lavigne et al., 2013; Estrada et al., 2014), an important particulate carbon export (Gogou et al., 2014) and a shift of zooplankton community toward larger size organisms (Auger et al., 2014).

Some objectives of the DeWEX (Deep Water formation EXperiment) project was to (i) better understand the impact of dense water formation on the marine biogeochemical cycles, and also (ii) to provide a coherent dataset of hydrological and biogeochemical parameters able to improve numerical modeling of the convection hydrology and coupled biogeochemical processes. To fulfill these objectives, oceanographic research vessels covered the area concerned by the deep convection, providing samples of hydrological and biogeochemical properties of the entire water column during each season from summer 2012 to summer 2013. Once calibrated and validated, numerical modeling is expected to achieve goals at different time scales. Firstly, in a short term, the model is expected to complete the temporal holes of the DeWEX observations in order to calculate a budget of nutrients and organic matter over an annual cycle. Secondly, at longer term, modeling will be held as an integrative tool in order to investigate the question of how climate change and anthropic activities could impact the cycle of biogenic elements and marine ecosystems.

This study aims to answer the first short-term objective of the numerical model in order to quantify the nutrients dynamics in the NW Med dense water formation area at the seasonal scale. After a brief description of the observation network, the modeling strategy is described (section 2), and then evaluated through confrontation with observations (section 3.1). The seasonal variability of atmospheric forcing and hydrology are then described (section 3.2), as well as their consequences on

the biogeochemical properties that drive the nitrogen and phosphorus cycles in the NW Med. Finally, a global annual budget of the region is proposed.

2. Method

2.1. Observations

The observations collected during three cruises, which covered the NW Med during the 2013 winter, spring and summer are used in this study. The major water masses observed in the Western Mediterranean Sea had been sampled. DeWEX Leg 1 was conducted from 1st to 21st February 2013 on board the R/V Le Suroît. Convection was documented by 75 hydrological profiles and 45 biogeochemical profiles (Fig. 1A) giving a global mapping of the convection area, of the distribution of new water formed and of the distribution of inorganic and organic matter. The DeWEX Leg 2 sampled the spring bloom from the 5 to 24th April 2013. It followed the same sampling network as the winter cruise with 99 hydrological profiles and 59 biogeochemical profiles (Fig. 1B). The third cruise had been carried out during the oligotrophic period, between July 24th and August 7th in the framework of the integrated observation network MOOSE (Mediterranean Ocean Observing System for the Environment) on board of the R/V Tethys II. About 100 biogeochemical profiles were measured (Fig. 1C).

Chlorophyll from the satellite MODIS type L3 at 4 km resolution was also used for the validation of the model. Daily maps have been interpolated on the grid of the model.

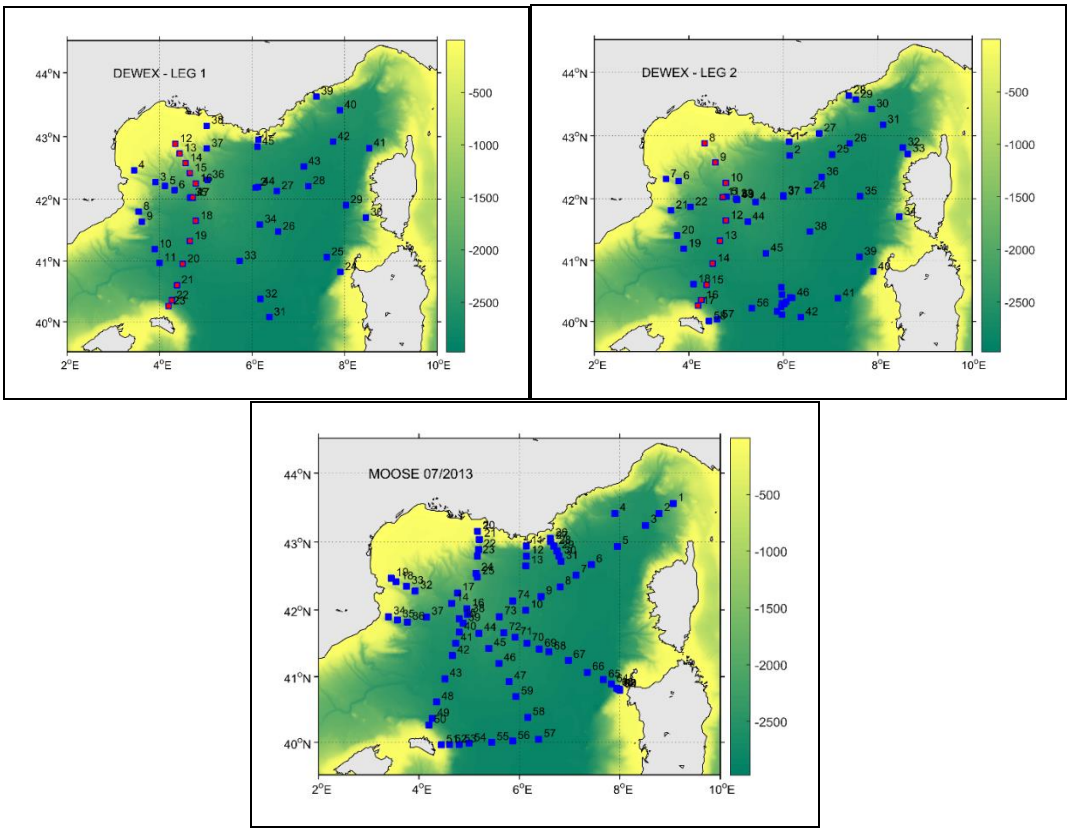

Figure 1: Maps representing the biogeochemical stations of (upper left panel): DeWEx Leg 1, (upper

right panel): Leg 2 and (lower panel): MOOSE. Stations in red represent the transect presented in Fig. 5.

2.2. Modelling

2.2.1. Hydrodynamics

The SYMPHONIE model used in this study is a 3D primitive equation, free surface and generalized sigma vertical coordinate, described by Marsaleix et al. (2009, 2011 and 2012). It was previously used in the Mediterranean Sea to simulate convection in the open sea (Herrmann et al. 2008), and coastal dense water formation (Estournel et al., 2005; Ulses et al., 2008). The horizontal grid presented in Fig. 2 covers a large part of the western Mediterranean basin. The horizontal resolution is about 1 km (variable from 0.8 to 1.4 km^2 from the north to the south of the domain) in order to represent the scales related to the Rossby radius, estimated between 5 km and 10 km. Forty vertical levels were used with closer spacing near the surface (15 levels in the first 100 meters in the center of the convection zone characterized by depths of ~2500 m). The model was initialized and forced at its lateral boundaries with daily analysis provided by the Mercator-Ocean operational system. The configuration of this model was the PSY2V2R4 prototype based on the NEMO Ocean modelling platform and the SAM data assimilation system (Lellouche et al., 2013) at a resolution of 1/12° over the Atlantic and the Mediterranean from 20° S to 80° N. As in Estournel et al. (2015), the initial field and open boundary conditions were corrected from stratification biases deduced from comparisons between analysis and observations taken during the MOOSE cruise of August 2012. The atmospheric forcing (turbulent fluxes) was calculated using the bulk formulae of Large and Yeager (2004). Meteorological parameters including radiative fluxes are given by the ECMWF operational forecasts at 1/8° horizontal resolution and 3 hours temporal resolution based on daily analysis at 00.00 UTC.

Rivers runoff were taken into account using realistic daily values for French rivers (data provided by Banque Hydro, www.hydro.eaufrance.fr) and Ebro (data provided by SAIH Ebro, www.saihebro.com) and mean annual values for the others.

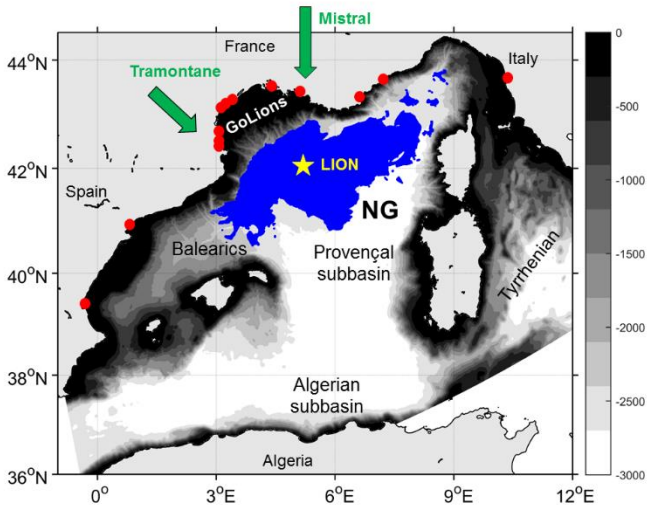

Figure 2: Bathymetry (m) in the domain of the Symphonie model. Red dots represent the modelled rivers locations and the blue area (northern gyre) the region used for the simulation analysis. The yellow star represents the point used for the time series of Fig. 9 (LION).

2.2.2. Biogeochemistry

The Eco3M-S model is a multi-nutrient and multi-plankton functional type model that simulates the dynamics of the biogeochemical decoupled cycles of several biogenic elements (carbon, nitrogen, phosphorus and silicon) and of non-redfieldian plankton groups. The model structure (Fig. 3) used in this study is based on the same pelagic plankton ecosystem model as the one fully described and used by Auger et al. (2011, 2014), Herrmann (2013) and (Kessouri et al., in prep-a). Eight compartments constitute the model. Phytoplankton classified by size (pico-phytoplankton [0.7–2 µm], nanophytoplankton [2–20 µm] and micro-phytoplankton [20–200 µm] represented by diatoms) is represented by the mechanistic formulations of the model Eco3M [Baklouti et al., 2006]. Zooplankton is composed by nano-zooplankton [5–20 µm] representing small flagellates, micro-zooplankton [20–200 µm] representing ciliates and large flagellates and meso-zooplankton [>200 µm] representing copepods and amphipods. Bacteria and zooplankton dynamics are derived from Anderson and Pondaven (2003) and adapted by Raick et al. (2005) for multi-group and multi-element modeling in the Ligurian Sea. The other compartments are dissolved organic matter, particulate organic matter (small and large, differentiated by the settling speed and origin), inorganic matter (nitrate, ammonium, phosphate and silicate) and dissolved oxygen. A total of 34 state variables are calculated.

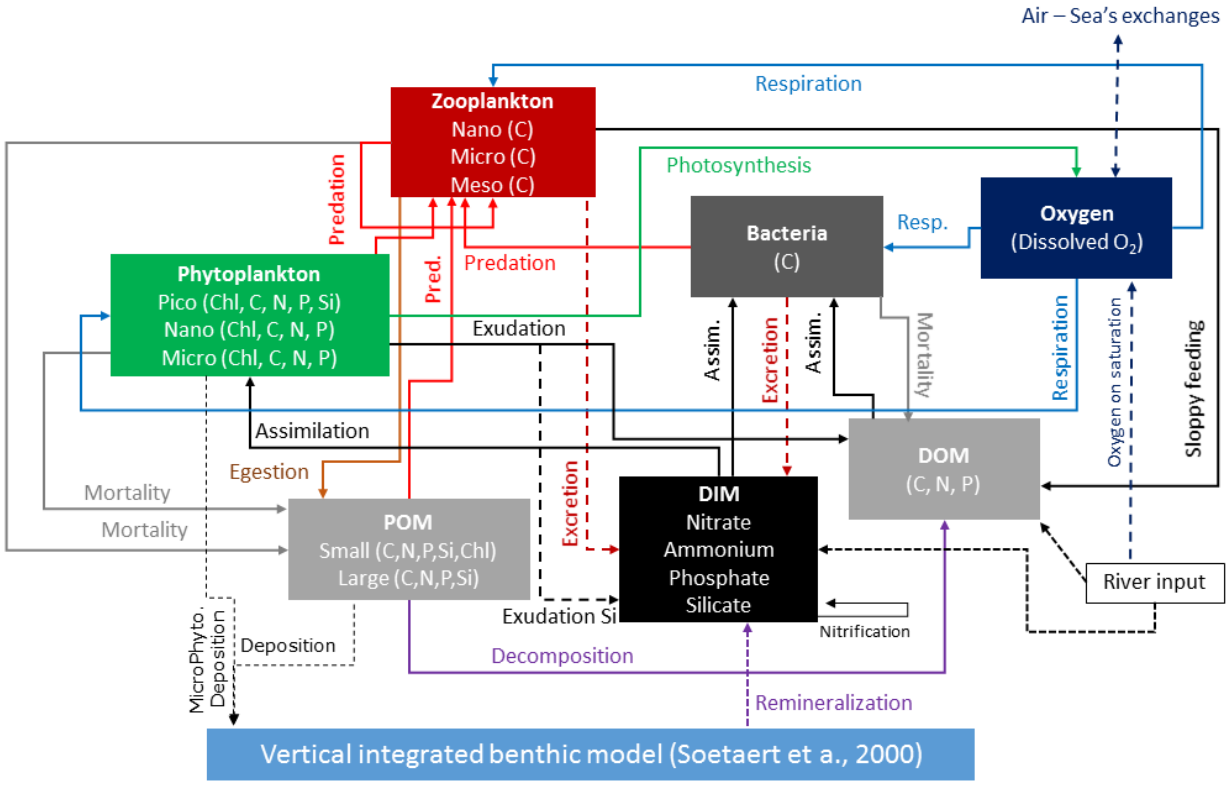

Figure 3: Eco3m-S biogeochemical model scheme.

2.2.3. Initial and boundary conditions

The biogeochemical model is downscaled from the Mediterranean basin scale to the regional scale described here. The biogeochemical basin scale model is forced by the daily fields from the NEMO model used for the boundary conditions of our hydrodynamic model. This configuration initialized in 2008 with climatological nutrients fields is described in Kessouri et al. (in prep-a). Daily values of all state variables are extracted from this run for the initial and lateral boundary conditions of the regional model. This nesting protocol ensures a coherence of the physical and biogeochemical fields at the open boundaries. The regional model is initialized in August 2012 and the simulation ends in October 2013.

The coupling method "Source Splitting" (Butenschön et al. 2012) has been used here. It consists on an offline forcing by the daily averaged outputs of the physical model using a time step of a few minutes for advection and diffusion of biogeochemical variables while Eco3M-S computes the biogeochemical fluxes with a time step of about one hour. It is then assumed that there is not impact of biogeochemical properties on hydrodynamics.

2.2.4. Derived variables

Other variables than state variables are used in the analysis of results. Their definition is given below.

The mixed layer depth (MLD) is defined as the depth where the potential density exceeds its value at 10 m below the surface by 0.01 kg m^{-3}. The stratification index is the difference between the potential density at 200 m and 10 m. Nutriclines (nitracline and phosphacline) correspond to the depth of the iso-concentrations: 1 $mmol.m^{-3}$ for nitrate and 0.05 $mmol.m^{-3}$ for phosphate. The amount of nutrients in the surface layer [0-150m] has been calculated in the simulation and in the observations. The calculation in the simulation is straightforward. It is performed on the NG area indicated in Fig. 2. For the observations, the nutrients measured during the cruises have been first interpolated over the model grid, then the amount of nutrients has been calculated in the [0-100m] layer as the model results. The total weight of the interpolation is computed using the vertical and horizontal distances, and the bathymetry and salinity differences between the observation point and the interpolation point. The information of bathymetry and salinity are used to take into account the coherence of the physical and biogeochemical fields at the scale of the northern gyre.

3. Results and discussion

3.1. Evaluation of the simulation

3.1.1. Surface chlorophyll

To assess the representation of the seasonal cycle simulated in the western basin, time series of chlorophyll are extracted from the model for four contrasted regions (Fig. 4): the Algerian basin zone (ALGZ), the shelf of the Gulf of Lions (GoL), the

Open Ocean area of the Gulf of Lions or Northern Gyre (OOC) and Ligurian Sea (LIG) and compared to satellite products. Simulated and satellite time series presents a correlation r_{coeff} higher than 0.7 (pvalue<0.05). Three regimes can be distinguished. The coastal area is characterized by ten months of efflorescence (from October 2012 to July 2013). Maximum concentrations are observed from February to April in the model probably explained by events of high river flows with high nutrient load, and by regions where vertical mixing is strong but limited by the topography. The Algerian basin is characterized by a winter efflorescence but no intense bloom behavior. The phytoplankton development starts in early December and lasts 4.5 months. The concentration increase is gradual. The open ocean convection zone (OOC) and Ligurian Sea show a bloom regime. Two periods of phytoplankton efflorescence can be noted: the first one, the weaker, in autumn between November and mid-January and the second one corresponding to the spring bloom in April lasting about four weeks. Between these two periods, winter is characterized by very weak concentrations. The model slightly over-estimates the Algerian concentrations and misses large peaks in the satellite data during the bloom events in convection zone. On the other side, the trends in each region is very correctly represented by the model.

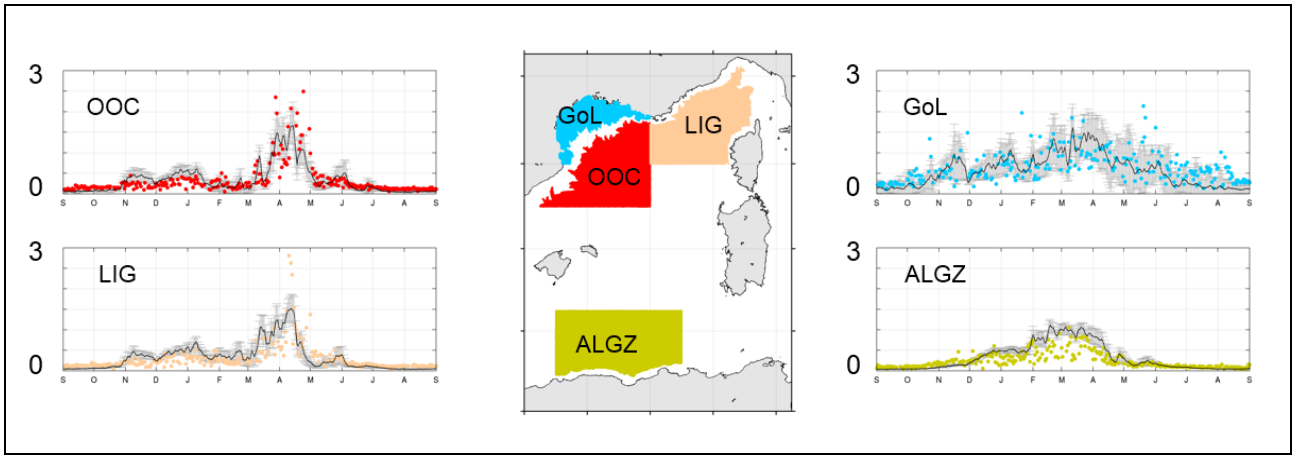

Figure 4: September 2012 to September 2013 Sea Surface Chlorophyll-a concentration [mg.m^{-3}] comparison between model outputs (black line for the spatial average and grey regions for the standard deviation) and MODIS 4km resolution satellite products (the colours refer to the regions of the map).

3.1.2. Horizontal and vertical biogeochemical patterns in winter and spring

In order to evaluate the model's performance to reproduce the horizontal and vertical biogeochemical patterns in relation with the hydrology, the simulation was compared to the cruises observations at the two key periods (winter and spring) for the ecosystem. First, surface concentrations of nutrients were compared to a snapshot of the model taken at the median day of the cruises. Then, a comparison of modeled and observed nutrients and chlorophyll was done for a vertical transect across the northern gyre from the Gulf of Lions to the Balearic Islands, corresponding to the red dots of Figure 1.

3.1.2.1. Winter

In winter, during the first leg of DeWEx cruise, maps of surface concentrations of nitrate and phosphate (Fig. 5a) show an expected heterogeneity induced by the strong gradients of MLD across the northern gyre. The model shows that the patch of very high concentrations (> 7.5 mmol.m^{-3} for nitrate and> 0.3 mmol.m^{-3} for phosphate) is located between 40.5°N and 43°N and between 3°E and 9°E. These characteristics and values match the measurements. The highest values correspond to the northern gyre where convection has upwelled nutrients. It is surrounded by the Northern Current to the north, the Western Corsican Current and the Balearic Front to the south with shallower mixed layer depth. The northern gyre is hydrologically and vertically homogenous at least over several hundred's meters. These findings are in agreement with the observations during the winter 2011 reported by Séverin et al. (2014). Other authors mentioned some homogeneous biogeochemical profiles and high surface enrichment by inorganic matter throughout convection in the eastern Mediterranean basin (Yilmaz and Tugrul, 1998; Gacic et al., 2002; Santinelli et al., 2012). Far outside the mixed patch, the nutrients concentrations are very low (<1 mmol.m^{-3} for nitrate and <0.05 mmol.m^{-3} for phosphate) as detected in the observations taken below latitude 41°N. Between these two regions, a strong gradient is observed on a narrow band where observed concentrations (~3 mmol.m^{-3} for nitrate and 0.15 mmol.m^{-3} for phosphate) are weaker than those of the model (~4 mmol.m^{-3} for nitrate and 0.18 mmol.m^{-3} for phosphate). Probably the horizontal gradient bounding the convective zone is not enough marked in the model. It is interesting to note the fine scale structures in the model's map which demonstrate the enrichment induced by the small scale dynamics.

Figure 5b gives complementary information on the vertical distribution of nutrients and chlorophyll concentration. The model gives values close to the observations. Between latitudes 41.5 °N and 42.5 °N, the water column is homogeneous, nitrate higher than 7 mmol.m^{-3}, phosphate higher than 0.25 mmol.m^{-3} (the model slightly underestimates the nutrient increases at the northern stations inside the NG) and chlorophyll lower than 0.1 mg.m^{-3}. The maximum nutrients vertical gradient corresponds to the isopycnal 29.05 (superimposed on vertical sections) on both sides of the northern gyre. Its depth varies between 100 m to the south to 400 m to the north. Beyond this threshold, nitrate increases from 3 to 8 mmol.m^{-3} and phosphate from 0.1 to 0.3 mmol.m^{-3}. The surface concentrations of chlorophyll outside the NG is around 0.5 mg.m^{-3}.

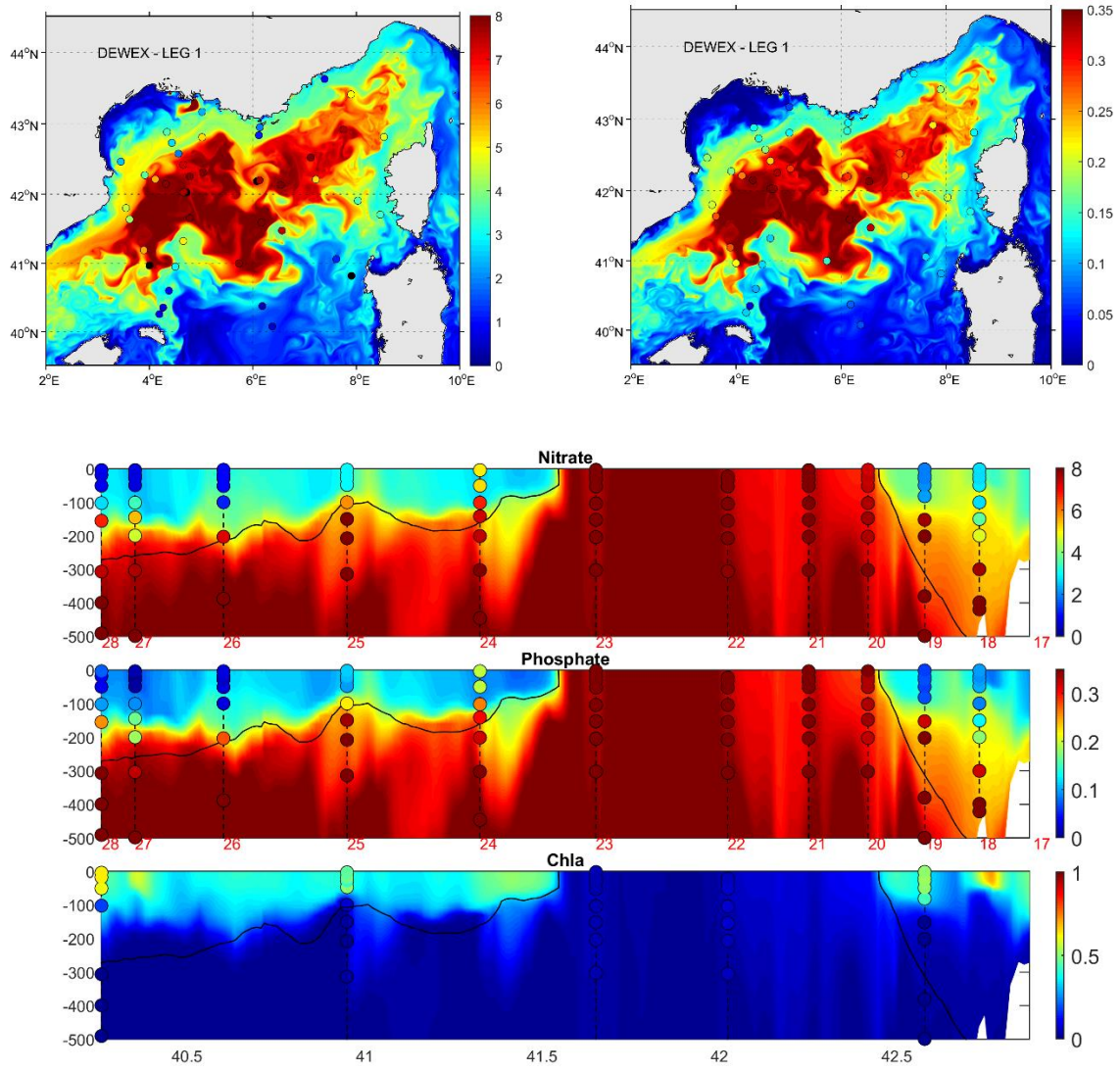

Figure 5: Comparison of nitrate, phosphate and chlorophyll from the model (background colors) and from the DeWEx Leg1 cruise in February 2013 (coloured circles). Unit: mMol.m^{-3}. Upper panel (a): Nitrate (left), Phosphate (right). Lower panel (b): Vertical section indicated by red dots on Fig. 1. Black line represents the 29.05 isopycnal.

3.1.2.2. Spring

In spring, during the second leg of DeWEx, conditions are completely different of those observed two months before. Surface nutrients concentrations are low (Fig. 6a) but remain stronger in the northern gyre than outside. In the observations as in the model, values of 2 to 3 mMol.m^{-3} for nitrate and 0.08 to 0.12 mMol.m^{-3} for phosphate stand out in the center of the basin. Elsewhere, it is the beginning of oligotrophic conditions. Far from the convection zone, the values are zero. In general, a low overestimation of nutrients, especially phosphate, concentrations are visible.

The gradients of nitrate and phosphate shows the vertical properties of the biogeochemistry in the basin. Figures 6b gives an estimation of the location of the nutriclines at about 90 m , and shows that they follows the density gradient, which is located at about 100 m depth. Inside the surface impoverished layer, chlorophyll cells are developed. The chlorophyll concentration exceeds 1.5 mg.m^{-3} in the first 30 meters and 0.5 mg.m^{-3} until 60 m depth. Chlorophyll is very low beyond. Again this comparison evidences a low overestimation of modeled surface nutrients concentrations.

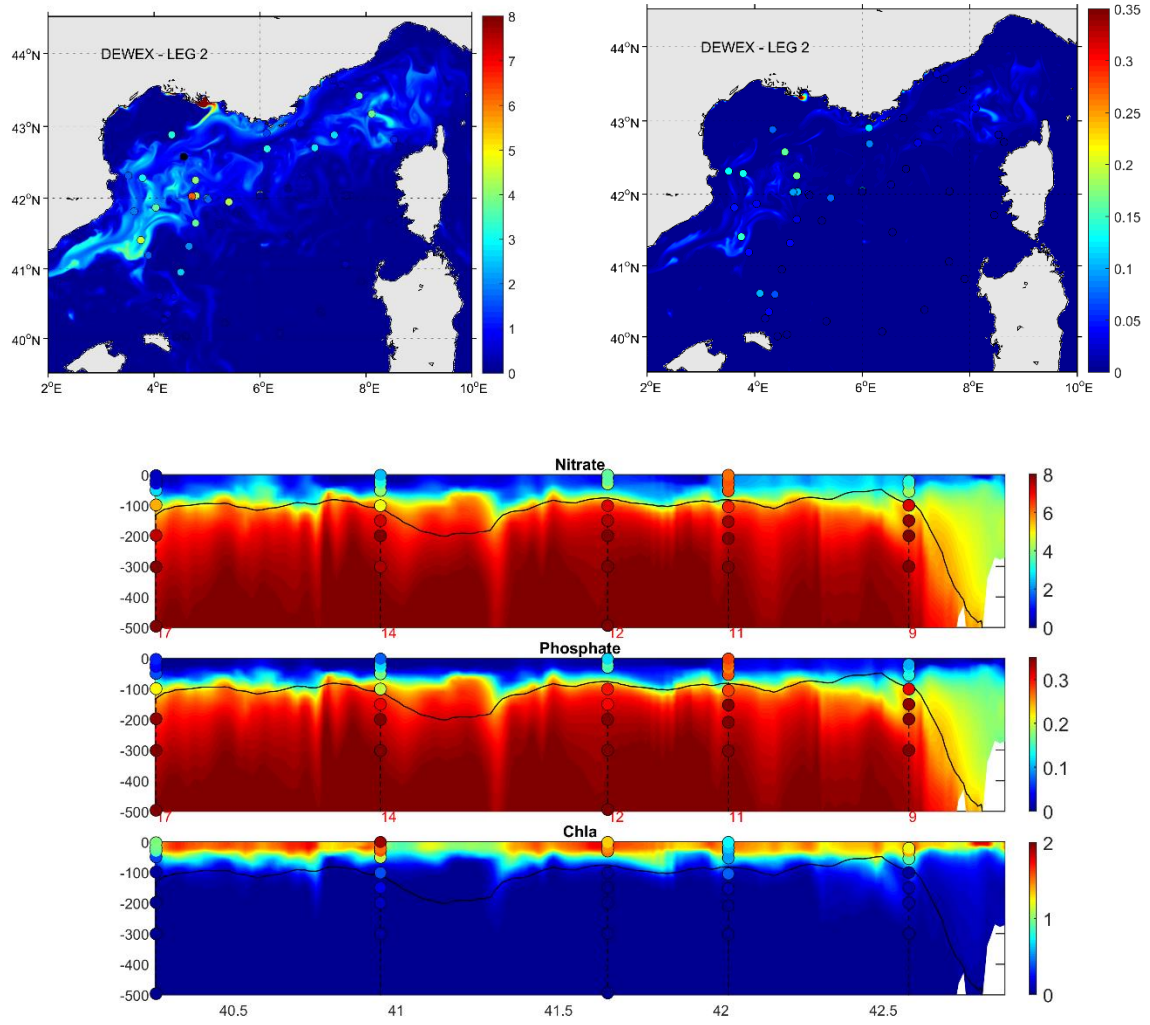

Figure 6: Same as Fig. 5 for DeWEx Leg 2 in April 2013. Black line represents the 29.05 isopycnal.

3.1.3. Variability between April and September 2013

The objective of this section is to evaluate the ability of the model to reproduce the variability of the biogeochemistry during a transition phase.

Figure 7 shows an evolution of nitrate concentration measured by the float and simulated by the model at the same points. The deepening of the nitracline in the model presents a delay as shown by surface layer nitrate measured by the float in

April which is higher than in the model. Then, in May, the modelled and the observed trends join as well as the position of the nitrate vertical gradient. Nitrate concentrations vary from 0 to 7 mMol.m^{-3} in less than 30 m. High frequency motions are clear in both observations and model results in April and May. These motions seem more efficient in the observations to supply pulses of nutrients in the MLD. However, after each pulse, the depletion of nutrients in the surface layer is fast and the nitracline deepens with time. From the beginning of June, the nitracline falls below 50 m depth and reaches 70 m during all the summer. At the same time, MLD is very shallow at 10-15

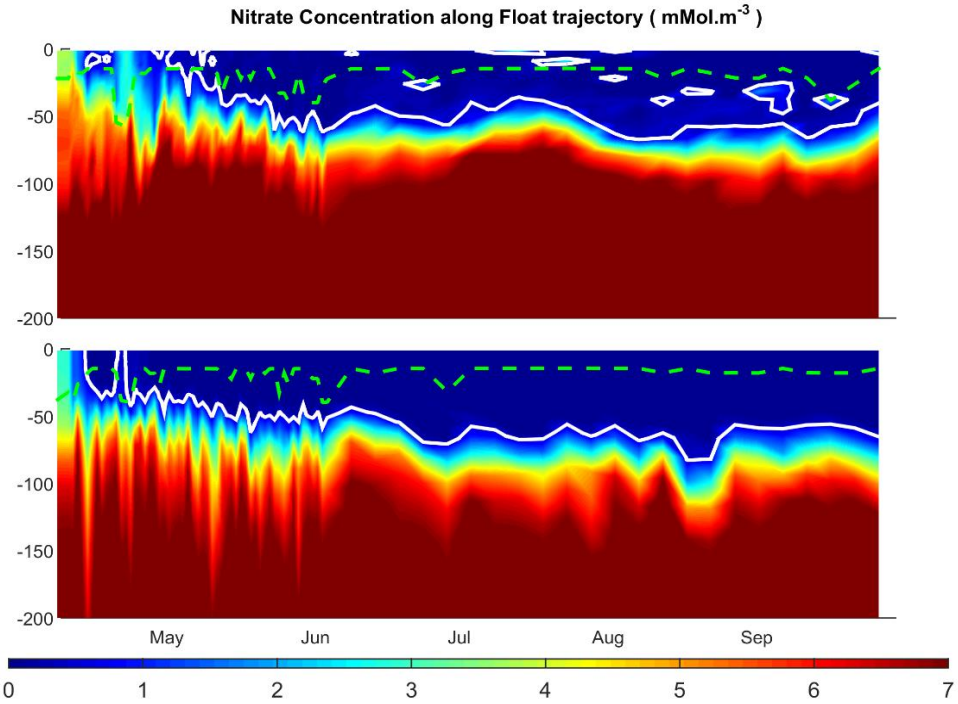

m.

Figure 7: Hovemöller representing the nitrate concentration [mMol.m^{-3}] along the float track. Data are extracted from the float lovbio-17B (upper panel) and from the model (lower panel). White line represents the nitracline (position of the concentration 1 mMol.m^{-3}) and the green dashed line represents the MLD.

3.1.4. Annual cycle of the nutrients stocks

Figure 8 presents the modeled annual cycle of the nitrate and phosphate stock in the first 150 m. The time series considered here corresponds to the average value in the NG area (indicated in Fig. 2). The area was selected with a criterion of convection reaching 1000 m in the simulation. It covers 5615 km^2. Stocks deduced from the interpolation of the cruises observations on the model grid have been reported on the figure with horizontal bars. The simulated fields reproduce correctly the seasonal trend and orders of magnitude of nutrients as estimated by the three snapshots of winter, spring and summer. These curves will be analyzed more into details in section 3.3 dealing with the stoichiometry of the surface waters.

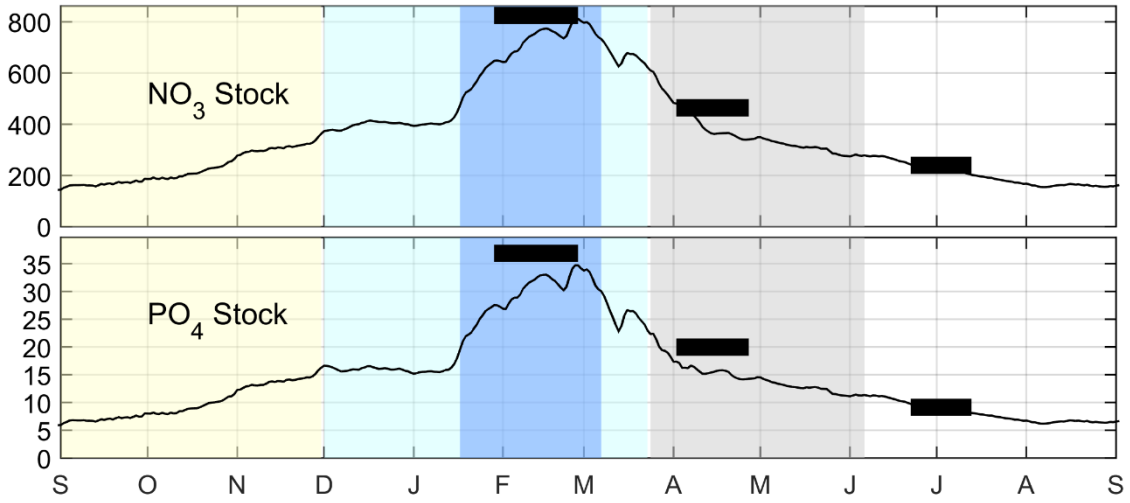

Figure 8: Nitrate (upper panel) and phosphate (lower panel) stock evolution in the upper layer [0-150 m] and the northern gyre region. Units: mmol.m^{-2}. Horizontal black bars correspond to the value averaged over the three cruises. The four seasons identified in section 3.3 have been highlighted with background colors (blue stands for the main convective period)

3.2. Atmospheric forcing and hydrology

Figure 9 presents the time series of the heat flux at LION (42°N 5°E) located in the center of the NG and Fig.10 presents the time series of the MLD averaged over the NG region (black curve). The seasonal variability of the atmospheric forcing is obvious. In September and October, positive heat fluxes are regularly interrupted by short events of heat losses corresponding to northern wind gusts. On October 28, 2012 an extreme event reaching 1300 W.m^{-2} strongly impacts the stratification of the 80 m upper layers.

From December, heat fluxes are almost exclusively negative. First, a strong wind event lasts three weeks in December and is followed by a succession of events during six weeks between mid-January and the end of February. From December, each event produces an increase of the MLD (Fig. 10). Around the beginning of February, the MLD reaches the seafloor in the center of the NG, when the spatially averaged deepening reaches 1500m. Then, a final short and strong episode is recorded between the second and third week of March. This event causes a breakdown of the weak surface restratification that established during the calm second week of March. During the last week of March, the heat flux becomes durably positive, except some few peaks. After March, the heat gain is a component of the progressive restratification of the surface layers, the development of instabilities around the mixed patch being the other component. Relatively large variations (0-50 m) of the MLD (Fig. 10) can be noted throughout the spring caused by the effect of wind over low stratified surface layers, as shown in the example of the third week of April.

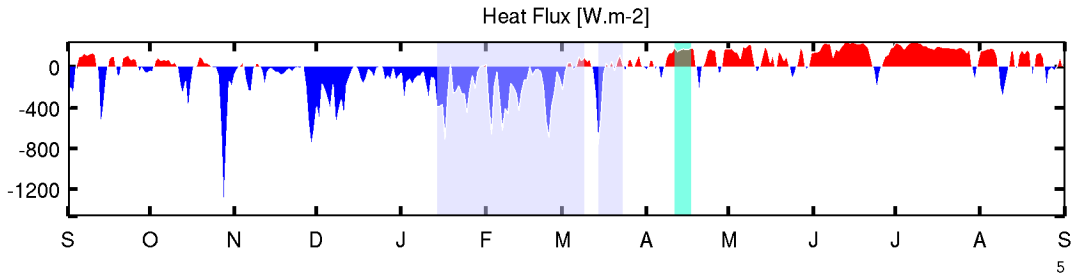

Figure 9: Time series of total heat flux (W m^{-2}) at the LION point indicated in Fig. 2. Blue strips represent the period when the MLD is higher than 1000m. The green strip represents the period when the phytoplankton bloom is maximum.

3.3. Consequences of hydrological variability on biogeochemical processes and stoichiometry

The biogeochemical interfaces (nutriclines and deep chlorophyll maximum – DCM) are plotted in Fig. 10. The year was divided into four periods corresponding to the seasons analyzed individually (they are indicated by coloured vertical bars in Fig. 10). The first one is autumn, from September 1st to December 1st 2012. Winter was chosen as the period of strong negative heat fluxes (from December 1st 2012 to March 23th 2013) (Fig. 9) and deep MLD (Fig. 10). Spring, which begins on March 24, corresponds to the period where the MLD becomes shallower than 100 m. It ends on June 6th when the MLD becomes very shallow (< 20 m) and the deep chlorophyll maximum (DCM) is setting up. Summer is the last stage, which starts on June 6th until September 1st 2013, the end of the time series.

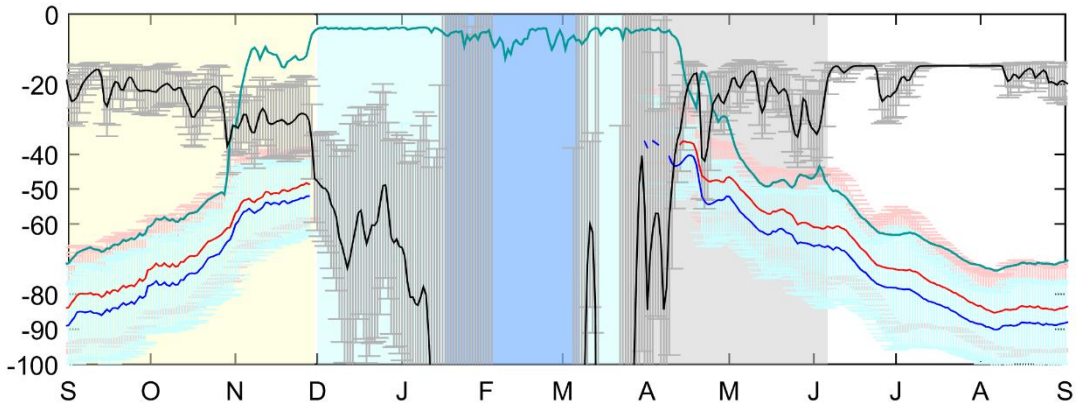

Figure 10: Time series of simulated mixed layer depth (in black), nitracline (in red), phosphacline (in dark blue) and DCM (in green) averaged over the NG (solid lines). Shaded areas correspond to the standard deviation simulated in the NG region.

In marine ecology, the nitrate to phosphate ratio was determined to be universally 16:1 because of the phytoplankton requirements which control the marine biogeochemistry (Redfield et al., 1963). Even if this averaged ratio has been reappraised several times (Banse, 1994; Geider and La Roche, 2002), its dynamics can still be used to understand the

nitrogen and the phosphorus reactivity (Arrigo, 2005). Indeed, the N:P stoichiometry reflects relations between several processes: nutrients uptake by phytoplankton and small heterotrophs, rate of mineralization of organic matter, inorganic matter excretion by heterotrophs (Eqs 1 and 2) and finally the effects of physical processes (mixing and advection, not included in these equations).

$$\frac{\partial[NO_3]}{\partial[t]} = Nitrification - BacteriaUptake - PhytoplanktonUptake \quad \text{(Eq. 1)}$$

$$\frac{\partial[PO_4]}{\partial t} = ZooplanktonExcretion + BacteriaExcretion - BacteriaUptake - PhytoplanktonUptake \quad \text{(Eq. 2)}$$

In the Mediterranean Sea, the ration N:P is higher than the canonical value of 16:1. It was estimated on average at 24 (Pujo-Pay et al., 2011) with a pronounced horizontal gradient from west to east. To the west, the ratio is 22 in the Levantine Intermediate Water and the Western Mediterranean Deep Water (Copin-Montegut, 1986) while in the Levantine Basin, the ratio reaches 27±3:1 below 200 m (Ribera d'Alcalà et al., 2003). The N:P ratio can be much higher above the thermocline (Raimbault and Coste, 1990) because of the preference of phytoplankton for phosphate compared to nitrate. These ratios confirm that the Mediterranean waters are limited by phosphate, especially in the eastern basin.

In the northwestern basin which is the heart of this study, Severin et al., 2014 showed during deep convection, strong variations of the N:P ratio. Values of 22 were measured in mixed water columns, 25 in stratified regions and up to 30 in regions where the efflorescence had already started.

The objective of this section is to use our simulation to characterize the time evolution of the stoichiometry over an annual cycle and then to describe the physical and biogeochemical processes responsible of these variations. The analysis begins with the steady-state period, the end of summer, when the surface layer is completely depleted in nutrients.

Figure 11 presents the time series of the sink and source biogeochemical terms of nitrate and phosphate as well as the trends induced by hydrodynamics. Figure 12 presents the time series of seawater N:P and of the biogeochemical and physical contributions to the N:P rate of change. These rates of change have been computed with Eq. 3:

$$\frac{\partial(N:P)}{\partial t} = \frac{P\frac{\partial N}{\partial t} - N\frac{\partial P}{\partial t}}{P^2} \quad \text{(Eq. 3)}$$

where N and P stand for nitrate et phosphate molar concentration. Concentrations and processes have been averaged over the 150 m upper layer.

A first general remark about the effect of biogeochemical processes on N:P is that uptake increases N:P while releases of nitrate and phosphate decrease N:P (Fig. 12). Indeed, the N:P ratio of uptake is lower than the ratio in seawater which presents an excess of nitrate compared to phosphate. The effect of uptake is then to increase the water N:P ratio. For the same reason, releases of nutrients by the ecosystem produce a decrease of water N:P. A second remark is that convective

mixing and upwelling produce a decrease of surface N:P ratio because of the positive gradient of N:P in the water column (Pujo-Pay et al., 2011 ; Huertas et al., 2012).

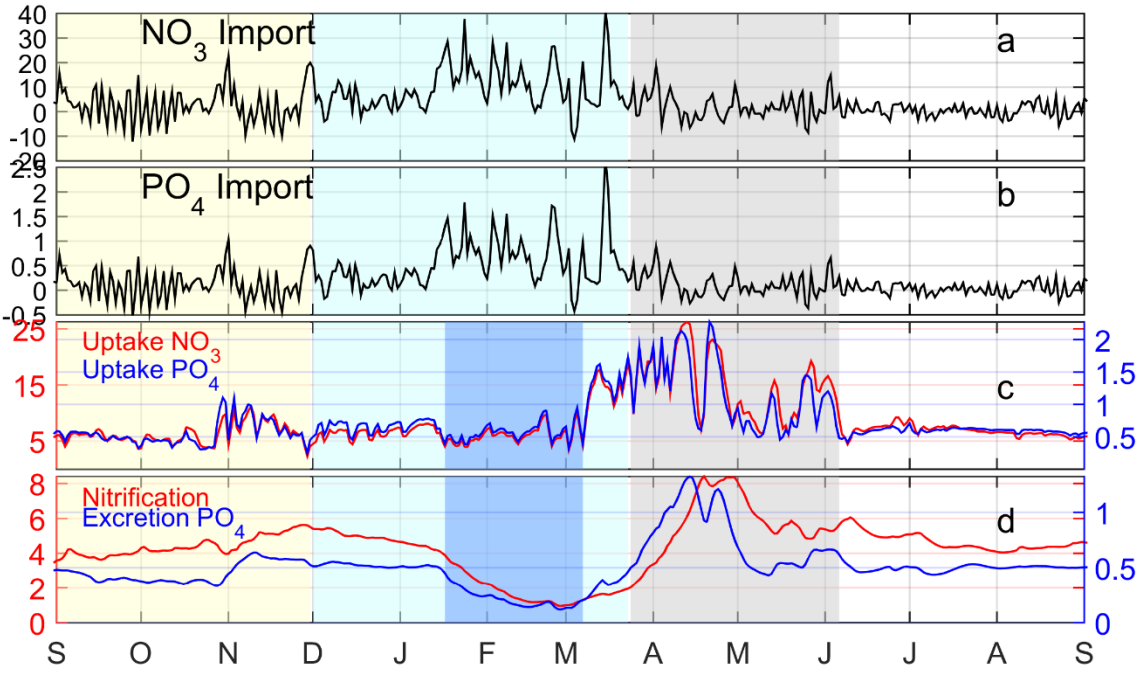

Figure 11: Time series of the nitrate (a) and phosphate (b) vertical import flux (Units: mmol.m^{-2}.day^{-1}) through the 150 m level for the northern gyre region. Time series of simulated source and sink biogeochemical terms for nitrate (c) and phosphate (d) averaged over the northern gyre region and the [0-150 m] upper layer

3.3.1.Autumn

From September to November, uptake of nitrate (resp. phosphate) is slightly higher than nitrification (resp. phosphate excretion). Besides, at the end of August, mean value of nutriclines are located at 80-90 m depth (Fig. 10). Starting from September, nutriclines become progressively shallower to reach 50 m at the end of November. This upward displacement of the nutriclines corresponds to the preconditioning phase of the deep convection process in the northern gyre. The addition of this displacement to the recycling of organic matter and subsequent nitrification, is larger than the uptake and is then the cause of the nutrients stock increase in the surface layer (Fig. 8).

The N:P ratio is on average 24:1 in the simulation at the beginning of September (Fig. 12). The deep values are weaker (23 in the model, a little bit higher than the observed values of 22) and the maximum N:P vertical gradient is located below the nutriclines (not shown). The impact of each biogeochemical process on the stoichiometry (N:P) is much larger than the effect of the physical processes (Fig. 12a). Yet the negative budget of physical processes is slightly higher than the positive budget of nearly balanced biogeochemical processes explaining the slow and regular drop of N:P. Indeed, the vertical

import of nutrients with relatively low ratio leads to reduce N:P. The horizontal advection also reduces N:P with comparable rates of change as vertical import during September and October.

November is the period of the autumn bloom as displayed by the increase of chlorophyll (Fig. 4) and by the increase of the nitrate and phosphate uptakes (Fig 11). The bloom is triggered by the strong wind event of the end of October (see section 3.2). An upward flux of nutrients is visible at 150 m (Fig. 11) as well as an increase of the MLD (Fig. 10) which in some places become deeper than the nutriclines. Pulses of nutrients reach the surface, then, are absorbed by phytoplankton and consequently the DCM shallows suddenly (Fig. 10). Phosphate and ammonium excretion progressively increases reflecting the development of heterotrophs grazing the phytoplankton produced during the bloom. Nitrification also increases but more slowly than excretion as it is a slow reaction.

The consequence of this sequence of processes is now examined regarding the N:P ratio. During the first days of the bloom, the biogeochemical processes (uptake) tend to strongly increase the seawater N:P (Fig. 12) but this increase is balanced by a sudden decrease trend mainly due to horizontal advection linked to the strong wind-induced currents disrupting the geostrophic equilibrium that keeps the gyre isolated from peripheric regions. During the second part of November, the heterotrophs development and the associated bloom decline lead to a negative biogeochemical trend for N:P. This trend is balanced by an opposite trend imposed by horizontal advection. N:P remains stationary.

3.3.2. Winter

Winter has been divided into three periods.

- 1 December – 15 January

At the end of November and beginning of December, a new sudden northern wind event thickens the MLD to 50-60 m on average (Fig. 10). The vertical mixing induces an increase of nutrient amount during this event and more generally during the whole period (Fig. 11). A part of these nutrients are advected out of the northern gyre. The autumn efflorescence continues until mid-January (Fig. 4) even if the low light availability reduces the nutrients uptake compared to the comparable situation of late October. During approximately one month (15 December-15 January) the source (vertical import and nitrification/phosphate excretion) and sink (mainly uptake) terms balance resulting in a nearly constant nutrients stocks (Fig. 8). This is not the case for N:P, as during the first part of December, this ratio increases rapidly from 22 to 25. During this period, opposite to the balance between the physical and the biogeochemical terms noticed in November, both the resultant of physical and biogeochemical processes favor this increase. The term responsible of this “anomaly” is the vertical import of nutrients which is no more associated to a drop of N:P. The reason is that the surface N:P has been progressively reduced from September to December to the value of the subsurface waters (22) preventing a supplementary decrease by vertical mixing.

- 16 January – 7 March

Deep convection is triggered on mid-January. Nutrients are upwelled, biogeochemical vertical gradients vanish. Nutrients stocks in the surface layer reach their maximum value (Fig. 8). Deep convection causes a sudden reduction of uptakes which remains however not negligible afterwards (Fig. 11). The phytoplankton biomass is vertically mixed resulting in a decoupling of preys and predators (Auger et al., 2014), and finally in zooplankton mortality as shown by the regular drop of excretion terms all along the period. The decrease of excretions is clearly more pronounced than the decrease of uptakes. During the convective period, all the contributions to N:P, except the one of vertical import, strongly reduce (Fig. 12). Nevertheless, the triggering of convection on mid-January creates an imbalance leading to a drop of N:P from 26 to 24 in a few days which is due to the asymmetry of the response of biogeochemical processes mentioned before (rapid response of uptake / slow response of excretion). The net effect of these processes on N:P which is usually positive becomes very low. Besides, the strong increase of the MLD on mid-January induces a decrease of N:P as the December increase of N:P had regenerated its vertical gradient. As could be anticipated for this period, physical processes dominate the N:P budget. During the rest of the convective period, N:P is quasi stationary as a result of a return to equilibrium between biogeochemical processes dominated by uptake and vertical imports of low N:P nutrients. The value of 23.5 simulated during this period is comparable to the mean value of 22.3 observed in February. Deep mixing temporarily stops on March 7.

- 8 March – 23 March

The phytoplankton development begins during the second week of March characterized by calm meteorological (section 3.2) and hydrodynamic conditions. This first efflorescence is characterized by a strong and sudden consumption of nutrients (Fig. 11) which increases the N:P ratio of seawater (Fig. 12). The excretion and nitrification increases appear lower compared to the uptake one leading to a net positive biogeochemical effect on N:P that reach 27.5. Contributions of physical processes is very low. The duration of this event is short as convection starts again on March 14 for a few days. This late mixing reduces N:P as it did on mid-January. As this event is short, the decrease of N:P is reduced (25.5). These results clearly show that intense events (physical, as the triggering of convection, or biogeochemical, as the start of efflorescence) induce rapid variations of seawater N:P. Convection definitely stops on March 21.

3.3.3. Spring

Spring has been divided into two periods.

- Bloom period: 24 March – 24 April

Maximum N:P corresponds to the transition between winter and spring, (8 March - 6 April), during the period of strong growth of the phytoplankton biomass (Fig. 8 and 12). Zooplankton biomass is still low (growth delayed compared to phytoplankton) resulting in a low excretion compared to uptake. However, it can be noted on Fig. 12 that the strong positive

N:P trend induced by biogeochemical processes is partly balanced by a negative trend due to physical processes (mixing is active until 10 April).

April is the month when the individual biogeochemical processes and their contribution to the stoichiometric changes are the strongest of the year. Around 10 April, the nutrients uptake is maximum, heterotrophic biomass has strongly increased during the preceding month. The rapid evolution of this heterotrophic biomass introduces an imbalance in the recycling of nutrients. The excretion of phosphate and ammonium indeed increases more rapidly than the production of nitrate by nitrification. This induces a strong negative tendency of N:P which temporarily cancels the positive tendency of uptake. The biogeochemical terms are then responsible of the N:P drop (Fig. 12). Phytoplankton biomass reaches its maximum. Nutrients stocks have strongly decreased (Fig. 8), a thin MLD develops with a surface stratification induced by positive heat fluxes, and nutriclines reappear. On April 19, a new wind gust increases briefly the MLD (Fig. 10) producing an enrichment of surface waters, itself producing a last strong and short pulse of uptake (Fig. 11). The resulting increase of N:P is very moderate as the event is short compared to the sequence of events of March. N:P is around 24 on mid-April which is close to the average value observed during the April cruise during which some values between 28 and 32 have been recorded.

- Post bloom period: 25 April – June

From April 25, the bloom is finished as observed on the sudden drop of uptakes even if they are still characterized by relatively strong variations until early June. Energetic mesoscale processes produce horizontal redistribution of light Atlantic water with low N:P and dense water from convection with high N:P. Brief increases of nutrients by horizontal advection (~12 May and last week of May) are rapidly consumed. The result of this complicated period is that N:P is affected by a succession of small increases and decreases. The nutrient stock at the beginning of June is at the level of the beginning of November (Fig. 8). As the nutrients stock continuously decreases, nutriclines as well as DCM depth increases (Fig. 10).

3.3.4. Summer

From early June, the surface layer (0-50 m) is definitely depleted from nutrients as can be observed on Fig. 10 where nutriclines become deeper than MLD. From a biogeochemical point of view, a steady state prevails for uptake, excretion and nitrification during summer. Variations of N:P are negligible until the beginning of August. Again, physical and biogeochemical processes balance, indicating a rapid reaction of organisms to physical processes. Then, from August, as explained at the beginning of this section, nutriclines begin to be upwelled and N:P to decrease.

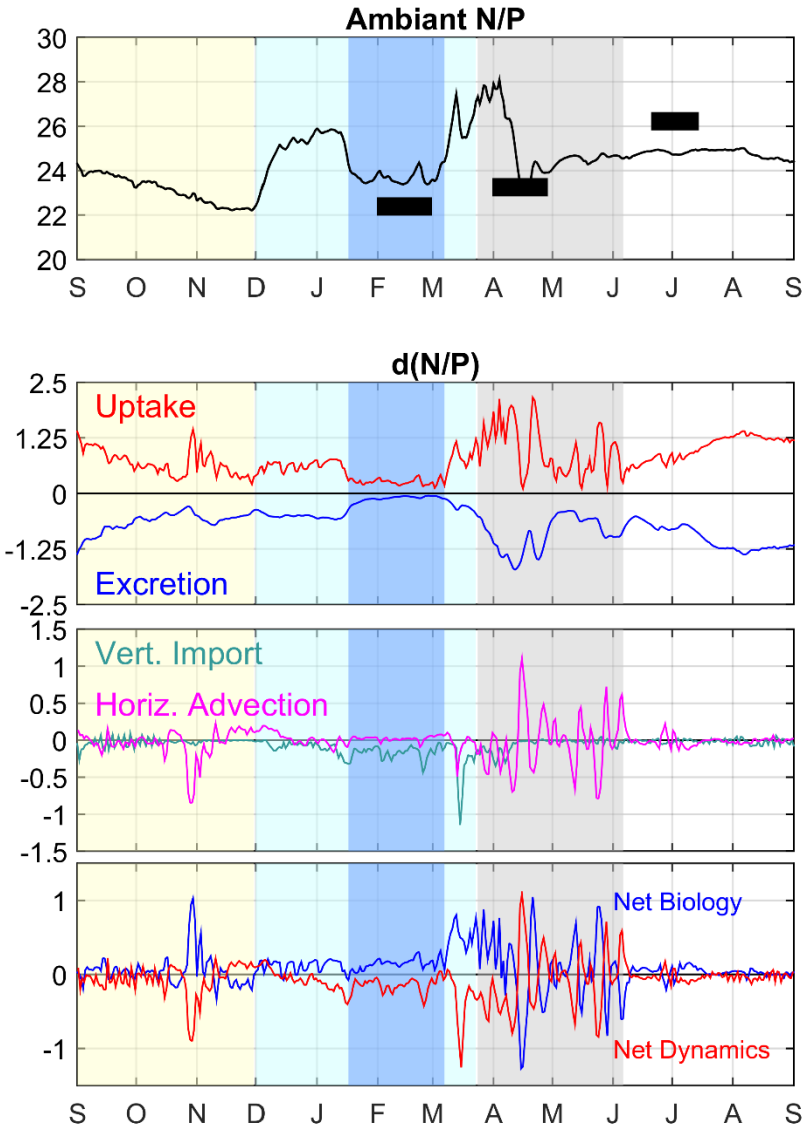

Figure 12: (upper panel): time series of N:P ratio averaged over the upper layer [0-150 m] of the northern gyre region, horizontal black bars correspond to the value averaged over the three cruises. (Lower panel): terms involved in the N:P time evolution as indicated in the figures (unit: day^{-1}).

3.4. Budget of the nitrogen and phosphorus in the northwestern Mediterranean basin

The annual nitrogen and phosphorus budgets of the northern gyre are calculated in the surface layer (0-150 m) with the model (Fig. 13). The annual vertical import of nitrate and phosphate is estimated at resp. 1.56 molN.m^{-2}.y^{-1}, and 0.08 molP.m^{-2}.y^{-1} which is, for nitrate, the same order of magnitude than the estimation of 1.4 molN.m^{-2}.y^{-1} in the convective Atlantic sub-polar region (Williams et al., 2000). The vertical organic nitrogen and phosphorus export under dissolved and particulate forms is resp. 1.03 molN.m^{-2}.y^{-1} and 0.07 molP.m^{-2}.y^{-1}. Horizontal advection exports negligible amounts of nitrate

and phosphate in the surface layer at the annual scale.

The transformation of organic matter by heterotrophs excretion is the other factor that controls phytoplankton production. The regenerated production based on ammonium ranges in the model between 53 and 78% of the total production, depending on the consideration of the nitrification in the calculation of the new production. It is significantly higher than new production based on nitrate from June to the end of October (not shown). The export of ammonium by horizontal advection out of the northern gyre is very important (0.74 molN.m^{-2}.y^{-1}) compared to nitrate and phosphate. The strong difference of ammonium with nitrate is that its biogeochemical source term is four times the one of nitrate, its cycle is rapid, and its concentration is low but relatively constant except between February (minimum value) and April (maximum value). We also can argue that during the oligotrophic period, production is limited by phosphate and the excess of ammonium is thus exported. At the opposite, the surface layers of northern gyre import organic nitrogen (0.46 molN.m^{-2}.y^{-1}) from the peripheric regions.

The biogeochemical fluxes lead to a gain (and as a consequence a loss) of 0.66 molN.m^{-2}.y^{-1} and 0.09 molP.m^{-2}.y^{-1} of organic (resp. inorganic) matter.

To synthesize, during the period from September 2012 to September 2013, the surface layer of the northern gyre receives about 0.37 molN.m^{-2}.y^{-1} from the deep reservoir and exports 0.28 molN.m^{-2}.y^{-1} to the peripheric region in the form of ammonium. The difference of these two terms and considering the biogeochemical fluxes the stocks increase as follows: 0.02 molN.m^{-2} of nitrate, 0.02 molN.m^{-2} of ammonium and 0.09 molN.m^{-2} of organic matter. As regards phosphorus, the same region receives 0.01 molP.m^{-2}.y^{-1} under inorganic form from the deep reservoir and exports 0.02 molP.m^{-2}.y^{-1} to the peripheric region under organic form. The stock mainly decreases of 0.01 molP.m^{-2} under inorganic form, while the organic phosphorus stock remains stable.

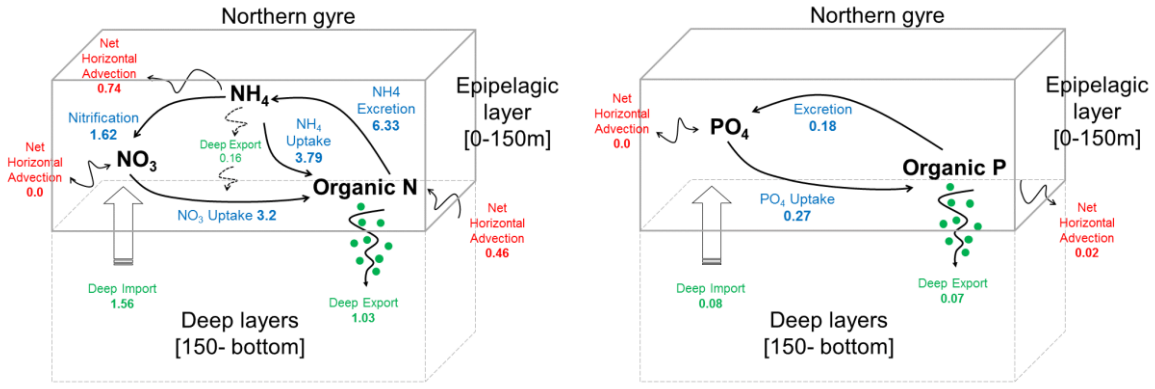

Figure 13: Annual budget of the nitrogen (left panel) and phosphorus (right panel) cycle in the surface layer of the northern gyre region [mol.m^{-2}.y^{-1}]

4. Conclusion

For the first time to our knowledge, a coupled physical biogeochemical model has been compared to a high resolution dataset taken at three seasons of the same year and documenting a strong convective winter, a bloom and the oligotrophic period. The study was focused on the dense water formation area of the northwestern Mediterranean (northern gyre). The model reproduces quite well the intensity and timing of the biogeochemical events concerning the efflorescence magnitude, the vertical nutrient intrusion in the epipelagic layer and the depth of the nutriclines. The model appears very stable as the nutrients stocks in the northern gyre do not vary significantly between the beginning and the end of the year.

The impact of the atmospheric variability on the water column stratification and the biogeochemical properties of the upper water has been shown. Preconditioning by the wind driven gyre in autumn produces a shallowing of nutriclines allowing the triggering of the autumn bloom. Convection in winter upwells large amounts of nutrients in the euphotic layer. When the conditions for chlorophyll development are gathered, a phytoplankton bloom is triggered with a massive consumption of nutrients during more than one month resulting at the end of April in a depletion of nutrients at the surface. Nutrients consumption continues to deplete nutrients at increasing depth, and to increase the nutriclines and DCM depths. That finally leads to the summer oligotrophy of the water column. Abiotic parameters, such as the vertical mixing, are not the only one responsible for this global dynamics. Coupling and decoupling of plankton groups could also influence the ecosystem dynamics (Behrenfeld et al., 2013) as suggested by the collapse of heterotrophs when the mixed layer strongly deepens (mid-January). The Mediterranean northern gyre therefore performs like the North Atlantic sub-polar gyre where winter, characterized by strong mixing (Barton et al., 2014) inhibits the development of phytoplankton.

The time-series of processes affecting nitrate, phosphate and the N:P ratio show periods of decoupling between nitrogen and phosphorus processes. The N:P ratio indeed changes mainly during transition periods whatever they are physically or biogeochemically driven. The first case is the triggering of convection through the enrichment of surface waters with nutrients from deep waters which suddenly reduces the ratio N:P. The second case is the start of the bloom which increases N:P by the nutrients uptake, especially because heterotrophs biomass is slightly developed and by consequence excretion is limited. The third case occurs at the peak of the bloom when nutrients stock strongly decreases, uptake decreases, and excretion by the heterotrophs is maximum. Nitrification creates a decoupling in the recycling of nutrients decreasing the ratio N:P. Besides these strong events, the N:P ratio of the epipelagic layer slowly decreases in autumn by the preconditioning which lifts the nutriclines and so upwells low N:P subsurface water.

A budget of nitrogen and phosphorus is proposed for the region. At the annual scale, the surface layer of the dense water formation area does not exchange nitrate with the peripheric regions while it is a source of ammonium and a sink of organic matter for the periphery. The deep layer is a source of about 0.37 molN.m^{-2}.y^{-1} for the surface layer (resultant of nitrate import/organic nitrogen export) while the surface layer is a source of 0.28 molN.m^{-2}.y^{-1} for the peripheric regions (mainly resultant of an export of 0.74 molN.m^{-2}.y^{-1} of ammonium and an import of 0.46 molN.m^{-2}.y^{-1} of organic nitrogen). The deep

layer is a source of 0.01 molP.m^{-2}.y^{-1} for the surface layer (resultant of phosphate import/organic phosphorus export). The surface layer exports 0.02 molP.m^{-2}.y^{-1} to the peripheric regions.

Appendix – Model parameters

Table A.1: List of state variables

State Variables	Description	Units
Nut_1 (NO_3), Nut_2 (NH_4), Nut_3 (PO_4), Nut_4 (SiO_4)	Nitrate, Ammonium, Phosphate, Silicate	mmol m^{-3}
$XPhy_1$, $XPhy_2$, $XPhy_3$	Pico-, nano-, micro- phytoplankton in X, X = C (carbon), N (nitrogen), P (phosphorus) or Si (silica)	mmolX m^{-3}
$ChlPhy_1$, $ChlPhy_2$, $ChlPhy_3$	Pico-, nano- micro- phytoplankton in chlorophyll	mgChl m^{-3}
$CZoo_1$, $CZoo_2$, $CZoo_3$	Nano-, micro- and meso-zooplankton	mmolC m^{-3}
Cbac	Bacteria	mmolC m^{-3}
DOX	Dissolved organic X, X=carbon, nitrogen, and phosphorus	mmolX m^{-3}
$XDet_Y$	Heavy (Y=H) and light (Y=L) particulate organic X, X= carbon, nitrogen, phosphorus, silica and chlorophyll	mmolX m^{-3}
Oxyg	Dissolved oxygen	$MmolO_2$ m^{-3}

Table A.2: List of parameters of the biogeochemical model and references.

Symbol	Description	Units		Values			Ref.
Phytoplankton				**Phy_1**	**Phy_2**	**Phy_3**	
φ_{max,Phy_i}	Maximum quantum yield	mmolC J^{-1}		2.2e-4	2.47e-4	3.45e-4	c
a_{Chl,Phy_i}	Chl-specific absorption coeff.	m^2 $mgChl^{-1}$		0.032	0.016	0.013	2,c
τ_{Phy_i}	Renewal time of photosystems	d		2.3e-8	3.5.e-8	4.7e-8	3,c
σ_{Phy_i}	Cross-section of photosystems	m^2 J^{-1}		18	12	9	4,5,c
k_d	Dimensionless photoinhibition rate	-		2.6e-8	2.6e-8	2.6e-8	6
k_{rep}	Rate of repair of photoinhibition damaged PSII	d		2e-4	2e-4	2e-4	6
$(N/C)_{min,Phy_i}$	Minimal internal N/C quota	molN $molC^{-1}$		0.05	0.05	0.05	7,8,9
$(N/C)_{max,Phy_i}$	Maximal internal N/C quota	molN $molC^{-1}$		0.2	0.2	0.2	7,8,9
$(P/C)_{min,Phy_i}$	Minimal internal P/C quota	molP $molC^{-1}$		0.004	0.002	0.002	8,10,11
$(P/C)_{max,Phy_i}$	Maximal internal P/C quota	molP $molC^{-1}$		0.019	0.019	0.019	8,10,11
$(Si/C)_{min,Phy_i}$	Minimal internal Si/C quota	molSi $molC^{-1}$		-	-	0.05	9,11
$(Si/C)_{max,Phy_i}$	Maximal internal Si/C quota	molSi $molC^{-1}$		-	-	0.19	9,11
$(Chl/N)_{max,Phy_i}$	Maximal internal Chl/N quota	molChl $molN^{-1}$		2.3	2.3	2.3	12,13,c
Q_{Phy}^{10}	Temperature coefficient	-		2.0	2.0	2.0	14
T_{Phy}^{REF}	Reference temperature	°C		14	14	14	c
k_{resp,Phy_i}	Respiration cost for growth	-		0.3	0.25	0.2	13,14,16,c
$\beta_{Phy_i,N}$	Nitrogen parameter for growth rate limitation	molN $molC^{-1}$		-	0.0072	0.002	c
$\beta_{Phy_i,P}$	Phosphorus parameter for growth rate limitation	molP $molC^{-1}$		-	0.0002	0.0005	c

$\beta_{Phy_i,Si}$	Silica parameter for growth rate limitation	molSi molC^{-1}		-	-	0.004	c
k_{Si}	Nitrogen parameter for growth rate limitation by silica	molN molC^{-1}		-	-	0.1	c
k_{Phy_i,NO_3}	Half saturation constant for NO_3	mmolN m^{-3}		0.5	0.7	1	11,15,17,18,c
k_{Phy_i,NH_4}	Half saturation constant for NH_4	mmolN m^{-3}		0.1	0.3	0.7	15,17,18,c
k_{inhib}	Inhibition coefficient by NH_4	mmolN m^{-3}		0.578	0.578	-	17
Inhib	Inhibition parameter by NH_4	-		0.82	0.82	-	17
k_{Phy_i,PO_4}	Half saturation constant for PO_4	mmolP m^{-3}		0.005	0.015	0.05	11,18,19,c
k_{Phy_i,SiO_4}	Half saturation constant for SiO_4	mmolSi m^{-3}		-	-	1.2	11,c
r_{Phy_i,NO_3}	Respiration cost for NO_3 uptake	molC molN^{-1}		0.397	0.397	0.397	16
r_{Phy_i,NH_4}	Respiration cost for NH_4 uptake	molC molN^{-1}		0.198	0.198	0.198	16
r_{Phy_i,PO_4}	Respiration cost for PO_4 uptake	molC molP^{-1}		0.155	0.155	0.155	16
r_{Phy_i,SiO_4}	Respiration cost for SiO_4 uptake	molC molSi^{-1}		-	-	0.140	16
τ_{mort,Phy_i}	Natural mortality rate	d^{-1}		0.2722	0.1944	0.1728	C
w_{s,Phy_i}	Sinking rate	m d^{-1}		-	-	0.6912	7,15,c

Zooplankton				**Zoo_1**	**Zoo_2**	**Zoo_3**	
g_{Zoo_i}	Maximum grazing rate	d^{-1}		3.89	2.59	1.30	7,21,22,c
k_{g,Zoo_i}	Half saturation constant	mmolC m^{-3}		5	8.5	20	23,c
Ψ_{Zoo_i}	Sloppy feeding fraction	-		0.23	0.23	0.23	7,24
β_{Zoo_i}	Assimilation efficiency	-		0.6	0.6	0.6	7,24
k_{c,Zoo_i}	Net growth efficiency	-		0.8	0.8	0.8	7,24

$(N/C)_{Zoo_i}$	Internal N/C quota	molN molC^{-1}		0.18	0.18	0.18	7,10,25
$(P/C)_{Zoo_i}$	Internal P/C quota	molP molC^{-1}		0.013	0.013	0.013	10,25,c
τ_{mort,Zoo_i}	Natural mortality rate	d^{-1}		0.22	0.17	-	20,c
τ_{pred}	Predation mortality rate	m^3 (mmolC d)$^{-1}$		-	-	0.061	20,c
$fr_{Det_L}^{Eges_{Si}}$	Ratio light/heavy Si detritus in residu of egestion			-	0.8	0.8	c
$fr_{Det_L}^{MortZoo_i}$	Ratio light/heavy detritus in zooplankton loss term	-		1	1	0.95	c
Q_{Zoo}^{10}	Temperature coefficient	-		2.0	2.0	2.0	7
T_{Zoo}^{REF}	Reference temperature	°C		18	18	18	C
$pref_{i,Prey}$	Preference of Zooplankton i for Prey		-				

Zooi/Prey	Bacteria	Phy_1	Phy_2	Phy_3	Zoo_1	Zoo_2	Det_L
Zoo_1	0.35	0.65	0	0	0	0	0
Zoo_2	0.08	0.06	0.3	0.15	0.25	0.12	0.04
Zoo_3	0	0	0	0.5	0	0.45	0.05

Bacteria

μ_{Bac}	Maximum DOC uptake	d^{-1}		3.672	c
k_{DOC}	Half-saturation for DOC uptake	mmolC m^{-3}		25	24
ω_{Bac}	Bacteria gross growth efficiency	-		0.3	24,c
$(N/C)_{Bac}$	Bacteria internal N/C quota	molN molC^{-1}		0.232	10
$(P/C)_{Bac}$	Bacteria internal P/C quota	molP molC^{-1}		0.022	10,28
$k_{NH_4,Bac}$	Half-saturation for NH_4 uptake	mmolN m^{-3}		0.2	24,c
$k_{PO_4,Bac}$	Half-saturation for PO_4 uptake	mmolP m^{-3}		0.007	25,c
$\tau_{mort,Bac}$	Bacteria natural mortality rate	d^{-1}		0.06	20
Q_{Bac}^{10}	Temperature coefficient	-		2.95	10
T_{Bac}^{REF}	Reference temperature	°C		20	c

Non-living matter					
$\tau_{decomp,CDet}$	Detritus decomposition rate, C	d^{-1}		0.1728	c
$\tau_{decomp,NDet}$	Detritus decomposition rate, N	d^{-1}		0.2074	c
$\tau_{decomp,PDet}$	Detritus decomposition rate, P	d^{-1}		0.1814	c
$\tau_{decomp,ChlDet}$	Detritus decomposition rate, Chl	d^{-1}		0.4009	c
$\tau_{decomp,SiDet}$	Detritus decomposition rate, Si	d^{-1}		0.02	c
w_{s,Det_L}	Light detritus sinking rate	m d^{-1}		0.7	15,c
w_{s,Det_H}	Heavy detritus sinking rate	m d^{-1}		90	15,c
Q_{decomp}^{10}	Temperature coefficient for decomposition	-		2.37	c
T_{decomp}^{REF}	Reference temperature for decomposition	°C		20	c
τ_{nitrif}	Nitrification rate	d^{-1}		0.05	15,c
Q_{nitrif}^{10}	Temperature coefficient for nitrification	-		2.37	10
T_{nitrif}^{REF}	Reference temperature for nitrification	°C		10	c

Oxygen				
N/O	Mol O2 needed to oxidize 1 mol of NHs in nitrification	molN/molC	2	29
C/O	Mol O2 used per mol C in oxic respiration	molC/molO	1	29

C: carbon ; N: nitrogen ; P: phosphorus ; Si: silicate ; NO3 : nitrate ; NH4 : ammonium ; PO4 : phosphate ; SiO4 : silica ; Phy1 : pico-phytoplankton ; Phy2: nano-phytoplankton ; Phy3: micro-zooplankton ; Zoo1 : nano-zooplankton ; Zoo2: micro-zooplankton ; Zoo3: meso-zooplankton ; DOC: Dissolved organic carbon ; (c) Calibration ; (1) (*Babin et al.*, 1996) ; (2) (*Claustre et al.*, 2005) ; (3) (*Laney et al.*, 2005) ; (4) (*Moore et al.*, 2003) ; (5) (*Gorbunov et al.*, 1999) ; (6) (*Oliver et al.*, 2003) ; (7) (*Raick et al.*, 2005) ; (8) (*Riegman et al.*, 2000) ; (9) (*Geider et al.*, 1998) ; (10) (*Vichi et al.*, 2007) ; (11) (*Sarthou et al.*, 2005) ; (12) (van den Meersche et al., 2004) ; (13) (Sondergaard and Theil-Nielsen, 1997) ; (14) (Soetaert et al, 2001) ; (15) (Lacroix et Grégoire, 2002) ; (16) (*Cannell and Thornley*, 2000) ; (17) (*Harrison et al.*, 1996) ; (18) (*Tyrrell and Taylor*, 1996) ; (19) *(Timmermans et al.*, 2005) ; (20) (*Fasham et al.*, 2006) ; (21) (*Christaki et al.*, 2002) ; (22) (*Nejstgaard et al.*, 1997) ; (23) (*Hansen et al.*, 1997); (24) (*Anderson and Pondaven*, 2003); (25) (*Goldman et al.*, 1987) ; (26) (*Liu and Dagg*, 2003) ; (27) (*Thingstad et al.*, 1993) ; (28) (*Thingstad*, 2005) ; (29) (Grégoire et al., 2008).

Appendix – State variables of the model

$$\frac{dCPhy_i}{dt} = GPP_i - RespPhy_i - Exu_{i,C} - MortPhy_{i,C} - \sum_{j=1}^{3} Graz_{j,CPhy_i}$$

$$\frac{dNPhy_i}{dt} = UptPhy_{i,NH_4} - UptPhy_{iNO_3} - Exu_{i,N} - MortPhy_{i,N} - \sum_{j=1}^{3} Graz_{j,NPhy_i}$$

$$\frac{dPPhy_i}{dt} = UptPhy_{i,PO_4} - Exu_{i,P} - MortPhy_{i,P} - \sum_{j=1}^{3} Graz_{j,PPhy_i}$$

$$\frac{dSiPhy_i}{dt} = UptPhy_{i,SiO_4} - Exu_{i,Si} - MortPhy_{i,Si} - \sum_{j=1}^{3} Graz_{j,SiPhy_i}$$

$$\frac{dChlPhy_i}{dt} = Synth_{i,Chl} - MortPhy_{i,Chl} - \sum_{j=1}^{3} Graz_{j,ChlPhy_i}$$

$$\frac{dCZoo_i}{dt} = GrowthZoo_{i,C} - MortZoo_{i,C} - \sum_{j=1}^{3} Graz_{j,CZoo_i} - RespZo_i^{add}$$

$$\frac{dCBac}{dt} = UptBac_{DOC} - RespBac - MortBac_C - \sum_{j=1}^{3} Graz_{j,CBac}$$

$$\frac{dCDet_S}{dt} = \sum_{i=1}^{3} MortPhy_{i,C} + \sum_{i=1}^{3} Eges_{i,C} + \sum_{i=1}^{2} fr_{Det_S}^{MortZoo_i} MortZoo_{i,C} + fr_{Det_S}^{MortZoo_3} PredZoo_{3,C} - Rem_{C,Det_S} - \sum_{i=1}^{3} Graz_{i,CDet_S}$$

$$\frac{dPDet_S}{dt} = \sum_{i=1}^{3} MortPhy_{i,P} + \sum_{i=1}^{3} Eges_{i,P} + \sum_{i=1}^{2} fr_{Det_S}^{MortZoo_i} MortZoo_{i,P} + fr_{Det_S}^{MortZoo_3} PredZoo_{3,P} - Rem_{P,Det_S} - \sum_{i=1}^{3} Graz_{i,PDet_S}$$

$$\frac{dNDet_S}{dt} = \sum_{i=1}^{3} MortPhy_{i,N} + \sum_{i=1}^{3} Eges_{i,N} + \sum_{i=1}^{2} fr_{Det_S}^{MortZoo_i} MortZoo_{i,N} + fr_{Det_S}^{MortZoo_3} PredZoo_{3,N} - Rem_{N,Det_S} - \sum_{i=1}^{3} Graz_{i,NDet_S}$$

$$\frac{dSiDet_S}{dt} = MortPhy_{3,Si} + fr_{Det_S}^{Eges_{Si}} . \sum_{i=2}^{3} Eges_{i,Si} - Decomp_{Si,Det_S}$$

$$\frac{dChlDet_S}{dt} = \sum_{i=1}^{3} MortPhy_{i,Chl} + \sum_{i=2}^{3} Eges_{i,Chl} - Decomp_{Chl,Det_S}$$

$$\frac{dCDet_L}{dt} = \sum_{i=1}^{3} (1 - fr_{Det_S}^{MortZoo_i}) MortPhy_{i,C} + (1 - fr_{Det_S}^{MortZoo_3}) MortPhy_{i,C} - Decomp_{C,Det_L} - \sum_{i=1}^{3} Graz_{i,CDet_L}$$

$$\frac{dPDet_L}{dt} = \sum_{i=1}^{3} (1 - fr_{Det_S}^{MortZoo_i}) MortPhy_{i,P} + (1 - fr_{Det_S}^{MortZoo_3}) MortPhy_{i,P} - Decomp_{P,Det_L} - \sum_{i=1}^{3} Graz_{i,PDet_L}$$

$$\frac{dNDet_L}{dt} = \sum_{i=1}^{3} (1 - fr_{Det_S}^{MortZoo_i}) MortPhy_{i,N} + (1 - fr_{Det_S}^{MortZoo_3}) MortPhy_{i,N} - Decomp_{N,Det_L} - \sum_{i=1}^{3} Graz_{i,NDet_L}$$

$$\frac{dSiDet_L}{dt} = (1 - fr_{Det_S}^{Eges_{Si}}) . \sum_{i=2}^{3} Eges_{i,Si} - Decomp_{Si,Det_L}$$

$$\frac{dDOC}{dt} = \sum_{i=1}^{3} Exu_{i,C} + \sum_{i=1}^{3} SloppyFeed_{i,C} + MortBac_C + Decomp_{CDet_S} + Decomp_{CDet_L} + UptBac_{DOC}$$

$$\frac{dNO_3}{dt} = Nitrif + \sum_{i=1}^{3} UptPhy_{i,NO_3}$$

$$\frac{dNH_4}{dt} = \sum_{i=1}^{3} ExcZoo_{i,NH_4} + ExcBac_{NH_4} + Nitrif - \sum_{i=1}^{3} UptPhy_{i,NH_4} - UptBac_{NH_4}$$

$$\frac{dPO_4}{dt} = \sum_{i=1}^{3} ExcZoo_{i,PO_4} + ExcBac_{PO_4} - \sum_{i=1}^{3} UptPhy_{i,PO_4} - UptBac_{PO_4}$$

$$\frac{dSiO_4}{dt} = Exu_{3,Si} + Rem_{SiDet_S} + Rem_{SiDet_L} - UptPhy_{3,SiO_4}$$

$$\frac{dO_2}{dt} = PPB \times C/O + Resp_{phy} \times C/O + Resp_{zoo} \times C/O + Resp_{bact} \times C/O + UptN \times N/O - Nitrif \times N/O$$

5. References

- Anderson, T. R., and P. Pondaven. Non-redfield carbon and nitrogen cycling in the Sargasso Sea: pelagic imbalances and export flux, Deep-Sea Res., Part I, 50, 573–591, 2003.
- Arrigo, K. R., 2005. Marine microorganisms and global nutrient cycles. Nature 437, 349–355.
- Auger, P. a., Diaz, F., Ulses, C., Estournel, C., Neveux, J., Joux, F., Pujo-Pay, M. and Naudin, J. J.: Functioning of the planktonic ecosystem on the Gulf of Lions shelf (NW Mediterranean) during spring and its impact on the carbon deposition: A field data and 3-D modelling combined approach, Biogeosciences, 8(11), 3231–3261, doi:10.5194/bg-8-3231-2011, 2011.
- Auger, P. a., Ulses, C., Estournel, C., Stemmann, L., Somot, S. and Diaz, F.: Interannual control of plankton communities by deep winter mixing and prey/predator interactions in the NW Mediterranean: Results from a 30-year 3D modeling study, Prog. Oceanogr., 124, 12–27, doi:10.1016/j.pocean.2014.04.004, 2014.
- Babin, M., D. Stramski, G.M. Ferrari, H. Claustre, A. Bricaud, G. Obolensky, and N. Hoepffner (2003), Variations in the light absorption coefficients of phytoplankton, nonalgal particles, and dissolved organic matter in coastal waters around Europe, J. Geophys. Res., 108, 3211, doi:10.1029/2001JC000882, 2003.
- Baklouti, M., Faure, V., Pawlowski, L. and Sciandra, A.: Investigation and sensitivity analysis of a mechanistic phytoplankton model implemented in a new modular numerical tool (Eco3M) dedicated to biogeochemical modelling, Prog. Oceanogr., 71(1), 34–58, doi:10.1016/j.pocean.2006.05.003, 2006.
- Banse, K. 1994. Grazing and zooplankton production as key controls of phytoplankton production in the open ocean. Oceanography, 7, 13–20.
- Barton, A. D., Lozier, M. S. and Williams, R. G.: Physical controls of variability in North Atlantic phytoplankton communities, Limnol. Oceanogr., 60(1), 181–197, doi:10.1002/lno.10011, 2015.
- Behrenfeld, M. J.: Abandoning Sverdrup ' s Critical Depth Hypothesis on phytoplankton blooms Critical Depth Hypothesis Abandoning Sverdrup ' s on phytoplankton, , 91(4), 977–989, doi:10.1890/09-1207.1, 2013
- Bethoux, J.P., Gentili, B., Raunet, J., Tailliez, D., 1990. Warming trend in the western Mediterranean deep water. Nature 247, 660–662
- Butenschön, M., M. Zavatarelli, and M. Vichi (2012), Sensitivity of a marine coupled physical biogeochemical model to time resolution, integration scheme and time splitting method, Ocean Modell., 52–53, 36–53, doi:10.1016/j.ocemod.2012.04.008.
- Cannell, M. G. R., and J.H.M. Thornley (2000), Nitrogen States in Plant Ecosystems: A Viewpoint, Ann. Bot.-London, 86, 1161–1167.
- Christaki, U., C. Courties, H. Karayanni, A. Giannakourou, C. Maravelias, K.A. Kormas, and P. Lebaron (2002), Dynamic Characteristics of Prochlorococcus and Synechococcus Consumption by Bacterivorous Nanoflagellates, Microb. Ecol., 43, 341–352.

- Claustre, H., M. Babin, D. Merien, J. Ras, L. Prieur, S. Dallot, O. Prasil, H. Dousova, and T. Moutin, T. (2005), Toward a taxon-specific parameterization of bio-optical models of primary production: A case study in the North Atlantic, J. Geophys. Res., 110, C07S12, doi:doi:10.1029/2004JC002634.
- D'Ortenzio, F. and Ribera d'Alcalà, M.: On the trophic regimes of the Mediterranean Sea: a satellite analysis, Biogeosciences Discuss., 5(4), 2959–2983, doi:10.5194/bgd-5-2959-2008, 2009.
- Durrieu de Madron, X., et al.: Marine ecosystems' responses to climatic and anthropogenic forcings in the Mediterranean, Prog. Oceanogr., 91(2), 97–166, doi:10.1016/j.pocean.2011.02.003, 2011.
- Estrada, M., Latasa, M., Emelianov, M., Gutiérrez-Rodríguez, A., Fernández-Castro, B., Isern-Fontanet, J., Mouriño-Carballido, B., Salat, J. and Vidal, M.: Seasonal and mesoscale variability of primary production in the deep winter-mixing region of the NW Mediterranean, Deep Sea Res. Part I Oceanogr. Res. Pap., 94, 45–61, doi:10.1016/j.dsr.2014.08.003, 2014.
- Estournel, C., Zervakis, V., Marsaleix, P., Papadopoulos, A., Auclair, F., Perivoliotis, L., Tragou, E., 2005. Dense water formation and cascading in the Gulf of Thermaikos (North Aegean), from observations and modelling. Continental Shelf Research 25, 2366–2386.
- Estournel., C, Testor., P, Damien., P, D'Ortenzio., F, Marsaleix., P, Conan., P, Kessouri., F, Durrieu de Madron., X, Coppola., L, Lellouche., J.M, Belamari., S, Mortier., L, Ulses., C., Prieur., L. High resolution modelling of dense water formation in the north-western Mediterranean: benefits from an improved initial state in summer. 2015.
- Fasham, M. J. R., K.J. Flynn, P. Pondaven, T.R. Anderson, and P.W. Boyd (2006), Development of a robust marine ecosystem model to predict the role of iron in biogeochemical cycles: A comparison of results for iron-replete and iron-limited areas, and the SOIREE iron-enrichment experiment, Deep-Sea Res. Pt. 1, 53, 333–366.
- Gačić, M., Civitarese, G., Miserocchi, S., Cardin, V., Crise, a. and Mauri, E.: The open-ocean convection in the Southern Adriatic: A controlling mechanism of the spring phytoplankton bloom, Cont. Shelf Res., 22(14), 1897–1908, doi:10.1016/S0278-4343(02)00050-X, 2002.
- Geider, R. J., and J. LaRoche, Redfield revisited : variability of C :N :P in marine microalgae ane its biochemical base, European Journal of Phycology, 37, 1–17, 2002.
- Geider, R. J., H.L. Macintyre, L.M. Graziano, and R.M.L. McKay (1998), Responses of the photosynthetic apparatus of Dunaliella tertiolecta (Chlorophyceae) to nitrogen and phosphorus limitation, Eur. J. Phycol., 33, 315–332.
- Gogou, A., Sanchez-Vidal, A., Durrieu de Madron, X., Stavrakakis, S., Calafat, A. M., Stabholz, M., Psarra, S., Canals, M., Heussner, S., Stavrakaki, I. and Papathanassiou, E.: Reprint of: Carbon flux to the deep in three open sites of the Southern European Seas (SES), J. Mar. Syst., 135, 170–179, doi:10.1016/j.jmarsys.2014.04.012, 2014.
- Goldman, J. G., D.A. Caron, and M.R. Dennett (1987), Nutrient cycling in a microflagellate food chain: IV. Phytoplankton microflagellate interactions, Mar. Ecol.-Prog. Ser., 38, 75–87.

- Gorbunov, M. Y., Z.S. Kolber, and P.G. Falkowski.(1999), Measuring photosynthetic parameters in individual algal cells by Fast Repetition Rate fluorometry, Photosynth. Res., 62, 141–153.
- Gorbunov, M. Y., Z.S. Kolber, and P.G. Falkowski.(1999), Measuring photosynthetic parameters in individual algal cells by Fast Repetition Rate fluorometry, Photosynth. Res., 62, 141–153.
- Grégoire, M., Raick, C. and Soetaert, K.: Numerical modeling of the central Black Sea ecosystem functioning during the eutrophication phase, Prog. Oceanogr., 76(3), 286–333, doi:10.1016/j.pocean.2008.01.002, 2008.
- Harrison, W. G., L.R. Harris, and B.D. Irwin (1996), The kinetics of nitrogen utilization in the oceanic mixed layer: Nitrate and ammonium interactions at nanomolar concentrations, Limnol. Oceanogr., 41, 16–32.
- Hansen, P. J., P.K. Bjørnsen, and B.W. Hansen (1997), Zooplankton grazing and growth: Scaling within the 2–2,000-∼III body size range, Limnol. Oceanogr., 42, 687–704.
- Herrmann, M., Somot, S., 2008. Relevance of ERA40 dynamical downscaling for modeling deep convection in the Mediterranean Sea. Geophysical Research Letters 35.
- Herrmann, M., Diaz, F., Estournel, C., Marsaleix, P., Ulses, C. Impact of atmospheric and oceanic interannual variability on the Northwestern Mediterranean Sea pelagic planktonic ecosystem and associated carbon cycle. Journal of Geophysical Research – Oceans 118, 5792–5813. 2013
- Huertas, I. E., Ríos, a. F., García-Lafuente, J., Navarro, G., Makaoui, a., Sánchez-Román, a., Rodriguez-Galvez, S., Orbi, a., Ruíz, J. and Pérez, F. F.: Atlantic forcing of the Mediterranean oligotrophy, Global Biogeochem. Cycles, 26(2), n/a–n/a, doi:10.1029/2011GB004167, 2012.
- Kessouri et al., Biogeochemical cycles of the Mediterranean Sea: climatologies and budget. (In prep-a).
- Lacombe, H., Tchernia, P., Gamberoni, L., 1985. Variable bottom water in the Western Mediterranean Basin. Progress in Oceanography 14, 319–338.
- Lacroix, G., and M. Grégoire (2002), Revisited ecosystem model (MODECOGeL) of the Ligurian Sea: seasonal and interannual variability due to atmospheric forcing, J. Marine Syst., 37, 229–258
- Laney, S. R., R.M. Letelier, and M.R. Abbott (2005), Parameterizing the natural fluorescence kinetics of Thalassiosira weissflogii, Limnol. Oceanogr., 50, 1499–1510.
- Large, W. G. and S. Yeager, 2009: The global climatology of an interannually varying air-sea flux data set. Climate Dynamics, 33, 341–364, doi:10.1007/s00382-008-0441-3
- Lellouche, J.-M., O. Le Galloudec, M. Drévillon, C. Régnier, E. Greiner, G. Garric, N. Ferry, C. Desportes, C.-E. Testut, C. Bricaud, R. Bourdallé-Badie, B. Tranchant, M. Benkiran, Y. Drillet, A. Daudin, and C. De Nicola (2013), Evaluation of global monitoring and forecasting systems at Mercator Océan, Ocean Sci., 9, 57-81, doi:10.5194/os-9-57-2013.
- Liu, H., and M. Dagg (2003), Interactions between nutrients, phytoplankton growth, and micro- and mesozooplankton grazing in the plume of the Mississippi River, Mar. Ecol.-Prog. Ser., 258, 31–42.

- Marsaleix P., Auclair F., Floor J. W., Herrmann M. J., Estournel C., Pairaud I., Ulses C., 2008. Energy conservation issues in sigma-coordinate free-surface ocean models. Ocean Modelling. 20, 61-89. http://dx.doi.org/10.1016/j.ocemod.2007.07.005
- Marsaleix P., Auclair F., Estournel C., 2009. Low-order pressure gradient schemes in sigma coordinate models: The seamount test revisited. Ocean Modelling, 30, 169-177. http://dx.doi.org/10.1016/j.ocemod.2009.06.011
- Marsaleix P., Auclair F., Estournel C., Nguyen C., Ulses C., 2011. An accurate implementation of the compressibility terms in the equation of state in a low order pressure gradient scheme for sigma coordinate ocean models. Ocean Modelling, 40, 1-13 http://dx.doi.org/10.1016/j.ocemod.2011.07.004
- Marsaleix P., Auclair F., Duhaut T., Estournel C., Nguyen C., Ulses C., 2012. Alternatives to the Robert-Asselin filter. Ocean Modelling, 41, 53-66 http://dx.doi.org/10.1016/j.ocemod.2011.11.002
- MEDOC Group, 1970. Observation of formation of deep water in the Mediterranean Sea, 1969. Nature, 227:1037-1040.
- Mertens, C. and F. Schott, 1998. Interannual Variability of Deep-Water Formation in the Northwestern Mediterranean. Journal of Physical Oceanography, 28(7):1410–1424. doi: 10.1175/1520-0485(1998)028<1410:IVODWF>2.0.CO;2.
- Moore, C. M., D. Suggett, P.M. Holligan, J. Sharples, E.R. Abraham, M.I. Lucas, T.P. Rippeth, N.R. Fisher, J.H. Simpson, and D.J. Hydes (2003), Physical controls on phytoplankton physiology and production at a shelf sea front: a fast repetition-rate fluorometer based field study, Mar. Ecol.-Prog. Ser., 259, 29–45.
- Nejstgaard, J. C., I. Gismervik, and P.T. Solberg (1997), Feeding and reproduction by Calanus finmarchicus, and microzooplankton grazing during mesocosm blooms of diatoms and the coccolithophore Emiliania huxleyi, Mar. Ecol.-Prog. Ser., 147, 197217.
- Oliver, R. L., J. Whittington, Z. Lorenz, and I.T. Webster (2003), The influence of vertical mixing on the photoinhibition of variable chlorophyll a fluorescence and its inclusion in a model of phytoplankton photosynthesis, J. Plankton Res., 25, 1107–1129.
- Ovchinnikov, I.M., 1984. The formation of IntermediateWater in theMediterranean. Oceanology, 24:168–173.
- Pollak, M. I., 1951. The sources of deep water of the EasternMediterranean Sea. Journal of Marine Research, Nittis, K. and A. Lascaratos, 1998. Diagnostic and prognostic numerical studies of LIW formation. Journal of Marine Systems, 18(1-3):179–195. doi: 10.1016/S0924-7963(98)00011-6.10:128–152.
- Pujo-Pay, M., Conan, P., Oriol, L., Cornet-Barthaux, V., Falco, C., Ghiglione, J. F., Goyet, C., Moutin, T. and Prieur, L.: Integrated survey of elemental stoichiometry (C, N, P) from the western to eastern Mediterranean Sea, Biogeosciences, 8(4), 883–899, doi:10.5194/bg-8-883-2011, 2011.
- Raick, C., Delhez, E. J. M., Soetaert, K. and Grégoire, M.: Study of the seasonal cycle of the biogeochemical processes in the Ligurian Sea using a 1D interdisciplinary model, J. Mar. Syst., 55(3-4), 177–203, doi:10.1016/j.jmarsys.2004.09.005, 2005.

- Raimbault P, Coste B Very high values of nitrate:phosphate ratio (>30) in the subsurface layers of the western Mediterranean Sea. Rapp P-V Reun Comm int Mer Med32(1):C-18. 1990.
- Redfield, A.C.,Ketchum,B.H.,Richards,F.A.,1963.Theinfluence of organisms on the composition of sea water. In: Hill, M.N.(Ed.),The Sea. Wiley Interscience, Hoboken, N.J.,pp.26–77.
- Ribera d'Alcalà, M.: Nutrient ratios and fluxes hint at overlooked processes in the Mediterranean Sea, J. Geophys. Res., 108(C9), doi:10.1029/2002JC001650, 2003.
- Riegman, R., W. Stolte, A.A.M. Noordeloos, and D. Slezak (2000), Nutrient uptake and alkaline phosphatase (ec 3:1:3:1) activity of emiliania huxleyi (Prymnesiophyceae) during growth under n and p limitation in continuous cultures, J. Phycol., 36, 87–96.
- Sarthou, G., K.R. Timmermans, S. Blain, and P. Tréguer (2005) Growth physiology and fate of diatoms in the ocean: a review, J. Sea. Res., 53, 25–42.
- Santinelli, C., Ibello, V., Lavezza, R., Civitarese, G., Seritti, A., 2012. New insights into C, N and P stoichiometry in the Mediterranean Sea : the Adriatic Sea case. Cont. Shelf Res.44,83–93.
- Schroeder, K., Gasparini, G. and Borghini, M.: Biogeochemical tracers and fluxes in the Western Mediterranean Sea, spring 2005, J. Mar. … [online] Available from: http://www.sciencedirect.com/science/article/pii/S0924796309002516 (Accessed 3 April 2013), 2010.
- Severin, T., Conan, P., Durrieu De Madron, X., Houpert, L., Oliver, M. J., Oriol, L., Caparros, J. and Pujo-Pay, M.: Impact of open-ocean convection on nutrient, phytoplankton biomass and activity, Deep Sea Res. Part I Oceanogr. Res. Pap., Submitted, 62–71, doi:10.1016/j.dsr.2014.07.015, 2014.
- Soetaert, K., P.M.J. Herman, J.J. Middelburg, C. Heip, C.L. Smith, P. Tett, and K. Wild-Allen (2001), Numerical modelling of the shelf break ecosystem: reproducing benthic and pelagic measurements. Deep-Sea Research II 48, 3141 – 3177.
- Soetaert, K., J.J. Middelburg, P.M.J. Herman, and K. Buis (2000), On the coupling of benthic and pelagic biogeochemical models. Earth-Sci. Rev. 51, 173–201.
- Sondergaard, M. and J. Theil-Nielsen (1997), Bacterial growth efficiency in lakewater cultures, Aquat. Microb. Ecol., 12, 115–122.
- Thingstad, T. F. (2005), Simulating the response to phosphate additions in the oligotrophic eastern Mediterranean using an idealized four member microbial food web model, Deep-Sea Res. Pt. 2, 52, 3074–3089.
- Thingstad, T. F., E.F. Skjoldal, and R.A. Bohne (1993), Phosphorus cycling and algal-bacterial competition in Sandsfjord, western Norway, Mar. Ecol.-Prog. Ser., 99, 239–259.
- Tyrrell, T., and A.H. Taylor (1996), A modelling study of Emiliania huxleyi in the NE atlantic, J. Marine Syst., 9, 83–112.

- Timmermans, K. R., B. Van der Wagt, M.J.W. Veldhuis, A. Maatman, and H.J.W. De Baar (2005), Physiological responses of three species of marine pico-phytoplankton to ammonium, phosphate, iron and light limitation, J. Sea Res., 53, 109–120.
- Tyrrell, T., and A.H. Taylor (1996), A modelling study of Emiliania huxleyi in the NE atlantic, J. Marine Syst., 9, 83–112.
- Ulses, C., Estournel, C., Puig, P., Durrieu de Madron, X. and Marsaleix, P.: Dense shelf water cascading in the northwestern Mediterranean during the cold winter 2005: Quantification of the export through the Gulf of Lion and the Catalan margin, Geophys. Res. Lett., 35(7), 2–7, doi:10.1029/2008GL033257, 2008.
- Van den Meersche, K., J.J. Middelburg, K. Soetaert, P. van Rijswijk, H.T.S. Boschker, and C.H.R. Heip (2004), Carbon-nitrogen coupling and algal-bacterial interactions during an experimental bloom: Modeling a ^{13}C tracer experiment, Limnology and Oceanography, 3, doi: 10.4319/lo.2004.49.3.0862.
- Vichi, M., N. Pinardi, and S. Masina (2007), A generalized model of pelagic biogeochemistry for the global ocean ecosystem. Part I: Theory, J. Marine Syst., 64, 89–109.
- Williams, R.G., A.J McLaren and M.J. Follows, 2000: Estimating the convective supply of nitrate and implied variability in export production over the North Atlantic. Global Biogeochemical Cycles, 14, 1299-1313.
- Yilmaz, A.,Tugrul,S.,1998.The effect of cold-and warm core eddies on the distribution and stoichiometry of dissolved nutrients in the north eastern Mediterranean.J.Mar.Syst.16,253–268.

Title: **Phytoplankton dynamics and biogeochemical fluxes in the western Mediterranean Sea using a 3D physical/biogeochemical coupled model**

Table des matières

1. Introduction 110
2. Methods 112
   2.1. The hydrodynamic model 112
   2.2. The biogeochemical model 113
   2.3. Areas of study 114
   2.4. MODIS satellite dataset 114
   2.5. Determination of the bloom onset 115
   2.6. Calculation of the F-ratio 115
3. Model evaluation 115
4. Results and discussion 117
   4.1. Atmospheric conditions 117
   4.2. Vertical mixing and chlorophyll concentration 118
      4.2.1. The Northern Gyre 118
      4.2.2. The shallow convection area 120
      4.2.3. The stratified region 120
   4.3. Conditions at the onsets of the phytoplankton efflorescence 122
   4.4. Primary production 124
   4.5. Particulate organic carbon export 125
   4.6 The trophic regimes 127
5. Conclusion 128
6. References 129

Authors:

F. Kessouri[1], C. Ulses[1], C. Estournel[1], P. Marsaleix[1], and DeWEx Group

[1] Laboratoire d'Aérologie, UMR 5560 CNRS, Université de Toulouse 3, 14 avenue Edouard Belin, 31400 Toulouse, France

Key points up to three (<100 characters)

- Seasonality of nutrients concentrations (nitrate, phosphate)
- Deep convection, light limitation
- Spring and autumn phytoplankton bloom

- Bloom initiation conditions
- Trophic regimes
- carbon export, primary production

Abstract

A 3D very high resolution coupled hydrodynamic biogeochemical model of the western Mediterranean basin has been used to study the chlorophyll dynamics in three hydrodynamic distinct regions, deep convection, shallow convection and stratified areas, along three directions. The first direction focuses on the conditions leading to the onset of the bloom in autumn and winter. In autumn the vertical inflow of nutrients triggers the bloom in the three regions while at the end of winter the shutdown of turbulent mixing is responsible of the bloom onset in the deep convection area. The decoupling of phytoplankton and zooplankton is also a factor fostering the phytoplankton growth. The second direction focuses on the primary production and the particulate organic carbon (POC) export. The comparison of convection areas and the stratified region shows that the second one exhibits a higher annual primary. The Algerian sub-basin, which includes the largest part of the stratified area, is apparently favored by a long period of enrichment and by a subsurface production higher in the deep chlorophyll maximum. When it comes to POC export flux below the photic layer, convection areas appear to be more efficient than stratified ones. Indeed, strong export events are predicted by the model during the mixing events. The exported matter stems from the biological production preceding the mixing events. The autumnal bloom starting in December is at the origin of an important part of this exported biological matter. The third direction concerns the trophic regimes of the western basin. The northwestern sub-basin is characterized by a eutrophic regime in late winter and spring, and an oligotrophic one in summer and fall. While deep convection is detrimental to the phytoplankton development during the first two months of winter, the enrichment in nutrients is then responsible of the post convective phytoplankton bloom encircled in the cyclonic gyre of the sub-basin. The Algerian sub-basin with its no bloom regime is oligotrophic because of its recycling based production all along the year.

1. Introduction

The Mediterranean Sea by its multiple trophic regimes hosts a high geographic heterogeneity in phytoplankton distribution. The scarcity of observations on phytoplankton prevents from a precise study of its spatial and temporal variability. The present understanding of the phytoplankton distribution relies essentially on sea surface remote sensing observations (Morel and André, 1991; Antoine et al., 1995; Bosc et al., 2004; D'Ortenzio and Ribera D'Alcalà. 2009). Recently, Lavigne et al. (2015) completed this surface description by showing the main properties of the deep chlorophyll variability over the Mediterranean Sea.

Many experimental studies focused on the understanding of the bloom initiation (Sverdrup. 1953; Townsend et al. 1992; Backhaus et al. 1999; 2011; Huisman et al. 2002; Behrenfeld. 2010; 2014; Chiswell. 2011; Brody et al. 2013; and others) in

the Ocean by investigating the atmospheric, hydrological and/or biological properties. Several hypothesises were exposed to explain the favourable conditions of the bloom development (Behrenfeld and Boss, 2014). The first hypothesis, the critical depth hypothesis, relies on the mixed layer depth (Sverdrup, 1953). According to this theory, the phytoplankton is homogeneously distributed inside the Mixed Layer Depth (MLD), the mixing below the euphotic layer limits its exposure to light. The bloom is triggered when the light exposure increases and ML becomes shallower than a critical depth where phytoplankton growth is higher than phytoplankton losses. This first theory was reconsidered by several studies displaying an onset of the bloom under deep MLD and/or low light conditions (Halldal 1953; Dale et al. 1999; Backhaus et al. 2003; Boss & Behrenfeld 2010; Behrenfeld et al. 2013). The second hypothesis relies on the magnitude of the turbulent kinetic energy. Using a diffusivity model, Huisman et al. (2002) showed that the bloom can develop when the turbulent mixing becomes smaller than a critical value, before a change of the density structure of the water column. Below this critical turbulent mixing, the residence time of phytoplankton in the euphotic layer is then sufficiently increased. Taylor and Ferrari (2011) showed that the depth of the turbulent mixing becomes shallow at the end of the deepening of the ML and as net heat flux becomes positive. This theory was also questioned by observations reported by Behrenfeld et al., (2013) showing a phytoplankton biomass increase during the deepening of the ML. A third theory of the bloom onset, the disturbance recovery hypothesis relies on the decoupling between phytoplankton growth and loss rates, in particular the loss rate corresponding to grazing, induced by a physical process. However this hypothesis can hardly be confirmed by *in situ* measurements.

Bernadello et al., 2012 studied the interannual variability of the bloom in the North-Western (NW) region based on a 3D coupled model. Their results showed that certain years the spring bloom is initiated whereas the MLD is still deep. Conditions of close-to-zero heat flux and low turbulence kinetic energy appear to be more appropriate conditions to trigger the bloom for every studied year (2002-2010). Using chlorophyll and nitrate observations Lavigne (2013) claimed that the bloom in the NW subbasin would not be driven by a decrease of grazing pressure but by a light deficit. Indeed during the mixing period, the nitrate uptake rate is smaller than the rate of nitrate injection. The likely decrease of grazing could not allow a phytoplankton development high enough to favour the consumption of the nutrients injected in the euphotic layer. Phytoplankton would then be limited by light when ML is deep. However these observations didn't allow concluding if stratification (first hypothesis) or stabilization (second hypothesis) of the water column would be at the origin of the bloom.

The Mediterranean Sea is generally considered as one of the most oligotrophic sea in the world (Azov, 1991, Antoine et al., 1995), with a clear west-east gradient (Siokou-Frangou et al., 2010). In many studies, relatively low productivity was deduced from in situ observations (Sournia 1973; Turley et al., 2000; Moutin and Raimbault, 2002) and ocean colour satellite data (Bosc et al., 2004; D'Ortenzio and Ribera d'Alcalà, 2009, Uitz et al., 2012). The most productive areas include the convection areas, in particular in the NW sub-basin, the Alboran Sea and the shelves influenced by large nutrient inputs. In the other regions, Deep Chlorophyll Maximum (DCM) structures prevail, except during mixing periods (Siokou-Frangou et

al., 2010). Based on 3D modelling, Macias et al. (2014) state that ~62% of the total primary production in the open seas may take place in these structures. Gogou et al. (2014) who investigated the strength and efficiency of the carbon sequestration in the Mediterranean Sea found that the fraction of primary production exported under the photic layer is in the order of 11% using sediment trap measurements and primary production estimations deduced from satellite data.

The objective of the present work is to describe phytoplankton dynamics and biogeochemical fluxes in the Western Mediterranean (WM) using a high resolution 3D hydrodynamic/biogeochemical coupled modelling. It also aims at gaining understanding on the conditions favoring the beginning of the phytoplankton efflorescence in this region. The DeWEx cruises have allowed a description of the spatial distribution of phytoplankton in the north-western Mediterranean in winter 2012-2013, during the deep convection period, and in spring 2013 during the phytoplankton bloom. This has offered the opportunity to calibrate and validate our 3D coupled modelling during two key seasons in order to use it to describe an entire seasonal cycle. The article starts with a presentation of the methods and an evaluation of the model. Atmospheric forcing, vertical mixing and chlorophyll profile seasonal cycles are then presented over the period Sept. 2012-Sept. 2013. The conditions favorable to phytoplankton development are investigated in the following section. Afterwards, the seasonal cycle of primary production and particulate organic carbon is described. Finally, the trophic regimes in the NW are evaluated and discussed.

2. Methods

2.1. The hydrodynamic model

The SYMPHONIE model used in this study is a 3D primitive equation, free surface and generalized sigma vertical coordinate, described by Marsaleix et al. (2009, 2011 and 2012). We used the configuration described by Kessouri et al. (in prep b). The horizontal grid presented in figure 1, covers a large part of the western Mediterranean basin. The horizontal resolution is about 1 km (variable from 0.8 to 1.4 km^2 from the north to the south of the domain) to represent the scales related to the Rossby radius, of the order of 10 km. Forty vertical levels were used with closer spacing near the surface (15 levels in the first 100 meters in the center of the convection zone characterized by depths of ~2500 m). The model was initialized and forced at its lateral boundaries with daily analysis PSY2V2R4 provided by the Mercator-Ocean operational system (Lellouche et al., 2013) at a resolution of 1/12° over the Atlantic and the Mediterranean from 20°S to 80°N. As in Estournel et al. (2015), the initial field and open boundary conditions were corrected from stratification biases deduced from comparisons between analysis and observations taken during the MOOSE cruise of August 2012. The atmospheric forcing (turbulent fluxes) was calculated using the bulk formulae of Large and Yeager (2004). Meteorological parameters including radiative fluxes are given by the ECMWF operational forecasts at 1/8° horizontal resolution and 3 hours temporal resolution based on daily analysis at 00.00 UTC.

Rivers runoff were taken into account using realistic daily values for French rivers (data provided by Banque Hydro, www.hydro.eaufrance.fr) and Ebro (data provided by SAIH Ebro, www.saihebro.com) and mean annual values for the others.

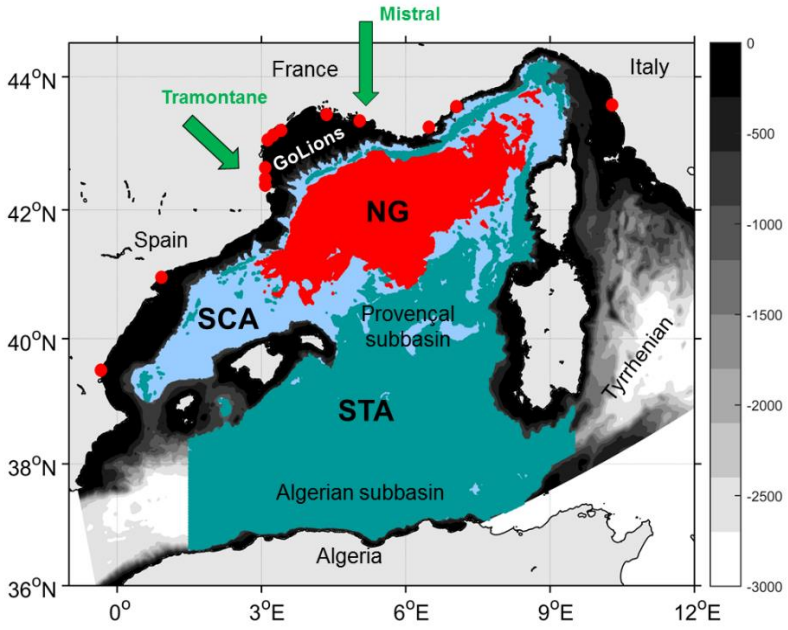

Figure 1: Bathymetry (m) of the modeled area in the Western Mediterranean Sea and location of the three regions analyzed in this study (Northern gyre: NG (in red), Shallow convection area: SC (in blue) and Stratified area: ST (in green)). The red points represent the location of the modeled rivers mouths.

2.2. The biogeochemical model

The Eco3M-S model is a multi-nutrient and multi-plankton functional type model that simulates the dynamics of the biogeochemical decoupled cycles of several biogenic elements (carbon, nitrogen, phosphorus and silicon) and of non-redfieldian plankton groups. The model structure used in this study is based on the same pelagic plankton ecosystem model as the one fully described and used by Auger et al. (2011; 2014), Herrmann et al. (2013) and Kessouri et al. (in prep b).. Eight compartments constitute the model: a first compartment of phytoplankton classified by size (pico-phytoplankton [0.7–2 µm], nanophytoplankton [2–20 µm] represented by dinoflagellates and micro-phytoplankton [20–200 µm] represented by diatoms) is represented by the mechanistic formulations of the model Eco3M (Baklouti et al., 2006), a second compartment of zooplankton is composed by nano-zooplankton [5–20 µm] representing small flagellates, micro-zooplankton [20–200 µm] representing ciliates and large flagellates and meso-zooplankton [>200 µm] representing copepods and amphipods, and a third compartment of bacteria. Bacteria and zooplankton dynamics are derived from Anderson and Pondaven (2003) and adapted by Raick et al. (2005) for multi-group and multi-element modeling in the Ligurian Sea. The other compartments are

dissolved organic matter, particulate organic matter (small and large, differentiated by the settling speed and origin), inorganic nutrients (nitrate, ammonium, phosphate and silicate) and dissolved oxygen. A total of 34 state variables are calculated.

The biogeochemical model is downscaled from the Mediterranean basin scale to the regional scale described here. The biogeochemical basin scale model is forced by the daily fields from the NEMO model used for the boundary conditions of our hydrodynamic model. This configuration initialized in 2008 with climatological nutrients fields is described in Kessouri et al. (in prep-a). Daily values of all state variables are extracted from this run for the initial and lateral boundary conditions of the regional model. This nesting protocol ensures a coherence of the physical and biogeochemical fields at the open boundaries. The regional model is initialized in August 2012.

The deposition of organic and inorganic matter from the atmosphere is neglected in this study. The benthic fluxes of inorganic nutrients are taken into account by coupling the pelagic model with a simplified version of the meta-model described by Soetaert et al. (2001). The parameters of this latter model have been set according to the modelling study in the Gulf of Lions shelf performed by Pastor et al. (2011).

Rivers runoff were taken into account using realistic daily values for French rivers (data provided by Banque Hydro, www.hydro.eaufrance.fr) and Ebro (data provided by SAIH Ebro, www.saihebro.com) and mean annual values for the others.

2.3. Areas of study

We investigate in this study the biogeochemical functioning in three different areas of the NW sea (indicated in Fig. 1). the first studied region is the Northern Gyre (NG), which includes the area surrounded by the Northern Current, the West Corsican Current, the Balearic front and the Northern Current recirculation at the eastern boundary of the Balearic Sea; it is defined here as the area where the daily averaged MLD exceeds 1000 depth at least one day during the winter convection. The second studied region is the Shallow Convection Area (SCA), defined as the area where the daily averaged MLD exceeds 150 m (and is lower than 1000 m). The third area, named the STratified area (STA), corresponds to a region covering a large part of a deep pelagic zone of the southwestern Mediterranean (Algerian subbasin) where winter maximum MLD has been lower than 150 m. These regions are characterized by different phenology as showed by D'Ortenzio and Ribera d'Alcalà (2009) and Lavigne et al. (2013). Heat fluxes, hydrodynamic and biogeochemical variables presented in the following are averaged on these three areas.

2.4. MODIS satellite dataset

Daily mean surface chlorophyll concentrations have been extracted from MODIS (or Moderate Resolution Imaging

Spectroradiometer) Aqua (EOS PM) satellites data set (Ocean Biology Processing Group, 2014) on the period Sept. 2012-Sept. 2013, in order to evaluate the intensity and the temporal evolution of the modeled surface in the three selected regions defined in 2.3.

2.5. Determination of the bloom onset

Several methods have been used to determine the date of the onset of the phytoplankton bloom in order to understand the physical, biogeochemical and environmental factors that control the bloom. The method established by Siegel et al. (2002) defines the onset as the first day of the year (starting end of June) when surface chlorophyll concentration exceeds the annual median plus 5 %. Adjustments of this method was made for instance in order to avoid taking the autumnal bloom by considering the beginning of the investigated year after this bloom (Henson et al. 2006; 2009), or in order to avoid considering a small transient concentration increase by changing the value of the threshold (10% instead of 5% as in Bernardello et al. 2012).

Behrenfeld (2014) proposed another method based on rates of biomass change. He argued that this method is more appropriate than the median method mentioned above to detect the bloom onset when the phytoplankton biomass is low at the beginning of the bloom. In this study, we have used this second type of methods. The onsets of the bloom correspond to the days where the rate of change, defined in Eq. 1, is higher than 50 % of the maximal annual rate of change.

$$Rate\ of\ Change = \frac{\log(Int\_Chla_t - Int\_Chla_{t-1})}{\partial t} \qquad with\ \partial t = 3\ days \quad Eq.1$$

Where *Int_Chla* is the depth-integrated chlorophyll concentration and *∂t* the time step set here to three days.

2.6. Calculation of the F-ratio

In order to understand what drives the primary production in each region the *F-ratio* (Eppley and Peterson, 1979) (Eq. 3) has been evaluated. In the first calculation, the remineralized nitrate throughout nitrification are taking into account.

$$F_{ratio} = New\ Primary\ Production\ /(New + Regenerated) Primary\ Production \quad \text{(Eq. 3)}$$

With, $New\ Primary\ Production = [N0_3\ uptake - nitrification]$,

And $Regenerated\ Primary\ Production = [NH_4\ uptake\ ]$.

3. Model evaluation

A validation of the hydrodynamic and the biogeochemical coupled models has been described in extension in Estournel et al. (2015), and Kessouri et al., (in prep-b). It was performed through a comparison of the model results to nutrient and

chlorophyll observations collected during DeWEx campaigns. It was concluded that the model reproduces the timing of the convection and bloom events, the depth of the DCM and nutriclines and the intensity of the efflorescence in the north-western Mediterranean basin. Here, the seasonal evolution of surface chlorophyll modeled and observed by the satellite MODIS is presented over the period Sept. 2012-Sept. 2013 for three WM regions, the NG, the SCA and the STA, defined in section 2.3 (Fig. 2). It is completed by a statistical analysis through Taylor diagrams (Fig. 3).

The timing of the phytoplankton development in surface and its intensity are generally correctly represented by the model in the three studied regions (Fig. 2). The Pearson correlation between surface chlorophyll from the model and from the satellite is equal to 0.78 in the NG, 0.84 in the SCA and 0.86 in the STA (Fig. 3). Low values in the NG region, around 0.1 $mg.m^{-3}$, are attained during the period of deep convection, between January 16 and March 7th, both in the model and satellite data. Maximum values in this area are reached between 9 and 15 April 2013 in both time-series. In the SC region, they are reached the third week of March and in the ST region in mid-March.

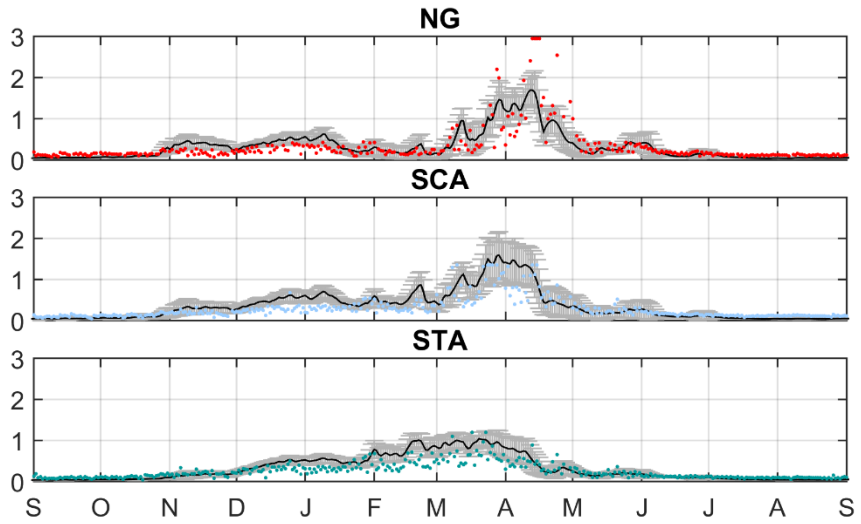

Figure 2: Surface chlorophyll concentration ($mg.m^{-3}$) times series in the northern gyre, shallow convection area and stratified area (indicated in Fig. 1)

Figure 3 shows that the RMS error is around 0.26 $mg.m^{-3}$ in the NG where the signal is high during the bloom. It is smaller in both surrounding areas (0.19 $mg.m^{-3}$ in SCA, 0.16 $mg.m^{-3}$ in STA).

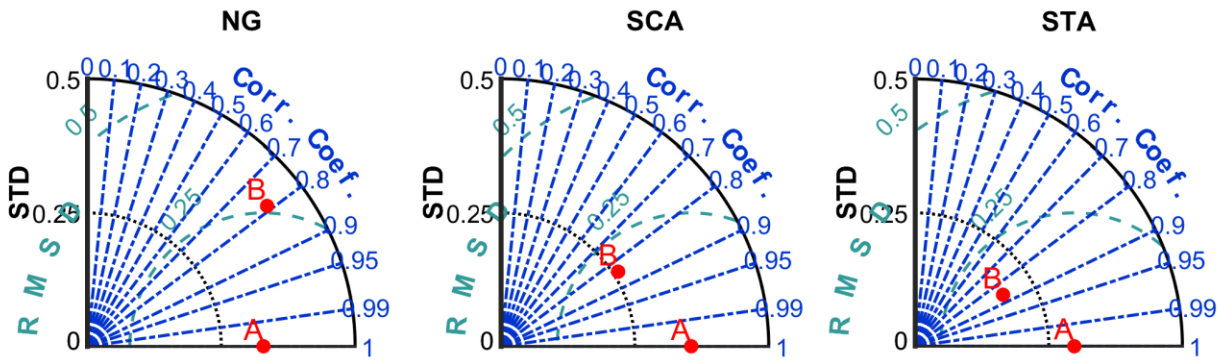

Figure 3: Taylor diagram presenting the comparisons between modeled and observed surface chlorophyll in three western Mediterranean regions, NG, SCA and STA. A is the observations from MODIS and B is the model outputs.

4. Results and discussion

4.1. Atmospheric conditions

The heat flux evolution follows the same trend in the three studied regions (Fig. 4). The time correlation coefficients between SCA and NG regions, and between STA and NG subbasins heat fluxes are resp. 0.96 and 0.93. Each region is characterized by a significant heat loss with a great variability between mid-October 2012 and mid-March 2013 and a clear heat gain from mid-March 2013 to September 2013. However one can notice that the intensity is different. Heat losses are more intense in the NG, directly exposed to the Mistral and Tramontane winds, than in the two other regions. They reach 1200 W/m^2 in October 2012 in the NG. In this region, heat flux presents a winter average around -180 W/m^2 while it is equal to -140 W/m^2 in the SCA and -130 W/m^2 in the STA. The heat loss exceeds 400 W/m^2 several times during the studied period in the NG whereas it rarely exceeds this value in the two other regions.

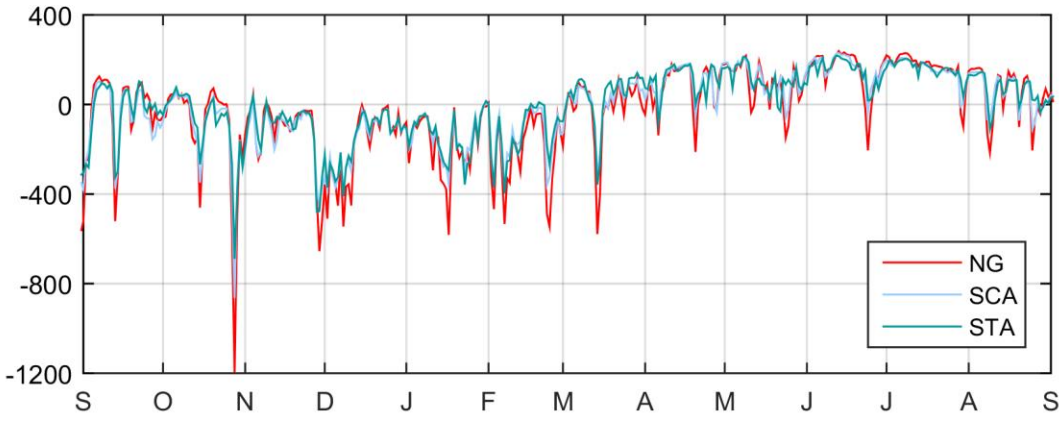

Figure 4: Time series of total heat flux (W m^{-2}) in the three studied regions.

4.2. Vertical mixing and chlorophyll concentration

4.2.1. The Northern Gyre

Figure 5 presents the modeled evolution of the MLD and the chlorophyll concentration profiles from September 2012 to September 2013 averaged over the NG region.

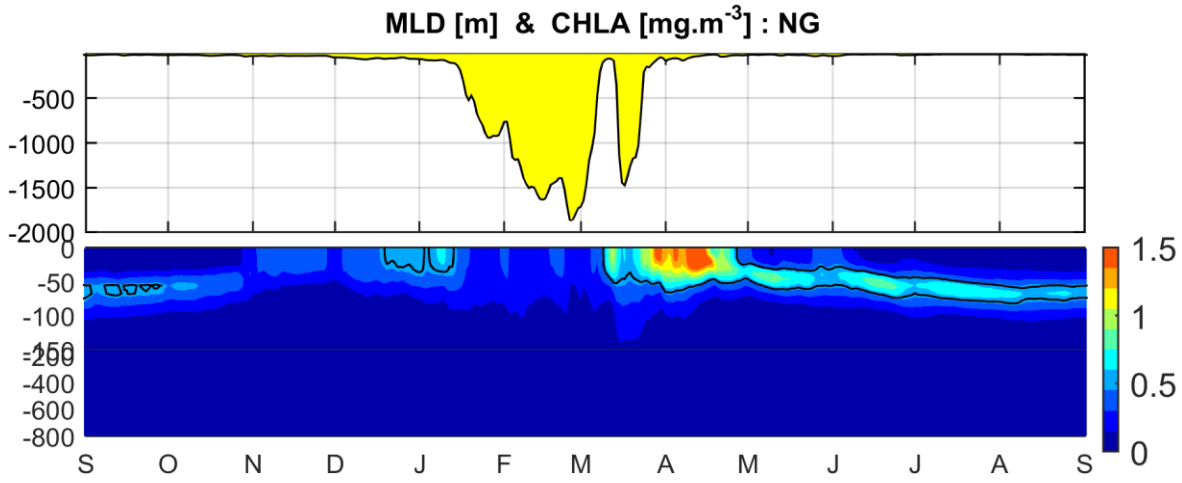

Figure 5: Mixed layer depth and chlorophyll evolution in the NG region indicated in Figure 1.

The ML starts to deepen in November. The mixing intensifies in January. Three successive and progressive mixing events are distinguishable between January and early March. The MLD reaches its maximal depth (area's averaged around 1870 m) on 25 February. A last strong mixing event occurs then in mid-March.

The deep chlorophyll maximum (DCM) is positioned at about 60-70 m depth at the beginning of autumn. It progressively approaches the surface until disappearing at the beginning of November during wind-induced mixing that also provokes an enrichment of nutrients in the upper layer. Nitrate concentration reaches more than 1 mmol.m^{-3} and phosphate more than 0.05 mmol.m^{-3} at the surface at this period (Kessouri et al., in prep. b). Phytoplankton efflorescence is then visible at the surface between early December and early January, chlorophyll concentration reaching 0.6 mg.m^{-3} over this period. The use of the rate of change method gives an autumnal bloom onset on 1st December 2012. The chlorophyll concentration decreases during the three strong mixing events mentioned above and at the date of the maximum MLD, the concentration surface is very low (< 0.1 mg.m^{-3}). In early March, an important efflorescence occurs in the surface layer (0-50 m depth). We have found that the onset of the late winter bloom corresponds to the 4th of March. This winter efflorescence is followed by the last strong event of mixing that induces the dilution of phytoplankton over 1000 m depth. When the mixing decreases, a spring surface efflorescence appears at the end of March and lasts three weeks. During this phytoplankton efflorescence,

chlorophyll intensity remains highly variable. Maximum surface values (> 1.5 mg.m^{-3}) are reached between 9th and 15th April. Between May and August, the chlorophyll maximum gradually deepens to reach back 70 m depth in mid-summer.

It is noteworthy that both deep convection zone, marked by a minimum of chlorophyll (Fig. 6a), and bloom area, marked by maximum surface chlorophyll concentrations (Fig. 6b), are confined in the NG. Both areas followed globally the sea surface height (SSH) shape (Fig. 6c and 6d). Little contradictions are observed at the western boundary of the convection and bloom areas which is due to the advection of the surface chlorophyll. The depression is caused by a doming "up" of the temperature and salinity iso-lines that is compensated by a doming "down" of SSH by a mass conservation mechanism. The extension of the NG is variable in time nevertheless the area characterized by a minimum chlorophyll threshold of 0.1 mg.m^{-3} (cf. on February 18th: maximum extension day of the deep convection area) and the area covered by high chlorophyll concentrations (>2 mg.m^{-3}) concerns a large area which covers a mean surface of about 2 000 km^2 in mid-April. While chlorophyll concentrations (>1 mg.m^{-3}) covers about 15 000 km^2.

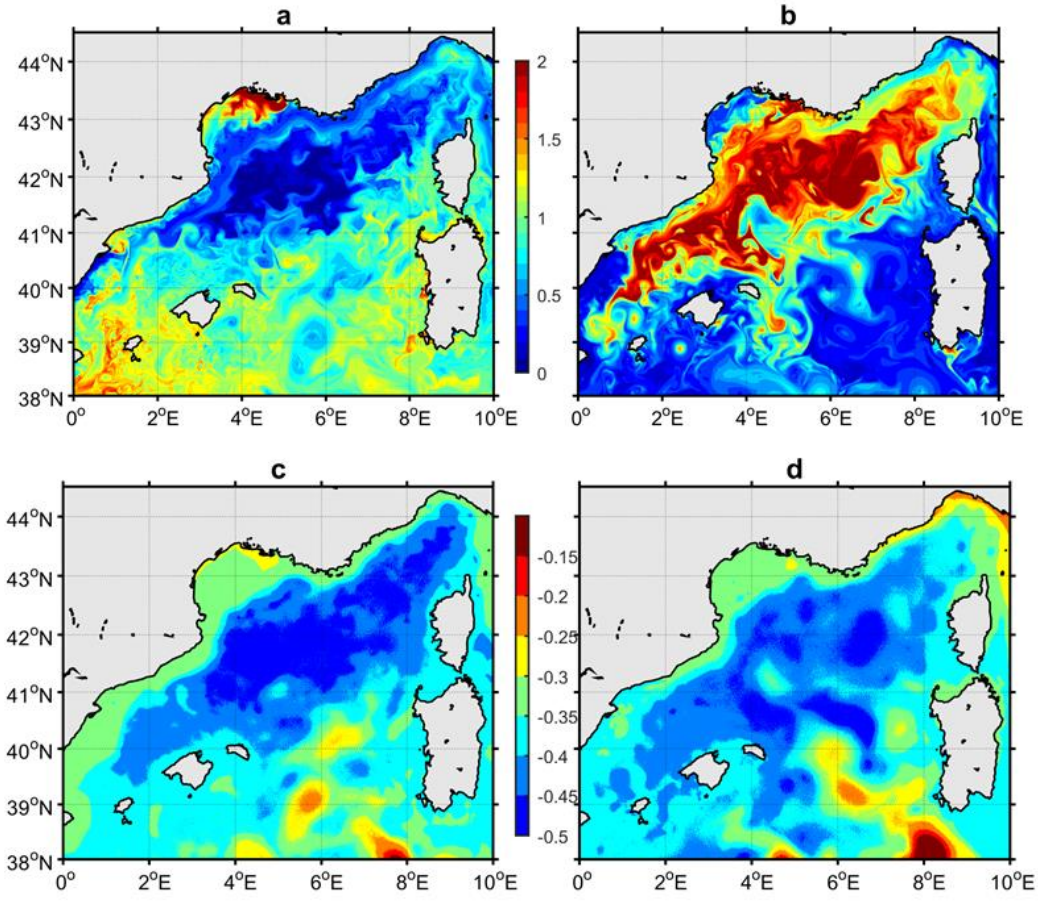

Figure 6: (a) Winter and (b) spring snapshot (13th April 2013) of the surface chlorophyll concentration from the model. (c) Winter and (d) spring snapshot of the sea surface high [cm]

4.2.2. The shallow convection area

Figure 7 shows the modeled annual cycle of the MLD and the chlorophyll concentration profile in the SCA region. The time evolution of MLD is similar (r^2=0.98, p<0.01) to the one in the NG. The depth of the ML is however lower than in the NG. The maximum MLD is around 380 m.

The time evolution of the chlorophyll profile in the SCA region is also very close to the one in the NG. At the beginning of autumn, the DCM is located at 90 m depth and progressively shallows until it disappears in the beginning of November. Chlorophyll concentration increases at the surface from the end of November. We have calculated an onset of the autumnal efflorescence on 30 November (one day before the date of autumnal bloom onset in the NG). During the following strong winter mixing the surface efflorescence is reduced. Afterwards, a late winter bloom starts end of January (26 January is identified as the onset of this bloom). During a month, chlorophyll concentration increases until reaching 1.5 mg.m^{-3} over more than 30 m depth. The bloom area extends in the whole SCA. At the third week of April, the DCM appears and deepens progressively.

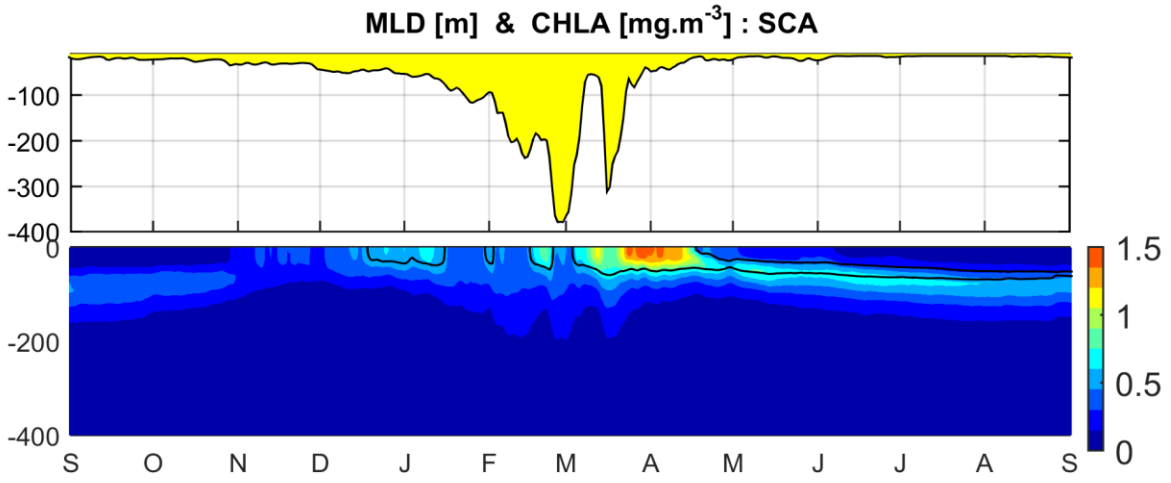

Figure 7: Same as Fig. 5 in the shallow convection region

4.2.3. The stratified region

Figure 8 displays the modeled evolution of the MLD and the chlorophyll concentration profile over the studied year in the STA. The evolution of the MLD is different, in particular in its intensity, from the one in the NG and SC regions. The ML deepens progressively from September to mid-February when it reaches 60 m. It shallows then until June. In this region, the ML never deepens below the photic zone.

The evolution of the chlorophyll profile is similar to the convection ones until mid-January when the mixing strongly intensifies in these latter regions. We have calculated that the onset of the bloom takes place on 4th December. The surface efflorescence continues until mid-April (from mid-February to the end of March, chlorophyll concentration varies between 0.8 and 1.1 mg.m^{-3} at the surface), when the chlorophyll maximum starts to deepen progressively. It stabilizes around 85 m in late June. Its intensity is about 0.5 mg.m^{-3} during the summer.

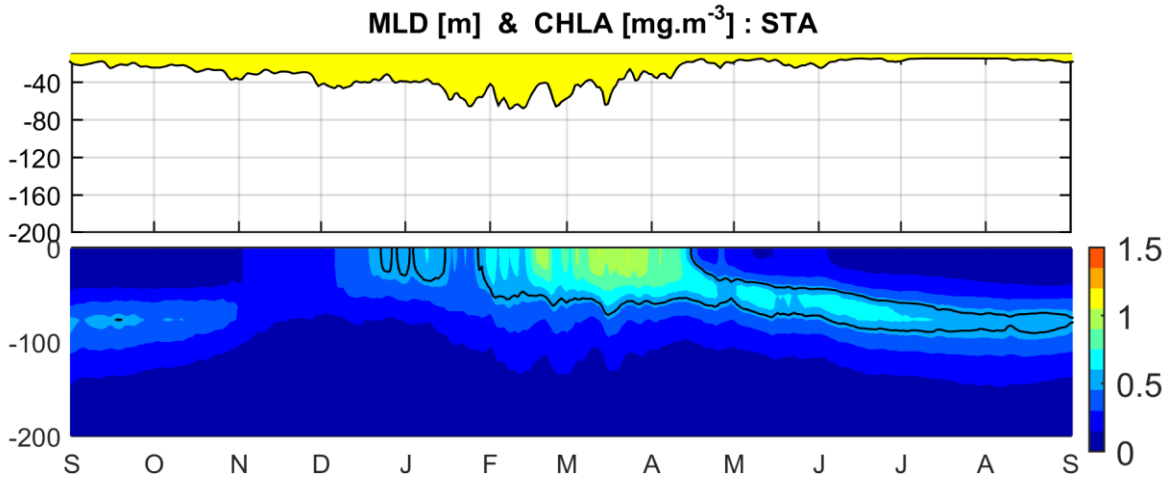

Figure 8: Same as Fig. 4 in the stratified region. Chlorophyll concentration profile and MLD depths have different scales than previous figures.

The chlorophyll concentration is maximum in mid-February in the STA. The highest values (Fig. 9a) are modeled on the edge of the anticyclonic eddies where the maximum gradient of density in subsurface waters emerges (Fig. 9b). The high chlorophyll concentration at the surface is due to the enhanced productivity recorded within filaments which surround eddies as well reported by numerical experiments of Lévy et al. (2001a) and Lévy and Klein (2004).

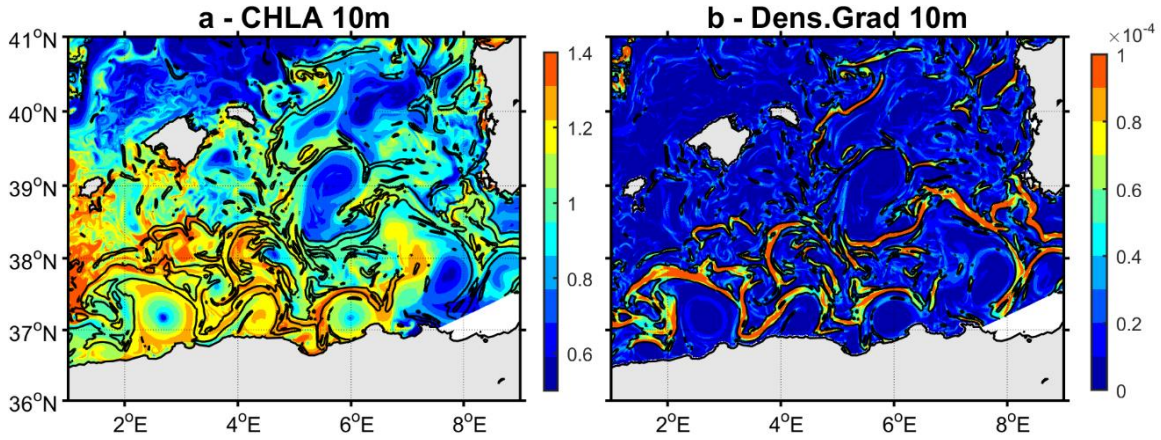

Figure 9: Snapshot (20th March 2013) of the chlorophyll concentration (mg.m^{-3}) and the potential density gradient (kg.m^{-3}) at 10 m depth in the Algerian sub-basin. Contours in both maps represent 0.3 10^{-4} kg.m^{-3} density gradient, in order to show how the water physical properties can drive phytoplankton distribution.

4.3. Conditions at the onsets of the phytoplankton efflorescence

As mentioned before, based on the rate of change method (Behrenfeld, 2014), the autumnal bloom onsets are found in the model results on 1st December in the NG, 30 November in the SCA and 4th December in the STA. This is in agreement with the study of Lavigne et al. (2013) who found, using the onset threshold method (Siegel et al., 2002) that the bloom starts in November or early December in all Mediterranean bio-regions. In the two convection regions, vertical mixing provokes temporary interruption and reduction of the phytoplankton development in early winter. A decrease in both surface and depth-integrated chlorophyll is found in January in these two regions (Fig. 10a and g). However, this decrease of biomass is distinctly more pronounced in the NG than in the SCA. We found that afterwards an intense phytoplankton development starts in late winter on 4th March in the NG and on 26th January in the SCA. In the STA, the vertical mixing remains shallow and only small decreases in the depth-integrated phytoplankton biomass take place (Fig. 10m). The maximum value of the depth-integrated biomass and its increase are clearly weaker than in the convection regions, in consistency with the classification of this region as a no-bloom regime by D'Ortenzio and Ribera d'Alcalà (2009) and Lavigne et al. (2013).

The conditions at the onset of the autumnal bloom are similar in the three studied regions: (1) the heat loss is quite important (-358 W.m^{-2} in the NG, -364 W.m^{-2} in the SCA and -230 W.m^{-2} in the STA, Fig. 10b,h,n), (2) the ML starts increasing (it deepens from 10 to 48 m in the NG, to 44 m in the SCA and to 46 m in the STA, Fig. 10c,i,o), (3) turbulent diffusivity is low (4 10^{-5} m^2.s^{-1} in the NG, 1 10^{-5} m^2.s^{-1} in the SCA and 2 10^{-4} m^2.s^{-1} in the STA, Fig. 10d,j,p), (4) zooplankton biomass have strongly decreased (245 mgC.m^{-2} in the NG, 288 mgC.m^{-2} in the SCA, 258 mgC.m^{-2} in the STA, Fig. 10e,k,q) and (5) nitrate concentration at the surface starts increasing (Fig. 10 f,l,r). Consequently, the availability of nutrients injected into the surface layer during wind-induced events, together with a decreasing grazing pressure, seem to be triggered conditions to the autumnal bloom.

In winter in the SCA, surface and depth-integrated chlorophyll do not evolved by the same trend. The rate of change method shows that the initiation happens early in winter when (1) the heat flux is negative (-124 W.m^{-2}, Fig. 10h), (2) ML is deepening (-117 m, Fig. 10i), (3) turbulence is still low (8 10^{-4} m^2.s^{-1}, Fig. 10j, it increases up to 0.01 m^2.s^{-1} during the phytoplankton development), (3) zooplankton pressure is minimum and nitrate is available (Fig. 10k,l). The onset of winter bloom detected in the shallow convection follows a short decrease of phytoplankton activity (between 15th January and 25th January) at the beginning of the convection at mid-January. The increase of nutrient stocks induced by the mixing events associated to an interruption of the mixing are in this area the conditions that favoured the beginning of the winter bloom.
In the NG, the conditions at the onset of the late winter NG bloom is different from the autumnal bloom. Indeed the late

winter bloom starts when the heat flux becomes positive (30 $W.m^{-2}$, Fig. 10b), and the vertical turbulence strongly decreases (0.01 $m^2.s^{-1}$, Fig. 10d). However, at the onset date, the water column is still homogenous: the ML is 1192 m deep (Fig. 10c). The surface concentration of nitrate is maximum (> 6.5 $mmol.m^{-3}$, Fig. 10f) and zooplankton pressure is minimum (183 $mgC.m^{-2}$, Fig. 10e). Low turbulent mixing seems then to be the main factor controlling this bloom onset. This result is consistent with the study of Bernardello et al. (2012) and Lavigne (2013) who showed that in the NG the phytoplankton development in winter is limited by a deficit in light and that the late winter bloom is triggered under low mixing. As in the results of Bernadello et al. (2012), we find that conditions of low heat flux and turbulent mixing are favorable to the bloom onset in consistency with the theory proposed by Huisman et al. (1999) and Taylor and Ferrari (2011).

As expected, the SCA presents an intermediate functioning between the ones of the NG and the STA. As in the NG, a second onset of the bloom is detected by the rate of change method. Indeed, in both convection areas, the first autumnal bloom was interrupted by a deficit of light due to mixing. However in the SCA, this interruption period is very short and the second bloom begins earlier in winter and under different atmospheric and hydrodynamic conditions than in the NG. This is explained by the functioning during the heart of the convection event. During that period, the availability of nutrients prevails on the deficit of light in the SCA, while it is the inverse in the NG. We remark that the surface nitrate and depth-integrated chlorophyll concentrations are temporally correlated in the SCA (r^2=0.75) and in the STA (r2=0.76) while the relation does not exist in the NG (r^2=0.001), between the date of the first bloom onset and the date of the maximum surface chlorophyll concentration. Moreover, the delay of the depth-integrated chlorophyll maximum compared to the surface nitrate maximum and to the maximum MLD is found twice more important in the NG (45 days) than in the SCA (25 days). In the STA the depth-integrated chlorophyll maximum values are attained within the period of maximum MLD around 60 m.

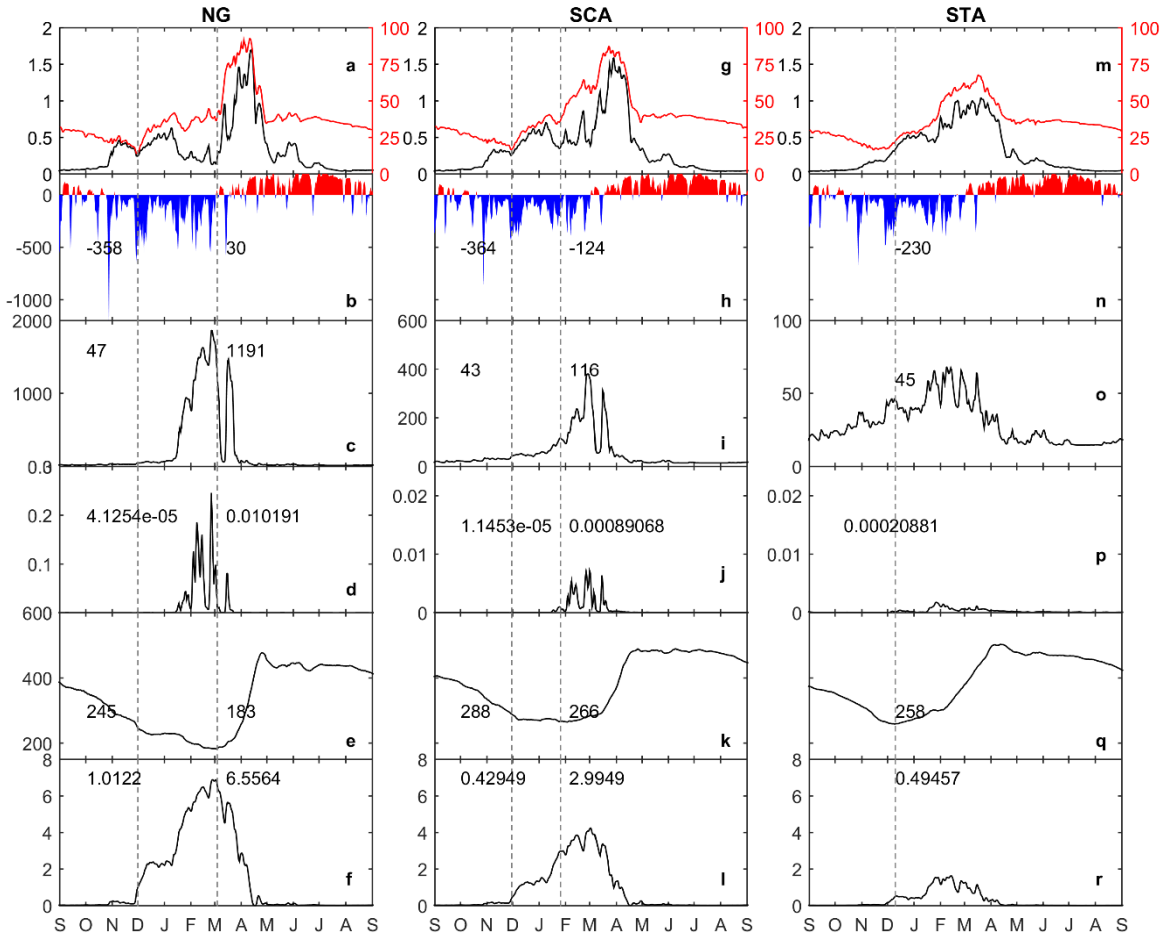

Figure 10: Conditions of the onset of the blooms in each region. Row 1. Average integrated chlorophyll in red (mgChl.m^{-2}) and surface chlorophyll in black (mgChl.m^{-3}). 2. Heat flux (W.m^{-2}). 3. MLD (m) 4. Turbulence average in the upper 75m (m^2.s^{-1}). 5. Integrated zooplankton biomass (mgC.m^{-2}). 6. Nitrate concentration at the surface (mmol.m^{-3}). Column 1: Northern Gyre. Column 2: Shallow convection area. Column 3: Stratified area.

4.4. Primary production

In the three investigated regions, the modeled net primary production (NPP) globally decreases slowly in fall and early winter (Fig. 11). However, in winter, it presents higher values by about 0.2 to 0.5 gC.m^{-2}.d^{-1} in the SCA and in the STA than in the NG, where deep mixing induces a strong decrease in productivity. At this period, the NPP reaches in this region a mean value of 0.1-0.15 gC.m^{-2}.d^{-1}. An increase of NPP starts then at the end of January in the SC and ST regions, while it starts one month later in the NG. The NPP is maximum in the three regions in spring (1.6 gC.m^{-2}.d^{-1} in the NG, 1.46 gC.m^{-2}.d^{-1} in the SCA, and 1.42 gC.m^{-2}.d^{-1} the STA). A secondary peak, more pronounced in the deep convection area than in the two other regions, occurred between mid-May and early June From early June to September NPP is then relatively stable:

around 0.6 $gC.m^{-2}.d^{-1}$ in the NG and SC regions and around 0.8 $gC.m^{-2}.d^{-1}$ in the ST area.

On an annual scale, we estimate a NPP of 235 $gC.m^{-2}.y^{-1}$ in the NG, 243 $gC.m^{-2}.y^{-1}$ in the SCA and 266 $gC.m^{-2}.y^{-1}$ in the STA. Despite a lower depth-integrated biomass maximum, the production is then higher in stratified regions where phytoplankton development is less interrupted by vertical dynamics. The excess of production in spring seems not to entirely compensate the deficit of production in winter in convection areas compared to stratified ones.

The modeled seasonal evolution is in agreement with previous results based on in situ (located in the Ligurian Sea) and remote sensing observations (Marty and Chiavérini, 2002; Bosc et al., 2004; Uitz et al., 2012). However, one can notice that our estimations of NPP maximum are generally higher compared to satellite-based studies and that the modeled summer NPP is higher that the estimations based on the various observations. As a consequence, our annual estimations are in the upper range or higher than the one based on observations. The same assessment is obtained from some comparisons with other 3D coupled physical/biogeochemical modelling studies (Crispi et al., 2002; Allen et al., 2002; Lazzari et al., 2012).

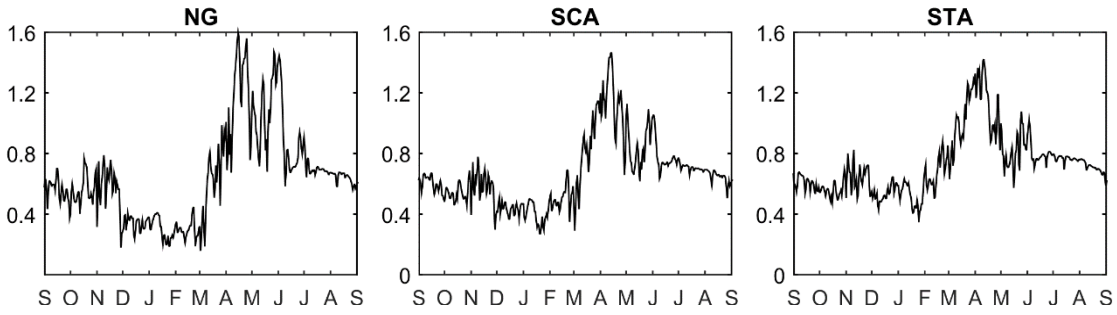

Figure 11: Integrated primary production ($gC.m^{-2}.d^{-1}$) in the NG, Balearic Sea and the Algerian subbasin between September 2012 and September 2013.

4.5. Particulate organic carbon export

Figure 12 displays the seasonal evolution of the Particulate Organic Carbon (POC) exported below 150 m depth in the NG, the SCA and the STA. During summer and autumn conditions, the vertical export is low in the three regions (the mean value

from September to November is equal to 0.04 $gC.m^{-2}.d^{-1}$ in the NG, 0.07 in the SCA $gC.m^{-2}.d^{-1}$ and 0.05 $gC.m^{-2}.d^{-1}$ in the STA) and slightly variable (STD= 0.01 $gC.m^{-2}.d^{-1}$). In December, when the winter mixing intensifies, a first peak of export is simulated in the NG region, while small increases are visible in the SCA and STA. In the NG, when the spatial mean ML reaches 500 m, starting from mid-January until the first week of March, the particulate carbon flux becomes very strong and very variable. It exceeds 0.4 $gC.m^{-2}.d^{-1}$ in January and 0.6 $gC.m^{-2}.d^{-1}$ in February, at the end of the first convection episode. The mean value of export during the long period of mixing is 0.25 $gC.m^{-2}.d^{-1}$ and varies around 0.10 $gC.m^{-2}.d^{-1}$. The export flux cumulated over this period represents 34 % of the annual export. In mid-March, during the last mixing event that lasts for 6 days and occurs after the onset of the late winter bloom, a high peak of export (1$gC.m^{-2}.d^{-1}$) is recorded. The flux during this short period represents 9 % of the annual export. In the SCA, the export flux is also maximum during the mixing events. It exceeds 0.4 $gC.m^{-2}.d^{-1}$ during three mixing events. In the STA, where between the MLD and the vertically integrated bio mass is correlated, the export is related to both surface layer POC stock and mixing. It is noteworthy that the peak of the export is located then during a mixing event taking place during the period of maximum efflorescence. After the last strong mixing events, the export flux decreased to ~ 0.2 $gC.m^{-2}.d^{-1}$ and after the surface development, it progressively stabilized below 0.1 $gC.m^{-2}.d^{-1}$.

At the annual scale, the POC export is evaluated at 38 $gC.m^{-2}.y^{-1}$, 40 $gC.m^{-2}.y^{-1}$ and 29 $gC.m^{-2}.y^{-1}$ in resp. NG, SC and ST regions. We find thus that the export flux is lower in the STA and close in both convection areas, the NG being characterized by stronger winter mixing but lower annual production than the SCA.

A comparison of the modeled seasonal evolution with the one based on sediment traps measurements in convection areas is difficult due to the low reliability on these measurements during strong mixing events (Buesseler et al., 2007). Nevertheless, outside convection periods, our estimations appear to be higher than the sediment traps observations in the Ligurian Sea reported by Miquel et al. (2011). We also find at the LION station (42°N 5°E) a higher annual value at 100 m depth than the estimation of Gogou et al. (2014) deduced from 1000 m sediment trap measurements and Martin et al (1987) formulations (38 $gC.m^{-2}.y^{-1}$ vs 23 $gC.m^{-2}.y^{-1}$).

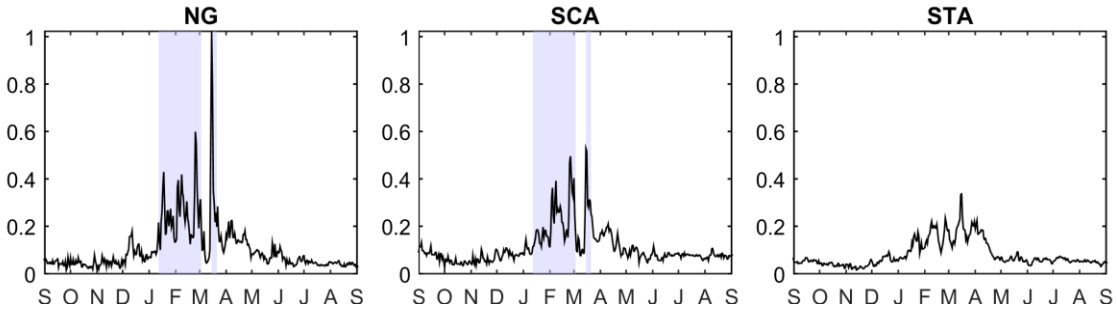

Figure 12: Particulate organic carbon export ($gC.m^{-2}.d^{-1}$) under 150 m depth in the NG, SCA and the STA between September 2012 and September 2013. The first strip reports the main deep convection event, the second one concerns the short strong deep mixing of March.

4.6 The trophic regimes

The evolution of the *F-ratio* for the three hydrodynamic regions is presented in Figure 13a. In the NG, high values of *F-ratio* (> 0.5) are attained from the end of January to mid-April. The trophic regime during this period is thus eutrophic, the new production dominating the regenerated one during the second part of winter and spring. This is due to large nutrient enrichment during convection and consumption during spring in this area over that period. *F-ratio* reaches a maximum value of 0.76 on 11 March at the maximum rate of change after the bloom onset, and 0.49 at the bloom maximum. In the SCA, the period of eutrophic regime is shorter: it lasts from mid-February to end of March, whereas in the ST area, eutrophic regime is never encountered. Conversely, the oligotrophic period, when the primary production is mostly maintained by regenerated production (*F-ratio* lower than 0.2) and located in a DCM, is obviously longer in the STA (326 days) than in the SCA (275 days) and in the NG (261 days).

The annual mean *F-ratio* is equal to 0.22 in the NG, 0.20 in the SCA and 0.12 in the STA. Despite a relatively high primary production, we find thus that each region is characterized by an oligotrophic regime at the annual scale. The values of *F-ratio* are comparable to the *E-ratio*, which represents the ratio between the total exported organic carbon (dissolved + particular) and the net primary production (Murray et al., 1989). Indeed annual averaged *E-ratio* is equal to 0.24 in the NG, 0.25 in the SCA and 0.17 in the STA. Laws et al. (2000) found also that the *E-ratio* is close to the *F-ratio* because all the production at the upper layer was considered to be vertically exported. Here the values of *E-ratio* are slightly higher than to the *F-ratio*. This could be explained by an underestimation of the *F-ratio* which is due because nitrate originated from nitrification is not totally absorbed by phytoplankton, then new primary production could be overestimated.
Figure 13b displays the spatial heterogeneity of the annual *F-ratio* in the WM. The most important values (> 0.3) are located on the shelves, in the deep convection area and in the western Algerian sub-basin, where water masses are horizontally advected through gyres from the Alboran Sea characterized in its northern part by strong vertical velocities inducing a surface enrichment with nutrients. In the eastern Algero-Provençal sub-basin and almost the whole SC region, annual F-*ratio* is below 0.04.

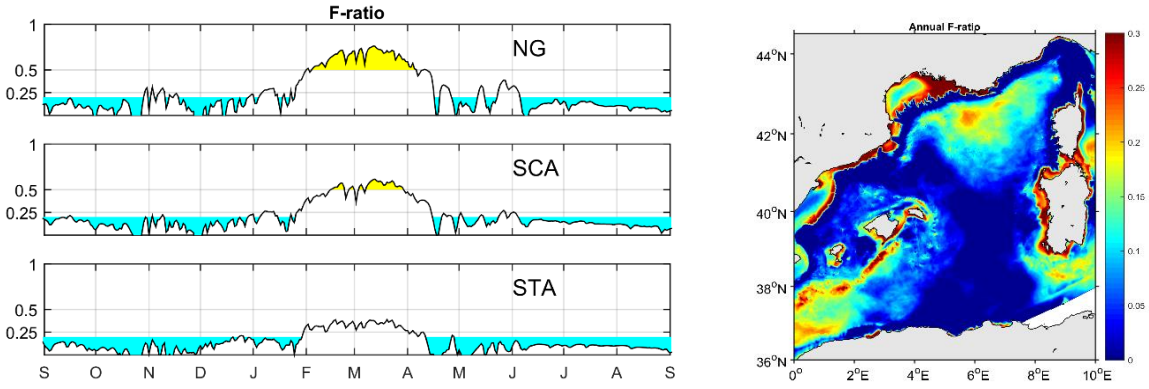

Figure 13: Time-series of minimum and the extension of the annual average of* F-ratio *(calculated following Eq. 3) in the western Mediterranean basin.

5. Conclusion

A 3D very high hydrodynamic/biogeochemical coupled model has been used to study phytoplankton dynamics and biogeochemical fluxes in three hydrodynamically distinct regions of the western Mediterranean Sea (deep convection, shallow convection and stratified areas). First a comparison of the model results with ocean colour satellite observations allows showing that the model correctly represents the time evolution of surface chlorophyll concentration. Then, this study shows the different phytoplankton phenology in the three investigated regions. A first phytoplankton efflorescence starts at the end of November/early December in the three regions, as zooplankton pressure decreases and surface nutrient concentrations increase in response to the intensification of the vertical mixing. In both convection regions, the efflorescence is then interrupted by strong mixing events, whereas it continues in the ST region. The interruption of the efflorescence is nevertheless clearly shorter in the shallow convection area related to the deep convection one. In the former region, a second bloom onset is identified at the beginning of the convection period when the effect of nutrient availability dominates the mixing-induced deficit of light. In the deep convection area, the bloom onset is detected at the end of the convection period; a huge phytoplankton bloom takes place when the heat flux and turbulent mixing decrease, as well as the zooplankton biomass is minimum.

We investigate then the biogeochemical fluxes. The primary production presents globally a similar seasonal evolution in the three regions, except during the maximum mixing period. In the deep convection area, the intense mixing reduces first the production by inducing a strong deficit in light and then when it stops strongly favors it through the previous upwelling of large amount of nutrients. In more stratified areas, the production is rapidly favored by the injection of nutrients. On an annual scale, the primary production appears to be higher in stratified regions than in the deep convection area. Concerning

the export flux of POC, we estimate a higher value in convection areas compared to stratified regions, winter mixing appearing as an important driving factor.

Finally, the calculation of the F-ratio shows that the convection areas present a eutrophic regime in late winter and spring period and shift the rest of the year to an oligotrophic regime when nutrients are depleted in the surface layer and a DCM structure forms. The stratified region exhibits no eutrophic regime, primary production being mostly maintained by regenerated production all year long.

6. References

Allen, J. I., Somerfield, P. J. and Siddorn, J.: Primary and bacterial production in the Mediterranean Sea: A modelling study, J. Mar. Syst., 33-34, 473–495, doi:10.1016/S0924-7963(02)00072-6, 2002.

- Anderson, T. R., and P. Pondaven. Non-redfield carbon and nitrogen cycling in the Sargasso Sea: pelagic imbalances and export flux, Deep-Sea Res., Part I, 50, 573–591, 2003.
- Auger, P. a., Diaz, F., Ulses, C., Estournel, C., Neveux, J., Joux, F., Pujo-Pay, M. and Naudin, J. J.: Functioning of the planktonic ecosystem on the Gulf of Lions shelf (NW Mediterranean) during spring and its impact on the carbon deposition: A field data and 3-D modelling combined approach, Biogeosciences, 8(11), 3231–3261, doi:10.5194/bg-8-3231-2011, 2011.
- Auger, P. a., Ulses, C., Estournel, C., Stemmann, L., Somot, S. and Diaz, F.: Interannual control of plankton communities by deep winter mixing and prey/predator interactions in the NW Mediterranean: Results from a 30-year 3D modeling study, Prog. Oceanogr., 124, 12–27, doi:10.1016/j.pocean.2014.04.004, 2014.
- Baklouti, M., Faure, V., Pawlowski, L. and Sciandra, A.: Investigation and sensitivity analysis of a mechanistic phytoplankton model implemented in a new modular numerical tool (Eco3M) dedicated to biogeochemical modelling, Prog. Oceanogr., 71(1), 34–58, doi:10.1016/j.pocean.2006.05.003, 2006.
- Antoine, D., Morel, A., Gordon, H. R., Banzon, V. F. and Evans, R. H.: Bridging ocean color observations of the 1980s and 2000s in search of long-term trends, J. Geophys. Res., 110(C06009), 2005.
- Backhaus, J. O., Hegseth, E. N., Wehde, H., Irigoien, X., Hatten, K. and Logemann, K.: Convection and primary production in winter, Mar. Ecol. Prog. Ser., 251(1953), 1–14, doi:10.3354/meps251001, 2003.
- Behrenfeld, M. 2010. Abandonding Sverdrup's crtical depth hypothesis on phytoplankton blooms. Ecology 91: 977–989. doi:10.1890/09-1207.1
- Behrenfeld, M. J.: Abandoning Sverdrup ' s Critical Depth Hypothesis on phytoplankton blooms Critical Depth Hypothesis Abandoning Sverdrup ' s on phytoplankton, , 91(4), 977–989, doi:10.1890/09-1207.1, 2013
- Behrenfeld, M. J., and E. S. Boss. 2014. Resurrecting the ecological underpinnings of ocean plankton blooms. Ann. Rev. Mar. Sci. 6: 167–194. doi:10.1146/annurev-marine- 052913-021325.

- Bernardello, R., Cardoso, J. G., Bahamon, N., Donis, D., Marinov, I. and Cruzado, a.: Factors controlling interannual variability of vertical organic matter export and phytoplankton bloom dynamics-a numerical case-study for the NW Mediterranean Sea, Biogeosciences, 9(11), 4233–4245, doi:10.5194/bg-9-4233-2012, 2012.
- Bosc, E.: Seasonal and interannual variability in algal biomass and primary production in the Mediterranean Sea, as derived from 4 years of SeaWiFS observations, Global Biogeochem. Cycles, 18(1), 1–17, doi:10.1029/2003GB002034, 2004.
- Brody, S. R., and M. S. Lozier. 2014. Changes in dominant mixing length scales as a driver of subpolar phytoplankton bloom initiation in the North Atlantic. Geophys. Res. Lett. 41: 3197–3203. doi:10.1002/2014gl059707
- Buesseler, K. O., Ball, L., Andrews, J., Cochran, J. K., Hirschberg, D. J., Bacon, M. P., Fleer, A. and Brzezinski, M.: Upper ocean export of particulate organic carbon and biogenic silica in the Southern Ocean along 170W, Deep. Res. Part II Top. Stud. Oceanogr., 48(19-20), 4275–4297, doi:10.1016/S0967-0645(01)00089-3, 2001.
- Dale T, Rey F, Heimdal BR (1999) Seasonal development of phytoplankton at a high latitude ocean site. Sarsia 84:1–17DiBattista, M.,T., Majda A.J. and J. Marshall (2002). A Statistical Theory for the "Patchiness" of Open-Ocean Deep Convection: The Effect of Preconditioning. Journal of Physical Oceanography, 32, 599-626.
- Crispi, G., Crise, a. and Mauri, E.: A seasonal three-dimensional study of the nitrogen cycle in the Mediterranean Sea: Part II. Verification of the energy constrained trophic model, J. Mar. Syst., 20(1-4), 357–379, doi:10.1016/S0924-7963(98)00085-2, 1999.
- D'Ortenzio, F. and Ribera d'Alcalà, M.: On the trophic regimes of the Mediterranean Sea: a satellite analysis, Biogeosciences Discuss., 5(4), 2959–2983, doi:10.5194/bgd-5-2959-2008, 2009.
- Estournel., C, Testor., P, Damien., P, D'Ortenzio., F, Marsaleix., P, Conan., P, Kessouri., F, Durrieu de Madron., X, Coppola., L, Lellouche., J.M, Belamari., S, Mortier., L, Ulses., C., Prieur., L. High resolution modelling of dense water formation in the north-western Mediterranean: benefits from an improved initial state in summer. In press.
- Gogou, A., Sanchez-Vidal, A., Durrieu de Madron, X., Stavrakakis, S., Calafat, A. M., Stabholz, M., Psarra, S., Canals, M., Heussner, S., Stavrakaki, I. and Papathanassiou, E.: Reprint of: Carbon flux to the deep in three open sites of the Southern European Seas (SES), J. Mar. Syst., 135, 170–179, doi:10.1016/j.jmarsys.2014.04.012, 2014.
- Herrmann, M., Diaz, F., Estournel, C., Marsaleix, P., Ulses, C. Impact of atmospheric and oceanic interannual variability on the Northwestern Mediterranean Sea pelagic planktonic ecosystem and associated carbon cycle. Journal of Geophysical Research – Oceans 118, 5792–5813. 2013
- Halldal P. Phytoplankton investigations from the weather ship M in the Norwegian Sea. Hvalråd Skr 38:1–91. 1953.
- Henson, S., Dunne, J., and Sarmiento, J. 2009. Decadal variability in North Atlantic phytoplankton blooms. Journal of Geophysical Research, 114: C04013.

- Henson, S., Robinson, I., Allen, J., and Waniek, J. 2006. Effect of meteorological conditions on interannual variability in timing and magnitude of the spring bloom in the Irminger Basin, North Atlantic. Deep Sea Research Part I, 53: 1601–1615.
- Huisman J, Arrayas M, Ebert U, Sommeijer B. How do sinking phytoplankon species manage to persist? Am Nat 159(3):245–254. 2002.
- Kessouri et al., Nitrogen and phosphorus cycles in the western Mediterranean Sea using high resolution modeling: Processes and budget. (In prep-b).
- Large, W. G. and S. Yeager, 2009: The global climatology of an interannually varying air-sea flux data set. Climate Dynamics, 33, 341–364, doi:10.1007/s00382-008-0441-3
- Lavigne, H., D'Ortenzio, F., Ribera D'Alcalà, M., Claustre, H., Sauzède, R. and Gacic, M.: On the vertical distribution of the chlorophyll a concentration in the Mediterranean Sea: a basin scale and seasonal approach, Biogeosciences Discuss., 12(5), 4139–4181, doi:10.5194/bgd-12-4139-2015, 2015.
- Lavigne, H., F. D'Ortenzio, C. Migon, H. Claustre, P. Testor, M. R. d'Alcalà, R. Lavezza, L. 1156 Houpert, and L. Prieur (2013), Enhancing the comprehension of mixed layer depth control on 1157 the Mediterranean phytoplankton phenology, Journal of Geophysical Research: Oceans, 1158 118(7), 3416-3430, doi:10.1002/jgrc.20251.
- Lazzari, P., Solidoro, C., Ibello, V., Salon, S., Teruzzi, a., Béranger, K., Colella, S. and Crise, a.: Seasonal and inter-annual variability of plankton chlorophyll and primary production in the Mediterranean Sea: A modelling approach, Biogeosciences, 9(1), 217–233, doi:10.5194/bg-9-217-2012, 2012.
- Lellouche, J.-M., O. Le Galloudec, M. Drévillon, C. Régnier, E. Greiner, G. Garric, N. Ferry, C. Desportes, C.-E. Testut, C. Bricaud, R. Bourdallé-Badie, B. Tranchant, M. Benkiran, Y. Drillet, A. Daudin, and C. De Nicola (2013), Evaluation of global monitoring and forecasting systems at Mercator Océan, Ocean Sci., 9, 57-81, doi:10.5194/os-9-57-2013.
- Lévy, M.: Production regimes in the northeast Atlantic: A study based on Sea-viewing Wide Field-of-view Sensor (SeaWiFS) chlorophyll and ocean general circulation model mixed layer depth, J. Geophys. Res., 110(C7), C07S10, doi:10.1029/2004JC002771, 2005.
- Lévy, M., Klein, P., Treguier, A.-M. A.-M., Levy, M., Klein, P. and Treguier, A.-M. A.-M.: Impact of sub-mesoscale physics on production and subduction of phytoplankton in an oligotrophic regime, J. Mar. Res., 59(4), 535–565, doi:10.1357/002224001762842181, 2001.
- Raick, C., Delhez, E. J. M., Soetaert, K. and Grégoire, M.: Study of the seasonal cycle of the biogeochemical processes in the Ligurian Sea using a 1D interdisciplinary model, J. Mar. Syst., 55(3-4), 177–203, doi:10.1016/j.jmarsys.2004.09.005, 2005.
- Marsaleix P., Auclair F., Floor J. W., Herrmann M. J., Estournel C., Pairaud I., Ulses C., 2008. Energy conservation issues in sigma-coordinate free-surface ocean models. Ocean Modelling. 20, 61-89. http://dx.doi.org/10.1016/j.ocemod.2007.07.005

- Marsaleix P., Auclair F., Estournel C., 2009. Low-order pressure gradient schemes in sigma coordinate models: The seamount test revisited. Ocean Modelling, 30, 169-177. http://dx.doi.org/10.1016/j.ocemod.2009.06.011
- Marsaleix P., Auclair F., Estournel C., Nguyen C., Ulses C., 2011. An accurate implementation of the compressibility terms in the equation of state in a low order pressure gradient scheme for sigma coordinate ocean models. Ocean Modelling, 40, 1-13 http://dx.doi.org/10.1016/j.ocemod.2011.07.004
- Marsaleix P., Auclair F., Duhaut T., Estournel C., Nguyen C., Ulses C., 2012. Alternatives to the Robert-Asselin filter. Ocean Modelling, 41, 53-66 http://dx.doi.org/10.1016/j.ocemod.2011.11.002
- Marty, J., Chiaverini, J., Pizay, M. and Avril, B.: Seasonal and interannual dynamics of nutrients and phytoplankton pigments in the western Mediterranean Sea at the DYFAMED time-series station (1991–1999), Deep Sea Res. Part II Top. Stud. Oceanogr., 49(11), 1965–1985 [online] Available from: http://linkinghub.elsevier.com/retrieve/pii/S096706450200022X, 2002.
- Miquel, J. C., Martín, J., Gasser, B., Rodriguez-y-Baena, A., Toubal, T. and Fowler, S. W.: Dynamics of particle flux and carbon export in the northwestern Mediterranean Sea: A two decade time-series study at the DYFAMED site, Prog. Oceanogr., 91(4), 461–481, doi:10.1016/j.pocean.2011.07.018, 2011.
- Morel, A. and André, J.-M.: Pigment distribution and primary production in the western Mediterranean as derived and modeled from coastal zone color scanner observations, J. Geophys. Res., 96, 12685–12698, doi:10.1029/91JC00788, 1991.
- Pastor, L., Deflandre, B., Viollier, E., Cathalot, C., Metzger, E., Rabouille, C., Escoubeyrou, K., Lloret, E., Pruski, A. M., Vétion, G., Desmalades, M., Buscail, R. and Grémare, A.: Influence of the organic matter composition on benthic oxygen demand in the RhÔne River prodelta (NW Mediterranean Sea), Cont. Shelf Res., 31(9), 1008–1019, doi:10.1016/j.csr.2011.03.007, 2011.
- Siegel, D., Doney, S., and Yoder, J. 2002. The North Atlantic spring phytoplankton bloom and Sverdrup's critical depth hypothesis. Science, 296: 730–733.
- Siokou-Frangou, I., Christaki, U., Mazzocchi, M. G., Montresor, M., Ribera D'Alcala, M., Vaque, D. and Zingone, a.: Plankton in the open mediterranean Sea: A review, Biogeosciences, 7(5), 1543–1586, doi:10.5194/bg-7-1543-2010, 2010.
- Soetaert, K., Herman, P. M. J., Middelburg, J. J., Heip, C., Smith, C. L., Tett, P. and Wild-Allen, K.: Numerical modelling of the shelf break ecosystem: Reproducing benthic and pelagic measurements, Deep. Res. Part II Top. Stud. Oceanogr., 48(14-15), 3141–3177, doi:10.1016/S0967-0645(01)00035-2, 2001.
- Sverdrup, H. 1953. On conditions for the vernal blooming of phytoplankton. Journal du Conseil International Pour L'Exploration de la Mer, 18: 287–295.
- Taylor, J. R. and Ferrari, R.: Shutdown of turbulent convection as a new criterion for the onset of spring phytoplankton blooms, Limnol. Oceanogr., 56(6), 2293–2307, doi:10.4319/lo.2011.56.6.2293, 2011.

- Townsend, D. W., Cammen, L. M., Holligan, P. M., Campbell, D. E. and Pettigrew, N. R.: Causes and consequences of variability in the timing of spring phytoplankton blooms, Deep Sea Res. Part I Oceanogr. Res. Pap., 41(5-6), 747–765, doi:10.1016/0967-0637(94)90075-2, 1994.
- Uitz, J., Stramski, D., Gentili, B., D'Ortenzio, F. and Claustre, H.: Estimates of phytoplankton class-specific and total primary production in the Mediterranean Sea from satellite ocean color observations, Global Biogeochem. Cycles, 26(2), 1–10, doi:10.1029/2011GB004055, 2012.

Bibliographie supplémentaire

- Anderson, T. R., and P. Pondaven, Non-redfield carbon and nitrogen cycling in the Sargasso Sea: pelagic imbalances and export flux, Deep-Sea Res., Part I, 50, 573–591, 2003.
- Auger, P. a., Diaz, F., Ulses, C., Estournel, C., Neveux, J., Joux, F., Pujo-Pay, M. and Naudin, J. J.: Functioning of the planktonic ecosystem on the Gulf of Lions shelf (NW Mediterranean) during spring and its impact on the carbon deposition: A field data and 3-D modelling combined approach, Biogeosciences, 8(11), 3231–3261, doi:10.5194/bg-8-3231-2011, 2011.
- Auger, P. a., Ulses, C., Estournel, C., Stemmann, L., Somot, S. and Diaz, F.: Interannual control of plankton communities by deep winter mixing and prey/predator interactions in the NW Mediterranean: Results from a 30-year 3D modeling study, Prog. Oceanogr., 124, 12–27, doi:10.1016/j.pocean.2014.04.004, 2014.
- D'Ortenzio, F., S. Le Reste, H. Lavigne, F. Besson, H. Claustre, L. Coppola, A. Dufour, V. 1050 Dutreuil, A. Laes, and E. Leymarie (2012), Autonomously profiling the nitrate concentrations 1051 in the ocean: the Pronuts project, Mercator Ocean–CORIOLIS Quarterly Newsletter(45), 8-11.
- D'Ortenzio, F. and Ribera d'Alcalà, M.: On the trophic regimes of the Mediterranean Sea: a satellite analysis, Biogeosciences Discuss., 5(4), 2959–2983, doi:10.5194/bgd-5-2959-2008, 2009.
- Giorgi, F.: Climate change hot-spots, Geophys. Res. Lett., 33(8), 1–4, doi:10.1029/2006GL025734, 2006.
- Hamon. M , Beuvier. J , Somot. S , M. Lellouche .J.M. , Greiner. E , Jordà. G , Bouin. M.N , Arsouze. T , Béranger. K , Sevault. F , Dubois. C , Drevillon. M , and Drillet. Y. Design and validation of MEDRYS, a Mediterranean Sea reanalysis over 1992–2013. Sci. 2015.
- Herrmann, M.: Discipline : Océanographie présentée et soutenue par Formation et devenir des masses d'eau en Méditerranée nord-occidentale Influence sur l' écosystème planctonique pélagique Variabilité interannuelle et changement climatique, Sci. York, 2007.
- Herrmann, M., Estournel, C., Déqué, M., Marsaleix, P., Sevault, F. and Somot, S.: Dense water formation in the Gulf of Lions shelf: Impact of atmospheric interannual variability and climate change, Cont. Shelf Res., 28(15), 2092–2112, doi:10.1016/j.csr.2008.03.003, 2008a.
- Herrmann, M., Bouffard, J. and Béranger, K.: Monitoring open-ocean deep convection from space, Geophys. Res. Lett., 36(3), 1–5, doi:10.1029/2008GL036422, 2009.

- Johnson, K., Processing Argo Nitrate Data at the DAC Level Version 0.2. Document 1130 produced in response to action item 11 from the first Bio-Argo Data Management meeting in 1131 Hyderabad, India (November 12-13, 2012). 2014.
- Kriest, I.: Different parameterizations of marine snow in a 1D-model and their influence on representation of marine snow, nitrogen budget and sedimentation, Deep. Res. Part I Oceanogr. Res. Pap., 49(12), 2133–2162, doi:10.1016/S0967-0637(02)00127-9, 2002.
- Kriest, I. and Evans, G. T.: Representing phytoplankton aggregates in biogeochemical models, Deep. Res. Part I Oceanogr. Res. Pap., 46(11), 1841–1859, doi:10.1016/S0967-0637(99)00032-1, 1999.
- Kriest, I. and Oschlies, a.: On the treatment of particulate organic matter sinking in large-scale models of marine biogeochemical cycles, Biogeosciences Discuss., 4(4), 3005–3040, doi:10.5194/bgd-4-3005-2007, 2007.
- Lavezza, R., Dubroca, L., Conversano, F., Iudicone, D., Kress, N. and Herut, B.: MED – Nut , a new Quality Controlled nutrient data base for the Mediterranean Sea, , (November), 1–42, doi:10.1594/PANGAEA.771907.1, 2011.
- Manca, B., Burca, M., Giorgetti, a, Coatanoan, C., Garcia, M. J. and Iona, a: Physical and biochemical averaged vertical profiles in the Mediterranean regions: an important tool to trace the climatology of water masses and to validate incoming data from operational oceanography, J. Mar. Syst., 48(1-4), 83–116, doi:10.1016/j.jmarsys.2003.11.025, 2004.
- Moutin, T. and Prieur, L.: Influence of anticyclonic eddies on the Biogeochemistry from the Oligotrophic to the Ultraoligotrophic Mediterranean(BOUM cruise), Biogeosciences [online] Available from: http://biogeosciences.net/9/3827/2012/bg-9-3827-2012.pdf (Accessed 3 April 2013), 2012.
- Raick, C., Delhez, E. J. M., Soetaert, K. and Grégoire, M.: Study of the seasonal cycle of the biogeochemical processes in the Ligurian Sea using a 1D interdisciplinary model, J. Mar. Syst., 55(3-4), 177–203, doi:10.1016/j.jmarsys.2004.09.005, 2005.
- Ribera d'Alcalà, M.: Nutrient ratios and fluxes hint at overlooked processes in the Mediterranean Sea, J. Geophys. Res., 108(C9), doi:10.1029/2002JC001650, 2003.
- Siokou-Frangou, I., Christaki, U., Mazzocchi, M. G., Montresor, M., Ribera D'Alcala, M., Vaque, D. and Zingone, a.: Plankton in the open mediterranean Sea: A review, Biogeosciences, 7(5), 1543–1586, doi:10.5194/bg-7-1543-2010, 2010.

- Somot, S., Sevault, F., Déqué, M. and Crépon, M.: 21st century climate change scenario for the Mediterranean using a coupled atmosphere-ocean regional climate model, Glob. Planet. Change, 63(2-3), 112–126, doi:10.1016/j.gloplacha.2007.10.003, 2008.

5 Annexes

5.1 Annexe 1 : Déroulement de la thèse

Ce travail de recherche est financé par le programme de recherche européen PERSEUS (Policy-oriented marine Environmental Research for the Southern European Seas http://www.perseus-net.eu/site/content.php). Il s'agit d'un projet de recherche qui évalue le double effet de l'activité humaine et des pressions naturelles sur la Méditerranée et la mer Noire. PERSEUS fusionne sciences naturelles et sciences socio-économiques pour prédire les effets à long terme de ces pressions sur les écosystèmes marins. Le projet vise à concevoir un cadre de gouvernance pour une recherche efficace et innovante, qui servira de base pour les décideurs dans l'objectif de stopper la dégradation de la vie marine.

Cette thèse de doctorat a été effectuée au Laboratoire d'Aérologie (http://www.aero.obs-mip.fr/) de l'Observatoire Midi-Pyrénées (http://www.obs-mip.fr/), affilié à l'Université de Toulouse Paul Sabatier (http://www.univ-tlse3.fr/) et au CNRS.

Dans le cadre de ce projet, la thèse a été proposée et encadrée par Claude Estournel (directrice de recherche, CNRS) et Caroline Ulses (physicienne adjointe, CNAP) avec la collaboration permanente de Patrick Marsaleix (chargé de recherche, CNRS).

L'originalité de cette thèse tient dans la pluridisciplinarité qui relie les sciences de l'atmosphère, à l'hydrodynamique, à la biogéochimie marine, à la biologie des écosystèmes planctoniques marins et aussi dans l'association de la modélisation et l'observation.

Ma mission dans ce cadre était de préparer et d'exécuter des simulations océaniques, couplées physique–biogéochimie en Mer Méditerranée nord occidentale. Le sujet a beaucoup évolué au cours de ces trois années, pendant lesquelles nous sommes passés de la modélisation régionale à la

modélisation du bassin entier, travaillant désormais sur deux fronts : le bassin Méditerranéen et le sous-bassin occidental à très haute résolution.

Sur le plan technique, nous avons été assistés par Thomas Duhaut et Cyril Nguyen (Ingénieurs au Laboratoire d'Aérologie), spécifiquement pour résoudre des problèmes liés aux forçages océaniques ou atmosphériques ou encore dans la partie liée à la parallélisassions des grilles utilisées.

Au cours de cette thèse, j'ai eu l'opportunité de participer à une campagne en mer assez inédite, inscrite dans le projet DeWEx (Deep Water EXperiments). Il s'agit de deux legs du projet MISTRALS qui ont été faits en deux phases la même année, pendant la convection profonde au centre du Golfe du Lion et pendant le bloom printanier qui a suivi. Il s'agit d'une des rares campagnes pendant un bloom phytoplanctonique printanier en Méditerranée nord occidentale. Pendant cette mission j'étais chargé des prélèvements de pigments phytoplanctoniques, de leur filtration et de leur conditionnement sous la direction de Fabrizio D'Ortenzio (LOV-Villefranche-sur-Mer) et aussi chargé d'assister Tatiana Severin et Louise Oriol du Laboratoire LOMIC de Banyuls-sur-Mer pour les prélèvements, filtration et conditionnement des sels nutritifs et de la matière organique sous toutes ses formes. Et enfin, je m'occupais des prélèvements de l'oxygène dissous sous la responsabilité de Laurent Coppola (LOV-Villefranche-sur-Mer). Mon autre mission sur le N/O (navire océanographique) Le Suroît était d'effectuer des analyses graphiques des sorties du modèle physique-biogéochimie qui tournait en même temps sur les serveurs du Laboratoire d'Aérologie en mode prévisionnel en temps réel (à J+5) sous le monitoring de Claude Estournel et avec l'assistance de Pierre Damien (étudiant en thèse en physique au sein du même laboratoire), qui me communiquaient les résultats du modèle. En parallèle je devais présenter un état des lieux quotidien afin d'aider Pascal Conan (chef de mission) à orienter, lorsque les conditions le permettaient, l'échantillonnage au fur et à mesure que les conditions atmosphériques et océaniques évoluaient. Le modèle était quotidiennement confronté aux images satellites traitées par Fabrizio D'Ortenzio à bord, assisté par Vincent Taillandier et Luis Prieur à terre depuis leur laboratoire de Villefranche-sur-Mer ainsi qu'aux résultats du thermo-salinomètre placé sous la coque du navire et enfin à l'aide des mesures du courantomètre sous la responsabilité de Xavier Durrieu de Madron (directeur de recherches au CNRS, CEFREM - Perpignan).

Le travail à bord était continu pendant 21 jours avec un rythme quotidien de l'ordre de 16 à 19h par jour. Cette expérience a renforcé mes compétences techniques, scientifiques ainsi que mes aptitudes à la communication et à la collaboration avec tous les chercheurs, ingénieurs, techniciens expérimentateurs et membres de l'équipage du navire.

A terre, généralement deux fois par an, les nombreux acteurs de ce projet se réunissaient pour présenter les avancées liées à ces recherches. C'était l'occasion pour moi de présenter à chaque réunion mes nouvelles calibrations et modifications appliquées dans le modèle, faites progressivement à partir du panel de mesures. Un court passage au laboratoire de Banyuls pour assister aux dernières analyses biogéochimiques a été fait quatre mois après la campagne. Cela m'a donné un aperçu des méthodes de calibration des profils d'observation.

Ce projet m'a permis de rédiger deux articles en modélisation et de co-rédiger un article en observation. Les résultats ont été présentés au cours de deux grandes conférences (CIESM à Marseille et Ocean Sciences à Honolulu, EU) et pendant une école d'été sur la thématique de la matière organique à Holàr en Islande, organisée par l'université danoise DTU.

La suite de la thèse était focalisée sur la qualité du modèle. Au cours du travail sur les conditions limites, avec mes encadrants, nous nous sommes penchés sur la modélisation à l'échelle du bassin Méditerranéen. Ce dernier nous apportait un champ d'initialisation pour toutes les variables du modèle ainsi qu'un forçage aux frontières quotidien et le plus cohérent possible car nous avons réussi à paramétrer les deux modèles, forcé et forçant, de la même manière. Le travail de calibration manuelle a duré huit mois avec plus de 120 simulations tests en 3D.

Cette méthodologie est plus longue que les méthodes mathématiques appliquées généralement en 1D ou en 0D. À ce stade, seul des tests sur la totalité de la grille nous intéressaient pour pouvoir prendre en compte l'état de la turbulence, des vitesses verticales et autres paramètres pouvant impacter la distribution de la matière biogène afin d'obtenir une approche exhaustive de la calibration. Par ailleurs le modèle avait auparavant bénéficié des tests préliminaires qui ont permis de rétrécir les gammes de variation des paramètres préalablement déterminés par Caroline Ulses lors de la mise en œuvre du modèle ainsi qu'au cours des deux thèses de Marine Herrmann et de Pierre-Amaël Auger. De plus des tests étaient effectués en parallèle par Patrick Marsaleix sur les schémas d'advection des traceurs passifs biogéochimiques qui nécessitaient mes retours sur l'ensemble du bassin et notamment, dans les zones à forte dynamique à submésoéchelle telle que dans le bassin algérien.

L'imbrication des deux modèles bassin et régional m'a permis de faire partie d'un autre projet, AMICO-Bio (http://oliver.ross.p.luminy.univ-amu.fr/amico/) co-dirigé par Christel Pinazo et Oliver Ross du MIO – Marseille. Ce projet consistait à inter-comparer les méthodes de forçages aux frontières avec différents autres groupes de modélisateurs français. Il a fait objet de plusieurs présentations orales et de posters lors d'évènements scientifiques en France.

J'ai utilisé le modèle physique Nemo-Med12 de Jonathan Beuvier de Mercator-Ocean , en mode offline via la plateforme générique de couplage BLOOM développée au LA, pour mon forçage de Eco3m-S sur le bassin. Ce couplage méditerranéen nous a permis de faire partie du projet SIMED. Avec des réunions annuelles dirigées par Thomas Arsouze (LOCEAN-LSCE-ENSTA). Ces réunions regroupaient des modélisateurs utilisant le modèle Nemo-Med pour des buts variés, allant des tests de sensibilité, à la dynamique et à la biologie.

Un dernier volet a été effectué en dernière année thèse, c'est celui de la confrontation de nos simulations aux données des flotteurs BioArgo du projet NAOS (http://www.oao.obs-vlfr.fr/maps/en/?projectid=2) dirigé par Fabrizio D'Ortenzio et Hervé Claustre. Ce projet m'a mené à présenter nos travaux lors du 4ème meeting BioArgo-Users, ce qui représente une belle expérience parmi les expérimentateurs.

Le modèle de bassin a été traduit en une première prévision biogéochimique en 3D sur l'ensemble de la mer Méditerranée. Ce projet (http://moc.sedoo.fr/) dirigé par Claude Estournel avec la participation active de Thomas Duhaut, Cyril Nguyen, Caroline Ulses, Patrick Marsaleix et moi-même, a permis aux expérimentateurs sortant en mer de suivre l'évolution n'importe où en Méditerranée avec une avance de cinq jours ainsi que d'ajuster leur plan d'échantillonnage, y compris les positions de déploiement de flotteurs Argo et BioArgo.

Ce manuscrit de thèse de doctorat a été écrit par partie en deux langues. Les premiers chapitres de présentation et de description des méthodes et des objectifs ainsi que la conclusion sont rédigés en français, quant aux chapitres de résultats, ils sont présentés en anglais, sous forme de projets d'articles scientifiques et seront soumis, les jours suivant le dépôt du manuscrit de thèse, dans des revues scientifiques (Biogeosciences-EGU pour le premier et Journal of Geophysical Research-AGU pour les trois autres).

Ce manuscrit est également accompagné par un article de collaboration soumis par nos collaborateurs du LOV-Villefranche. Ce dernier est un article accepté à Deep Sea Research II. il s'agit d'une étude qui a permis de quantifier les dépôts de sels nutritifs en mer Ligure et comparés aux estimations des apports des sels nutritifs par la convection profonde. Ces estimations sont basées sur un exercice entre sorties modèle du forçage physique et mesure de surface.

5.2 Annexe 2 : Les bases de données et la calibration

La modélisation de l'écosystème planctonique nécessite une représentation tridimensionnelle de

l'environnement. Afin de configurer nos simulations couplées biogéochimiques, nous avons eu recours à de nombreuses bases de données. L'objectif de ce travail est d'initialiser le modèle, calibrer les paramètres et de valider les résultats. Chaque base de données utilisée nous a permis d'ajuster indépendamment plusieurs aspects de la modélisation (champs d'initialisation, valeurs de paramètres du modèle biogéochimique, apports des rivières et des frontières, flux solaire). La méthode a consisté principalement à balayer l'espace des paramètres, impliquant de très nombreuses simulations.

2.1. Base de données Lavezza et al (2011) pour l'initialisation des sels nutritifs, et initialisation de l'oxygène

Lavezza et al (2011) ont présenté une analyse permettant de sélectionner un nombre conséquent de profils de sels nutritifs ainsi que les profils hydrologiques associés. Pour discriminer les profils entre-eux, ils ont utilisé une méthode statistique de filtrage qui se base sur quatre indices de dispersions : « standard absolute deviation » (SAD), « median absolute deviation » (MAD), « the skewed adjusted outlyingness » (Skewed AO) et « the symmetric adjusted outlyingness » (symmetric AO). Le résultat est une classification des profils par qualité en 3 groupes dont [flag=1, Bonne ; flag=2, mauvaise]. Par un regroupement statistique, leurs travaux leur ont permis de déterminer différentes biorégions se basant sur la forme des profils de sels nutritifs. Lavezza et al (2011) ont obtenu 13 biorégions réparties sur la carte (Fig. 10.1).

Concernant notre étude, les profils de type flag=1 ont été repris en compte, puis un profil médian a été calculé par biorégion en respectant la distribution géographique proposée dans Lavezza et al (2011). Pour le bassin oriental, ces profils médians ont été par la suite interpolés sur la grille du modèle pour servir de base d'initialisation. Pour le bassin occidental, tout en prenant la même répartition géographique de Lavezza et al (2011), nous avons calculé des relations reliant la distribution de sels nutritifs et de l'oxygène aux profils de salinité. Ceci a donné des équations polynomiales pour extraire la distribution en trois dimensions des sels nutritifs partant des données hydrologiques de la simulation physique. Cette approche n'a pas été retenue pour le bassin oriental à cause du manque de profils verticaux principalement dans les eaux proches des talus. Cette approche d'initialisation par relation a déjà été effectuée par Auger et al (2014) et Prieur et al (2005) en utilisant un champ de densité. L'utilisation du champ de salinité a pour impact d'intensifier le gradient des éléments nutritifs et donc d'augmenter le réservoir en matières biogènes.

Un autre intérêt primordial de cet exercice est de démarrer le modèle avec des profondeurs de nutriclines correctes ce qui permet au modèle de trouver son équilibre dans un laps de temps

beaucoup plus court. Sans ce protocole d'initialisation, l'état d'équilibre du modèle s'établirait après une période de temps correspondant au renouvellement des masses d'eau intermédiaires, soit 70 ans en moyenne. Le même exercice a été appliqué sur les profils d'oxygène en s'appuyant sur les mêmes biorégions, avec la base de données provenant de la base de données MEDAR-MedAtlas 2002.

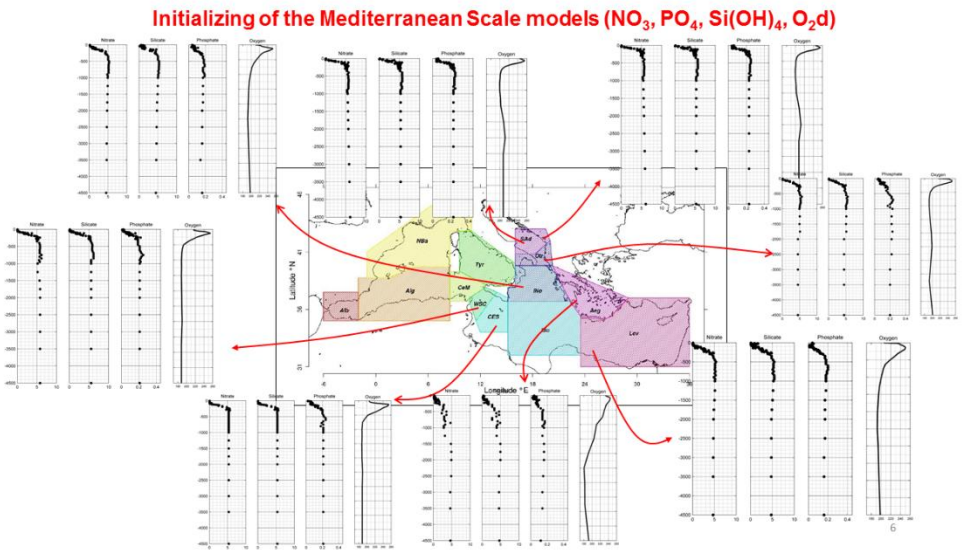

Figure 10.1: profiles médians issus de la climatologie du nitrate, du phosphate, du silicate et de l'oxygène, qui serviront comme champs initial du modèle de bassin.

- Base d'initialisation par région :

$NO_3 = (a\,.salt^2 - b)^2$

$(po_4, Si(OH)_4) = (-c + d.salt^2)^2$

Bioregion	Geographical limits				Nutrients = f (density)		
	East	West	North	South	NO3	PO4	Si(OH)4
Western Med Sea							
Gibraltar Strait	-5	Boundary	Coast	Coast			
Alboran	-2	-5	Coast	Coast			
Algerian	9.5	-2	39.5	Coast			
NWM	9.5	Coast	Coast	39.5	a= 1/36.0319 b= 1/1.23423	a= exp(164.933) b= exp(1/4828.84)	a= -1/37.9453 b= 1108.41
Tyrrhenian	16.5	9.5	Coast	41.5	a= 15.278 b= -435.513	a= 0.371067 b= -10.4974	a= 12.8943 b= -367.212

Initiation des nutriments dans le bassin occidental:

$NO_3 = (a\,.salt^2 - b)^2$
$PO_4, = (-c + d.salt^2)^2$
$Si(OH)_4 = (-e + f.salt^2)^2$

Bioregion	Geographical limits				Nutrients = f (density)		
	East	West	North	South	NO3	PO4	Si(OH)4
Western Med Sea							
Gib	-5	Boundary	Coast	Coast	$NO_3 = a\,.dens - b$ $PO_4, = c\,.dens - d$ $Si(OH)_4 = e\,.dens - f$ *a = 3.19339, b = 84.8924, c = 0.135093, d = 3.55102, e = 3.48983, f = 93.489*		
Alb	-2	-5	Coast	Coast	$NO_3 = (a\,.salt^2 - b)^2$ $PO_4, = (-c + d.salt^2)^2$ $Si(OH)_4 = (-e + f.salt^2)^2$ *a = 0.0389, b = 49.4811, c = 9.09731, d = 0.00656935, e = 21.0933, f = 0.0162298*		
Alg	9.5	-2	39.5	Coast	$NO_3 = (a\,.salt^2 - b)^2$ $PO_4, = (-c + d.salt^2)^2$ $Si(OH)_4 = (-e + f.salt^2)^2$ *a = 0.0230496, b = 31.2392, c = 7.0582, d = 0.00517724, e = 33.0298, f = 0.0242586*		
NBa	9.5	Coast	Coast	39.5	$NO_3 = e^{a.salt^2 - b}$ $PO_4 = (-c + d.salt^2)^2$ $Si(OH)_4 = 1/(a - b\,.salt^2)^2$ *a = 0.0508111, b = 73.2698, c = 16.5165, d = 0.0115393, e = 22.9274, f = 0.0153768*		
Tyr	16.5	9.5	Coast	41.5	$NO_3 = (a\,.salt^2 - b)^2$ $PO_4, = (-c + d.salt^2)^2$ $Si(OH)_4 = (-e + f.salt^2)^2$ *a = 0.0400278, b = 57.0955, c = 9.93055, d = 0.00700501, e = 62.7026, f = 0.0437829*		
With, salt is salinity and dens is density							

- Initialisation du basin oriental:

Eastern Med Sea					
Bioregion	Geographical limits				Median profiles from Lazzari et al reanalysis
	East	West	North	South	NO3 / PO4 / Si(OH)4 / O_{2d}
CeM	11	9.5	38	36.5	

					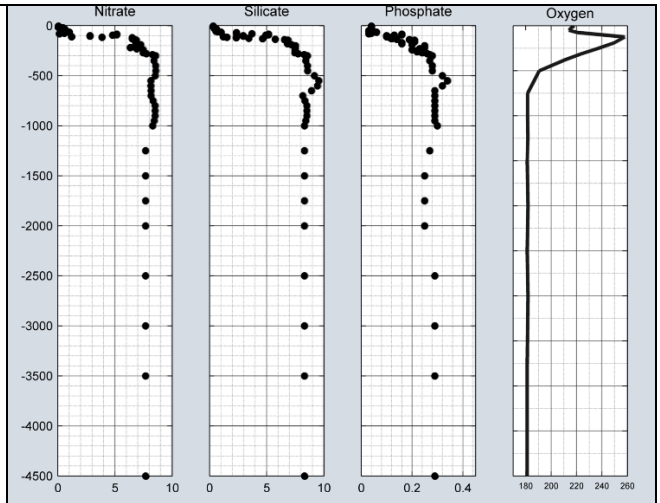
WSC	15	9.5	34	Coast	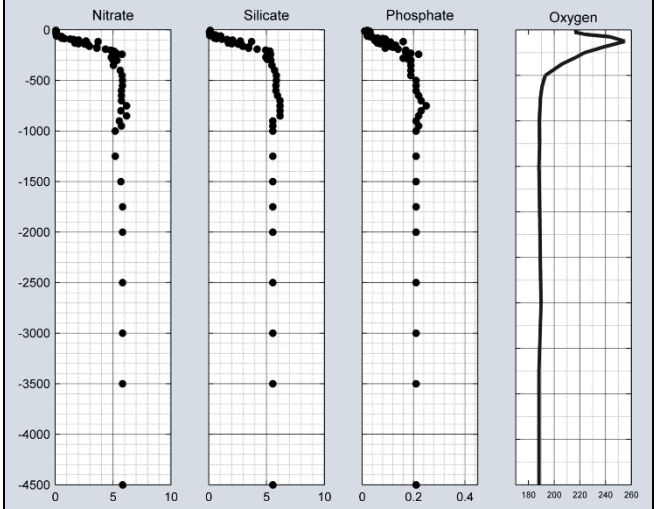
CES	15	10	38	34	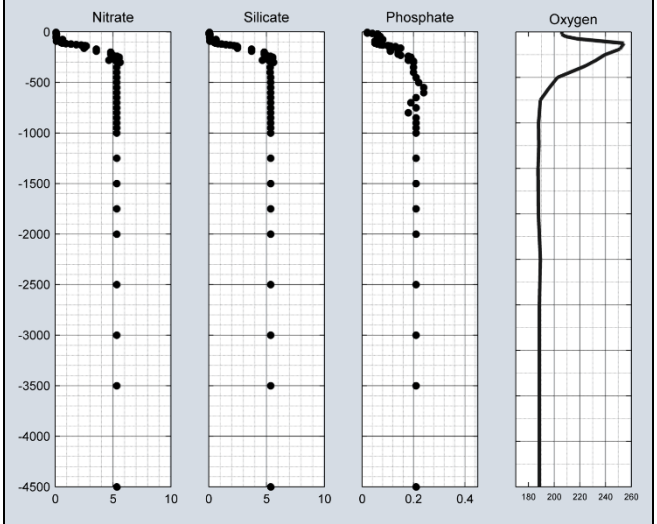
ISo + Lev	30 + Coast	15	37	Coast	

					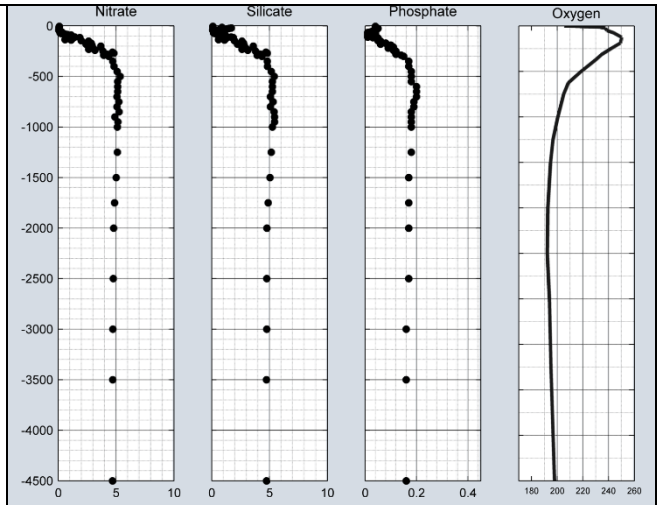
Ino	22	15	39	37	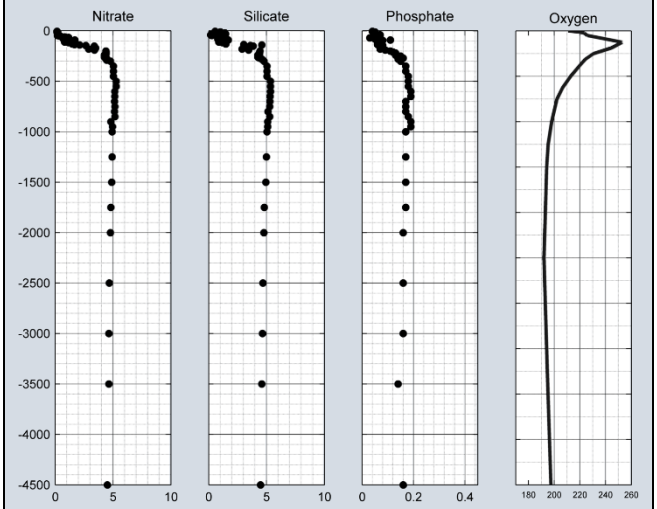
Otr	20.5	16	41	39	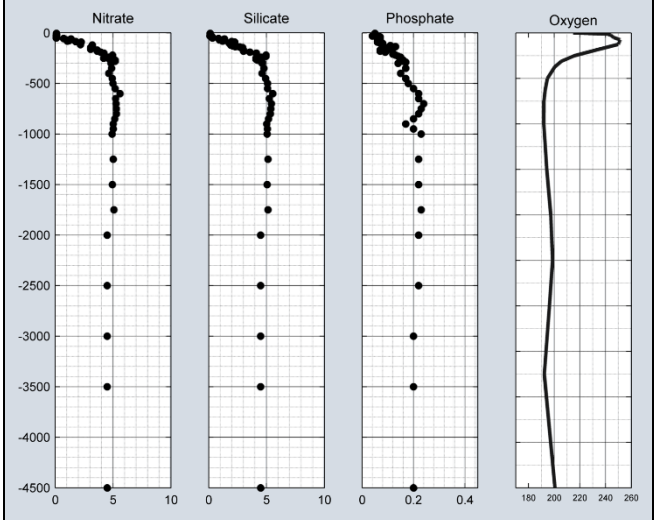
SAd	20	11	Coast	41	

					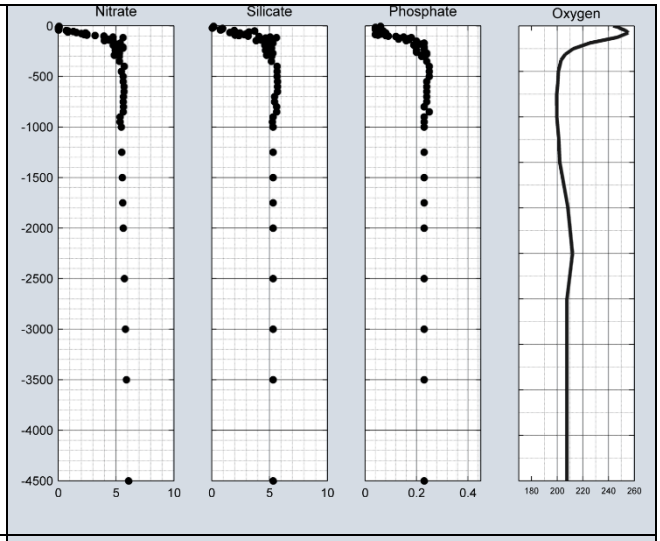
Aeg	30	23	Coast	37	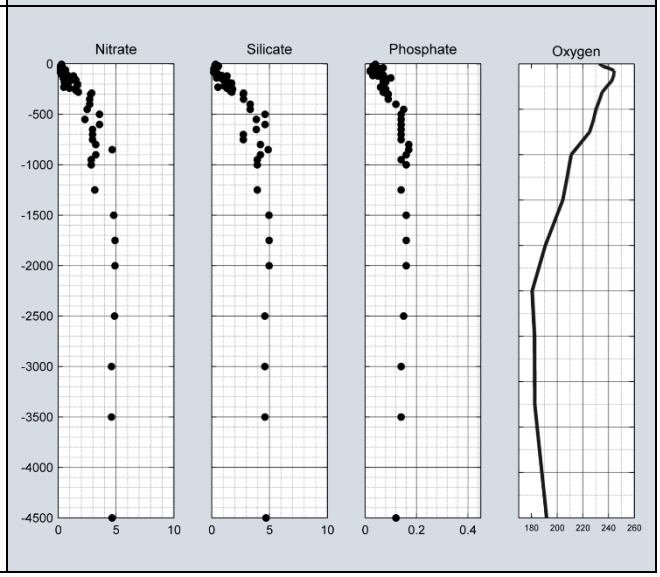

2.2. Le produit satellite MODIS

Les données satellite de chlorophylle « Ocean Colo Level 3 » du satellite MODIS-Aqua ont été téléchargées à partir du site de la NASA (http://oceancolor.gsfc.nasa.gov/cgi/l3). Les données ont une résolution horizontale de 4km avec des fréquences de sortie quotidiennes. Les champs de la Mer Méditerranée ont été sélectionnés puis interpolés sur nos grilles numériques. Des comparaisons ont été faites sur des séries temporelles moyennées par région ou par « point-référence » préalablement sélectionnés (cf : chapitre 6, 7 et 8). Des climatologies ont aussi été réalisées pour les comparer à celle du modèle. Les données MODIS sont actualisées quotidiennement et sont disponibles depuis 2002. Les séries temporelles utilisées dans cette thèse ont été automatisées pour une exploitation qui commence le 1er juin 2003 et se prolonge jusqu'en 2015.

Les images satellite ont joué un rôle très important pendant la campagne DeWEx, principalement au Leg 2. Elles ont, entre autre, permis le suivi d'un tourbillon cyclonique qui se déplaçait au sud de la zone d'étude.

Dans un plan beaucoup plus étendu, la chlorophylle du satellite MODIS a permis la calibration de la chlorophylle du modèle biogéochimique sur deux plans. Le premier plan est temporel. Le but était d'obtenir un bon « timing » du déclenchement du bloom sur la douzaine d'années simulées. Pour cela, les paramètres liés aux températures préférentielles de consommation pour le phytoplancton et le zooplancton ont été modifiées. Le second plan est celui de l'intensité de la production primaire, c'est à dire agir sur les paramètres liés au rendement quantique maximal et le coefficient d'absorption spécifique par groupe phytoplanctonique.

Le résumé des paramètres, ajustés par dichotomie à l'intérieur d'un intervalle mentionné dans la littérature, sont présentés dans le tableau 10.1. Les résultats montrent que la température de croissance optimale est de 14 °C pour le phytoplancton et de 18 °C pour le zooplancton. Le paramètre de rendement quantique augmente avec la taille du phytoplancton allant de 2.6 à 3.85^{e}-4 en mmolC/J. Pour le coefficient d'absorption, l'évolution est inversement proportionnelle à la taille, allant de 0.032 m^2/mgChl pour le picophytoplancton à 0.013 pour le microphytoplancton.

Nom du paramètre	Résultat final		
	Picophyto ou Nanozoo	Nanophyto ou Microzoo	Microphyto ou Mesozoo
Timing du développement planctonique optimal			
Température de croissance optimale : Phyto	14°C	14°C	14°C
Température de croissance optimale : Zoo	18°C	18°C	18°C
Intensité de l'efflorescence chlorophyllienne			
Rendement quantique : Phyto	2.6^{e}-4	2.87^{e}-4	3.85^{e}-4
Coefficient d'absorption : Phyto	0.032	0.016	0.013

Tableau 10.1 : Paramètres du modèle biogéochimique associés aux données MODIS.Les campagnes MOOSE, DoWEx et DeWEx

Les programmes d'observation combinés DeWEx, DoWEx et MOOSE ont recouvert un cycle annuel de juillet 2012 à septembre 2013 sur l'ensemble de la Méditerranée nord-occidentale (du golfe du Lion au golfe de Gènes). Quatre campagnes hauturières ont été organisées : deux campagnes sur le navire océanographique (N/O) Le Suroît en 2013 ont balayé les périodes de formation des eaux

denses (du 1er au 20 février) et d'efflorescence printanière (du 5 au 24 avril) ; elles ont été précédées puis suivies par deux campagnes dont les mesures ont été moins fréquentes et plus légères en ce qui concerne le nombre de paramètres biologiques mesurés, le tout à bord du N/O Téthys 2 (septembre 2012 et septembre 2013).

Les campagnes hauturières se sont déroulées le long d'un même parcours sous forme d'étoile qui traversa à plusieurs reprises le Courant Nord, le Courant Corse et le front des Baléares en effectuant des stations hydrologiques et biogéochimiques tous les 10 à 20 km, ce qui représente une échelle spatiale suffisante pour échantillonner correctement une gamme étendue de structures dynamiques. Les campagnes menées ont pu réaliser un échantillonnage sur quatre périodes clés de l'année et par chance cette année a connu une convection profonde et un bloom intense. Les deux autres saisons furent caractérisées par une stratification totale des masses d'eau, ce qui a permis d'avoir trois visions représentatives de trois états océanique totalement différents.

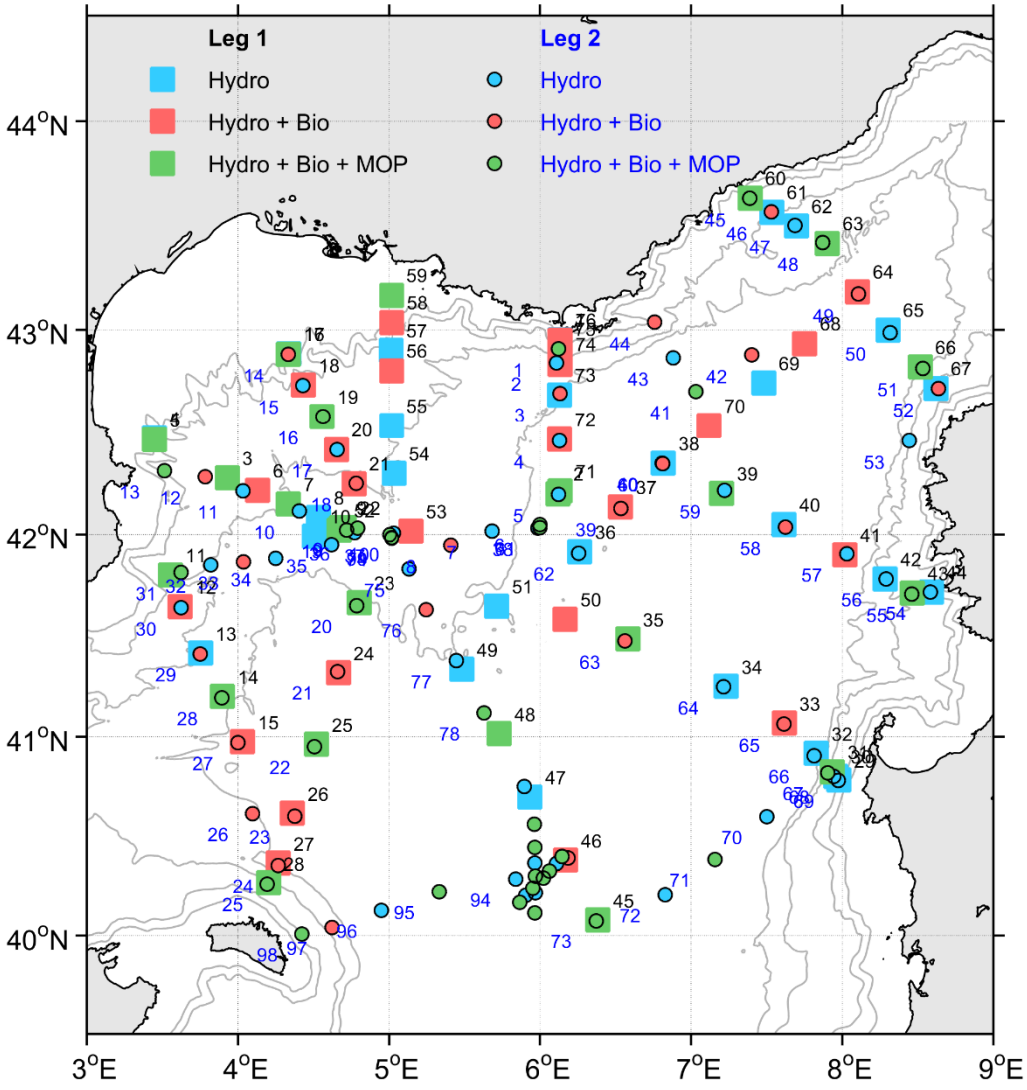

Figure 10.2 : position des stations superposées des deux legs DeWEX

L'objectif principal du projet DeWEx appuyé par la modélisation à l'échelle régionale est d'étudier un cycle hydrologique et biogéochimique annuel complet en Méditerranée nord-occidentale. Le projet DeWEx est une étape clé du projet MERMEX (Marine ecosystem response in the mediterranean experiment) visant à comprendre les changements susceptibles d'impacter les écosystèmes marins en Méditerranée dans les prochaines décennies, MERMEX étant une composante du programme MISTRALS. Le projet DeWEX partage également certains objectifs du projet HyMeX, une autre composante de MISTRALS.

La distribution spatiale des observations (Fig. 10.2.), principalement celles de l'hiver qui couvrent les zones représentatives des propriétés dynamiques de la région d'étude (convection, courant nord et front des Baléares), ont permis de calibrer très finement le modèle. Le but était de permettre de diminuer les concentrations en sels nutritifs sur les bords du courant nord afin d'obtenir des concentrations les plus proches possible des mesures. Les taux de consommation du phytoplancton par le coefficient de broutage maximal du zooplancton ont été calculés en prenant en considération les ajustements précédents. Les taux de mortalité du phytoplancton et du zooplancton ont également été testés.

Les résultats sont rappelés dans le tableau 10.2. Le coefficient de broutage est plus important pour le petit phytoplancton que pour les gros. Le taux de mortalité présente un minimum dans la classe moyenne, ce qui n'est pas le cas pour le zooplancton qui lui présente une variation du taux de mortalité décroissant avec la taille des individus.

Nom du paramètre	Résultat final		
	Picophyto ou Nanozoo	Nanophyto ou Microzoo	Microphyto ou Mesozoo
Coefficient de broutage	3.88 d^{-1}	2.59 d^{-1}	1.29 d^{-1}
Taux de mortalité du phyto	0.09 $m^{-3}.mMolC.d^{-1}$	0.0328 $m^{-3}.mMolC.d^{-1}$	0.0522 $m^{-3}.mMolC.d^{-1}$
Taux de mortalité du zoo	0.01134 d^{-1}	0.0081d^{-1}	0.0072 d^{-1}

Tableau 2.2 : Paramètres biogéochimiques du modèle associé aux données de la campagne DeWEX.

2.3. Les flotteurs BioArgo

Les flotteurs Argo sont des instruments autonomes qui permettent de réaliser des profils hydrologiques sur de grandes profondeurs [0-2000m]. La technologie des flotteurs a évolué et permet actuellement d'équiper certains flotteurs de capteurs biologiques. Les flotteurs déployés en Mer Méditerranée sont équipés de capteur SUNA (PROVBIO-V2). Ces flotteurs sont également équipés de capteurs de chlorophylle, de matière organique dissoute colorée (CDOM), et autres capteurs optiques et de moyens de télémétrie pour permettre la communication dans les deux sens, pour

récupérer les données à chaque surfaçage et aussi pour pouvoir guider la direction et les profondeurs de dérive à distance. Les flotteurs dérivent à une profondeur programmée (1000m) qui représente une couche d'eau profonde ouest méditerranéenne pendant un certain nombre de jours, établie en fonction des objectifs. Habituellement cette durée est de l'ordre de 10 jours, mais pourrait être choisie plus courte si l'on souhaitait un échantillonnage à plus haute résolution (3 jours pendant la période du bloom d'avril 2013 pour le flotteur lovbio017b).

Les mesures biogéochimiques sont effectuées tous les 10 m dans la couche supérieure [0-250m environ] puis tous les 30 m dans les couches plus profondes. Les mesures physiques ont une fréquence plus élevée avec un pas de 1 m dans la couche [0-100m] et de 10 m dans tout le restant de la colonne d'eau.

La calibration des capteurs de nitrate repose sur des algorithmes de déconvolution des mesures d'absorption de la lumière (D'Ortenzio et al. 2012 ; Johnson 2014). Plus de détails sont disponibles dans l'article (DeFommmervault et al. 2015).

La position de déploiement des flotteurs est choisi en fonction des répartitions des biorégions reconnues en Mer Méditerranée depuis le papier de D'Ortenzio et Ribera d'Alcalà en 2009. Actuellement 14 flotteurs sillonnent la mer Méditerranée. Cinq d'entre eux ont été analysés avec précision et utilisés dans un plan de validation et calibration des modèles couplés dans le cadre de cette thèse, les autres ont été utilisés dernièrement dans un projet de mise en place d'un projet de prévision sur 5 jours du couple physique – biogéochimique en 3D de l'ensemble du bassin (voir en annexe). Il s'agit d'après nos connaissances de la première prévision biologique de cette envergure. Plusieurs de ces flotteurs ont servi à la calibration du modèle utilisé dans cette étude.

Le flotteur bioargo017b avec ces capteurs de nitrate et de chlorophylle a été mis à l'eau pendant la campagne DeWEx en avril 2013 au centre du gyre nord-occidental pendant la période de bloom phytoplanctonique. Ce flotteur est resté dans le gyre pendant plus de 140 jours ce qui a permis d'échantillonner l'évolution de la consommation du nitrate par un développement planctonique intense. Le flotteur lovbio017b a permis la validation du modèle dans un plan temporelle (voir article – chapitre 6).

Le flotteur 035b échantillonnant uniquement un capteur de chlorophylle a été déployé pendant le Leg 1 de la campagne DeWEx en février 2013. Ce dernier a permis de suivre l'évolution de la

fluorescence depuis le grand mélange hivernal à l'intérieur du centre du gyre nord occidental, puis dans le courant nord au début du printemps et jusqu'en mer Alboran.

Ces deux flotteurs mis à l'eau pendant les campagnes DeWEx ont été analysées avec précision et confrontés aux images satellite de chlorophylle et de température de surface puis enfin comparés avec les résultats du modèle point par point.

Les flotteurs lovbio016c et lovbio018c ont été déployés dans le bassin oriental. Le premier en mer Ionienne et le second en mer Levantine en mai 2013. Les deux flotteurs ont effectué des échantillonnages intéressants car ils ont été pris dans des mouvements circulatoires pendant plus de deux ans et sont toujours en opération. Par la détermination de l'évolution de la profondeur de la couche de mélange et par des comparaisons point par point avec le modèle, ces informations temporelles et spatiales ont permis de bien calibrer le modèle biogéochimique.

En effet, la DCM, légèrement trop profonde avant calibration, a été améliorée avec l'ajustement des gradients biologiques tels que la nitracline, la phosphacline entraînant l'amélioration de la position définitive de consommation/production des sels nutritifs, ce qui a pour conséquence un positionnement plus correct de la profondeur de développement phytoplanctonique. Les premières retouches concernaient la vitesse de chute des particules organiques qui semblait être trop rapide, ce qui donnait par conséquent une reminéralisation plus intense à des profondeurs plus importantes. Le second ajustement a concerné le taux de reminéralisation qui finalement s'avère le seul paramètre qui a été modifié dans ce cadre précis. Les tests ont été effectués dans le but de faire remonter la profondeur des gradients biogéochimiques maximaux communément nommés «nutriclines ». La figure 10.3 montre une comparaison finale de l'évolution normalisée de la chlorophylle dans les trois bassins (nord occidental, ionien et levantin) pendant une année, entre le printemps 2013 et celui de 2014, sachant que l'hiver 2014 n'a pas connu de convection profonde. A première vue, on observe un cycle saisonnier de la profondeur de la DCM, avec une intensité variable, plus forte au printemps et plus faible en automne et en hiver dans les trois sous-bassins. On observe également que la profondeur de la DCM varie beaucoup d'un sous-bassin à l'autre, suivant un gradient d'approfondissement ouest-est assez bien représenté par le modèle. Le tableau 10.3 rappelle les résultats obtenus lors de la calibration.

Tableau 10.3 : Taux de décomposition associés aux données issues des BioArgo par élément biogéochimique.

Nom du paramètre	Résultat final	
	Petits détritus	Grand détritus
Cabrone	4.8 e-5 $.d^{-1}$	4.8 e-5 $.d^{-1}$
Azote	5.76^{e}-5 $.d^{-1}$	5.76^{e}-5 $.d^{-1}$
Phosphore	5.04^{e}-5 $.d^{-1}$	5.04^{e}-5 $.d^{-1}$
Silicium	5.54^{e}-6 $.d^{-1}$	5.54^{e}-6 $.d^{-1}$
Chlorophylle	1.5936^{e}-4 $.d^{-1}$	-

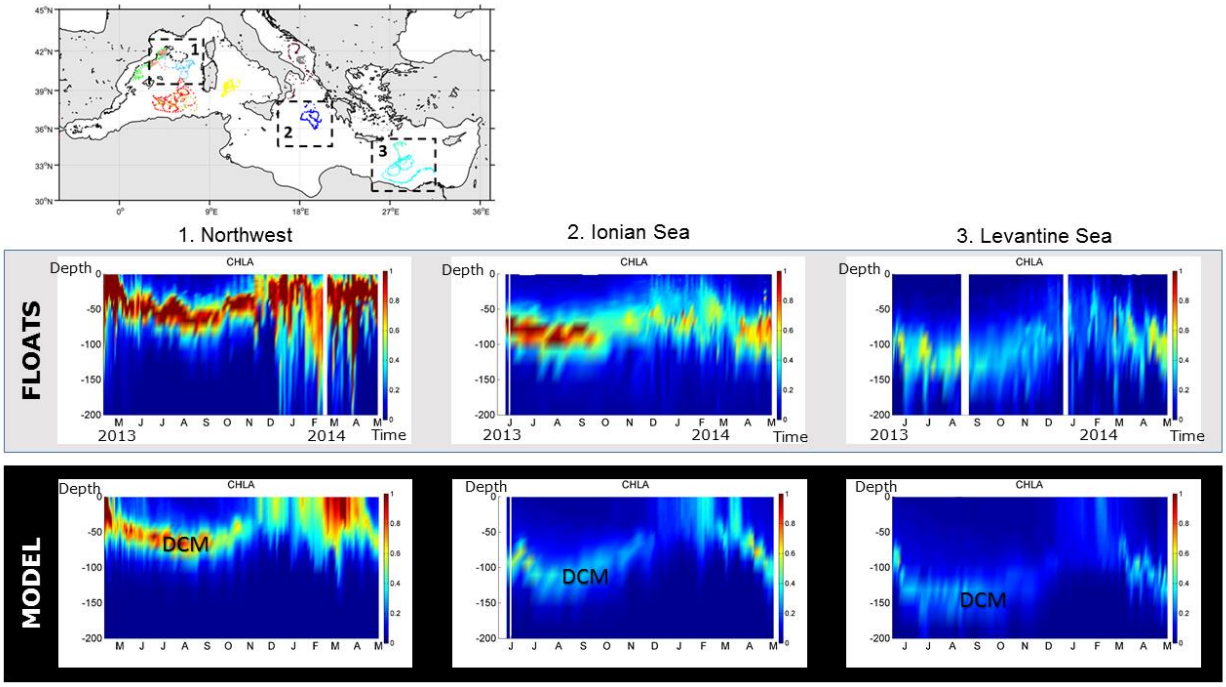

Figure 10.3 : Comparaisons entre les observations des flotteurs BioArgo et les sorties du modèle dans trois biorégions distinctes de la Mer Méditerranée.

2.4. Rappel de l'utilisation des bases de données pour la calibration et perfectionnement des modèles couplées

Objectifs	Variables	Sources des données	Résultats
Distribution verticale, profondeur des nutriclines	Compartiment inorganique (sels nutritifs), oxygène dissous	DEWEX, MOOSE, Base de données historique	Initialisation liée aux propriétés physiques permet d'obtenir un équilibre rapide des processus grâce au bon positionnement des gradients biogéochimiques Caractérisation propre aux biorégions

Processus biologiques	Compartiments organique, dissous, particulaire, phytoplancton, déductions sur le compartiment bactérien	DEWEX leg2, MODIS	Amélioration de la consommation des sels nutritifs et de la minéralisation de la matière organique Timing de l'efflorescence et son intensité Répartition améliorée des groupes phytoplanctoniques
Variabilité liée à la physique (convection, circulation générale)	- Compartiments inorganique, organique, oxygène, phytoplancton - Advection	DEWEX, MODIS	Amélioration des concentrations spécifiques aux courants (Courant Nord, Corse, Front des Baléares) Zones de mélanges et périphériques bien dissociées aussi bien biologiquement que physiquement
Derniers tests de sensibilité	Compartiment organique, phytoplancton	DEWEX, flotteurs NAOS, MODIS	Amélioration des profondeurs de DCM, nutriclines
Extension du domaine de modélisation, Amélioration des conditions aux limites	Toutes les variables biogéochimiques (Organiques, inorganiques, gaz dissous, bactérie, phytoplancton, zooplancton)	DEWEX, flotteurs NAOS, MODIS	Calibration extrapolée du modèle Eco3mS sur l'ensemble du bassin méditerranéen

5.3 Annexes 3 : Les « groupes de travail (WP)» du chantier Méditerranéen MISTRALS et la modélisation

La modélisation physique - biogéochimique 3D aux échelles spatio-temporelles fines donne l'opportunité de travailler sur un plan pluridisciplinaire. Tel était l'objectif de la thèse vis-à-vis de la communauté scientifique du chantier Méditerranéen : aborder les thèmes pluridisplinaires ouverts par les acteurs du chantier en s'appuyant sur une modélisation correctement calibrée et validée permettant d'établir des interactions constructives entre les différents groupes. A termes la modélisation devrait tenter d'apporter des réponses aux questions soulevées par les différents groupes de travail de MerMEx.

(1) Fort de la capacité du modèle à représenter la dynamique océanique à méso et submésoéchelle, le WP1 porte sur l'étude de l'impact de l'hydrodynamique sur la répartition de la matière organique et inorganique dans l'ouest de la Méditerranée. Le WP1 a comme objectif de quantifier le bilan et la variabilité temporelle des éléments biogènes impactés par la circulation océanique, à différentes échelles. Cet objectif ne peut être atteint sans l'association de la modélisation et de l'expérimentation in situ. Les données ponctuelles de campagnes, les images satellites et les robots autonomes sont utilisés pour calibrer puis consolider les résultats obtenus par la modélisation qui tentera de combler les vides laissés par l'observation puis de faire des scénarios de bilans futurs. Les principaux sujets d'étude tournent autour de la dynamique des sels nutritifs dans les zones à fortes dynamiques, dans les zones de mélanges profonds, les fronts et les courants puis sur la production planctonique qui résulte de cet enrichissement en matière inorganique. Son intensité dépendra de la fonction de la structure hydrologique et de la longévité des efflorescences printanières dans la couche superficielle. Dans ce présent travail, un bilan long d'une dizaine d'années a été effectué sur l'ensemble du bassin. Un bilan court, sur la seule année des missions DeWEx a été effectué dans le cadre d'une étude plus fine et plus résolue.

(2) Le modèle apportera certaines réponses à la problématique du WP2 à propos des processus écologiques. En effet, ce WP a pour objectifs de qualifier la variabilité à long terme des processus biologiques entre les communautés planctoniques dans le bassin nord occidental. Cette perspective a été plus longuement étudiée par Marine Herrmann et Pierre-Amaël Auger au cours de leurs thèses respectives. Dans ce présent travail, les réponses apportées concernent plus précisément la quantification de l'évolution de l'export du carbone hors de la couche épipélagique suite à la formation complexe et variable de la matière organique dans la couche euphotique. Ce qu'on appelle plus communément l'export de matière organique s'effectue suivant différentes formes, par advection, par turbulence et par sédimentation. La dernière forme d'export domine d'un point de vue temporel, car elle s'effectue plus principalement après le bloom printanier et pendant la période

stratifiée. D'un point de vue quantitatif, l'export par advection est plus fiable, il intervient pendant la convection profonde et exporte toute la matière présente en surface à la fin de l'automne dans un laps de temps court et avec flux vertical considérable.

(3) Le WP3 est spécialisé dans les apports terrigènes. Cette problématique est très étudiée mais pas totalement résolue par la communauté scientifique. Les difficultés rencontrées par les spécialistes de l'observation dépendent principalement des méthodes et des fréquences des mesures. Ici, les apports par les rivières constituent une variable importante pour deux raisons, d'une part pour pouvoir simuler une bonne efflorescence sur les plateaux et d'autre part pour avoir un bilan minéral correct. Le but commun que porte la modélisation avec ce WP est le suivi des apports inorganiques et organiques dans les couches de surface ou dans les couches plus profondes à travers le cascading, et ensuite voir l'assimilation de cette matière par les communautés marines, planctoniques ou bactériennes. La variabilité des apports est très forte donc l'impact sur les organismes marins est aussi important et doit être quantifié. Le sédiment aussi rétroagit avec la colonne d'eau de fond par des processus de reminéralisation également (Soetaert et al. 2000).

(4) Le WP4 consiste en l'étude des interactions air-mer d'un point de vue biogéochimique. Il s'agit des dépôts atmosphériques des particules organiques ou des sels nutritifs et leur assimilation par les écosystèmes planctoniques. Les efforts effectués dans la modélisation dans ce contexte cernent la mise en place des apports atmosphériques par sous-bassin dans un premier temps en utilisant des données issues de la littérature. D'autre part, des efforts ont été effectués pour imbriquer un modèle atmosphérique (RegCM) au modèle océanique couplé NemoMed12-Eco3m-S sur l'ensemble de la mer Méditerranée, dont les premiers tests montrent des modifications très localisées lors d'évènements extrêmes et des modifications légères liées à la quantité totale de production primaire du bassin. Des efforts sont prêts à être faits pour valoriser cette discipline de recherche dans le domaine de la modélisation et aussi pour promouvoir des exercices plus précis en termes de bilan de matière organique et inorganique dans les masses d'eau superficielles.

(5) Le WP5 est un compartiment de travail final qui permet de rassembler toutes les informations permettant la communication aux décideurs notamment à propos des impacts anthropiques sur les écosystèmes méditerranéens. Le but est de mettre en place un dispositif partant d'un système d'information géographique collectant des données de toutes les disciplines citées auparavant. Par le biais de la modélisation, dans le chapitre 3, nous avons tenté de fabriquer une biorégionalisation à partir d'un ensemble de jeux de données sur une simulation de 10 années. Cette dernière donne une

vue globale du fonctionnement de chaque biorégion. Une des biorégionalisations la plus citée dans la littérature est celle faite par D'Ortenzio and Ribera d'Alcalà (2009). Elle est basée sur la chlorophylle de surface issue des images satellites et qui a été reprise pour une description plus détaillée par Lavigne et al (2013) avec des bases de données historiques de profondeur de couche de mélange et de profils de nitrate. Nous avons testé une méthode de répartition des propriétés biogéochimiques (présentée dans le chapitre 4). Ces exercices de biorégionalisation permettront de mieux connaître le fonctionnement de l'ensemble du bassin et ainsi mettre en place des cartographies de surveillance de la mer et de son évolution en fonction des impacts anthropiques et climatiques.

5.4 Annexes 4 : Paramètres du modèle biogéochimique

Les flux que constituent les équations du phytoplancton sont détaillés comme suit :

Processus du compartiment du phytoplancton		
La production primaire brute	La production primaire est la quantité de carbone organique particulaire et dissous produite lors du processus biologique de la photosynthèse : $$\boldsymbol{GPP_i} = \frac{\boldsymbol{a_{Chl,Phy_i}.\sigma_{max,Phy_i}.PAR(z).f_{Phy}^{T}.ChlPhy_i}}{1+\boldsymbol{\tau_{Phy_i}.\sigma_{Phy_i}.PAR(z)}+\boldsymbol{\tau_{Phy_i}.\frac{k_d}{k_r}.(\sigma_{Phy_i}.PAR(z))^2}}$$	
L'absorption des sels nutritifs	L'absorption des sels nutritifs se fait en proportion de la quantité ambiante $\mu\frac{NR}{Phy_i} =. GPP_i.(^1/_{CPhy_i})$ $$\boldsymbol{UptPhy_{i,NO_3}} = \boldsymbol{v_{Phy_i,N}^{max}}.\frac{\boldsymbol{NO_3}}{\boldsymbol{NO_3}+\boldsymbol{k_{NO_3,Phy_i}}}.\boldsymbol{CPhy_i}.\left(1-(\boldsymbol{\delta_{i,1}}+\boldsymbol{\delta_{i,2}}).\boldsymbol{Inhib}.\frac{\boldsymbol{NH_4}}{\boldsymbol{NH_4}+\boldsymbol{k_{inhib}}}\right).$$ $$\boldsymbol{UptPhy_{i,NH_4}} = \boldsymbol{v_{Phy_i,N}^{max}}.\frac{\boldsymbol{NH_4}}{\boldsymbol{NH_4}+\boldsymbol{k_{NH_4,Phy_i}}}.\boldsymbol{CPhy_i}$$ $$\boldsymbol{UptPhy_{i,PO_4}} = \boldsymbol{v_{Phy_i,P}^{max}}.\frac{\boldsymbol{PO_4}}{\boldsymbol{PO_4}+\boldsymbol{k_{PO_4,Phy_i}}}.\boldsymbol{CPhy_i}$$ $$\boldsymbol{UptPhy_{i,SiO_4}} = \boldsymbol{v_{Phy_i,Si}^{max}}.\frac{\boldsymbol{SiO_4}}{\boldsymbol{SiO_4}+\boldsymbol{k_{SiO_4,Phy_i}}}.\boldsymbol{CPhy_i}$$ avec $v_{Phy_i,x}^{max} = \mu_{Phy_i}^{NR}.(^x/_C)_{Phy_i}^{max}$ (x=N, P,Si)	
Exsudation de la matière organique dissoute	L'exsudation ($Exu_{i,C}$) de matière organique dissoute représente le rejet de tout ce qui n'est pas assimilé par les cellules de phytoplancton, (sauf pour les silicates, qui sont rejetés sous forme inorganique dissoute). $$\boldsymbol{Exu_{i,C}} = (1-\boldsymbol{gml_i}).\boldsymbol{GPP_i}$$ Avec $gml_i = 0$ si $(^{x_{lim}}/_C)_{Phy_i} < (^{x_{lim}}/_C)_{Phy_i}^{min}$	

	ou $gml_i = f^{Q}_{x_{lim},Phy_i}$ si $(^{x_{lim}}/_{C})_{Phy_i} \in [(^{x_{lim}}/_{C})^{min}_{Phy_i}, (^{x_{lim}}/_{C})^{max}_{Phy_i}]$ ou $gml_i = 1$ si $(^{x_{lim}}/_{C})_{Phy_i} > (^{x_{lim}}/_{C})^{max}_{Phy_i}$ Avec x= N, P, Si Et, $x_{\lim} \; such as \; \frac{(^{x_{lim}}/_{C})_{Phy_i}}{(^{x_{lim}}/_{C})^{\max}_{Phy_i}} = \min\left(\frac{(^{x_{lim}}/_{C})_{Phy_i}}{(^{x_{lim}}/_{C})^{\max}_{Phy_i}}\right)$ $f^{Q}_{N_{lim},Phy_i} = 1 - \frac{(^{N_{lim}}/_{C})^{min}_{Phy_1}}{(^{N_{lim}}/_{C})_{Phy_1}}$ $f^{Q}_{P_{lim},Phy_i} = 1 - \frac{(^{P_{lim}}/_{C})^{min}_{Phy_1}}{(^{P_{lim}}/_{C})_{Phy_1}}$ $f^{Q}_{N_{lim},Phy_i} = \frac{(^{N_{lim}}/_{C})_{Phy_i} - (^{N_{lim}}/_{C})^{min}_{Phy_1}}{(^{N_{lim}}/_{C})_{Phy_i} - (^{N_{lim}}/_{C})^{min}_{Phy_1} + \beta_{NPhy_i}}$; i=2,3 $f^{Q}_{P_{lim},Phy_i} = \frac{(^{P_{lim}}/_{C})_{Phy_i} - (^{P_{lim}}/_{C})^{min}_{Phy_1}}{(^{P_{lim}}/_{C})_{Phy_i} - (^{P_{lim}}/_{C})^{min}_{Phy_1} + \beta_{PPhy_i}}$; i=2,3 $f^{Q}_{N_{lim},Phy_3} = \frac{(^{Si}/_{C})_{Phy_3} - (^{Si}/_{C})^{min}_{Phy_3}}{(^{Si}/_{C})_{Phy_3} - (^{Si}/_{C})^{min}_{Phy_3} + \beta_{SiPhy_3}} \frac{(^{N}/_{C})_{Phy_3}{}^{10}}{(^{N}/_{C})_{Phy_3}{}^{10} + (kSi)^{10}}$	
Exsudation de la matière inorganique (N,P) et du $Si(OH)_4$ résultant de l'absorption	$\boldsymbol{Exu_{i,N} = \sum_{j=1}^{2}\left(1 - f^{Q}_{Upt_{N,Phy_i}}\right).UptPhy_{i,Nut_j}}$ $\boldsymbol{Exu_{i,P} = \left(1 - f^{Q}_{Upt_{P,Phy_i}}\right).UptPhy_{i,Nut_j}}$; j=3,4 $\boldsymbol{Exu_{i,Si} = \left(1 - f^{Q}_{Upt_{Si,Phy_i}}\right).UptPhy_{i,Nut_j}}$; j=3,4 : $f^{Q}_{Upt_{x,Phy_i}} = \left(\frac{(^{x}/_{C})^{max}_{Phy_i} - (^{x}/_{C})_{Phy_i}}{(^{x}/_{C})^{max}_{Phy_i} - (^{x}/_{C})^{min}_{Phy_i}}\right)^{1/2}$; x= P, Si	
La respiration	La respiration dépend de l'absorption des nutriments. $\boldsymbol{RespPhy_i = k_{resp,Phy_i}.gml_i.GPP_i + \sum_j r_{Nut_j,Phy_i} UptPhy_{i,Nut_j}}$	
La synthese de la chlorophylle	$\boldsymbol{Synth_{i,Chl} = \rho_{Phy_i,Chl} \cdot \sum_{j=1}^{2} UptPhy_{i,Nut_j}}$ $\rho_{Phy_i,Chl} = \frac{(^{Chl}/_{N})^{max}_{Phy_i}.\mu_{Phy_i}}{a_{Chl,Phy_i}.\varphi_{max,Phy_i}.PAR(z).(^{Chl}/_{C})_{Phy_i}} . \frac{1 - \frac{(^{Chl}/_{N})_{Phy_i}}{(^{Chl}/_{N})^{max}_{Phy_i}}}{1.05 - \frac{(^{Chl}/_{N})_{Phy_i}}{(^{Chl}/_{N})^{max}_{Phy_i}}}$ $\mu_{Phy_i} = gml_i.\mu^{NR}_{Phy_I}$	

La sénescence	La mortalité est proportionnelle à la concentration et, est fonction de la température $\boldsymbol{MortPhy_{i,x} = \tau_{mort,Phy_i}.f_{Phy}^{T}.XPhy_i}$; x=C, N, P, Si, Chl	

Les processus impliquant les variabilités du zooplancton se détaillent comme suit :

Processus du compartiment zooplanctonique		
La croissance du zooplancton	La croissance du zooplancton dépend du bilan broutage, égestion et gaspillage, suivant : $\boldsymbol{GrowthZoo_{i,C} = k_{C,Zoo_i}.(Graz_{i,CPrey} - Eges_{i,C} - SloppyFeed_{i,C})}$	
Broutage	$Graz_{i,xPrey} = \frac{f_{Zoo}^{T} \cdot g_{Zoo_I} \cdot \varphi_{Prey,Zoo_i} \cdot (CPrey)^2 \cdot ({}^{x}/_{C})_{Prey} \cdot CZoo_i}{k_{g,Zoo_i} \cdot (\sum_{Prey} \varphi_{Prey,Zoo_i} CPrey) + \sum_{Prey} \varphi_{Prey,Zoo_i} (CPrey)^2}$ X= C, N, P, Si, Chl	
Sloppy feeding (Gaspillage de nourriture)	$SloppyFeed_{i,x} = \Psi_{Zoo}.\sum_{Prey} Graz_{i,xPrey}$; x=C, N, P	
L'égestion	L'égestion est la production de matière organique particulaire rejetée par le zooplancton qui sédimente par force de gravité $Eges_{i,x} = (1 - \beta_{Zoo_i}).(1 - \Psi_{Zoo}).\sum_{Prey} Graz_{i,xPrey}$; x=C, N, P $Eges_{i,x} = \sum_{Prey} Graz_{i,xPrey}$; x=Si, Chl	
La respiration basale	Il s'agit de la production du dioxyde de carbone par la respiration du zooplancton $\boldsymbol{RespZoo_i = (1 - k_{C,Zoo_i}).(Graz_{i,CPrey} - Eges_{i,C} - SloppyFeed_{i,C})}$	
L'excrétion de la matière inorganique dissoute et respiration additionnelle	$FoodZoo_{i,C} = k_{C,Zoo_i}.(Graz_{i,CPrey} - Eges_{i,C} - SloppyFeed_{i,C})$ $FoodZoo_{i,N} = Graz_{i,NPrey} - Eges_{i,N} - SloppyFeed_{i,N}$ $FoodZoo_{i,P} = Graz_{i,PPrey} - Eges_{i,P} - SloppyFeed_{i,P}$ $({}^{N}/_{C})_{FoodZoo_i} = \frac{FoodZoo_{i,N}}{FoodZoo_{i,C}}$ and $({}^{P}/_{C})_{FoodZoo_i} = \frac{FoodZoo_{i,P}}{FoodZoo_{i,C}}$ 1. Si l'élément le plus limitant est le carbone; $({}^{N}/_{C})_{FoodZoo_i} > ({}^{N}/_{C})_{Zoo_i}$ and $({}^{P}/_{C})_{FoodZoo_i} > ({}^{P}/_{C})_{Zoo_i}$: $ExcZoo_{i,NH_4} = FoodZoo_{i,N} - ({}^{N}/_{C})_{Zoo_i}.FoodZoo_{i,C}$ $ExcZoo_{i,PO_4} = FoodZoo_{i,P} - ({}^{P}/_{C})_{Zoo_i}.FoodZoo_{i,C}$ 2. Si la nourriture est enrichie de carbone et que les éléments les plus limitants sont le N et le P	
Mortalité	$\boldsymbol{MortZoo_{i,C} = \tau_{mort,Zoo_i}.f_{Zoo}^{T}.CZoo_i}$ $\boldsymbol{MortZoo_{i,N} = ({}^{N}/_{C})_{Zoo_i}.MortZoo_{i,C}}$	

	$\boldsymbol{MortZoo_{i,P} = (P/C)_{Zoo_i} . MortZoo_{i,C}}$	
Prédation du méso zooplancton	La prédation ne concerne que le mésozooplancton $\boldsymbol{GrazZoo_{3,C} = \tau_{pRED} . f^{T}_{Zoo} . (CZoo_3)^2}$ $\boldsymbol{GrazZoo_{i,N} = (N/C)_{Zoo_3} . GrazZoo_{3,C}}$ $\boldsymbol{GrazZoo_{i,P} = (P/C)_{Zoo_3} . GrazZoo_{3,C}}$	

Les processus intervenants dans l'équation d'état de l'évolution des bactéries sont détaillés comme suit :

Les processus du compartiment des bactéries (adapté du modèle decrit dans (Anderson and Pondaven, 2003)		
Absorption de la matiere organique dissoute	L'absorption de la matière organique est fonction d'un coefficient d'absorption maximal, de diverses fonctions de limitation et de la quantité de carbone disponible dans les cellules bactériennes. $\boldsymbol{UptBac_{DON} = \mu_{Bac} . \left(\frac{DOC}{DOC + k_{DOC}}\right) . (N/C)_{DOM} . CBac}$ $\boldsymbol{UptBac_{DOP} = \mu_{Bac} . \left(\frac{DOC}{DOC + k_{DOC}}\right) . (P/C)_{DOM} . CBac}$ $Absorption\ de\ la\ matière\ organique = Taux\ d'absorption\ max + fonction\ de\ régulation + \frac{Concentration\ ambiante\ de\ l'élément\ N ou\ P}{ambiant\ concentration\ of\ element\ C} + carbon\ amount\ in\ the$	
Production bactérienne nette	La production bactérienne nette est un diagnostic qui permet de représenter quantité effective dans l'eau de mer $NBP = \varepsilon_{Bac} . UptBac_{DOC}$	
Absorption et et libération des nutriments	Les bactéries ont un ratio (N or P/C)$_{bac}$ constant et dépendant du ratio de l'absorption de la matière organique dissoute et de l'excrétion de l'ammonium et du phosphate, ainsi que de la respiration (rejet du CO_2). Le rapport alimentaire est calculé en fonction de l'absorption de la matière organique dissoute $(N\ or\ P/C)_{DOM}$ et de la croissance des bactéries $\frac{1}{\varepsilon_{Bac}}$. $(N/C)_{Food\ Bac} = \frac{1}{\varepsilon_{Bac}} . (N/C)_{DOM}$ $(P/C)_{Food\ Bac} = \frac{1}{\varepsilon_{Bac}} . (P/C)_{DOM}$ La fonction de régulation de l'absorption de la matière inorganique (taux maximale d'absorption)	

$$UptBac_{N\ or\ P}^{max} = Taux\ de\ croissance \max \times \frac{Concentration\ ambiante\ de\ l'élément\ Nor\ P}{Concentration\ ambiante\ de\ l'élément} \times Terme\ Michaelian \times\ Quantité\ de\ carbon\ dans\ les\ bactéries$$

$$\boldsymbol{UptBac_{NNut}^{max} = \mu_{Bac}.\left({}^{N}/_{C}\right)_{Bac}.\left(\frac{NNut}{NNut + k_{NNut,Bac}}\right).CBac}$$

$$\boldsymbol{UptBac_{PO_4}^{max} = \mu_{Bac}.\left({}^{P}/_{C}\right)_{Bac}.\left(\frac{PO_4}{PO_4 + k_{PO_4,Bac}}\right).CBac}$$

Michaelian est un terne de limitation spécifique à chaque élément X. il est extrait selon trois cas:

1. Lorsque l'élément le plus limitant est le carbone;
$\left({}^{N}/_{C}\right)_{FoodBac} > \left({}^{N}/_{C}\right)_{Bac}$ et $\left({}^{P}/_{C}\right)_{FoodBac} > \left({}^{P}/_{C}\right)_{Bac}$:

$$UptBac_{NNut} = 0\ ;\ UptBac_{PNut} = 0$$

$$\boldsymbol{ExcBac_{NNut} = UptBac_{DON} - \varepsilon_{Bac}.UptBac_{DOC}.\left({}^{N}/_{C}\right)_{Bac}}$$
$$\boldsymbol{ExcBac_{PO_4} = UptBac_{DOP} - \varepsilon_{Bac}.UptBac_{DOC}.\left({}^{P}/_{C}\right)_{Bac}}$$

$$NBP = \varepsilon_{Bac}.UptBac_{DOC}$$

2. Si l'alimentation présente un élément déficitaire $x_1(N, P)$; en même temps que les autres éléments $x_2 \neq x_1\ (N,P)$ sont en excès par rapport au carbone:
$\left({}^{x_1}/_{C}\right)_{FoodBac} \leq \left({}^{x_1}/_{C}\right)_{Bac}$ et $\left({}^{x_2}/_{C}\right)_{FoodBac} > \left({}^{x_2}/_{C}\right)_{Bac}$:

$$UptBac_{x_1Nut} = \min\left[UptBac_{x_1Nut}^{max}, \varepsilon_{Bac}.UptBac_{DOC}.\left({}^{x_1}/_{C}\right)_{Bac} - UptBac_{DOx_1}\right]\ ;\ UptBac_{DOx_2} = 0$$

$$ExcBac_{x_1Nut} = 0$$
$$ExcBac_{x_2Nut} = UptBac_{DOx_2} - \varepsilon_{Bac}.UptBac_{DOC}.\left({}^{x_2}/_{C}\right)_{Bac}$$

$$NBP = \frac{UptBac_{Dox_1} + UptBac_{x_1Nut}}{\left({}^{x_1}/_{C}\right)_{Bac}}$$

	3. Si l'alimentation comporte un déficit en azote et en phosphore et qu'un de ces deux éléments x1 (N, *P)* soit le plus limitant: $(^{x_1}/_{C})_{FoodBac} \leq (^{x_2}/_{C})_{Bac}$ *et* $(^{x_2}/_{C})_{FoodBac} \leq (^{x_2}/_{C})_{Bac}$ *With*: $(^{x_2}/_{x_1})_{FoodBac} \leq (^{x_2}/_{x_1})_{Bac}$: $UptBac_{x_1Nut} *= \min\left[UptBac^{max}_{x_1Nut}, NPB \,.\, (^{x_1}/_{C})_{Bac} - UptBac_{DOx_1}\right]$ Si $UptBac_{DOx_2} \leq UptBac_{DOx_1} + UptBac_{x_1Nut}) \,.\, (^{x_1}/_{x_2})_{Bac}$ $UptBac_{x_1Nut} = \min\left[UptBac^{max}_{x_1Nut}, \left(UptBac_{DOx_2} + UptBac_{x_2Nut} *\right) .(^{x_1}/_{x_2})_{Bac} - UptBa$ $ExcBac_{x_1Nut} = 0$ $UptBac_{x_2Nut} = \min\left[UptBac^{max}_{x_2Nut}, \left(UptBac_{DOx_1} + UptBac_{x_1Nut} *\right) .(^{x_2}/_{x_1})_{Bac} - UptBa$ $ExcBac_{x_2Nut} = 0$ $NPB = \dfrac{UptBac_{DOx_1} + UptBac_{x_1Nut}}{(^{x_1}/_{C})_{Bac}}$	
	Ou alors: $UptBac_{x_2Nut} = 0$ $ExcBac_{x_2Nut} = UptBac_{DOx_2} - (UptBac_{DOx_1} + UptBac_{x_1Nut}) \,.\, (^{x_2}/_{x_1})$ $UptBac_{x_1Nut} = UptBac_{x_1Nut}$ $UptBac_{x_1Nut} = 0$ $NPB = \dfrac{(UptBac_{DOx_1} + UptBac_{x_1Nut}}{(^{x_1}/_{C})_{Bac}}$	
Respiration	$\boldsymbol{RespBac = NBP \,.\, (\dfrac{1}{\varepsilon_{Bac}} - 1)}$ La respiration est reliée au taux de croissance et à la libération du CO_2.	
Mortalité	$\boldsymbol{MortBac_C = \tau_{mort,Bac}.f^T_{Bac}.(^{C}/_{C})_{Bac}.CBac}$ $\boldsymbol{MortBac_N = \tau_{mort,Bac}.f^T_{Bac}.(^{N}/_{C})_{Bac}.CBac}$ $\boldsymbol{MortBac_P = \tau_{mort,Bac}.f^T_{Bac}.(^{P}/_{C})_{Bac}.CBac}$ La cause principale de la mortalité des bactéries est cause par des attaques virales (Bratbak et al., 1992). La mortalité des bactéries produit de la matière organique dans cet environnement.	

Les processus qui interviennent dans l'évolution de la matière organique particulaire se fait comme suit :

Processus spécifiques du compartiment organique

Nitrification	La nitrification est un processus biologique bactérien dans lequel l'ammonium est transformé en nitrate suivant deux étapes, d'abord la nitritation puis la nitratation. $Nitrif = \tau_{nitrif} . NH_4 . f^T_{Nitrif} . (1 - \frac{PAR(z)}{PAR_{surf}})$ $Nitrification = taux\ de\ nitrification\ max\ at\ 0°$ $\times [NH_4] \times rfonction\ de\ régulation\ de\ la\ température\ \times fonction\ de\ régulation\ de\ la$ $(la\ nitrification\ est\ favorisée\ en\ subsurface)$	
La décomposition	La décomposition de la matière organique particulaire en matière organique dissoute est faite par l'activité bactérienne dans la colonne d'eau $Decomposition$ $= taux\ de\ décomposition\ \times fonction\ de\ régulation\ dée\ la\ temprature$ $\times concentration\ en\ détritus\ (organic\ particulate\ form)$ $Decomp_{xDet_{S,L}} = \tau_{rem,xDet} . xDet_{S,L}$	

Constantes pour le calcul de l'oxygène à saturation:

$$\mathrm{ox_{A0}} = 2.00907, \quad \mathrm{ox_{A1}} = 3.22014, \quad \mathrm{ox_{A2}} = 4.05010, \quad \mathrm{ox_{A3}} = 4.94457,$$
$$\mathrm{ox_{A4}} = -0.256847, \quad \mathrm{ox_{A5}} = 3.88767, \quad \mathrm{ox_{B0}} = -6.24523\mathrm{e}^{-3},$$
$$\mathrm{ox_{B1}} = -7.37614\mathrm{e}^{-3}, \quad \mathrm{ox_{B2}} = -1.03410\mathrm{e}^{-2}, \quad \mathrm{ox_{B3}} = -8.17083\mathrm{e}^{-3},$$
$$\mathrm{ox_{C0}} = -4.88682\mathrm{e}^{-7}, \quad \mathrm{ox_{A}} = 1638, \quad \mathrm{ox_{B}} = 81.83, \quad \mathrm{ox_{C}} = 1.483, \quad \mathrm{ox_{D}} = 0.008004$$

Liste des variables d'état du modèle biogéochimique:

State variables	Description	Unit
Phytoplankton		
*C*Phy$_i$ *N*Phy$_i$ *P*Phy$_i$ *Si*Phy$_3$	*i*(1,2,3)=pico, nano, micro phytoplankton	mmol*x* m^{-3}
Zooplankton		
*C*Zoo$_i$	*i*(1,2,3)=nano, micro meso zooplankton	mmol*C* m^{-3}
Bacteria		
*x*Bac	*x*=C	mmol*C* m^{-3}
Particulate organic matter		
*x*Small	*x*=Chl, C, N , P, Si	mmol*x* m^{-3}
*x*Large	*x*=C, N , P, Si	mmol*x* m^{-3}
Dissolved organic matter		
DOC, DON, DOP		mmol*x* m^{-3}
Dissolved inorganic matter (Nutrients)		
NO_3, NH_4, PO_4, $Si(OH)_4$	Nitrate, Ammonium, Phosphate, Silicate	mmol m^{-3}
Dissolved Oxygen		mmol m^{-3}

Flux biologiques:

Parameters	Description	Unit	Syne, nano, micro
φ_{max,Phy_i}	Maximum quantum yield	mmolC J^{-1}	2.2e-4, 2.47e-4, 3.45e-4
a_{Chl,Phy_i}	Chl-specific absorption coeff.	m^2 mgChl^{-1}	0.032, 0.016, 0.013
τ_{Phy_i}	Renewal time of photosystems	d	172.8, 259.2, 354.24
σ_{Phy_i}	Cross-section of photosystems	m2 J^{-1}	18, 12, 9
k_d	Dimensionless photoinhibition rate	-	2.6e-8
k_r	Rate of repair of photoinhibition damaged PSII	d	2.e-4
$N/C_{Phy_i}^{min}$	Minimal internal N/C quota	molN molC^{-1}	0.05, 0.05, 0.05
$N/C_{Phy_i}^{max}$	Maximal internal N/C quota	molN molC^{-1}	0.2, 0.2, 0.2
$P/C_{Phy_i}^{min}$	Minimal internal P/C quota	molP molC^{-1}	0.004, 0.002, 0.002
$P/C_{Phy_i}^{max}$	Maximal internal P/C quota	molP molC^{-1}	0.019, 0.019, 0.019
$Si/C_{Phy_i}^{min}$	Minimal internal Si/C quota	molSi molC^{-1}	-,-, 0.05
$Si/C_{Phy_i}^{max}$	Maximal internal Si/C quota	molSi molC^{-1}	-,-, 0.19
$Chl/N_{Phy_i}^{max}$	Maximal internal Chl/N quota	molChl molC^{-1}	
Q_{Phy}^{10}	Temperature coefficient	-	2
T_{Phy}^{REF}	Reference temperature	°C	14
β_{N,Phy_i}	Nitrogen parameter for growth rate limitation	molN molC^{-1}	0.397, 0.198
β_{P,Phy_i}	Phosphorus parameter for growth rate limitation	molP molC^{-1}	0.155
β_{Si,Phy_i}	Silica parameter for growth rate limitation	molSi molC^{-1}	0.140
k_{Si}	Nitrogen parameter for growth rate limitation by silica	molN molC^{-1}	1.2
k_{resp,Phy_i}	Respiration cost for growth	-	0.3, 0.25, 0.2
k_{NH_4,Phy_i}	Half saturation constant for NH_4	mmolN m^{-3}	0.1, 0.3, 0.7
k_{NO_3,Phy_i}	Half saturation constant for NO_3	mmolN m^{-3}	0.5, 0.7, 1
k_{inhib}	Inhibition coefficient by NH_4	mmolN m^{-3}	0.578
$Inhib$	Inhibition parameter by NH_4	-	0.82
k_{PO_4,Phy_i}	Half saturation constant for PO_4	mmolP m^{-3}	0.005, 0.015, 0.05

k_{SiOH_4,Phy_i}	Half saturation constant for SiO_4	mmolSi m^{-3}	1.2
r_{NO_3,Phy_i}	Respiration cost for NO_3 uptake	molC $molN^{-1}$	0.397
r_{NH_4,Phy_i}	Respiration cost for NH_4 uptake	molC $molN^{-1}$	0.198
r_{PO_4,Phy_i}	Respiration cost for PO_4 uptake	molC $molP^{-1}$	0.155
r_{SiO_4,Phy_i}	Respiration cost for SiO_4 uptake	molC $molSi^{-1}$	0.140
τ_{mort,Phy_i}	$Phytoplankton_i$ senescence rate	d^{-1}	0.2722, 0.1944, 0.1728
w_{s,Phy_i}	Sinking rate of $Phytoplankton_i$	m d^{-1}	-0.6912

Parameters	Description	Unit	Nano, micro, meso
g_{Zoo_i}	Maximum grazing rate	d^{-1}	3.888, 2.592, 1.296
k_{g,Zoo_i}	Half saturation constant	mmolC m^{-3}	5, 8.5, 20
k_{c,Zoo_i}	Net growth efficiency	-	0.8
Ψ_{Zoo}	Sloppy feeding fraction	-	0.23, 0.23, 0.23
β_{Zoo_i}	Assimilation efficiency	-	0.6
N/C_{Zoo_i}	Internal N/C quota	molN $molC^{-1}$	0.18
P/C_{Zoo_i}	Internal P/C quota	molP $molC^{-1}$	0.013
τ_{mort,Zoo_i}	Natural mortality rate	d^{-1}	0.0902, 0.0328, 0.0522
τ_{pred}	Predation mortality rate	(mmolC $d)^{-1}$	
$fr_{Det_s}^{MortZoo_i}$	Ratio small/large particulate organic silica in residues of egestion	-	0.8
$fr_{Det_s}^{Eges_{Si}}$	Ratio small/large detritus in zooplankton loss term	-	0.95
Q_{Zoo}^{10}	Temperature coefficient	-	2
T_{Zoo}^{REF}	Reference temperature	°C	18

Parameters	Description	Unit	
μ_{Bac}	Maximum DOC uptake	d^{-1}	3.672
k_{DOC}	Half-saturation for DOC uptake	mmolC m^{-3}	25.
$k_{NH_4,Bac}$	Half-saturation for NH4 uptake	mmolN m^{-3}	0.2

$k_{PO_4,Bac}$	Half-saturation for PO4 uptake	mmolP m^{-3}	0.007
N/C_{bAC}	Bacteria internal N/C quota	mmolN m^{-3}	0.232
P/C_{bAC}	Bacteria internal P/C quota	mmolP $molC^{-1}$	0.022
ε_{Bac}	Bacteria gross growth efficiency	-	0.3
$\tau_{mort,Bac}$	Bacteria mortality rate	d^{-1}	0.0596
Q_{Bac}^{10}	Temperature coefficient	-	2.95
T_{Bac}^{REF}	Reference temperature	°C	20

Parameters	Description	Unit	
$\tau_{rem,CDet}$	Detritus remineralisation rate, C	d^{-1}	0.1728
$\tau_{rem,NDet}$	Detritus remineralisation rate, N	d^{-1}	0.2074
$\tau_{rem,PDet}$	Detritus remineralisation rate, P	d^{-1}	0.1814
$\tau_{rem,ChlDet}$	Detritus remineralisation rate, Chl	d^{-1}	0.4009
$\tau_{rem,SiDet}$	Detritus remineralisation rate, Si	d^{-1}	0.02
w_{s,Det_S}	Small detritus sinking rate	$m.d^{-1}$	-0.6912
w_{s,Det_L}	Large detritus sinking rate	$m.d^{-1}$	-89.8560
τ_{nitrif}	Nitrification rate	d^{-1}	0.0511
Q_{nitrif}^{10}	Temperature coefficient for nitrification	-	2.37
T_{nitrif}^{REF}	Reference temperature for nitrification	°C	10
Q_{rem}^{10}	Temperature coefficient for remineralization	-	2.95
T_{rem}^{REF}	Reference temperature for remineralization	°C	20

Parameters	Description	Unit	
N/O	Mol O2 needed to oxidize 1 mol of NHs in nitrification	mmolN/m3	2
C/O	Mol O2 used per mol C in oxic respiration	molO2/molC	1